

**School of Chemical and Petroleum Engineering
Department of Chemical Engineering**

**Development of an Efficient Photobioreactor for CO₂ Mitigation and
Microalgae Biomass Production: Simulation and Optimisation**

Gita Naderi

**This thesis is presented for the Degree of
Doctor of Philosophy
of
Curtin University**

November 2016

Declaration

To the best of my knowledge and belief this thesis contains no material previously published by any other person except where due acknowledgment has been made. This thesis contains no material which has been accepted for the award of any other degree or diploma in any university.

Name: Gita Naderi

Signature:

A handwritten signature in black ink, appearing to be 'Gita Naderi', written in a cursive style.

Date: November 2016

Abstract

Recently, microalgae cultivation has been intensively investigated as a sustainable and eco-friendly approach for CO₂ mitigation, biofuel production, and wastewater treatment as well as for high value products. In addition to the microalgae species, parameters that affect the cultivation process include CO₂ concentration, light source and intensity, temperature, pH, agitation, and aeration rate. Among these parameters, light availability is considered to be one of the most outstanding limiting factors. The complex hydrodynamics of the microalgae cultivation in any type of photobioreactors causes complex nature of light distribution and its availability inside the culture which remains an obstacle in commercialising microalgae cultivation as well as for photobioreactor design and scale up. The current study has focused on light-related factors such as light intensity, photo period, light distribution inside the culture, and their influence on the performance of the photobioreactor (PBR) in terms of biomass growth, CO₂ biofixation and CO₂ utilisation efficiency.

The influence of light intensity on biomass productivity and CO₂ biofixation of fresh water alga, *Chlorella vulgaris*, in the photobioreactor was investigated. Incident light intensity was adjusted to different levels (30, 50, 100, 185 and 300 $\mu\text{mol m}^{-2} \text{s}^{-1}$). The maximum biomass concentration of 1.83 g L⁻¹ was obtained at a light intensity of 100 $\mu\text{mol m}^{-2} \text{s}^{-1}$ and 2 L min⁻¹ of 2 % CO₂ enriched air aeration. Microalgae still grew relatively well at 50 $\mu\text{mol m}^{-2} \text{s}^{-1}$, but at 30 $\mu\text{mol m}^{-2} \text{s}^{-1}$ led to photo-limitation. The other two light intensities of 185 and 300 $\mu\text{mol m}^{-2} \text{s}^{-1}$ also caused photo-inhibition. In addition, pH and DO variation during cultivation and at different light intensities are discussed.

Further investigation of the influence of other parameters simultaneously is the key for a successful PBR design. Therefore, in this study, the synergistic effect of the key important factors (injected CO₂ %, light intensity, and the photo period) on the biomass growth, CO₂ biofixation rate and CO₂ utilisation using *Chlorella vulgaris* in a batch system was thoroughly investigated and optimised. Response surface methodology based on Central Composite Design (CCD) was employed and a set of experiments was designed based on rotatable CCD at five levels while light intensity ranges between 65.6 and 334.4 $\mu\text{mol m}^{-2} \text{s}^{-1}$, the light period was between 9.3 and

22.7 h and the CO₂ concentration was from 1.3 to 14.7 %. It was deduced that optimum conditions of 112 μmol m⁻² s⁻¹ light intensity, for 17 h light period and 8.7 % CO₂ concentration should be applied to achieve maximum CO₂ biofixation rate of 0.3504 g CO₂ L⁻¹d⁻¹. Within the range of the investigated parameters, the best among the studied conditions CO₂ utilisation efficiency of 0.82 % was achieved at 140 μmol m⁻² s⁻¹, 17.4 h and 1.3 %, respectively. In addition to environmental stress optimisation, the individual and synergistic effects of these parameters on biomass growth and carbon dioxide fixation are discussed.

Evaluating the light intensity inside the culture at different locations (light distribution) is significantly important. Therefore, in this study, the light distribution inside the culture in different incident light intensities and biomass concentrations for various configurations of vessels and illuminations are investigated and discussed. It was observed how quickly light diminished in close distances from the surface, especially in high biomass concentration. Even increasing the incident light intensity did not prevent low light availability in high biomass concentration. Reducing the traveling distance of the light seems to have given the most operative solutions. Finally, experimental light distribution data was used to develop a mathematical model for local light intensity. The exponential dependence of light attenuation on the light path and biomass concentration, as described by the Beer-Lambert law, was improved by using experimental data of the local light intensity at different values of incident light intensity, biomass concentration and light path, and it assisted in developing a more proper model. How this model can more accurately estimate the local light intensity is also demonstrated. The model was then used to mathematically calculate the average light intensity in an evenly illuminated cylindrical photobioreactor to simulate the growth kinetic.

Acknowledgements

I would like to express my sincere gratitude to all those who supported me in bringing this study into reality. I would also like to thank Curtin University for giving me the opportunity of undertaking my PhD.

First, I thank my research supervisor, Dr Hussein Znad, for persuading me to take on this research, and his constructive recommendations and encouragement. I am extremely grateful to my associate supervisor, Prof Moses Tade, for giving me valuable advice, assistance and support.

I would also like to thank Jason Wright for his endless and valuable suggestions and assistance in the setting up of the laboratory equipment and facilities used in this study. My sincere thanks to Dr Roshanak Doroushi for always being ready to help and her kind encouragement and friendship during the years I have been doing this research study.

I would like to thank ANACC, and the CSIRO in Tasmania for the microalgae supply, and I am grateful to Cathy Johnston for her generous assistance and taking the time to answer my questions on microalgae culturing.

I would like to thank the Department of Chemical Engineering and Chemical Engineering Laboratories of Curtin University for all their kind administrative assistance and the carrying out my laboratory work. I am extremely grateful to Tammy Atkins, Karen Haynes, Andrew Chan, Ross Haynes, Joe Justin, Araya Abera, Xiao Hua, Ann Carroll, Surudee Bunpitakgate and Lemlem Selemon for their support.

I would like to acknowledge my gratitude to all my family and friends for helping me survive all the stress and not letting me give up. This thesis would not have been possible without the support and love of my family: my spouse, Mehran; my children, Hiran and Helia; and my parents, Aliakbar and Safieh.

Dedication

To my beloved spouse, Mehran,

Thanks for your great support and encouragement

To our children, Hiran and Helia

I am really grateful to both of you

List of Publications

Book chapter:

- Znad, H., Naderi, G., Ang, H. M., & Tade, M. O., (2012). CO₂ Biomitigation and Biofuel Production Using Microalgae: Photobioreactors Developments and Future Directions. *Advances in Chemical Engineering*, Book Chapter, ed. Nawaz, Z. and Naveed, S., 229-244. Croatia: InTech.
- Znad, H., Naderi, G., Ang, H. M., & Tade, M. O., (2016). Photosynthesis efficiency and light intensity in a microalgae photobioreactor. (to be submitted soon)

Journal paper:

- Naderi, G., Tade, M. O. and Znad, H. (2015) Modified Photobioreactor for Biofixation of Carbon Dioxide by *Chlorella vulgaris* at Different Light Intensities. *Chemical engineering & technology*, 38(8), pp. 1371-1379.
- Naderi, G., Tade, M. O. and Znad, H. (2017) Investigating and modelling of light intensity distribution inside algal photobioreactor. *Chemical Engineering & Processing: Process Intensification*, <https://doi.org/10.1016/j.cep.2017.04.014>.
- Naderi, G., Tade, M. O. and Znad, H. (2016) Enhancement of CO₂ Biofixation Rate and CO₂ Utilisation Efficiency in Algal Photobioreactor (to be submitted to Bioresource Technology).

Conference paper:

- Naderi, G., Tade, M. O., & Znad, H., (28 Sep-01 Oct 2014) Biofixation of Carbon Dioxide by *Chloralla vulgaris* at Different Light Intensities. Poster presentation, *Chemeca Conference*, Perth, Australia.
- Naderi, G., Tade, M. O., & Znad, H., (19-23 Sep 2016) Understanding and developing a novel mathematical model for light distribution inside the microalgae culture, Oral presentation, *XXII International Conference on Chemical Reactors (CHEMREACTOR-22)*, London, UK.

Table of Contents

	Page
Abstract.....	i
Acknowledgements.....	iii
List of Publications	v
Table of Contents	vi
List of Figures	xi
List of Tables.....	xvi
Nomenclature.....	xvii
1 Thesis Overview.....	1
1.1 Background	1
1.2 Research Objectives.....	2
1.3 Research Significance.....	3
1.4 Thesis Structure	3
2 Background and Literature Review.....	6
2.1 Introduction.....	6
2.2 CO ₂ Emission and Environmental Impacts.....	6
2.3 CO ₂ Mitigation Approaches	7
2.4 Biochemistry of Photosynthesis	8
2.5 Cultivation Methods and Systems.....	10
2.5.1 Open System.....	10
2.5.2 Closed Systems (Photobioreactors).....	10
2.5.2.1 Vertical Tubular PBRs.....	11
2.5.2.2 Horizontal Tubular PBRs	11
2.5.2.3 Flat Plate PBRs	12
2.5.2.4 Stirred Tank PBRs	12

2.5.3	Microalgae Photobioreactors.....	13
2.6	Cultivation Factors	15
2.6.1	Temperature.....	15
2.6.2	PH.....	15
2.6.3	CO ₂ Concentration.....	16
2.6.4	Aeration	17
2.6.5	Agitation.....	18
2.6.6	Source of CO ₂	19
2.6.7	Algae Species	20
2.6.8	Quality of Light	22
2.6.8.1	Light Intensity	23
2.6.8.2	Light period.....	24
2.6.8.3	Light Source	25
2.7	Light Distribution inside the Culture	27
2.7.1	Beer-Lambert Model	27
2.7.2	Average Light Intensity	32
2.7.2.1	One-Dimensional Model for Parallelepiped	33
2.7.2.2	Bi-Dimensional Model for Cylindrical Vessel	34
2.7.2.3	Three-Dimensional Model.....	37
2.7.3	Radiative Transfer Model.....	39
2.8	Photosynthesis Efficiency.....	42
2.9	Absorbed Photon Flux	44
2.10	Optical Properties.....	46
2.10.1	Attenuation Coefficient.....	46
2.11	Growth Kinetic Models.....	49
2.12	Response Surface Methodology for Optimisation	52
2.13	Summary	55

3	Experimental Methods and Design	57
3.1	Introduction	57
3.2	Microalgae and Medium	58
3.3	Subculturing	59
3.4	Cultivation System	61
3.4.1	Bioreactor	61
3.4.2	Light Enclosure	65
3.4.3	Cultivation procedure	66
3.4.4	Calibration and sterilisation	68
3.5	Analytical Procedures	69
3.5.1	Culture Sampling	69
3.5.2	Optical Density Measurement	69
3.5.3	Biomass Dry Weight Method	71
3.5.4	Calibration Equation for Biomass Concentration	73
3.5.5	Light Intensity Measurement	74
3.5.6	Elemental Analysis of Microalgae	76
3.5.7	Calculation of Microalgae Growth Rate, Biomass Productivity and CO ₂ Biofixation	77
3.6	Light Distribution Measurement	79
3.7	Experimental Design for Optimisation by RSM	80
4	Influence of Light Intensity on Growth and CO₂ Biofixation by <i>C. vulgaris</i>	82
4.1	Introduction	82
4.2	Materials and Methods	83
4.3	Results and Discussion	84
4.3.1	Carbon content and elemental analysing	84
4.3.2	Effect of light intensity on <i>C. vulgaris</i> growth	84
4.3.3	Effect of light intensity on specific growth rate	86

4.3.4	Effect of biomass growth on PH at different light intensities	87
4.3.5	Effect of light intensity and biomass growth on DO.....	90
4.3.6	Interaction between light intensity and biomass growth.....	91
4.3.7	Specific growth rate, productivity and CO ₂ biofixation at various light intensities.....	92
4.3.8	Experimental results at two different light intensities	95
4.4	Summary	100
5	Enhancement of CO₂ Biofixation Rate and CO₂ Utilisation Efficiency in an Algal PBR	102
5.1	Introduction.....	102
5.2	Materials and Methods	105
5.3	Results and Discussion	108
5.3.1	Experimental results	108
5.3.1.1	Influence of light intensity	109
5.3.1.2	Influence of light period.....	110
5.3.1.3	Influence of CO ₂ concentration.....	112
5.3.2	RSM results.....	114
5.3.3	Statistical analysis.....	115
5.3.4	Validation of the model	116
5.3.5	Individual influence of parameters on CO ₂ biofixation	117
5.3.6	Synergistic effect of parameters on CO ₂ biofixation.....	121
5.3.7	Maximising CO ₂ biofixation	122
5.3.8	Maximising CO ₂ utilisation efficiency	123
5.3.9	Verification of optimisation results.....	126
5.3.10	Regression Analysis and Statistically Significant Terms.....	126
5.3.11	Scatter plots	128
5.3.12	Residual and interaction plots	129
5.4	Summary	131

6 Investigating and Modelling of Light Intensity Distribution inside the Photobioreactor	132
6.1 Introduction.....	132
6.2 Materials and Methods	134
6.3 Results and Discussion	135
6.3.1 Light distribution at constant incident irradiance in a rectangular vessel	135
6.3.2 Light distribution at different incident irradiance in rectangular vessel.....	137
6.3.2.1 Effect of incident light intensity	138
6.3.2.2 Effect of biomass concentration	140
6.3.2.3 Effect of distance.....	142
6.3.3 Light distribution in cylindrical vessels	143
6.3.3.1 Single direction illumination	143
6.3.3.2 Even illumination	145
6.3.4 Light distribution modelling	147
6.3.4.1 Model validation	149
6.3.4.2 Average light intensity.....	150
6.3.4.3 Comparison of improved model with Beer-Lambert model.....	154
6.3.5 Kinetic modelling	155
6.3.5.1 Molina-Grima model.....	155
6.3.5.2 Muller-Feuga model	157
6.3.5.3 Comparing results from different kinetic models	158
6.3.6 Summary	159
7 Conclusions and Recommendations.....	160
7.1 Introduction.....	160
7.1.1 Conclusions.....	160
7.1.2 Recommendations for future research.....	162
8 References	166

List of Figures

Figure 1-1 Thesis structure	5
Figure 2-1 Schematic diagram of photosynthesis mechanism.....	9
Figure 2-2 Diagram of Beer-Lambert absorption of a light beam as it travels through a cuvette	28
Figure 2-3 Unidirectional Collimated light flux in a parallelepiped vessel.....	29
Figure 2-4 Cylindrical vessel illuminated by unidirectional parallel flux	29
Figure 2-5 Cylindrical vessel evenly illuminated by unidirectional parallel flux from different sides.....	30
Figure 2-6 Schematic representation of one-half of a cross section through a cylindrical vessel.....	30
Figure 2-7 Schematic of three-dimensional light distribution model	37
Figure 2-8 Radiation Balance.....	40
Figure 2-9 Radiation direction and solid angle.....	41
Figure 2-10 Culture absorbance with different pigment composition as a function of biomass concentration.....	47
Figure 2-11 Absorption coefficient as a function of total pigment mass fraction	48
Figure 2-12 Central composite design for three variables.....	53
Figure 3-1 Lab work diagram	58
Figure 3-2 a) Tissue-culture flask from CSIRO, and b) microscopic photograph of <i>Chlorella vulgaris</i>	59
Figure 3-3 a) Refrigerated incubator, and b) shaker.....	60
Figure 3-4 Schematic diagram of subculturing procedure.....	61
Figure 3-5 a) Bioreactor. b) Control cabinet.....	62
Figure 3-6 a) DO probe and b) pH probe	63
Figure 3-7 a) CO ₂ analyser and b) CO ₂ analyser connected to experimental setup.....	64
Figure 3-8 a) Experimental set up for the photobioreactor and b) Photobioreactor in the light enclosure.	65
Figure 3-9 Light enclosure.....	66
Figure 3-10 Autoclave	67
Figure 3-11 Diagram of cultivation procedure	68
Figure 3-12 UV-Vis spectrophotometer	70

Figure 3-13 Absorbance spectra for two samples of <i>C. vulgaris</i> culture	71
Figure 3-14 Millipore unit and vacuum pump for biomass filtration.....	72
Figure 3-15 Optical density calibration line	73
Figure 3-16 Quantum sensor (LI-192SA).....	74
Figure 3-17 Spherical micro quantum sensor (US-SQS/L)	75
Figure 3-18 Light meter (LI-250).....	76
Figure 3-19 Elemental analyser	77
Figure 3-20 Light distribution experimental setup with rectangular vessel.....	79
Figure 3-21 Light distribution experimental setup with cylindrical vessel	80
Figure 4-1 Growth curve of microalgae <i>C. vulgaris</i> at different light intensities in 17 days	85
Figure 4-2 Daily specific growth rate at different incident light intensities of 30, 50, 100, 185 and 300 $\mu\text{mol m}^{-2} \text{s}^{-1}$	86
Figure 4-3 pH evolution for experiments in different light intensities of 30, 50, 100, 185 and 300 $\mu\text{mol m}^{-2} \text{s}^{-1}$ over cultivation time	87
Figure 4-4 Effect of biomass growth on pH in experiment with 185 $\mu\text{mol m}^{-2} \text{s}^{-1}$ light intensity.....	89
Figure 4-5 Biomass concentration at day 6 and day 17 and pH when culture was illuminated by various light intensities of 30, 50, 100, 185 and 300 $\mu\text{mol m}^{-2} \text{s}^{-1}$	89
Figure 4-6 Biomass concentration and DO evolution over cultivation time, at light intensities of a) 50, b) 100 and c) 185 $\mu\text{mol m}^{-2} \text{s}^{-1}$	91
Figure 4-7 Maximum specific growth rate, productivity and CO_2 biofixation rate vs light intensity.....	92
Figure 4-8 Effect of light intensity on specific growth rate, productivity and CO_2 biofixation rate.....	93
Figure 4-9 a) Biomass concentration , b) specific growth rate and c) productivity vs cultivation time for two light intensities of 120 and 280 $\mu\text{mol m}^{-2} \text{s}^{-1}$	96
Figure 4-10 Biomass concentration, daily specific growth rate and daily production rate vs time at two different incident light intensities: a) 120 $\mu\text{mol m}^{-2} \text{s}^{-1}$ & b) 280 $\mu\text{mol m}^{-2} \text{s}^{-1}$	98
Figure 4-11 Biomass concentration and light intensity at centre of the bioreactor vs cultivation time at two different incident light intensities: a) 120 $\mu\text{mol m}^{-2} \text{s}^{-1}$ b) 280 $\mu\text{mol m}^{-2} \text{s}^{-1}$	100
Figure 5-1 Biomass concentration vs cultivation time for incident light intensities of 65.6, 200 & 334.4 $\mu\text{mol m}^{-2} \text{s}^{-1}$ with light period of 16 h and CO_2 concentration of 8 %.....	110

Figure 5-2 Maximum specific growth rate, CO ₂ biofixation rate and CO ₂ utilisation efficiency under different light intensities	110
Figure 5-3 Biomass concentration vs cultivation time for light periods of 9.3, 16 and 22.7 h, with light intensity of 200 μmol m ⁻² s ⁻¹ and CO ₂ concentration of 8 %.....	111
Figure 5-4 Maximum specific growth rate, CO ₂ biofixation rate and CO ₂ utilisation efficiency at different light periods.....	112
Figure 5-5 Biomass concentration vs cultivation time for CO ₂ concentrations of 1.3, 8.0 and 14.7 % with light intensity of 200 μmol m ⁻² s ⁻¹ and light period of 16 h	113
Figure 5-6 Maximum specific growth rate, CO ₂ biofixation rate and CO ₂ utilisation efficiency at different CO ₂ concentrations.....	114
Figure 5-7 Correlation of modelled and observed CO ₂ biofixation rates.....	117
Figure 5-8 Three dimensional plots for CO ₂ biofixation rate vs a) light intensity and light period, b) CO ₂ concentration and light intensity, and c) light period and CO ₂ concentration. In each plot the third parameter was kept constant at central point...	119
Figure 5-9 Contour plots of CO ₂ biofixation rate for two of the three influencing factors. The third factor was kept constant at central value.....	120
Figure 5-10 CO ₂ biofixation rate optimisation results.....	122
Figure 5-11 Three dimensional plots of CO ₂ utilisation efficiency vs two of the three influencing factors (light intensity, light period, CO ₂ concentration)	124
Figure 5-12 Contour plots of CO ₂ utilisation according to a) light intensity vs light period, b) light intensity vs CO ₂ concentration, and c) light period vs CO ₂ concentration	125
Figure 5-13 Pareto charts of ANOVA and regression.....	128
Figure 5-14 Scatter plots for CO ₂ biofixation vs a) light intensity, b) light period and c) CO ₂ percentage.....	129
Figure 5-15 Residual plot vs run order	130
Figure 5-16 Interaction plot	130
Figure 6-1 Local light intensity vs distance from the vessel surface and biomass concentration at an incident light intensity of 120 μmol m ⁻² s ⁻¹ when was measured in 1 cm intervals.....	136
Figure 6-2 Local light intensity vs distance from the vessel surface and biomass concentration at an incident light intensity of 190 μmol m ⁻² s ⁻¹ when was measured in 1 cm intervals.....	137
Figure 6-3 Local light intensity vs distance from the vessel surface for various incident light intensities (I ₀) at five different biomass concentrations (C _b).....	139

Figure 6-4 Local light intensity vs distance from the vessel surface for various biomass concentrations (C_b) at different incident light intensities (I_0)	141
Figure 6-5 Transmittance (I/I_0) vs biomass concentration at different distances (p) from the illuminated surface.....	142
Figure 6-6 Transmittance (I/I_0) vs distance at different biomass concentrations (C_b).....	143
Figure 6-7 Light distribution in a single-direction illuminated cylindrical vessel at various incident intensities (I_0) and biomass concentrations (C_b).....	144
Figure 6-8 Light distribution two different geometries (rectangular and cylindrical) at biomass concentrations of 0.09 and 0.9 g L ⁻¹	145
Figure 6-9 Light distribution in evenly illuminated cylindrical vessel at different biomass concentrations.....	146
Figure 6-10 Light distribution in a cylindrical vessel illuminated evenly or from a single direction, at two biomass concentrations (C_b).....	147
Figure 6-11 Transmittance (I/I_0) versus $K_a \cdot C_b \cdot p$ at different distances from the illuminated surface.....	148
Figure 6-12 Surface fitting of the light distribution model (Equation 6-1) to experimental data of light intensity, light path and biomass concentration (blue dots).....	150
Figure 6-13 Experimental and modelled results for light intensity vs light path at biomass concentrations (C_b) of 0.09, 0.18, 0.47, 0.75 and 1.34 g L ⁻¹	151
Figure 6-14 Average light intensity vs biomass concentration at an incident light intensity of $I_0 = 120 \mu\text{mol m}^{-2} \text{s}^{-1}$	153
Figure 6-15 Average light intensity vs time for various incident light intensities.....	153
Figure 6-16 Growth rate vs average light intensity	154
Figure 6-17 Light distribution in a rectangular vessel with single-sided illumination at different incident light intensities and biomass concentrations, dots represent experimental data, while dash and solid lines are show the predicted results using the Beer-Lambert model and the new model, respectively.....	155
Figure 6-18 Molina-Grima hyperbolic model of specific growth rate (d^{-1}) vs average light intensity ($\mu\text{mol m}^{-2} \text{s}^{-1}$), compared with experimental observations.....	156
Figure 6-19 Muller-Feuga model of specific growth rate (d^{-1}) vs average light intensity ($\mu\text{mol m}^{-2} \text{s}^{-1}$), compared with experimental data	157
Figure 6-20 Biomass concentration vs time predicted by Grima and Muller models and compared with experimental data.	158

Figure 6-21 Growth rate vs time predicted by Grima and Muller models and compared with experimental data.....158

List of Tables

Table 2-1 Comparison of different cultivation systems	12
Table 2-2 Comparison of the three most popular algae culture systems (Shen et al., 2009).....	13
Table 2-3 Different microalgae species and their CO ₂ biofixation rate.....	21
Table 2-4 High temperature and CO ₂ concentration tolerant microalgae species.....	22
Table 2-5 Comparison of cell growth rate of microalgae strains reported in literatures	26
Table 2-6 Static kinetic models for light-dependent specific growth rate	52
Table 3-1 Elemental analysis of <i>Chlorella vulgaris</i>	77
Table 4-1 Light enclosure set-up.....	83
Table 5-1 CO ₂ biofixation rate for various microalgae species under various conditions	104
Table 5-2 Independent variable values for different levels of experimental design.....	105
Table 5-3 Experimental runs, actual and coded levels of variables	107
Table 5-4 Model coefficients for both coded and actual values of parameters.....	114
Table 5-5 Experimental conditions and observed and predicted results.....	115
Table 5-6 ANOVA results	116
Table 5-7 Regression table	127
Table 5-8 Significant terms.....	127

Nomenclature

Symbols

At	attenuation, <i>unit less</i>
At_{max}	model parameter, <i>unit less</i>
α	light beam angle in evenly illuminated cylindrical vessel,
C_b	biomass concentration, $g L^{-1}$ or $kg m^{-3}$
E_a	absorption mass coefficient, $m^2 kg^{-1}$
E_s	scattering mass coefficient, $m^2 kg^{-1}$
F	mean radiant energy flux, $\mu mol m^{-2} s^{-1}$
F_T	total absorbed photon flux, $\mu mol s^{-1}$
F_{Vol}	absorbed photon flux in unit volume, $\mu mol m^{-3} s^{-1}$
F_λ	spectral radiant energy flux, $\mu mol m^{-3} s^{-1}$
f	void fraction, <i>dimensionless</i>
G	total local incident radiation intensity, $\mu mol m^{-2} s^{-1}$
G_λ	spectral local incident radiation intensity, $\mu mol m^{-3} s^{-1}$
H	height of the vessel, m
I_\circ	incident light intensity, $\mu mol m^{-2} s^{-1}$
I	light intensity, $\mu mol m^{-2} s^{-1}$
I_{av}	average light intensity, $\mu mol m^{-2} s^{-1}$
I_{pi}	local light intensity in the element, $\mu mol m^{-2} s^{-1}$
I_p	local light intensity, $\mu mol m^{-2} s^{-1}$
I_s	saturation light intensity, $\mu mol m^{-2} s^{-1}$
I_λ	spectral light intensity, $\mu mol m^{-3} s^{-1}$
K_a	absorption coefficient, $m^2 kg^{-1}$
K_{at}	model parameter, $kg m^3$
K'_a	absorption coefficient of hyperbolic expression, $m^2 kg^{-1}$

L_0	distance between the light source and surface of the vessel, m
L	length and/or width of the vessel, m
p	light path, m
P_b	biomass productivity, $g DW L^{-1} d^{-1}$ or $g DW m^{-3} d^{-1}$
R	radius, m
r	position vector, <i>dimensionless</i>
S	crossed surface, m^2
S	substrate concentration, $kg m^{-3}$
s	vertical distance from surface of the cylinder, m
\hat{s}	unit direction vector, <i>dimensionless</i>
t	time, d
V_i	volume of the element, m^3
V_T	total volume, m^3
x	distance from the illuminated surface, m
x_r	vertical distance from central line of the cylinder, m

Greek symbols

ε_c	extinction coefficient, $m^2 kg^{-1}$
λ	wavelength, nm
μ	specific growth rate, d^{-1}
φ	angle with central line of cylindrical vessel,
Ω	solid angle, <i>dimensionless</i>
θ	angle with r axis, Rad
ψ	azimuthal angle in spherical coordinate, Rad
Ψ	bioenergetics yield,
μ_{max}	maximum specific growth rate, d^{-1}
μ_s	saturation specific growth rate, d^{-1}

Subscripts

<i>b</i>	biomass
<i>eff</i>	effective
λ	spectral
<i>X</i>	cell particles
<i>B</i>	gas bubbles

Abbreviations

RSM	Response Surface Methodology
CCD	Central Composite Design
BBD	Box-Behnken Design
GHG	Greenhouse gas
CDIAC	Carbon Dioxide Information Analysis Centre
CCS	Carbon Capture and Storage
PBR	Photobioreactor
vvm	gas volume flow per unit of liquid volume per minute
rpm	revolutions per minute
ppm	parts per million
PAR	Photosynthetic Absorbed Radiation
HID	High Intensity Discharge
LED	Light Emitting Diodes
RTE	Radiative Transfer Equation
DCW	Dry Cell Weight

1

Thesis Overview

1.1 Background

Currently, the world is facing crises of environmental degradation and worldwide health due to elevated concentrations of greenhouse gases in the atmosphere. It is estimated that carbon dioxide (CO₂) accounts for up to 68 % of the greenhouse gases responsible for global climate change (Ho et al., 2011). These environmental impacts, and diminishing reserves of fossil fuels, have motivated many researchers to investigate and commercialise microalgae cultivation for the purposes of CO₂ biofixation and biofuel production.

Biological CO₂ mitigation, which is the conversion of CO₂ into organic matter, has received much attention as an alternative sustainable strategy. Biofixation of CO₂ produces biomass which can be used as a source of energy and feedstock for biofuel production, and also produces other valuable products (Wang et al., 2008). Biological CO₂ mitigation can be achieved through terrestrial plants and an enormous number of photosynthetic microorganisms. Microalgae are unicellular, photosynthetic microorganisms which require minimal nutrients and grow extremely rapidly in comparison to plants (Ho et al., 2011, Wang et al., 2008). Biofixation of CO₂ via microalgae culturing is one of the most promising ways to mitigate CO₂ due to the possibilities of producing high valued co-products such as biofuel and supplementary foods, or combining this technique with wastewater treatment.

Many factors such as temperature, pH, light intensity, aeration rate and agitation affect microalgae growth. However, light intensity is one of the most significant and key factors because it can limit or inhibit microalgae growth. Microalgae need a day/night light regime with sufficient photon flux during the day for productive photosynthesis. Nevertheless, due to shading effects, including photon-absorption by cells and scattering by particles, there are light gradients within

microalgae cultures, especially in dense ones. This is one of the remarkable obstacles to high density biomass production facing the development of photobioreactors (PBRs).

There are many strains of microalgae suitable for CO₂ mitigation; specifically, the strain *Chlorella vulgaris* has shown great promise. In this study, light distribution inside cultures, as well as the influences of light intensity, light period and CO₂ concentration on the biomass production rate and CO₂ biofixation rate of *C. vulgaris* in a batch photobioreactor were investigated. Optimisation and modelling were also addressed in this work.

1.2 Research Objectives

To address environmental issues related to greenhouse gas emissions and renewable energy production, the major objective of this PhD thesis was to enhance photobioreactor performance for microalgal CO₂ biofixation and biomass production. To achieve this aim, the present study will investigate the most significant issues in a stirred tank reactor using synthetic gas, as listed below:

- Investigate and discuss the influence of light intensity on the performance of photobioreactors. Conduct preliminary experiments to determine the optimum light intensity as well as photolimitation and photoinhibition areas for the selected algal strain.
- Explore the influences of irradiance, light period and % CO₂ in inlet gas for achieving rapid growth and high CO₂ uptake.
- Maximise CO₂ biofixation rate and CO₂ utilisation efficiency by optimising biomass growth conditions and growth rate of *Chlorella vulgaris* by varying light intensity, light period and CO₂ concentration.
- Investigate light distributions inside cultures in photobioreactors with different geometries and configurations.
- Investigate growth kinetics and the influence of light distribution on photobioreactor performance.
- Propose a new, modified light distribution equation to estimate local light intensity and use it to simulate photobioreactor performance.

1.3 Research Significance

- Light intensity, light period and CO₂ concentration are critical factors affecting the performance of photobioreactors for CO₂ biofixation and biomass production. Most of the available studies have investigated these factors individually, and only in relation to biomass production. Therefore, the merit of this study is that all these factors will be investigated and optimised simultaneously.
- Previous studies have used a photobioreactor with relatively limited ranges of CO₂ concentration and light irradiance. To the best of our knowledge, there has been no detailed study simultaneously varying irradiance and the initial CO₂ mole fraction in the gas phase to quantitatively assess CO₂ fixation and biomass production. Moreover, none of the available studies evaluated the relationship between algal growth and the potential for direct removal of CO₂ from a gas stream. The distribution of light throughout the photobioreactor is expected to affect CO₂ uptake rates. This needs to be further investigated to achieve optimal growth rates.
- Another innovative component of this research is the integration of models (models that relate biomass growth to light, considering kinetic and average light intensity) for analysis and optimisation. The formulation of an integrated model will significantly improve the understanding of photobioreactor function.

Overall, this study aims to contribute significantly to the understanding of the critical factors, and their influences, on the performance of photobioreactors. The outcomes will provide recommendations for the development of an efficient microalgal photobioreactor.

1.4 Thesis Structure

This thesis consists of 8 chapters that are linked systematically to achieve the targeted objectives. The following section briefly describes these chapters, and Figure 1-1 shows the thesis structure:

Chapter One Provides a general overview of the present research work which includes a brief background of the thesis topic, the key factors affecting photobioreactor (PBR) performance for efficient CO₂ biofixation and biomass production, and the thesis's main objectives, significance and structure.

Chapter Two Covers existing CO₂ mitigation technologies, microalgal CO₂ biofixation, factors affecting PBR performance and a review of relevant literature. The chapter also focuses on the light distribution and kinetic models and their limitations.

Chapter Three Describes the experimental methods, materials, microalgae cultivation techniques, and analytical equipment used in this study. This chapter also introduces the Response Surface Methodology (RSM) by applying Central Composite Design (CCD) for PBR optimization.

Chapter Four Reports the results and discussion of the experiments investigating the influence of light intensity on PBR performance. Specifically, it focuses on biomass growth, CO₂ biofixation, pH and dissolved oxygen levels in a PBR using *C. vulgaris*.

Chapter Five Demonstrates and explains the influences of the key factors (light intensity, photoperiod, inlet CO₂ concentration) on the CO₂ biofixation rate and utilisation efficiency. Then, these factors are optimised by conducting 17 systematic experiments and employing the CCD of RSM to achieve maximum biomass productivity, CO₂ biofixation and CO₂ utilisation efficiency.

Chapter Six Investigates light distribution inside microalgae cultures. It will reveal how it varies during the cultivation process according to different PBR geometries (rectangular and cylindrical), and under different light intensities and biomass concentrations. Then, it will propose and discuss an improved model for simulating light distribution inside microalgae cultures, and estimation of specific growth rates considering different kinetic models.

Chapter Seven Draws the conclusions from the study and makes some suggestions and recommendations for future research directions.

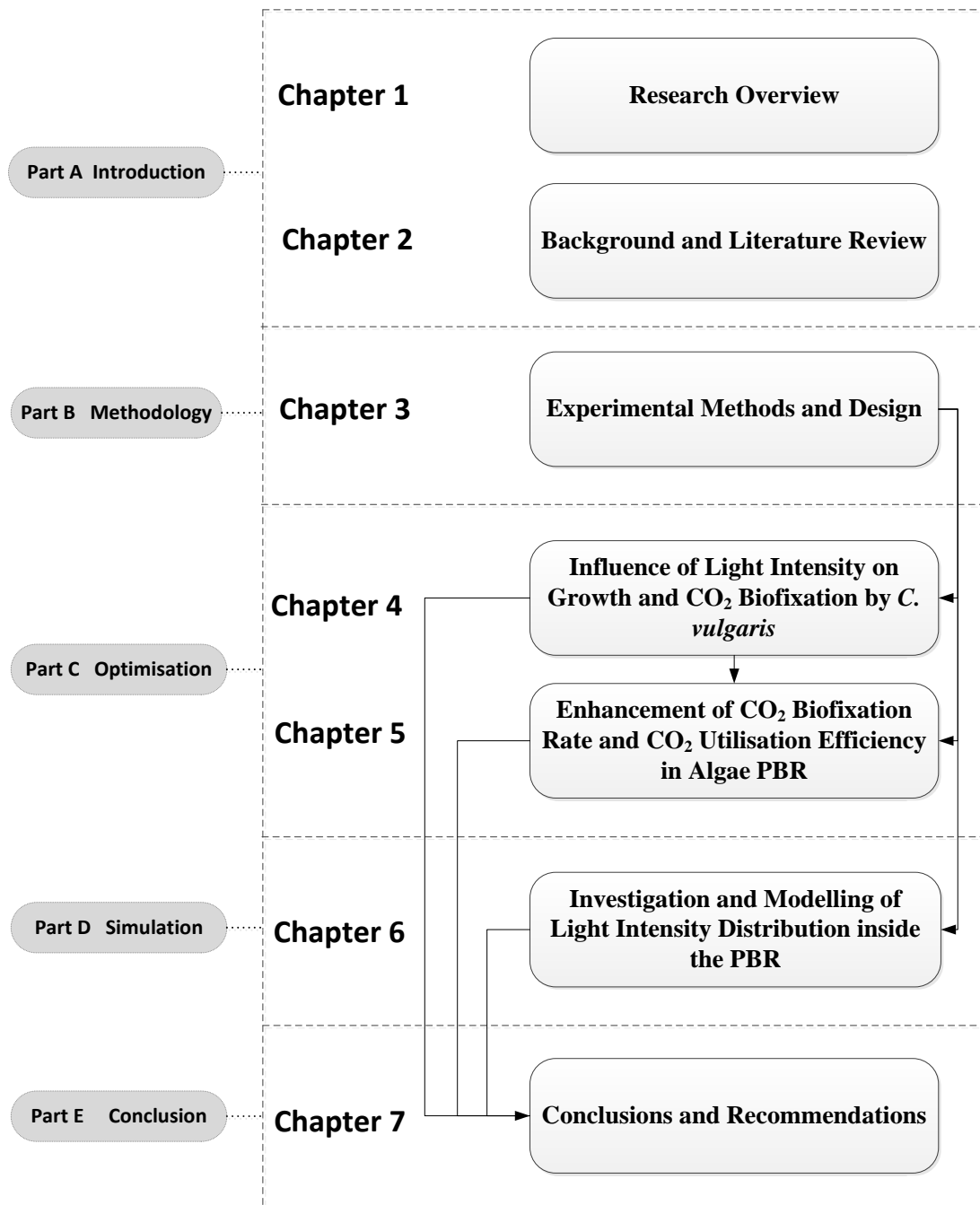


Figure 1-1 Thesis structure

2

Background and Literature Review

2.1 Introduction

Phototrophic CO₂ biofixation using fast-growing microalga species is a promising alternative approach to conventional CO₂ sequestration, as CO₂ is converted to microalgae biomass, which could be utilised to produce commercially valuable products. Compared to current chemical/physical CO₂ removal processes, biomitigation of CO₂ by microalgae can be handled easily and is more environmentally friendly and sustainable. This fixation method is a promising way that can contribute to the atmospheric CO₂ mitigation that causes global warming. In theory microalgae can use up to 9 % of the incoming solar energy to produce 280 tons of dry biomass per hectare per year while consuming roughly 513 tons of CO₂ (Bilanovic et al., 2009). Current studies to identify microalgae species containing high levels of fatty acids, with high ability for CO₂ biofixation and the development of improved biomass production techniques are being performed extensively. Despite all the advantages, relatively high operation cost bioreactors still remains a limitation and much research is required. In fact, the development of efficient mass production of microalgae is critical for commercialisation of this technique.

2.2 CO₂ Emission and Environmental Impacts

The world has been faced with two main crises of environmental degradation and fossil fuels depletion. More than 80 % of total globally produced energy is generated via fossil fuels combustion (Sayre, 2010), which is the major source of CO₂ emission. In fact, approximately one-third of carbon dioxide in the atmosphere originates from fossil fuels combustion in power plants worldwide (Chai et al., 2012). Carbon dioxide emissions to the atmosphere lead to the elevated greenhouse gas (GHG)

levels and subsequently cause other problems including global warming and acid rain. It is believed that carbon dioxide accounts for up to 68 % of total GHGs that are responsible for global climate change (Ho et al., 2011). According to the report published by Carbon Dioxide Information Analysis Centre (CDIAC), CO₂ emission has shown an enormous increase from 3 metric tons to 8230 metric tons in the years between 1971 and 2006 (Kumar et al., 2011). As per measurements in Mauna Loa observatory in Hawaii, US, CO₂ emissions reached 390 ppmv in 2010 while it was 280 ppmv in 1958 (Kumar et al., 2011).

Due to elevated CO₂ level in the atmosphere and so ever-increasing problems about global warming, the United Nations promoted Kyoto Protocol (1997) with the objective of decreasing greenhouse gases by 5.2 % based on emission in 1990 (Gutierrez-Sanchez and Nafidi, 2008). The Australian obligation under the Kyoto protocol requires a reduction of greenhouse gas emissions to 108 % of the 1990 levels by 2008–2012 (Harrington and Foster, 1999) and 5 % reduction base on 1990 levels by 2013-2020 (Newell et al., 2013). Moreover, a carbon credit system was proposed by the United Nations in 2010 (Stewart and Hessami, 2005b). Not only; the world's reserves of fossil fuels are limited, but also they cause severe environmental impacts. Therefore, researchers have been interested in non-petroleum eco-friendly fuels and CO₂ sequestration approaches (Ho et al., 2011). Researches have been accomplished toward reducing CO₂ emissions and still are seeking new more effective strategies for CO₂ sequestration.

2.3 CO₂ Mitigation Approaches

Carbon dioxide fixation is receiving increasing attention due to the impact associated with CO₂ elevation in the atmosphere. CO₂ mitigation strategies can be classified into three groups: (i) chemical reaction-based approaches for instant carbonation/de-carbonation reactions in which gaseous carbon dioxide reacts with solid metal oxide to produce metal carbonate (Wang et al., 2008); (ii) physical approach of carbon separation and direct injection to underground or into the ocean which is called carbon capture and storage (CCS) (Ho et al., 2011), but recently due to ecological problems associated with CO₂ injection to the oceans, it is no longer considered feasible; and (iii) biological CO₂ mitigation, which is biological conversion of CO₂

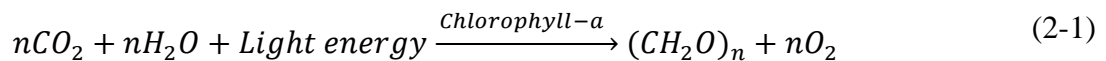
into organic matters. While chemical reaction-based and direct injection strategies are relatively costly and energy-consuming, biological CO₂ fixation has recently received much attention as an alternative and sustainable strategy (Kumar et al., 2011). On the other hand, CO₂ biofixation leads to biomass production which can be used as a clean renewable source of energy and feedstock for biofuel production as well as some other valuable products (Wang et al., 2008). However, in spite of sustainability and being cost effective, the low efficiency of CO₂ biofixation needs to be enhanced before commercialisation.

Biological CO₂ mitigation can be achieved through both terrestrial plants and an enormous number of photosynthetic microalgae microorganisms. Nevertheless, while the potential of CO₂ absorption by terrestrial plants is only 3-6 % of CO₂ discharges from fossil fuels, microalgae have the ability to absorb CO₂ with the efficiency of 10 to 50 times more (Ho et al., 2011, Wang et al., 2008). 1.83 kg of CO₂ is absorbed by 1 kg of dry microalgae and fixing one mole of CO₂ via photosynthesis results approximately 114 kilocalories of stored energy in the biomass (Miyamoto, 1997, Chisti, 2007). Microalgae are unicellular microorganisms that are living in freshwater or saline environments and photosynthetically convert light energy to algal biomass. Since microalga has a simple structure and rapid growth rate (Salih, 2011), it has the potential to produce considerably greater amounts of biomass than any kind of terrestrial biomass, so they have more photosynthesis efficiency which leads to more CO₂ mitigation. Meanwhile, producing biomass from terrestrial plants accompany with impact of land use and human food, indeed, terrestrial plants need obvious area of agricultural lands to be grown in (Demirbas and Demirbas, 2010). In addition to CO₂ removal and biomass production through microalgae cultivation, it also can be combined with wastewater treatment.

2.4 Biochemistry of Photosynthesis

Photosynthesis is a light-dependent carbon-fixation reaction which encompasses two major groups of reactions. Those in the first group are called light dependent reactions, including absorption and transferring of photon energy and generating chemical potential. The second group, light independent reactions, involves a set of

reactions to use this chemical potential to fix carbon dioxide (Barsanti and Gualtieri, 2014). Photoautotrophic microorganisms like eukaryotic green microalgae, possess chlorophyll and other pigments to capture sunlight energy and use photosynthetic systems to carry out plant-like oxygenic photosynthesis. In a multistep process of photosynthesis, plants and algae convert CO_2 into sugar using light and water as energy and electron source, respectively. The chemical equation for photosynthesis is given by (Kumar et al., 2011):



CO_2 is one of the nutrient that can be supplied from atmospheric air or power plant flue gas, and also light energy as a substrate can be furnished from sunlight or artificial light, chlorophyll-a is a catalytic agent, $(\text{CH}_2\text{O})_n$ represents biomass or organic matter. The first step uses the energy of sunlight to oxidise water to O_2 , and, ultimately, to produce ATP (Adenosine Triphosphate). In the second step (Calvin cycle) the actual fixation of carbon dioxide is carried out. This process consumes ATP and NADPH (Nicotinamide adenine dinucleotide phosphate) to produce sugar (Figure 2-1). The Calvin cycle in plants accounts for the majority of carbon fixation on land. Algae and cyanobacteria account for the majority of carbon fixation in the oceans. The Calvin cycle converts carbon dioxide into sugar, as triose phosphate (TP), which is glyceraldehyde 3-phosphate (GAP) together with dihydroxyacetone phosphate (DHAP) (Barsanti and Gualtieri, 2014, Kumar et al., 2011).

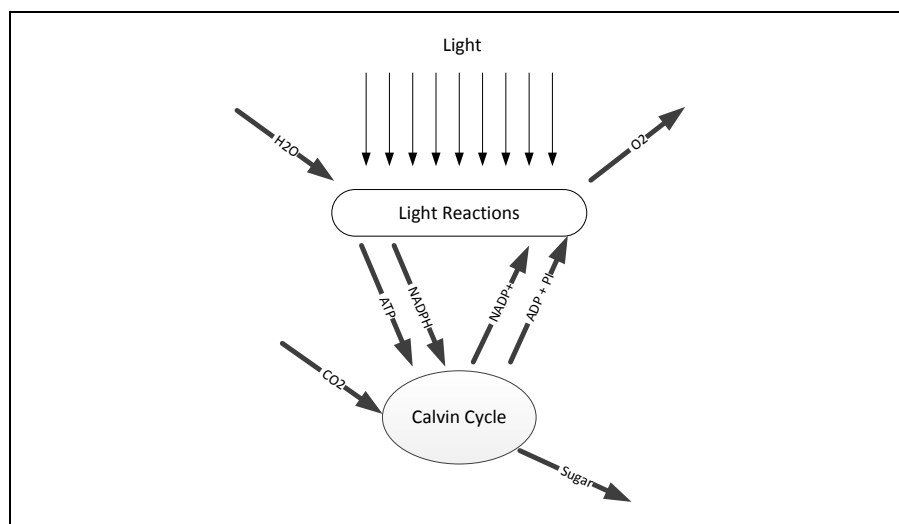


Figure 2-1 Schematic diagram of photosynthesis mechanism

2.5 Cultivation Methods and Systems

The two popular systems to cultivate microalgae are open systems and closed systems; each system might run in batch, continuous or semi-continuous mode. Generally, open systems are raceway ponds containing growth medium exposed to environment and sunlight. Closed systems are those where growth medium is enclosed away from the environment and mostly are engineered photobioreactors (PBRs). Indoor close culture allows control over temperature, illumination, nutrient level, contamination with predators as well as competing algae strains, whereas outdoor open algal systems, though cheaper, make it very difficult to grow specific algal cultures for extended periods.

2.5.1 Open System

Open pond systems, (raceway ponds, circular ponds and unstirred ponds) are the most widely and cost effective systems used for commercial microalgae cultivation (Ho et al., 2011). However, its usage is significantly limited because of several drawbacks such as high evaporative losses, difficulty in control of both temperature and light intensity, poor light utilisation by the cells, high risk of contamination (Carvalho et al., 2006). They are mainly used only for biomass production (Dasgupta et al., 2010) and not for CO₂ removal due to diffusion of CO₂ to the atmosphere. Because of these drawbacks, valuable CO₂ mitigation is not feasible using open systems (Pulz, 2001); therefore, the focus has shifted to closed systems.

2.5.2 Closed Systems (Photobioreactors)

Generally, closed systems, photobioreactors (PBRs), are well-controlled with the additional benefits of high CO₂ biofixation efficiency and biomass productivity, low contamination risk, and large surface area (Grima et al., 1999, Sierra et al., 2008). Nevertheless, the scaling up of PBRs faces some serious limitations regarding light utilisation, mass transfer, growth parameters control, and biomass circulation (Grima et al., 1999).

Considering all the limitations and shortcomings of the pond systems, most researchers, had oriented their research works towards the development of an

unconventional way for micro-algae culture, which should be fully closed and compact with high surface-to-volume ratio and all the growth factors be optimised. High surface-to volume ratio of photobioreactor allow to reach high productivity and biomass concentration in compare with open systems (Borowitzka and Moheimani, 2013).

Generally use of closed PBRs today can be classified into vertical tubular such as bubble column and air lift; horizontal tubular and flat panel photobioreactors, those are designed with non-mechanical agitation and mixing is carried out by gas sparging; or stirred tank which provide mechanical mixing in addition to gas bubbling (Kumar et al., 2011, Jacob-Lopes et al., 2008a, Shen et al., 2009). Obviously each of them has some advantages and disadvantages.

2.5.2.1 Vertical Tubular PBRs

Bubble column reactors are cylindrical vessel, usually with a ratio of height to diameter greater than two, and gas sparger at the bottom. Bubble column PBRs are relatively low cost, easy to operate with low shear stress and energy consumption but have small illumination surface area. Air lift reactor is a vertical vessel with two interconnecting tube; one tube is riser where gas is sparged and another tube with no gas sparging called downcomer. Air lift photobioreactor is one of the best for CO₂ sequestration due to high mass transfer, providing good mixing associated with low hydrodynamic stress, and ease of control (Kumar et al., 2011, Shen et al., 2009). It was shown that using membrane contactor in photobioreactor can significantly enhance the mass transfer rate of CO₂ and O₂ in a bubble column or airlift bioreactor and therefore, greater microalgae growth and CO₂ biofixation can be achieved (Fan et al., 2007a).

2.5.2.2 Horizontal Tubular PBRs

Tubular PBRs are parallel set of tubes with different configuration of straight horizontal, straight vertical, helical, α -shape and inclined. Tubular PBRs have large illumination area and thus fairly high biomass productivity and also relatively cheap, however, hard to control temperature, possibility of photoinhibition and O₂ accumulation, and also large area of land needed (Dasgupta et al., 2010, Shen et al., 2009).

2.5.2.3 Flat Plate PBRs

Flat plate or flat panel reactor is a cuboidal vessel with minimal light path (usually between 1 cm and 30 cm) which can be aligned vertically or inclined. Flat plate PBRs can provide huge illumination surface area and therefore high photosynthesis efficiency and biomass productivity, relatively low O₂ accumulation, also it is easy to scale up, but some problems related to high hydrodynamic stress and hard to control temperature are associated with them (Shen et al., 2009, Pires et al., 2012).

2.5.3 Stirred Tank PBRs

Stirred tank are well mixed PBRs since agitation is provided mechanically by the impeller. Meanwhile, gas is bubbled at the bottom of the vessel to provide carbon source and externally illuminated by fluorescent lamps or optical fibers. Agitation provide uniform distribution of nutrient and light for the cells and prevent sedimentation, however, it can impose high shear stress. In addition, the disadvantage of low light harvesting efficiency associated with them due to low surface area to volume ratio (Kumar et al., 2011).

Advantages and disadvantages of different photobioreactor systems has been summarised in Table 2-1.

Table 2-1 Comparison of different cultivation systems

Cultivation System	Advantages	Disadvantages
Open ponds	Low cost and easy to use	High vapour losses, difficulty of temperature control, high risk of contamination, low productivity
Veridical tubular PBRs	Relatively low cost, easy to operate, low shear stress and energy consumption	Small illumination area
Horizontal tubular PBRs	Large illumination area, high productivity, relatively cheap	Hard to control temperature, possibility of photoinhibition and O ₂ accumulation
Flat plate PBRs	Huge illumination area, high photosynthesis efficiency and biomass productivity, relatively low O ₂ accumulation, easy to scale up	High hydrodynamic stress and hard to control temperature
Stirred tank PBRs	Well mixed and uniform distribution of nutrients and light, low cost	Low surface area to volume ratio, possibility of high shear stress

Table 2-2 compare specifications for the three most popular systems for microalgae cultivation.

Table 2-2 Comparison of the three most popular algae culture systems (Shen et al., 2009)

Parameter	Raceway	Flat Panel PBR	Tubular PBR
Volume (m ³)	1,000	5	5
Volume to surface ratio (m ³ m ⁻²)	0.2	0.07-0.1	0.04-0.08
Gas holdup	0.01	0.05	0.01
Mass transfer coefficient (m s ⁻¹)	0.0005	0.005	0.003
Typical biomass productivity (g m ⁻² d ⁻¹)	15	35	50
Typical biomass concentration (g L ⁻¹)	0.25	1	1.5
Construction cost (\$ m ⁻³)	270	2,700	6,750

2.5.4 Microalgae Photobioreactors

Some results for microalgae productivity and CO₂ fixation rate at various bioreactor designs is discussed here. Overall, vertical tubular-type photobioreactors, such as bubble column and air-lift photobioreactors have often been thought to achieve the most efficient mixing and the best volumetric gas transfer (Chiu et al., 2009).

Jacob-Lopes et al. (2008a), observed CO₂ removal by *Aphanothece microscopica Nageli* in a bubble column photobioreactor under different conditions of temperature (21.5–38.5 °C), CO₂ concentration (3–62 %) and light intensity (0.96–11 klux), maintaining continues illumination. The strain was cultivated in a bubble column with an internal diameter of 7.5 cm, height of 75 cm and nominal working volume of 3.0 L. The carbon fixation rate varied between 3.45 to 45.78 mg L⁻¹ h⁻¹ under tested conditions and among the experimental results the highest biofixation rate was achieved at 35 °C, 9 klux and 15 %. Then through optimisation results it was deduced that under optimum operational conditions of 11 klux, 35 °C and 15 % CO₂ maximum specific growth rates and carbon biofixation rates can be achieved which are 0.04 h⁻¹ and 109.2 mg L⁻¹ h⁻¹, respectively.

Sierra et al. (2008), used a flat panel photobioreactor (0.07 m wide, 1.5 m height and 2.5 m length) for the production of microalgae and compared this bioreactor with bubble columns and tubular photobioreactors. They showed that a power supply of 53 W m⁻³ can provide a mass transfer rate high enough to avoid the undesired dissolved oxygen accumulation in this flat panel photobioreactor. This is

very close to 40 W m^{-3} power supplies that are necessary in bubble columns and much lower than the required power in tubular photobioreactors ($2000\text{-}3000 \text{ W m}^{-3}$). Even at low power supplies the mixing time for this photobioreactor was shorter than 200 s, although it is a little longer than the 60 s measured for bubble columns, but still it is quite faster than the typical values found for tubular photobioreactors (1-10 h). While the low power consumption (53 W m^{-3}) and the high mass transfer capacity (0.007 s^{-1}) are the main advantages of this bioreactor, potential high stress damage associated with aeration is the major disadvantages.

In another study, a marine microalga, *Chlorella* sp. NCTU-2, was used to assess biomass production and CO_2 removal when three types of photobioreactors were designed and compared: (i) a bubble column, (ii) air lift and (iii) air lift with a porous centric-tube column (Chiu et al., 2009). The airlift photobioreactor with the centric tube could provide a regular circulation of the culture so that the air rising from the inner column and cause liquid circulation and then airlift reactor with a porous centric tube could provide more turbulence. The cultivation was performed in 4 L working volume at temperature of $26 \text{ }^\circ\text{C}$ by furnishing continuous light intensity of approximately $300 \mu\text{mol m}^{-2} \text{ s}^{-1}$ at the surface of the photobioreactor provided by cool white fluorescent lamps. The specific growth rates of the batch cultures in the bubble column, air lift and the porous centric-tube air lift photobioreactor were 0.180, 0.226 and 0.252 d^{-1} , respectively.

Chiang et al. (2011), used a bubble column with internal illumination of $250 \mu\text{mol m}^{-2} \text{ s}^{-1}$ by cold cathode fluorescent lamps. A maximum CO_2 biofixation rate of $1.01 \text{ g CO}_2 \text{ L}^{-1} \text{ d}^{-1}$ was measured experimentally. Yoo et al. (2012), investigated the effect of aeration rate, H/D ratio, sparger diameter and slope of the V-shaped bottom on the performance of a V-shaped bottom bubble column. The performance of the photobioreactor was improved at an air flow rate of 0.2 vvm, a 6:1 H/D ratio, a 1.3 cm diameter sparger, and $60 \text{ }^\circ\text{C}$ V-shaped bottom. Fan et al. (2007b), compared performance of a membrane photobioreactors, with a draft tube airlift photobioreactor and a bubble column, when cultivated *Chlorella vulgaris* at $25 \text{ }^\circ\text{C}$, 1 % CO_2 and 10.8 klux. The maximum CO_2 biofixation rate of $0.275 \text{ g L}^{-1} \text{ h}^{-1}$ was obtained in membrane photobioreactor which was 1.95 and 2.15 times higher than in the airlift photobioreactor and bubble column, respectively.

2.6 Cultivation Factors

In addition to the design and configuration of the photobioreactors, there are many factors such as temperature, O₂ and CO₂ concentration, pH, nutrients supply, algae species, turbulence, shear stress, aeration and light illumination that could significantly influenced the photobioreactor performance (Salih, 2011, Wang, 2010). Generally, microalgae can use light from both the sun and artificial sources and grow in a temperature between 18-28 °C, and pH range 7-9 (Wang, 2010).

2.6.1 Temperature

Temperature should be controlled as close as possible to the temperature of the place where the strain was collected, typically, polar strains (<10 °C); temperate (10-25 °C); and tropical (>25 °C) (Barsanti and Gualtieri, 2014). As it is investigated by Jacob et al. (2008a), optimum temperature to grow *Aphanothece microscopica Nägeli* was 35 °C in a bubble column photobioreactor under 15 % CO₂ aeration and 11 klux illumination. An optimum CO₂ biofixation rate was found at 35.5 °C for freshwater cyanobacterium *Synechocystis* sp. under average light intensity of 686 μmol m⁻² s⁻¹ (Martinez et al., 2011). The growth of *Pavlova lutheri* was optimal at 26.17 °C in a 2 L flask under 100 μmol m⁻² s⁻¹ illumination (Ryu et al., 2012). Generally, microalgae grows in temperature range of 20-35 °C (Pires et al., 2012, Dasgupta et al., 2010), however, some high temperature tolerant species have been identified as well; for example, *Cyanidium caldarium* and *Synechococcus elongatus* at 60 °C (Seckbach and Ikan, 1972a, Miyairi, 1995), *Chlorella* sp. at 45 °C (Hanagata et al., 1992b) and cyanobacteria *Chlorogleopsis* sp. at 50 °C (Ono and Cuello, 2007). These strains are beneficial to be used for direct CO₂ sequestration from flue gas emitted from power plants and also for outdoor culturing. (Naderi et al., 2015)

2.6.2 PH

The optimum pH ranges between 7 and 9 for most algal species, and if it exceeds a value of 9.0 might cause to precipitate calcium salts, also has been reported greater pH around 11 (depends on species) has negative effect on the growth (Sacasa Castellanos, 2013). As it has been stated by Widjaja et al. (2009), *Chlorella vulgaris* can survive in a wider range of pH from 5 to above 8. The pH of the broth can be

influenced by dissolved CO₂ and also SO_x in the case of using flue gas as source of carbon. Indeed, pH can drop to 5 when CO₂ concentration elevate in the medium (Kumar et al., 2011), even down to pH 2.6 has been reported (Westerhoff et al., 2010). It has been shown that pH 7.3 of the medium sharply dropped to 5.6 after culture started and then as a result of inorganic carbon consumption due to photosynthesis reaction and cell growth, it slowly increased when *Chlorella vulgaris* was cultured with pure CO₂ and no inhibition was observed (Concas et al., 2013, Jacob-Lopes et al., 2008a). Overall, rise in CO₂ concentration can cause minor change in pH and no negative effect on algae growth, however SO_x can lead to strong change in pH and growth inhibition (Kumar et al., 2011).

pH can be controlled by manipulating CO₂ concentration in inlet gas and since it can affect the microalgae growth it is a key factor to optimise CO₂ biofixation (Concas et al., 2012). Optimum pH was 8.0 when *Chlorococcum* was cultured under pH 5.6, 8.0 and 10 (Chai et al., 2012). Overall, pH increases every day after starting cultivation, however, pH values decrease during dark period in compare with the light period.

2.6.3 CO₂ Concentration

Adjusting CO₂ percentage in the inlet gas or controlling CO₂ concentration in the culture to optimum value is one of the significant approaches to achieve efficient CO₂ removal. Sparging atmospheric air with around 300 ppm CO₂ cannot be efficient for purpose of CO₂ biofixation and leads to very low fixation rate. In contrast, using high CO₂ concentration flue gas can be beneficial for both CO₂ removal efficiency and a low cost CO₂ source. In the case of injecting high CO₂ concentration gas to the bioreactor, preadaptation of the cells to high concentration of CO₂ can be helpful (Yun et al., 1997).

Yun, Lee et al. (1997) investigated effect of CO₂ percentage in the inlet gas on growth of *Chlorella vulgaris* and they found better growth at 5 % CO₂ in compare with 15 %, however in another experiment, result for 15 % CO₂ improved when the strain was adapted to 5 % CO₂ before cultivation. Meanwhile, this strain showed a good adaptability and growth even at 30 % CO₂ when CO₂ increased gradually. Morais and Costa (2007c) cultivated *Chlorella kessleri* and *Scenedesmus obliquus* at different CO₂ concentrations and maximum growth of 0.60 g L⁻¹ and 1.14 g L⁻¹ for

them was achieved at 10 % and 12 %, respectively. Furthermore, *Scenedesmus obliquus* grew well even at 18 % CO₂ and reached to 1.12 g L⁻¹ and still continued to grow without any inhibition. Among the % CO₂ investigated (3-62), 15 % found to be the best when *Aphanothece microscopica Nägeli* was cultivated under different conditions of CO₂ concentration, light intensity and temperature for CO₂ removal (Jacob-Lopes et al., 2008a). Chiu et al. (2009) could achieved 0.61 g L⁻¹ biomass concentration when they cultivated *Chlorella* sp. under 10 % CO₂ in a porous centric-tube photobioreactor in semicontinuous operation mode with harvesting one fourth of broth every 2 days.

Maximum CO₂ fixation rate of 1.01 g CO₂ L⁻¹ d⁻¹ was achieved at 10 % CO₂ when *Anabaena* sp. CH1 was cultivated at 0.4 vvm aeration of 5 %, 10 % and 15 % CO₂ enriched air at room temperature and continuous illumination while CO₂ uptake rate at 15 % CO₂ was very close to 10 % CO₂ with around 33 % higher than 5 % CO₂ (Chiang et al., 2011).

2.6.4 Aeration

Generally, aeration rate directly influence on gas bubble residence time and size, and so on interfacial area and CO₂ mass transfer rate. Taking into considering CO₂ has a small mass transfer coefficient, optimising aeration rate to achieve the extensive gas/liquid interface area to improve mass transfer can play a significant role (Pires et al., 2012, Ho et al., 2011). Meanwhile, gas bubbling create mixing and turbulence in the culture and help for consistent availability and better distribution of nutrient and light over all the cells, in addition to avoid sedimentation and temperature gradient as well as to prevent toxic levels of dissolved oxygen (Sánchez et al., 2012). On the other hand, aeration rate take into account to calculate CO₂ injection rate which has effect on CO₂ biofixation efficiency and hence production cost. However, High aeration can cause shear and results in cell damage and so less growth. Therefore, it is necessary to optimise aeration rate that could efficiently enhance the photobioreactors performance. Despite of that bubble column bioreactor offers minimum shear, in high aeration rate damage to the cells because of shear may be not ignorable. In a stirred tank, shear has the maximum value around the impeller (Dasgupta et al., 2010).

As it has been demonstrated by Chai et al. (2012), higher aeration rate contributes to higher mass transfer coefficient, but lower CO₂ fixation efficiency. In that study, 0.013 vvm (volume per volume. minute) aeration rate was enough to accomplish mass transfer requirements and satisfy CO₂ demand of photosynthesis. It is stated by Sánchez et al. (2012) that aeration rate above 0.5 vvm results in shear rate higher than 60 s⁻¹ and consequently to cell damage. They observed abatement of biomass concentration and CO₂ fixation rate by 20 % and 25 %, respectively, for increasing aeration rate from 0.25 to 0.75 vvm in constant dilution rate and different light intensities between 625 to 1625 μmol m⁻² s⁻¹. The aeration rate that could lead to cell damage varies depending on algae species and the system. For instance, it has been reported that biomass productivity diminished at aeration rate above 1.3 vvm, 2 vvm, 1.0 vvm for *Phaeodactylum tricornutum* (Mirón et al., 2003), *Porphyridium cruentum* (Camacho et al., 2000) and *Dunaliella salina* (Silva et al., 1987), respectively.

The growth of *Haematococcus pluvialis* was improved at 0.2 vvm flow rate in compare with 0.05 and 0.1 vvm, but the performance did not amend for flow rates more than 0.2 vvm (Yoo et al., 2012). Ryu et al. (2009), examined the effect of aeration rate on *Chlorella* sp. when 5 % CO₂ gas mixture in aeration rates of 0.06, 0.1, 0.2 and 0.4 vvm was supplied. They showed that irrespective of increasing biomass productivity by increasing aeration rate, CO₂ removal efficiency decreased so that optimal aeration rate with respect to both productivity and fixation efficiency was 0.2 vvm. CO₂ biofixation rate was maximised at aeration of 6.5 % CO₂ enriched air at the rate of 0.5 vvm for cultivation of *Chlorella vulgaris* in a bubble column photobioreactor (Anjos et al., 2013). Biomass concentration maintained at 5.15 g L⁻¹ and maximum CO₂ removal efficiency of 63 % achieved in semi-continuous cultivation of *Chlorella* sp. at aeration rate of 0.125 vvm of 10 % CO₂ enriched air (Chiu et al., 2009).

2.6.5 Agitation

Mixing is one of the important parameters that could minimise sedimentation as well as temperature, light and nutrient gradient and also enhances gas exchange between the liquid and gas phases (Dasgupta et al., 2010, Barsanti and Gualtieri, 2014). On the other hand, mixing can cause shear stress and in the case of high shear stress,

cells are damaged and it leads to less productivity. Despite of that bubble column bioreactor offers minimum shear, in high aeration rate damage to the cells because of shear might be not ignorable. In a stirred tank, shear has the maximum value around the impeller (Dasgupta et al., 2010).

Actually, in a bubble column photobioreactor (or totally vertical tubular bioreactors) with a high H/D ratio which is around 6:1 (Yoo et al., 2012), and a gas sparger at the bottom of the bioreactor, mixing can be done quiet perfectly by gas bubbling, however in the case of using a stirred tank for cultivation, bubbling is not enough for well mixing. Stirred tanks have been used for microalgae culturing with various impeller speeds within range of 100-1200 rpm (Sacasa Castellanos, 2013), however maximum speed that strain can tolerate without cell damage is different for each species.

Funahashi et al. (1999) pointed out that mixing at 250 rpm is the best for *Chlorella* species. Specific growth rate and biomass concentration increased from 0.123 to 0.205 d⁻¹ and from 0.470 to 0.590 g L⁻¹, respectively, when mixing speed increased from 150 to 350 rpm in a 14 liter-stirred tank used to cultivate *Chlorella vulgaris* with constant air flowrate (Sacasa Castellanos, 2013). Indeed, smaller gas bubble size in higher mixing speed leads to mass transfer improvement and more CO₂ availability to the cells. In spite of considerable improve in cell growth by increasing impeller speed from 150 up to 350 rpm, by further increase in the impeller speed to 450 rpm, biomass concentration just slightly increased from 0.637 to 0.656 g L⁻¹, nevertheless no cell damage was observed even at 450 rpm (Sacasa Castellanos, 2013). Biomass concentration of two strains, *Phaedactylum tricornutum* and *Porphyridium cruentum*, was increased with increasing agitation speed up to 350 and 550 rpm, respectively (Sobczuk et al., 2006).

2.6.6 Source of CO₂

There are different sources of carbon dioxide that can be utilised by algae species such as: (i) CO₂ from atmosphere, (ii) CO₂ from industrial exhaust gases, and (iii) fixed CO₂ from soluble carbonates. Since the atmosphere contains only 0.03-0.06 % CO₂; some limitation in mass transfer and so in cell growth of microalgae is expected (Wang et al., 2008). In contrast, industrial exhaust gases such as flue gas from power plants contains up to 15 % CO₂, so it provides a CO₂-rich source which is potentially

more efficient for microalgae culturing and CO₂ biofixation. Using fixed CO₂ in the form of carbonates is not an atmospheric CO₂ removal process unless combined with an upstream process to fix CO₂ by chemical reaction to produce carbonates. However, as mentioned before CO₂ fixation via chemical reaction is a relatively expensive process. Conversely, CO₂ from flue gas of power plants, which is responsible for more than 7 % of total CO₂ emission worldwide (Wang et al., 2008), is available at little or no cost.

Flue gas mostly contains nitrogen, oxygen, carbon dioxide, water vapour, as well as minor amount of NO_x, SO_x and CO. Depending on the type of fuel and combustion process, CO₂ percentage in flue gas can be 4-14 % and also NO_x and SO_x around 200 ppm (Berberoglu et al., 2009). There is no major problem associated with presence of NO_x for algae growth, but SO_x may be toxic since it reduces pH due to sulphurous acid formation (Pires et al., 2012, Kumar et al., 2011). No negative affect has been observed when 50 ppm of SO_x is present in the inlet gas, however, pH dropped and growths was stopped with 400 ppm of SO_x in the inlet gas (Pires et al., 2012). In the case of using flue gas of power plant as source of carbon, the tolerance of microalgae species to high concentration of CO₂, high temperature and low pH would be advantageous.

2.6.7 Algae Species

More than 40,000 different microalgae species have been recognised so far (Bhola et al., 2011). Typical molecular formula for microalgae biomass can be represented by CO_{0.48}H_{1.83}N_{0.11}P_{0.01} (Chisti, 2007) or CO_{0.40}H_{1.61}N_{0.15}P_{0.01} (Ríos et al., 1998). Cornet et al. (1992a) obtained CO_{0.53}H_{1.65}N_{0.17}P_{0.006} for elemental composition of *Spirulina*.

Selecting appropriate microalgae strain plays a significant role to achieve an efficient and economically feasible CO₂ mitigation. The desired microalgae species should have high CO₂ biofixation ability, high growth rate, low operation cost, low contamination risk, easy harvesting and rich in valuable components. Meanwhile, species that can tolerate high light intensity and can grow well in natural day/night cycle are suitable for outdoor cultivation (Stewart and Hessami, 2005a).

Different algae species have been investigated for purpose of CO₂ biofixation. CO₂ biofixation rate for different algae species has been summarised in Table 2-3. *Chlorella vulgaris* is one of the most favoured species for purpose of CO₂

biofixation and a CO₂ biofixation of 0.624 g CO₂ L⁻¹ d⁻¹ was achieved when it was cultivated in 15 % CO₂ concentration (Yun et al., 1997). An amount of 0.497 g CO₂ L⁻¹ d⁻¹ was fixed by *Botryococcus braunii* at CO₂ concentration of 5 % (Ho et al., 2011). Biofixation rate for *Aphanothece microscopica Nägeli* in aeration of 15 % CO₂ enriched air was 1.44 g CO₂ L⁻¹ d⁻¹ (Jacob-Lopes et al., 2009a). More results can be seen in Table 2-3.

Since microalgal CO₂ biofixation involves photoautotrophic growth of the cells, the CO₂ fixation rate directly depends on cell growth rate and light utilisation efficiency (Ho et al., 2011) and maximises in optimum conditions which is specific to each microorganism and depends on physiological characteristics and their environmental factors and habitat (Martinez et al., 2011).

Table 2-3 Different microalgae species and their CO₂ biofixation rate

Algae Species	CO ₂ % at influent (%v/v)	Flow rate (vvm)	CO ₂ Fixation rate (g CO ₂ L ⁻¹ d ⁻¹)	References
<i>Anabaena</i> sp.	Air	0.2	1.45	Lopez et al. (2009)
<i>Anabaena</i> sp.	10	0.04	1.01	Chiang et al. (2011)
<i>Anabaena</i> sp.	Air	0.13-0.75	1	Sánchez et al. (2012)
<i>Synechocystis aquatilis</i> SI-2	10	0.05	3.3	Zhang et al. (2001)
<i>Chlorella vulgaris</i>	4	-	0.148	Bhola et al. (2011)
<i>Chlorella vulgaris</i>	5	-	0.252	Sydney et al. (2010)
<i>Chlorella vulgaris</i>	15	2	0.624	Yun et al. (1997)
<i>Chlorella vulgaris</i>	10-13 (flue gas)	-	4.4	Douskova et al. (2009)
<i>Chlorella vulgaris</i>	1	0.5	6.24	Cheng et al. (2006)
<i>Chlorococcum</i> sp.	10	0.004	0.305	Chai et al. (2012)
<i>Aphanothece microscopica Nägeli</i>	15	1	1.44	Jacob-Lopes et al. (2009a)
<i>Dunaliella salina</i>	3	-	0.091	Kim et al. (2012)
<i>Synechocystis</i> sp.	10	0.4	1.96	Martinez et al. (2012)
<i>Chlorella</i> sp.	5	0.2	0.7	Ryu et al. (2009)
<i>Chlorella</i> sp.	2	0.25	7.83	Chiu et al. (2008)
<i>Spirulina</i> sp.	6	0.075	0.39	De Morais and Costa (2007b)
<i>Scenedesmus obliquus</i>	6	0.075	0.2	De Morais and Costa (2007b)
<i>Scenedesmus obliquus</i>	12	0.038	0.26	De Morais and Costa (2007a)
<i>Chlorella kessleri</i>	6	0.075	0.12	De Morais and Costa (2007b)
<i>Spirulina platensis</i>	5	-	0.319	Sydney et al. (2010)
<i>Botryococcus braunii</i>	5	-	0.497	Sydney et al. (2010)

The strains that are tolerant to high CO₂ concentration, high temperature and toxic components like SO_x and NO_x are advantageous since flue gas of power plants can be used directly. It has been demonstrated that high level of carbon dioxide were

tolerated by many microalga species, for instance, *Chlorococcum littorale*, is a marine algae which can tolerate up to 40 % of CO₂ and grow well (Murakami and Ikenouchi, 1997); even *Chlorococcum littorale* can tolerate 70 % CO₂ concentration (Ota et al., 2009). *Spirulina* sp., *Chlorella* sp., *Botryococcus braunii* and *Scenedesmus obliquus* are some other strains with high tolerance to CO₂ concentration (Wang et al., 2008). Because of high temperature of flue gas from thermal power station, microalgae species with high temperature tolerance should be considered to avoid necessity of the flue gas cooling system (Ono and Cuello, 2003). *Chlorella* species which were isolated from hot springs in Japan grew at temperatures up to 42 °C and more than 40 % CO₂ (Ono and Cuello, 2003). Additionally, *Synechococcus elongatus* and *Cyanidium caldarium* can grow well even at 60 °C (Miyairi, 1995, Seckbach and Ikan, 1972b). Meanwhile, high tolerant species are suitable for outdoor cultivation due to possibility of high temperature especially in summer time. Some of tolerant microalgae species to high temperature and high CO₂ concentration have been listed in Table 2-4. Also there is a potential of improving microalgae species by genetic engineering to obtain better growth and higher production rate or increasing lipid content of algae or escalating temperature tolerance of the species.

Table 2-4 High temperature and CO₂ concentration tolerant microalgae species

Algae species	Maximum temperature tolerance (°C)	Maximum CO ₂ % tolerance	References
<i>Chlorella</i> sp.	42	40	Ono and Cuello (2003)
<i>Cyanidium caldarium</i>	60	100	Seckbach and Ikan (1972b)
<i>Scenedesmus</i> sp.	30	80	Hanagata et al. (1992b)
<i>Synechococcus elongatus</i>	60	60	Miyairi (1995)
<i>Chlorococcum littorale</i>	-	70	Ota et al. (2009)
<i>Eudorina</i> sp.	30	20	Hanagata et al. (1992b)
<i>Scenedesmus obliquus</i>	40	13.8	Basu et al. (2013)
<i>Chlorella vulgaris</i>	25	100	Concas et al. (2012)

2.6.8 Quality of Light

Light is an electromagnetic radiation that provides energy needed for photosynthesis and is the most significant parameter that influences the growth kinetic of microalgae (Pires et al., 2012).

Sun's radiation wavelength ranges between 100-4000 nm and within this solar radiation three different forms of energy exists; harmful ultraviolet radiation (100-400 nm), visible light (400-700 nm), and heat (infrared radiation 700-4000 nm)

(Barsanti and Gualtieri, 2014). Only visible light which is a tiny fraction of sunlight is responsible for photosynthesis which is called photosynthetically active radiation (PAR) and expressed as the radiant energy incident per unit of surface per unit of time, now internationally states in mole of photons per area per time ($\mu\text{mol m}^{-2} \text{s}^{-1}$).

When light wave travels, in interaction with matter, it can be scattered or absorbed. Small particles in a medium defuse a portion of incident light in all direction and it is called scattering phenomena. Light can be retained by a molecule and this process is defined absorption. Absorbed photon flux can be used to carry out work, or can be emitted as fluorescent or can be converted to heat energy. Amount of light absorbed by a molecule is basically described by Beer-Lambert law. This law expressed a logarithmic relationship between absorbance and the ratio of incident and transmitted light while absorbance is a linear function of biomass concentration, light path and absorption coefficient (Barsanti and Gualtieri, 2014).

All parameters of intensity, duration and quality of irradiance influence on biomass growth. These factors will be discussed at following sections.

2.6.8.1 Light Intensity

Light intensity refers to the available photons for photosynthesis, has a remarkable effect on photobioreactor performance (Gadhamshetty et al., 2010). Indeed, photon flux decreases exponentially with distance from illuminated surface. Therefore, the cells near irradiance source exposed to high light intensity while the cells far from the irradiance source receive less light as a result of shading. Light availability depends on the depth and cell density of algal culture, as cells grow to a high cell density, the light penetration distance inside the culture becomes shorter. Cells can absorb more light, and consequently, can grow more rapidly if the intensity of incident light increases within the optimum limit (Chiang et al., 2011). Growth rate increases by increasing light intensity until a certain value at saturation light intensity, afterward, growth rate shows decrease when light intensity further increased. While lack of light limits cell growth, too high light intensity may result in photoinhibition.

Optimum light intensity to reach maximum productivity is different for different species and generally ranges between 50-200 $\mu\text{mol m}^{-2} \text{s}^{-1}$, higher intensities may cause inhibitory effect (Dasgupta et al., 2010). On the other hand it has been

reported that most of the microalgae species illuminated by natural solar energy are saturated at 1700-2000 $\mu\text{mol m}^{-2} \text{s}^{-1}$ (Ho et al., 2011). However, many other parameters such as light period, light source or temperature, can affect the optimum light intensity. As it has been reported by Ho et al. (2012), maximum productivity and CO_2 biofixation rate for *Scenedesmus obliquus* CNW-N was about 420 $\mu\text{mol m}^{-2} \text{s}^{-1}$ and increasing light intensity to 540 $\mu\text{mol m}^{-2} \text{s}^{-1}$ led to less biomass growth which is due to photoinhibition. Jacob-Lopes et al. (2008a) found that maximum carbon dioxide removal for *Aphanothece microscopica* Nägeli can be obtained under 11 klux light illumination when temperature and CO_2 concentration are 35 °C and 15 %, respectively. Nevertheless, some species can tolerate high irradiance and are more suitable for outdoor culturing. For instance, *Synechocystis* sp. represented maximum productivity and CO_2 removal under irradiance of 1600 $\mu\text{mol m}^{-2} \text{s}^{-1}$ when 10 % CO_2 enriched air was bubbled at rate of 0.4 vvm (Martinez et al., 2012). On the other hand, CO_2 biofixation was optimum at 686 $\mu\text{mol m}^{-2} \text{s}^{-1}$ and 35.3 °C when *Synechocystis* sp. was investigated at different conditions of light intensity, temperature and pH (Martinez et al., 2011). Optimum light intensity of 391 $\mu\text{mol m}^{-2} \text{s}^{-1}$ have been reported for *Selenastrum tricorutum*, (Benson and Rusch, 2006), for microalgae *Porphyridium cruentum* 485 $\mu\text{mol m}^{-2} \text{s}^{-1}$ of light intensity has been stated as optimum light intensity (Muller-Feuga, 1999) and for *Haematococcus pluviialis* a range of 170-200 $\mu\text{mol m}^{-2} \text{s}^{-1}$ of light intensity has been reported (Benson and Rusch, 2006).

2.6.8.2 Light period

Light period also plays an important role in microalgae growth. Although phytoplankton can be normally cultivated under continuous illumination, most of the algae species do not grow well under constant illumination, and hence a light/dark cycle should be applied (Barsanti and Gualtieri, 2014). Optimum light period varies from 12:12 to 16:08 h light:dark, for different species and also it is affected by light intensity (Andersen, 2005).

Not many researches have investigated the influence of light period on the growth. Jacob-Lopes et al. (2009b) investigated 13 light periods ranges 0:24 to 24:0 h for cultivating cyanobacteria *Aphanothece microscopica* Nägeli using standard BG11 medium at 150 $\mu\text{mol m}^{-2} \text{s}^{-1}$ and 15 % CO_2 enriched air, and 12:12 h light

period was identified as the most effective light period. Among three various light periods of 24:00, 18:06 and 12:12 h that examined for *Nannochloropsis* sp., 18:06 h was the optimum when light intensity was $100 \mu\text{mol m}^{-2} \text{s}^{-1}$ (Wahidin et al., 2013). Photoinhibition was observed for very long light period of 24:00 h accompanied by cells' colour change and sharp drop in microalgae growth. Maximum biomass concentration and CO_2 biofixation rate was achieved at light period of 16:8 h when *Chlorococcum* sp. was cultured under different light periods of 24:00, 16:08 and 12:12 h (Chai et al., 2012). Besides, the trend of cell growth at light period of 24:00 h was similar to 16:08 h light period up to first three days, but then it experienced a sharp drop which can be related to cell damage due to high photon flux.

2.6.8.3 Light Source

Light energy can be provided by sunlight or artificial light or both. While the sunlight is the cost effective light source, it is subject to change by varying weather conditions, geometric location and day period. From other hand, artificial light source can be controlled to the desired intensity and even wavelength or light period. Controlled illumination by artificial light can enhance biomass productivity (Blanken et al., 2013).

Numerous types of artificial light source are available including: fluorescent tubes (cool white or day light), high intensity discharge lamps (HID), and light emitting diodes (LED). Fluorescent tubes are the common type of artificial light source used for microalgae cultivation with a PAR (400 and 700 nm) efficiency of $1.25 \mu\text{mol s}^{-1} \text{W}^{-1}$. HID and LED lamps exhibit PAR efficiency of 1.65-1.87 and $1.91 \mu\text{mol s}^{-1} \text{W}^{-1}$, respectively (Blanken et al., 2013). Although LED lamps would be the best due to the highest PAR efficiency, but the relatively high cost limits their large scale applications. Optical fiber excited by metal-halide lamp or solar energy have been also used (Chen et al., 2011).

Specific growth rate and productivity for different algae species that have been investigated by researchers can be found in Table 2-5. Cultivation conditions including temperature, light intensity, light period, % CO_2 and reactor type have been recommended.

Table 2-5 Comparison of cell growth rate of microalgae strains reported in literatures

Microalgae Species	Temperature °C	Light Intensity $\mu\text{mol m}^{-2} \text{s}^{-1}$	Light period Light:Dark h:h	CO ₂ %	Specific growth rate d ⁻¹	Biomass Productivity g L ⁻¹ d ⁻¹	Rector type	References
<i>Chelorella</i> sp.	40	500	24:0	20	5.76	0.7	Tubular	(Sakai et al., 1995)
<i>Synechocystis aquatilis</i>	N.A	N.A	24:0	N.A	5.5	0.59	N.A	(Murakami and Ikenouchi, 1997)
<i>Scenedesmus obliquus</i>	30	3200 lux	12:12	12	0.22	0.14 ^a	Tubular	(De Morais and Costa, 2007a)
<i>Spirulina</i> sp.	30	3200 lux	12:12	6	0.44	0.2 ^a	Tubular	(De Morais and Costa, 2007a)
<i>Chelorella vulgaris</i>	25	3600 lux	24:0	0.093	N.A	0.15	Membrane tubular	(Fan et al., 2008)
<i>Chelorella</i> sp.	26	300	24:0	2	0.49	0.17	Bubble column	(Chiu et al., 2008)
<i>Chelorella</i> sp.	Ambient	100	N.A	5	N.A	0.34	Tubular	(Ryu et al., 2009)
<i>Aphanothece microscopica</i> Nägeli	35	150	24:0	15	N.A	0.77	Bubble column	(Jacob-Lopes et al., 2009a)
<i>Scenedesmus obliquus</i>	28	60	24:0	10	1.19	0.29	N.A	(Ho et al., 2010)
<i>Anabaena</i> sp.	30	1625	N.A	300 ppm	N.A	0.5	Bubble column	(Sánchez et al., 2012)
<i>Synechocystis</i> sp.	25	1600	16:8	5	0.095	1.56	Bubble column	(Martinez et al., 2012)
<i>Chlorella</i> sp.	27	100	12:12	1	0.58	0.028	Tubular	(Kim et al., 2012)
<i>Dunaliella salina</i>	27	80	12:12	3	0.78	0.054	Tubular	(Kim et al., 2012)
<i>Dunaliella</i> sp.	25	100	12:12	1	0.56	0.03	Tubular	(Kim et al., 2012)
<i>Nannochloropsis</i> sp.	23	100	18:6	300 ppm	0.34	N.A	N.A	(Wahidin et al., 2013)
<i>Spirulina platensis</i>	25	90-125	24:0	300 ppm	N.A	0.087	Bubble column	(Arata et al., 2013)
<i>Tetraselmis suecica</i>	Ambient	Sunlight	-	N.A	N.A	0.52	Tubular	(Michels et al., 2014)
<i>Scenedesmus obliquus</i>	25	150	16:8	350 ppm	0.18	0.077	Airlift	(Massart et al., 2014)
<i>Chelorella vulgaris</i>	30	250	N.A	2	N.A	0.72	Airlift	(Fernandes et al., 2014)
<i>Scenedesmus obliquus</i>	23	350	N.A	5	0.49	0.35	Flat plate	(Gris et al., 2014)

In all cases except one, artificial light sources were used. A biomass productivity of $1.56 \text{ g L}^{-1} \text{ d}^{-1}$ was stated for *Synechocystis* sp. when cultivated under conditions of $25 \text{ }^\circ\text{C}$, 5 \% CO_2 , $1600 \text{ } \mu\text{mol m}^{-2} \text{ s}^{-1}$ and 16 h light period in a bubble column photobioreactor. *Chlorella vulgaris* productivity was $0.72 \text{ g L}^{-1} \text{ d}^{-1}$ in an airlift photobioreactor illuminated by $250 \text{ } \mu\text{mol m}^{-2} \text{ s}^{-1}$ and aerated by 2 \% CO_2 enriched air.

2.7 Light Distribution inside the Culture

Light distribution in the vessel cannot be considered homogeneous particularly in dense culture of microalgae due to the mutual shading that cannot be ignored unless at a very low biomass density (Sevilla et al., 1998, Grima et al., 1994, Evers, 1991).

Shading phenomena occurs due to absorption of photons by medium or cell pigments as well as scattering by cell particles or gas bubbles (Cornet et al., 1992b). Indeed, mean volumetric growth rate must be calculated for working illuminated volume considering local availability of light energy in the culture which is quite heterogeneous (Cornet et al., 1995). This means there is different amount of light intensity inside the photobioreactor so that light availability is a function of light path, the incident irradiance, biomass concentration and optical properties (Martínez et al., 2012, Grima et al., 1994). Accordingly, a quantitative description of the light regime inside the photobioreactor is necessary for kinetic modelling of the growth and calculation of the photosynthesis efficiency.

2.7.1 Beer-Lambert Model

In order to develop a mathematical model which describes photosynthesis efficiency or microalgae growth, accurate information of light attenuation through the microalgae suspension is required. For this purpose, direct measurement of light intensity at two points inside the culture and adjustment to a mathematical model (usually Lambert Beer model) is employed in most cases (Yun and Park, 2001). Assuming that the light obeys Beer-Lambert Law, the light beam is reduced when it passes through the culture, Figure 2-2, so that irradiance in any point inside the culture can be calculated as a function of incident light intensity, distance and biomass concentration.

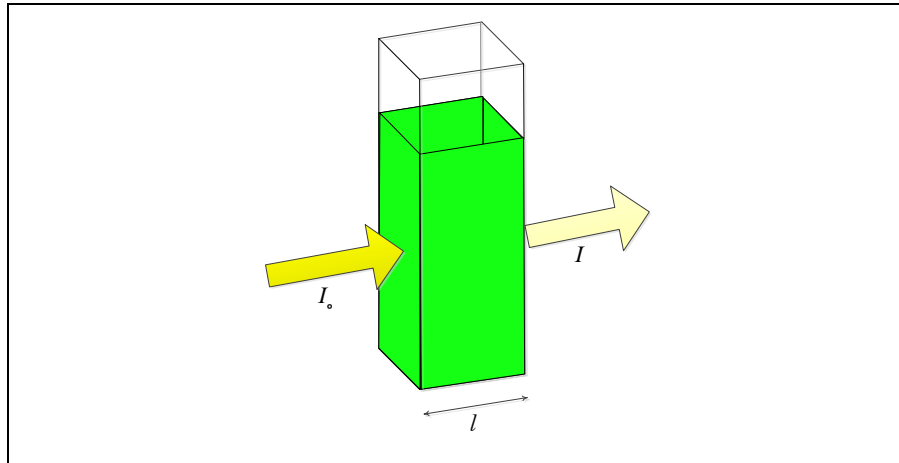


Figure 2-2 Diagram of Beer-Lambert absorption of a light beam as it travels through a cuvette

Based on Beer-Lambert Law, Equation (2-2), there is a logarithmic dependence between the transmission of the light through a substance and the parameters of the incident light intensity, I_0 , the absorption coefficient, K_a , the length of the light path, p , and the biomass concentration, C_b :

$$I(p, C_b) = I_0 \cdot \exp(-p \cdot K_a \cdot C_b) \quad (2-2)$$

It should be mentioned that there are two assumptions: (i) the monochromatic light beam illuminated to the vessel is parallel and remains parallel throughout the vessel, and (ii) scattering by particles is ignorable. Despite that this model developed for mono-chromatic radiation, it can be used for polychromatic radiation when absorption coefficient averaged for all wavelength (Sevilla and Grima, 1997).

The vessel shape/configuration has a significant influence on the light attenuation inside the vessel, for instance, the unidirectional collimated light flux in a parallelepiped vessel (Figure 2-3), the irradiance at any point inside the vessel (at distance x from the wall) with irrespective of the top and bottom effects can be calculated by Beer-Lambert law while $p = x$ (Grima et al., 1997).

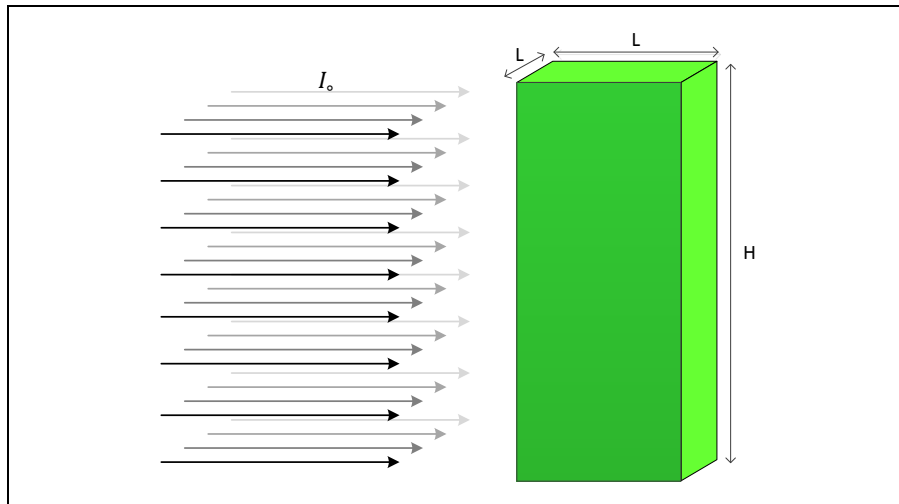


Figure 2-3 Unidirectional Collimated light flux in a parallelepiped vessel

In the case of a cylindrical geometry still illuminated by unidirectional parallel flux, it can be easily considered a collection of parallelepiped as shown in Figure 2-4. Then each parallelepiped has a different length of path, p , which is equal to $2\sqrt{R^2 - x_r^2}$, when x_r is vertical distance from central line as shown in Figure 2-4 (Grima et al., 1997).

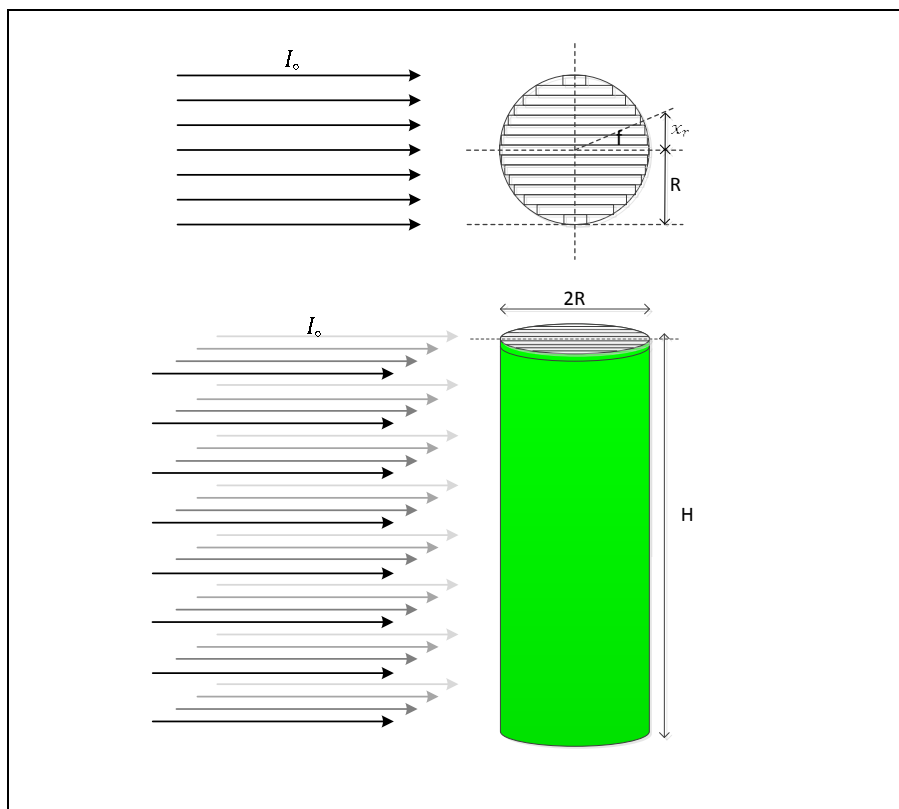


Figure 2-4 Cylindrical vessel illuminated by unidirectional parallel flux

However, the most common type of vessel is a cylindrical vessel which is illuminated from all sides, Figure 2-5.

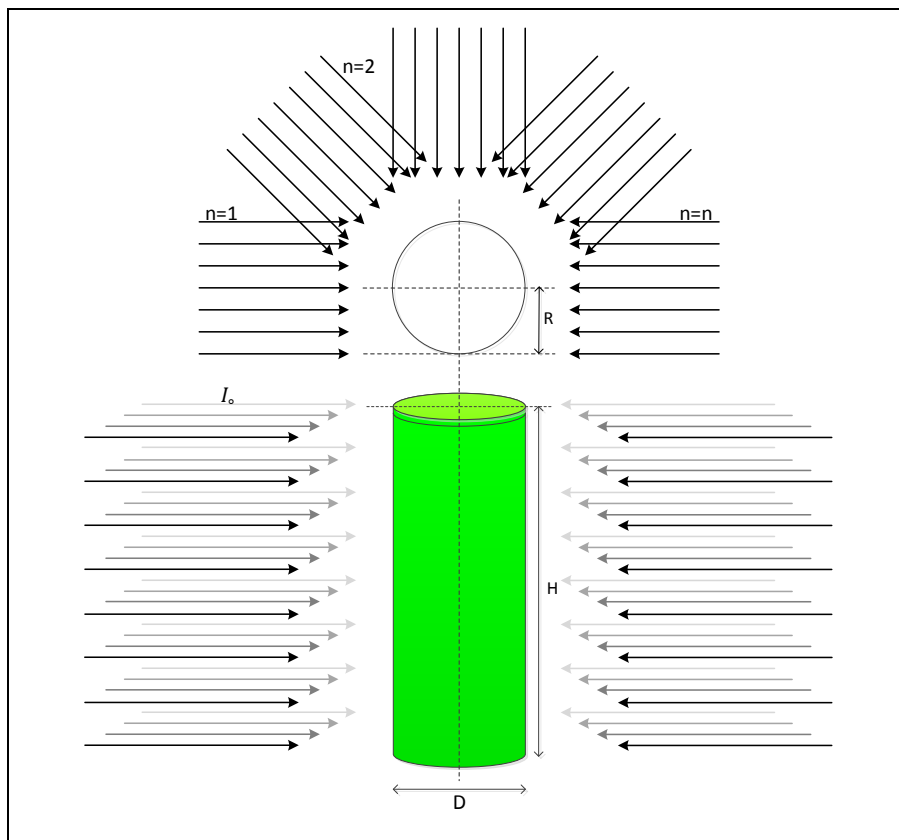


Figure 2-5 Cylindrical vessel evenly illuminated by unidirectional parallel flux from different sides

The path length of the light, p , at any point inside the vessel at vertical distance, s , from the vessel surface can be estimated by Equation (2-3), as demonstrated in Figure 2-6 (Evers, 1991).

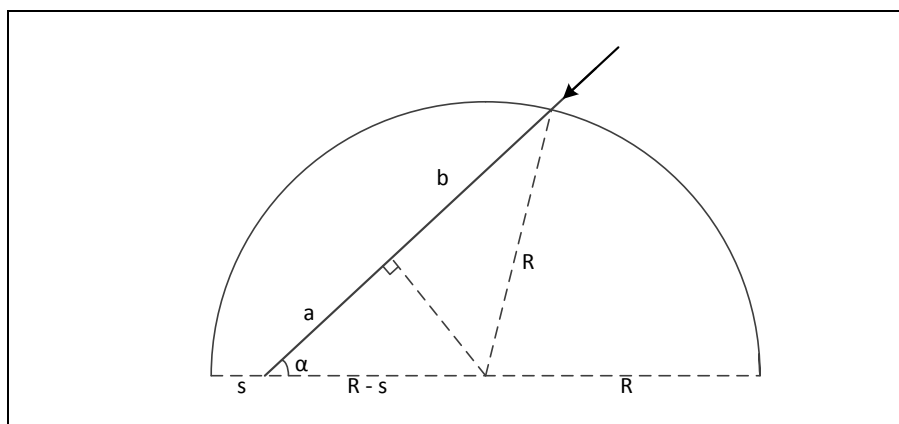


Figure 2-6 Schematic representation of one-half of a cross section through a cylindrical vessel

$$p = a + b = (R - s) \cos \alpha + [R^2 - (R - s)^2 \sin^2 \alpha]^{0.5} \quad (2-3)$$

Although the Beer-Lambert model is the simplest equation to predict light attenuation, it has extensively been used for modelling light distribution (Janssen et al., 2000, Suh and Lee, 2003, Benson et al., 2007, Bosma et al., 2007, Elyasi and Taghipour, 2010, Li et al., 2010). Nevertheless, this oversimplified model is an inappropriate model for light distribution modelling especially in high biomass concentration (Sevilla and Grima, 1997), since modelling results are only correct when very diluted culture illuminated by parallel beam of mono-chromatic light (Rosello Sastre et al., 2007, Suh and Lee, 2003, Lee et al., 2010, Li et al., 2010, Imoberdorf and Mohseni, 2011). Actually, scattering effect has been neglected in this model which leads to inaccurate prediction of photon flux distribution even for simple geometries but dense culture (Cornet et al., 1992a, Cornet et al., 1998). So, two independent coefficients of absorption by algae pigments and scattering coefficient by cells should be considered.

Although, using extinction coefficient, ε_c , in Beer-Lambert equation allows improvement by considering both absorption and out-scattering in one parameter, still accurate modelling is not achievable, because by extinction coefficient only out-scattering takes into account and in-scattering still neglected (Pilon et al., 2011).

$$I(p, C_b) = I_o \cdot \exp(-p \cdot \varepsilon_c \cdot C_b) \quad (2-4)$$

Beer-Lambert model has been also further modified by considering the effect of wavelength, λ and distance between the light source and surface of the vessel, L (Gadhamshetty et al., 2010, Katsuda et al., 2002) as represented by following equation:

$$I = \frac{L^2}{(p + L)^2} \Sigma I_{o\lambda} \cdot \exp(-p \cdot \varepsilon_c \cdot C_b) \quad (2-5)$$

This equation can be used to predict light attenuation profiles in photobioreactors with different sizes, meanwhile, spectra properties and extinction coefficient can easily be determined via spectrophotometric results.

Acién Fernández et al. (2013) compared the mathematical modelling results of light attenuation for an outdoor tubular photobioreactor when considered Beer-Lambert model, and a new hyperbolic expression to calculate absorption coefficient of Beer-Lambert model was proposed (Sevilla and Grima, 1997):

$$At = p \cdot K_a \cdot C_b \quad (2-6)$$

$$At = \frac{At_{max} \cdot C_b}{K_{at} + C_b} \quad (2-7)$$

$$K'_a = \frac{1}{p} \cdot \frac{At_{max}}{K_{at} + C_b} \quad (2-8)$$

$$I = I_o \cdot \exp(K'_a \cdot p \cdot C_b) \quad (2-9)$$

While Beer-Lambert model only accurately predicted light attenuation in low concentration, the new proposed hyperbolic equation to calculate absorption coefficient contributed to predict light attenuation and growth kinetics properly.

2.7.2 Average Light Intensity

Light gradients leads microalgae cells expose to different irradiance when they move along the culture. It is not well-known how the relation between growth rate and photosynthetic rate with irradiance will be in a dense culture (Grima et al., 1996). Nevertheless, it is consistently accepted that average should be taken into account due to physiological adaptation of the algae (Grima et al., 1994, Grima et al., 1993, Terry, 1986). One approach is calculation of average irradiance and then calculating growth rate with respect to average light (Grima et al., 1997), however, there is another possibility that estimate average growth rates from local growth rate at different places with various local light intensities inside the vessel (Evers, 1991). In the later model, they do growth rate calculation as function of local irradiance at every point in a vessel and then averaging them for whole the vessel. In this way, it is assumed that a cell moving in the culture adopt itself to different irradiance inside the vessel rapidly enough. Nevertheless, in the former model, it is assumed that each cell

is influenced by average light intensity in the culture instead of dealing with different light intensities in different points.

As it is expressed by Grima et al (1997), average irradiance, I_{av} which can be used to calculate total amount of absorbed photon flux, for any given geometry can be represented by:

$$I_{av} = \frac{\sum_{i=1}^n V_i \cdot I_{pi}}{\sum_{i=1}^n V_i} = \frac{\sum_{i=1}^n V_i \cdot I_{pi}}{V_T} \quad (2-10)$$

where V_i stands for a small volume element with constant local irradiance, I_{pi} and V_T stands for the total vessel volume. This equation is a basic definition for calculating average light intensity in various geometries that has been applied by many researchers (Brindley et al., 2011). However, in order to calculate average light intensity, the first step is to find the irradiance at any point inside the bioreactor. This may be achieved experimentally or analytically. Obviously, finding data through experiments would be complicated. In contrast, the latter option is much more convenient.

2.7.2.1 One-Dimensional Model for Parallelepiped

With employing Equation (2-10) for unidirectional collimated illumination to a parallelepiped vessel shown in Figure 2-3, and combining with Beer-Lambert Law (Grima et al., 1997):

$$I_{av} = \frac{\int I_p(x) \cdot dV}{V_T} = \frac{\int_0^L I_o \cdot \exp(-K_a C_b x) \cdot H \cdot L \cdot dx}{H \cdot L^2} \quad (2-11)$$

$$I_{av} = \frac{I_o}{L \cdot K_a \cdot C_b} \cdot [1 - \exp(-L \cdot K_a \cdot C_b)] \quad (2-12)$$

Equation (2-12) has been applied widely to determine average light intensity available to the cells. Martinez L. et al. (2011), have been studied growth condition's optimisation for purpose of CO₂ biofixation by native *Synechocystis* species. Equation (2-12) was used to determine average light intensity inside the reactor, and by applying response surface methodology (RSM) the maximum CO₂ biofixation of

2.07 g CO₂ L⁻¹ d⁻¹ was achieved when an average light intensity of 686 μmol m⁻² s⁻¹ applied (Martinez et al., 2011). Garcia-Malea et al. (2005 and 2006), in batch cultures of *Haematococcus pluvialis* for modelling of the growth and accumulation of carotenoids and then in continuous production of *Haematococcus pluvialis*, for modelling the irradiance effect have applied same equation for calculation average light intensity (Garcia-Malea et al., 2006, García-Malea et al., 2005, Ríó et al., 2005). Equation (2-12) has been applied for investigating the effects of light on *Synechocystis* species and for simulations of light intensity regime inside the photobioreactor (Martinez et al., 2012). In this study, specific growth rate was calculated for average light intensity when different external light furnished. Therefore, a maximum specific growth rate of 0.108±0.03 h⁻¹ at an average light intensity of 930±22 μmol m⁻² s⁻¹ was observed by both mathematical calculation and experimental results (Perner-Nochta and Posten, 2007, Martínez et al., 2012). In another recent research, for algal growth in bubble column, a theoretical model to predict biomass concentration in semi continues culturing with CO₂ enriched air was developed (Pegallapati and Nirmalakhandan, 2012). In this model, gas-liquid mass transfer, CO₂ uptake rate by microalgae, growth kinetic, average light intensity and temperature effects have been considered. Baliga and Powers (2010) have calculated average light intensity with Equation (2-12) for modelling hypothetical microalgae photobioreactor and determining the most suitable operating conditions for algae production in cold climates. Also Sánchez et al. (2012) successfully applied Equation (2-12) for modelling of *Anabaena* sp. cultivation under different conditions of dilution rate, irradiance and aeration rate.

2.7.2.2 Bi-Dimensional Model for Cylindrical Vessel

Unidirectional Illumination

As it mentioned, a cylindrical reactor which illuminated by unidirectional parallel beam can be divided into parallelepiped elements with different length (different value of p), Figure 2-4. So the average irradiance in the corresponding element and then for whole the vessel can be calculated (Grima et al., 1997):

$$x = R \sin \varphi \quad \text{so} \quad dx = R \cos \varphi d\varphi \quad (2-13)$$

$$p = 2\sqrt{R^2 - x_r^2} = 2\sqrt{R^2 - R^2 \sin^2 \varphi} = 2R \cos \varphi \quad (2-14)$$

$$V_i = Hpdx \quad \& \quad V_T = \pi R^2 H \quad (2-15)$$

$$I_{av} = \frac{2 \int_0^R \int_0^p I_o \cdot \exp(-K_a C_b s) H ds dx}{\pi R^2 H} \quad (2-16)$$

$$I_{av} = \frac{2 \int_0^{\pi/2} \frac{I_o HR}{K_a C_b} [1 - \exp(-K_a C_b p)] \cos \varphi d\varphi}{\pi R^2 H} \quad (2-17)$$

$$I_{av} = \frac{2I_o}{\pi K_a C_b R} \left[1 - \int_0^{\pi/2} \exp(-2K_a C_b R \cos \varphi) \cos \varphi d\varphi \right] \quad (2-18)$$

Average light intensity in a cylindrical vessel can be properly estimated by this equation and it has been employed by many researches for irradiance modelling. For instance, average active radiation in modelling of a semi-batch photobioreactor has been calculated with Equation (2-18) by Concas et al. (2012), (Concas et al., 2013). Equation (2-18) is also valid when vessel is evenly illuminated from all directions, because the irradiance is an additive property and for every parallel beam can apply Equations (2-11) and (2-18).

Evenly Illuminated

As explained by Evers (1991), the path length of the light in any point inside the vessel at vertical distance, s , from the vessel surface with respect to Figure 2-6 should be calculate based on Equation (2-19):

$$p(\alpha, s) = a + b = (R - s) \cos \alpha + [R^2 - (R - s)^2 \sin^2 \alpha]^{0.5} \quad (2-19)$$

A reasonable assumption is that the total irradiance at a given point inside the photobioreactor can be estimated by integrating all the contributions' irradiance from all direction. Any point inside the vessel receives light from all directions ($0 \leq \alpha \leq$

2π), but because of symmetry, it is sufficient to integrate Beer-Lambert Law for $0 \leq \alpha \leq \pi$:

$$I(s, \alpha) = \frac{1}{\pi} \int_0^\pi I_o \cdot \exp(-K_a C_b [(R - s) \cos \alpha + [R^2 - (R - s)^2 \sin^2 \alpha]^{0.5}]) d\alpha \quad (2-20)$$

This is a bi-dimensional model proposed by Evers (1991) for an evenly illuminated cylindrical vessel when ignores top and bottom effects.

Grima et al. (1994, Grima et al., 1993) proposed an equation for calculation of average light intensity inside an evenly illuminated cylindrical vessel considering the path length, p , and light intensity, $I(s, \alpha)$:

$$I_{av} = \frac{I_o}{\pi R} \int_0^R \int_0^\pi \exp(-K_a C_b [(R - s) \cos \alpha + [R^2 - (R - s)^2 \sin^2 \alpha]^{0.5}]) ds d\alpha \quad (2-21)$$

This equation has been successfully employed to investigate on-line control of light intensity in microalgae production (Meireles et al., 2008), development and scale up of photobioreactor (Walter et al., 2003) as well as cultivation optimisation in photobioreactors (Barbosa et al., 2003).

Furthermore, as explained above, average light can be calculated through equations (2-10) and (2-16), then for a cylindrical reactor evenly illuminated from all sides, Figure 2-5, and if use r instead of $(R - s)$ and remembering that $dV = \pi r H dr$, is differential volume for every element in a semicircle (Grima et al., 1997):

$$I_{av} = \frac{\frac{1}{\pi} \int_0^R \int_0^\pi I_o \cdot \exp[-K_a C_b (r \cos \varphi + (R^2 - r^2 \sin^2 \varphi)^{0.5})] \pi r H dr d\varphi}{\pi R^2 H} \quad (2-22)$$

$$I_{av} = \frac{I_o}{\pi R^2} \int_0^R \int_0^\pi \exp(-K_a C_b [r \cos \varphi + [R^2 - r^2 \sin^2 \varphi]^{0.5}]) r dr d\varphi \quad (2-23)$$

All these bi-dimensional Equations ((2-18), (2-21) and (2-23)) were used in expounding light gradients, nevertheless, they neglect light variations along the vertical axis.

2.7.2.3 Three-Dimensional Model

The following model is a three-dimensional model for estimation of the radiation field at any point inside a reactor which indicates variations with height, H , light path, P , and angle of incidence of the light ray, ϕ . In this model, two concentric right cylinders have been considered (Figure 2-7). The inner cylinder with radius, R , represents bioreactor while the outer cylinder with radius, R_s , represents the light source. It is assumed that the light source is continuous with uniform intensity (Zolner and Williams, 1971).

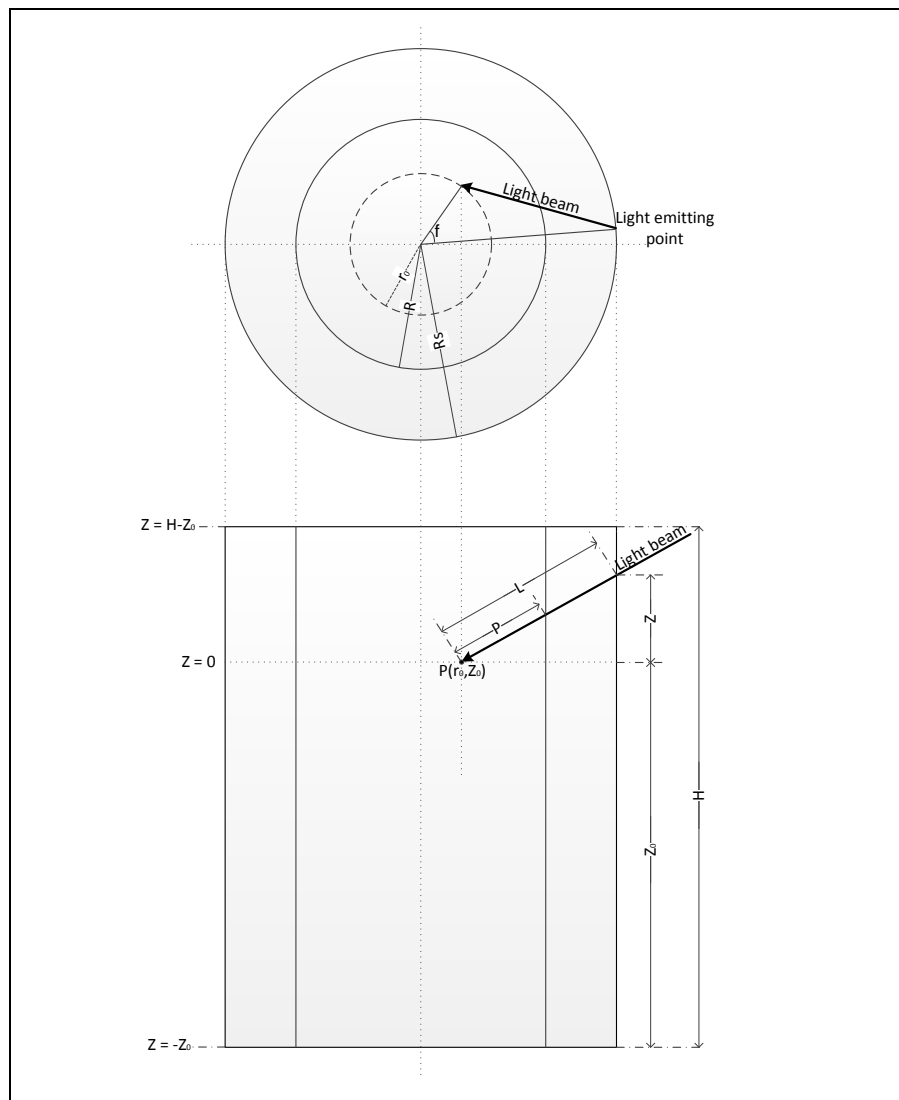


Figure 2-7 Schematic of three-dimensional light distribution model

So the local light intensity can be calculated by:

$$I_p(r_o, z_o) = \int_0^{z_o} \int_0^{2\pi} \exp(-K_a C_b P(r_o, z, \varphi) dI_o(z, \varphi) + \int_0^{H-z_o} \int_0^{2\pi} \exp(-K_a C_b P(r_o, z, \varphi) dI_o(z, \varphi) \quad (2-24)$$

$$dI_o(z, \varphi) = \frac{I_o R_s d\varphi dz}{R_s^2 + r_o^2 + z^2 - 2R_s r_o \cos(\varphi)} \quad (2-25)$$

$$P(r_o, z, \varphi) = \sqrt{R^2 - 2r_o R \cos(\varphi) + r_o^2 + z^2} \quad (2-26)$$

when $R_s \rightarrow \infty$, the model is reduced to a bi-dimensional model same as that used by Evers (1991) and there is a flat radiation profile along the vertical axis (Grima et al., 1996). It has been proved that both two-dimensional and three-dimensional models acceptably resemble I_p against the experimental data, although the more complex model being found more accurate (Grima et al., 1996).

Again Equation (2-10) can be used for average irradiance calculation while Equations (2-24) and (2-26) are using to estimate local light intensity. As stated by Grima et al (1996):

$$I_{av} = \frac{\int_0^H \int_0^R \int_0^{2\pi} I_p(r_o, z_o) d\varphi dr dz}{V_T} \quad (2-27)$$

Then calculated average irradiance is used to estimate growth rate, μ . This means growth rate is assumed to be a function of average irradiance. It is different from calculating growth rate in any point as a function of local irradiance and then averaging growth rate for the whole culture volume. Evers (1991) considered later procedure, which not only is difficult to give a physiological meaning to model parameters, but also is unrealistic to assume that a cell can adopt itself to different amount of light in the vessel quick enough (Grima et al., 1996). Actually, there is experimental evidence that shown growth rate does not change by short variations in light regime. It seems that photosynthetic cell is able to reserve a certain amount of light energy so that it can continue to do photosynthesis for a short time after light

reduction or interruption, as stated by Grima (1996), this has been approved for both flashing light (Phillips Jr and Myers, 1954) and for light/dark cycle (LEE and PIRT, 1981).

2.7.3 Radiative Transfer Model

The bottleneck of light transfer in microalgae culture due to both absorption and scattering of light by bubbles, medium and microalgae particles is why many researchers investigated and still looking for an accurate modelling equation. Indeed, heterogeneous light distribution inside the culture leads to local reaction rates, therefore local equation must be derive to calculate local available light intensity and total absorbed photon flux. The well-known and simple Beer-Lambert model is widely used for light attenuation modelling inside the photobioreactor, but because of inaccuracy of this model, some researchers have tried to use radiative transfer concept to model light distribution inside the photobioreactors.

Radiation transfer takes into account both phenomena of absorption by pigment of the cell and scattering by the cell which is called shading effect (Cornet et al., 1992b, Modest, 2013), by two independent parameters. In fact, the amount of absorbed photon flux depends not only on the light source intensity and adsorption properties but also on scattering properties. So the available photon in any control volume in the photobioreactor comes from light source and in-scattered light by particles from all directions. Also photon loses due to absorption and out-scattering by particles (Figure 2-8) (Pareek et al., 2008). Difficulty of light distribution modelling inside the vessel is a consequence of heterogeneity of radiation field, unequal distribution of available light energy in any point due to absorption and scattering, as well as various scattering depend on phase function over a 4π solid angle. Radiation energy balance results in complex integro-partial differential equation called Radiation Transfer Equation (RTE) which needs complicated numerical methods and computational developments to be solved. Indeed, there is no analytical solution for RTE and numerical method should be applied (Pareek et al., 2008, Cornet et al., 1992b, Pilon et al., 2011) which is quite sophisticated long calculation solution especially for modelling of dynamic process of microalgae growth.

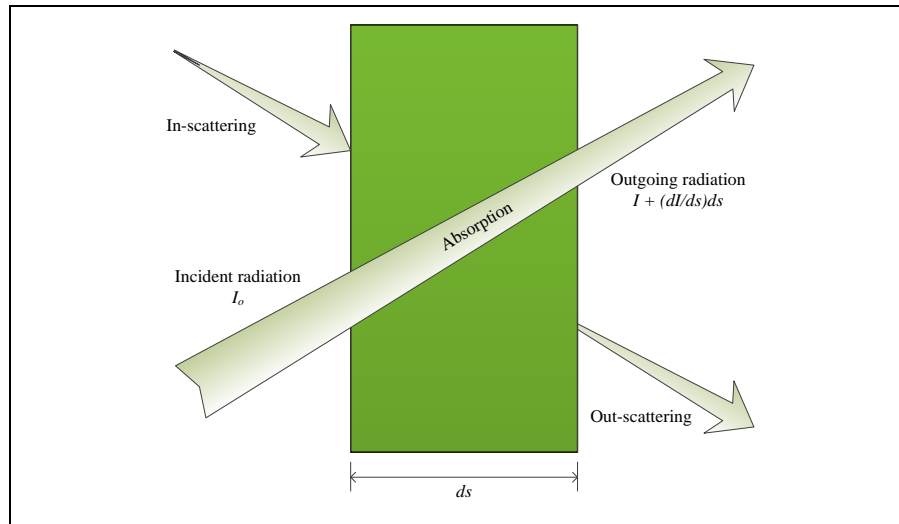


Figure 2-8 Radiation Balance

The radiative heat transfer and also thermal radiation occurred due to electromagnetic waves since all material can absorb or emit electromagnetic waves or photons (massless energy parcels) when their molecular energy raises or lowers. Thermal radiation is different and more powerful than other energy transferring mechanism including conduction and convection. While movement of electrons and molecules through medium are responsible for transferring energy in conduction and convection, respectively; thermal radiation does not need medium for transferring. On the other hand, thermal radiation is proportional to the fourth power of temperature instead of linearly depends on temperature differences (Modest, 2013). An electromagnetic wave can be partially or totally reflected or absorbed when travel through a medium. Furthermore, a medium continuously emits thermal radiation depends on its temperature and material.

Solid angle is two-dimensional angular space and can be vary between 0 and 2π while one-dimensional angle is between 0 and π (Modest, 2013). Figure 2-9 is an illustration of solid angle, Ω , and it can be calculated from bellow equation for seeing infinitesimal surface dA_j from point P :

$$d\Omega = \sin\theta \, d\theta \, d\psi \quad (2-28)$$

When θ is the angle with z axis and ψ is the azimuthal angle in spherical coordinate. By integration this equation over all possible directions:

$$\int_{\psi=0}^{2\pi} \int_{\theta=0}^{\pi} \sin \theta \, d\theta \, d\psi = 4\pi \quad (2-29)$$

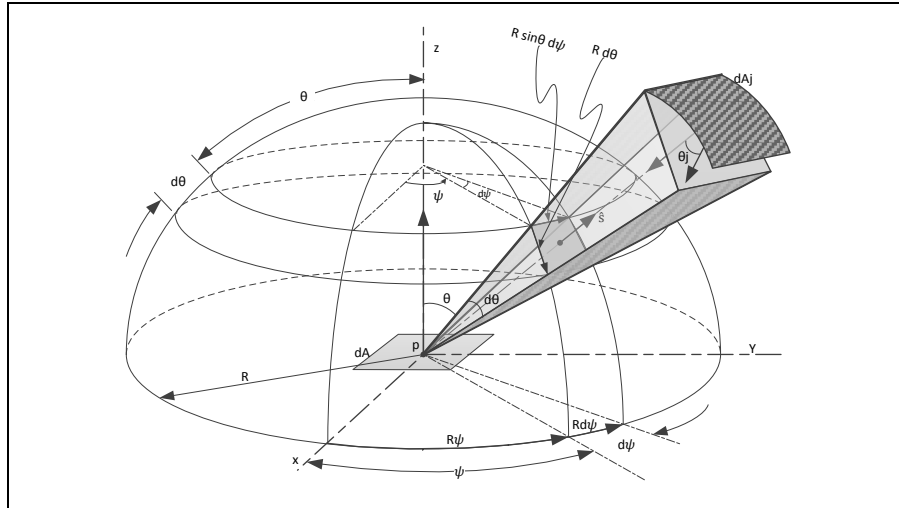


Figure 2-9 Radiation direction and solid angle

Two parameters of position and direction are necessary to characterize the light path. Then total radiative intensity per unit area and unit solid angle, I , is defined (Modest, 2013):

$$I(r, \hat{s}) = \int_0^{\infty} I_{\lambda}(r, \hat{s}, \lambda) \, d\lambda \quad (2-30)$$

When I_{λ} is spectral radiative intensity, r , is position vector and \hat{s} is unit direction vector. Then local incident radiation intensity at any point from all direction for isotropic radiation is equal to:

$$G_{\lambda}(r) = \int_{\Omega=0}^{\Omega=4\pi} I_{\lambda}(r, \vec{s}) \, d\Omega \quad (2-31)$$

By integration Equation (2-31), total local incident radiation intensity can be calculated for polychromatic radiation (Zhongming et al., 2012):

$$G(r) = \sum_{\lambda_{min}}^{\lambda_{max}} G_{\lambda}(r) \quad (2-32)$$

Therefore, this total local instantaneous irradiance can be coupled with growth kinetic model to predict local instantaneous microalgae growth which must be integrated over working volume to find average volumetric growth rate (Cornet et al., 1998). Meanwhile, volumetric averaged local intensity can be calculated as following (Pareek et al., 2008):

$$\langle G \rangle = \frac{1}{V} \int_0^V G dV = \frac{\sum_{i=1}^{N_c} G_i \Delta V_i}{\sum_{i=1}^{N_c} \Delta V_i} \quad (2-33)$$

and net radiant energy flux:

$$F_{\lambda} = \int_{4\pi} I_{\lambda}(\vec{s}) \cos\theta d\Omega \quad (2-34)$$

The radiative transfer theory which proposed by Chandrasekhar (1960) for astrophysical field has been successfully used to model light distribution in photobioreactors (Aiba, 1982, Cornet et al., 1992b, Cornet et al., 1994, Daniel et al., 1979, Incropera and Thomas, 1978, Spadoni et al., 1978) afterward.

2.8 Photosynthesis Efficiency

Microalgae do not absorb all incoming light (due to reflection, respiration requirements of photosynthesis) and do not convert all harvested energy into biomass, which results in low photosynthetic efficiency. Nevertheless, while the potential of CO₂ absorption by terrestrial plants is only 3-6 % of CO₂ that discharge from fossil fuels, microalgae have the ability to absorb CO₂ with the efficiency of 10 to 50 times more. Furthermore, appropriate cultivation systems of microalgae may lead to higher efficiency (Lan, Wang et al., 2008). Therefore, the first step is that to determining the efficiency based on productivity and/or CO₂ biofixation that can be achieved by selected microorganism. Photosynthetic efficiency can be evaluated

from O₂ generation as a function of absorbed light, but to find a technically reliable yield, measuring biomass production rate instead of O₂ generation has been suggested (Grima et al., 1997). So the best suggestion is quantum yield based on biomass generation since it can give us a sense of the biomass productivity caused by absorbed light.

Quantum yield is considered to be scale of photosynthesis efficiency. It is defined as the ratio of produced biomass to absorbed photon flux (Grima et al., 1997). Hence, it can be calculated by the following expression:

$$\Psi_E = \frac{P_b}{F_{Vol}} \quad (2-35)$$

where P_b stands for the biomass productivity and F_{Vol} for absorbed photon flux, both in volume unit. Mentioned yield based on mass of biomass (g E^{-1}) can be converted to energy unit which is named Ψ_{KJ} (KJ E^{-1}). Also the bioenergetics yield, Ψ , can be calculated by taking into account the biomass combustion heat, Q_b :

$$\Psi = \Psi_{KJ} \cdot Q_b \quad (2-36)$$

In this way, the percent of the light energy that is converted to chemical energy is quantified. As stated by Bergeijk (2010) photosynthesis efficiency is defined as the energy stored in biomass per unit of used light (van Bergeijk et al., 2010), which is in agreement with Equation (2-36):

$$\begin{aligned} & \text{photosynthesis efficiency} \\ & = \frac{\text{productivity (g DW m}^{-3}\text{d}^{-1}) \times \text{energy content (kJ g}^{-1})}{\text{irradiance (kJ m}^{-3}\text{d}^{-1})} \times 100 \% \end{aligned} \quad (2-37)$$

when:

$$\text{productivity (g DW m}^{-3}\text{d}^{-1}) = P_b = \frac{C_{bt} - C_{b_0}}{t} \quad (2-38)$$

Biomass productivity, P_b , can be calculated when biomass concentration, C_b and initial biomass concentration, C_{b_0} , are given. Therefore, with estimation of

absorbed photon flux, F_{Vol} , yields defined by Equations (2-35) and (2-36) can be readily evaluated. The major question is how to assess the absorbed light by the culture. In fact there is a light gradient along the radius of the culture because of light scattering, shading as well as light absorption. Therefore, the necessity of real understanding of light distribution inside the culture can be deduced.

2.9 Absorbed Photon Flux

The major goal is assessment of photosynthesis efficiency which has been defined by Equation (2-35). The most important factors that could lead to misevaluation is light scattering, therefore, is necessary to evaluate every case by direct measurement of outlet light. Consider the following photon flux balance:

$$\text{Incoming flux} = \text{Absorbed flux} + \text{Outgoing flux} \quad (2-39)$$

For a parallelepiped vessel with vessel optical path, L and crossed surface by light rays, S , it gives:

$$F_T = S \cdot I_o - S \cdot I_o \cdot \exp(-K_a C_b L) \quad (2-40)$$

where F_T stands for total absorbed photon flux. Dividing this equation by the vessel volume can be readily estimated the volumetric photon flux:

$$F_{Vol} = \frac{F_T}{V} = \frac{S \cdot I_o}{L \cdot S} (1 - \exp(-K_a C_b L)) = \frac{I_o}{L} (1 - \exp(-K_a C_b L)) \quad (2-41)$$

Compare Equation (2-41) with Equation (2-12) which is average light intensity inside the reactor, prove that:

$$F_{Vol} = I_{av} \cdot K_a \cdot C_b \quad (2-42)$$

Thus, absorbed photon flux in unit volume, F_{Vol} , can easily be obtained once I_{av} is known and in this case it is independent of system geometry (Grima et al., 1997). That means Equation (2-42) can be used for any type of reactor as long as I_{av} is distinguished. Therefore, by calculating the average light intensity and absorbed

photon flux, it is easy to estimate photosynthesis efficiency by Equations (2-35) and (2-36).

The validity of the results from Grima et al (1997) has been proved with data published by Lee et al (1984) (1987). Based on this comparison, Equations (2-27) and (2-35) are accepted as a reliable procedure for calculation of quantum yield. Lee et al (1984) used differences between the incoming and outgoing photon flux to calculate absorbed light and then Equations (2-44) and (2-45) for efficiency estimation:

Total light energy in

= energy incorporated into biomass

+ energy leaving by radiation, conduction and convection (2-43)

Therefore:

$$I_a \cdot A = \frac{q_v \cdot C_b \cdot \sigma_b \cdot \gamma_b \cdot q_o}{12} + Q_h \quad (2-44)$$

or:

$$\Psi = \frac{D \cdot \sigma_b \cdot \gamma_b \cdot q_o}{12 \cdot \left(\frac{I_a \cdot A}{C_b \cdot V}\right)} \quad (2-45)$$

where $q_v, C_b, \sigma_b, \gamma_b, I_a, A, V, D$, represent volumetric flow rate (L/h), biomass concentration (g/L), the weight fraction of carbon in biomass, the degree of reduction, absorbed energy (kcal/cm² h), illuminate surface (cm²), volume of the culture (L) and dilution rate (h⁻¹), respectively, and q_o is the energetic content equivalent of electrons of organic carbon which is equal to 113 kJ eq⁻¹ e⁻¹ (Lee et al., 1984).

Therefore, Ψ can easily be estimated as long as the value of Q_b is known. This can be calculated by considering the average biochemical profile of the biomass with considering enthalpy of different substances in biomass such as Protein, Lipids and Glucides. In this way, mean value for Q_b obtained 21.4 kJ g⁻¹ by Grima et al (1997) which is in agreement with 22.2 kJ g⁻¹ from Payne (1970), 21.0 kJ g⁻¹

proposed by Aiba (1982) and/or 22.15 kJ g⁻¹ through Renaud's research (Renaud et al., 2002) .

According to Lee et al (1987), the combustion heat, Q_b can deduce from following equation when $C_1H_bO_cN_d$ express the stoichiometry of the biomass:

$$Q_b = \frac{\sigma_b \cdot \gamma_b \cdot q_o}{12} \quad (2-46)$$

where the carbon fraction, σ_b and degree of reduction, γ_b can be calculated from:

$$\sigma_b = \frac{12}{1 \times 12 + b \times 1 + c \times 16 + d \times 14} \quad (2-47)$$

$$\gamma_b = 4 + b - 2 \times c - 3 \times d \quad (2-48)$$

As explained, absorbed photon flux can be calculated by Equation (2-42) for a certain biomass concentration when absorption coefficient and average light intensity are known.

2.10 Optical Properties

2.10.1 Attenuation Coefficient

Based on Beer-Lambert Law the attenuation of light through the culture depends on attenuation coefficient, K_a . It can be assumed constant and be calculated through experimental spectrophotometric absorbance measurements for samples at different biomass concentrations. Although attenuation coefficient can be assumed constant for each species, several researchers have reported that it strongly depends on the pigment content of the biomass (Grima et al., 1994, Sukenik et al., 1991, Evers, 1991). For a specific algae species, it is possible to obtain a linear relationship between absorption coefficient and total pigment content. This approach has been adopted by Grima et al. (1994) for *Isochrysis galbana* via measuring light absorbance under different light condition. From plotting absorbance as a function of

biomass concentration and employing Beer-Lambert Law, K_a can readily calculate for each condition:

$$\text{Absorbance} = pK_a C_b \quad (2-49)$$

Figure 2-10 is a schematic plot to show this procedure. Amounts of absorption coefficient for different pigment content can be calculated through Figure 2-10 and Equation (2-50). Plotting these absorbance coefficients as a function of pigment content has shown in schematic Figure 2-11, and simply from this plot can be estimated a linear relationship between absorbance coefficient and total pigment content. The following equation for marine microalga *Isochrysis galbana* is given by Grima et al. (1997):

$$K_a = 1.7356 X_p + 0.0199 \quad (2-50)$$

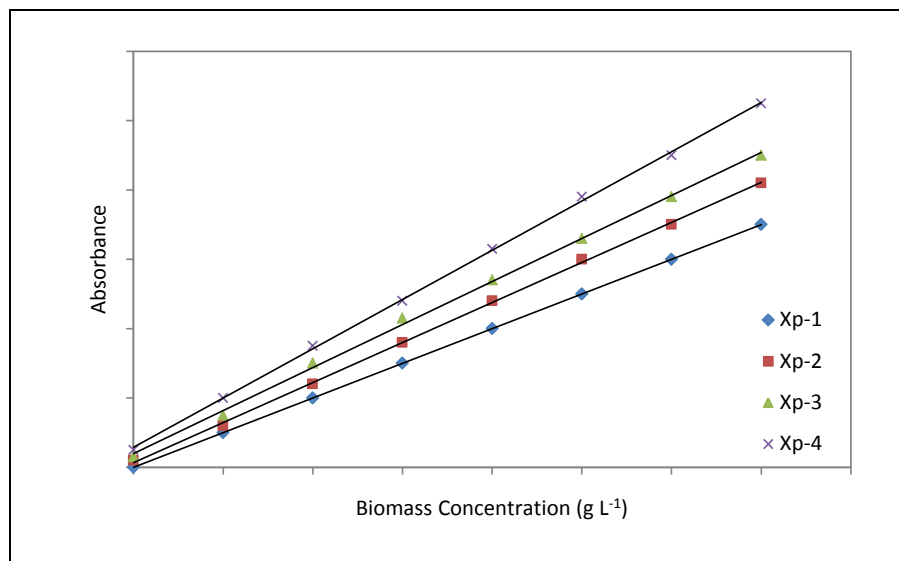


Figure 2-10 Culture absorbance with different pigment composition as a function of biomass concentration

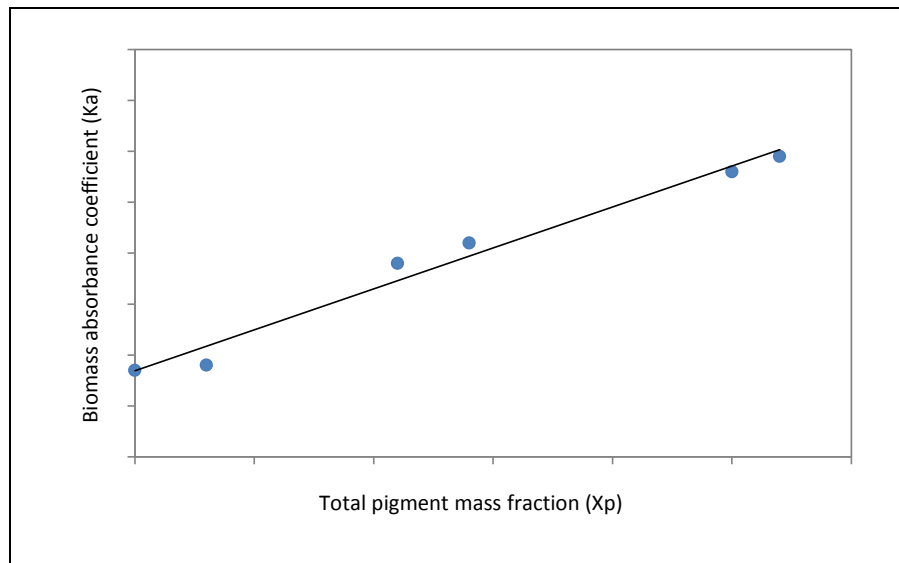


Figure 2-11 Absorption coefficient as a function of total pigment mass fraction

Another example is the following equation which has been used for estimating extinction coefficient of *Haematococcus pluvialis* (García-Malea et al., 2005, Garcia-Malea et al., 2006):

$$K_a = 0.086 + 0.0065 X_{Chlorophylls} - 0.016 X_{Carotenoids} \quad (2-51)$$

where $X_{Carotenoids}$ and $X_{Chlorophylls}$ are the dry weight content of Carotenoids and Chlorophylls, respectively.

Equation (2-52) is another example which was developed to calculate absorption coefficient by linear regression to pigment content when *Phaeodactylum tricornutum* was cultured:

$$K_a = 2.99 X_p + 0.0105 \quad (2-52)$$

Furthermore, light attenuation in microalgae suspension can be estimated by hyperbolic model as a function of biomass concentration, since attenuation does not change linearly with biomass concentration, except in very low concentration of the biomass, (Yun and Park, 2001, Sevilla and Grima, 1997, Lehana, 1990):

$$K_a = \frac{K_{a,max} \cdot C_b}{b + C_b} \quad (2-53)$$

where $K_{a,max}$ and b are maximum attenuation coefficient (m^{-1}) and model parameter, respectively; and they can be estimated by fitting the data for any microalgae species.

Generally, light attenuation coefficient is experimentally calculated by direct measurement of light intensity at two positions with certain path length. To prevent direct measurement errors, light attenuation coefficient, K_a , can theoretically be estimated for different biomass concentration with respect to spectral irradiance of incident light and light absorption spectra of algae suspension (Yun and Park, 2001). In spite of appropriate estimation of attenuation by hyperbolic model, it is not perfect since it does not have logical justification and it just established with respect to curve shape.

2.11 Growth Kinetic Models

A kinetic model which describe specific growth rate as a function of culture conditions is a useful tool for estimating the biomass productivity and viability of the photosynthesis process. Growth rate of microalgae depends on nutrients and light intensity. Actually light intensity besides being energy source, is a substrate. Furthermore, in the case of culturing with excess nutrients, it can be limiting substrate or inhibiting substrate. Overall, growth rate of microalgae depends on amount of light received by the cells (Martinez et al., 2012). Therefore, response to irradiance must be studied for microalgae cultivation in a photobioreactor. Due to the heterogeneous light distribution inside the culture, average light intensity is used to represent available light to the cells. Generally, growth rate increases with increasing irradiance until it reaches to a maximum value, μ_{max} . Further increase in light intensity may actually inhibit growth and photoinhibition occur. Many kinetic models have been proposed to estimate specific growth rate of microalgae, μ , as a function of average light intensity, I_{av} , but not all of them take into account the photoinhibition.

The simple most widely mathematical equation to estimate growth rate of any microorganism is Monod model. In this model effect of substrate on growth rate is described as per Equation (2-54) (Chojnacka and Noworyta, 2004):

$$\mu = \frac{\mu_{max}S}{K_s + S} \quad (2-54)$$

when S stands for substrate concentration, K_s is model parameter and μ_{max} is the maximum value of μ . In a photobioreactor average light intensity, I_{av} , can be consider as substrate while cultivation is carried out under nutrient saturation condition, so Monod equation can be rewritten as:

$$\mu = \frac{\mu_{max}I_{av}}{I_k + I_{av}} \quad (2-55)$$

However, when growth is inhibited by a limiting substrate or limiting light intensity, there will be optimum substrate concentration or optimum light intensity at which the maximum specific growth rate is obtained. To satisfy this condition minimum of two model parameters are needed. Then, the most common kinetic model with two model parameters is a hyperbolic model, Molina-Grima model which is proposed by Grima et al. (1994):

$$\mu = \frac{\mu_{max}I_{av}^n}{I_k^n + I_{av}^n} \quad (2-56)$$

where n and I_k are the model parameters. In this model there is a hyperbolic relation between specific growth rate and average light intensity, thus the growth rate increases with average light intensity until it reaches to maximum growth rate in saturated light intensity. Thereafter, specific growth rate does not change by increasing light intensity, but lack of growth due to photoinhibition and damage of the cells has not been included in this model (Grima et al., 1999, Martinez et al., 2012). This model is a well-known and the most popular equation and has been used by many researchers. This equation applied to simulate biomass growth and productivity in a tubular photobioreactor when average light intensity estimated by the Equation (2-12) (Molina et al., 2001), in spite of popularity, photoinhibition has been disregarded in this Equation (Grima et al., 1999).

Molina-Grima model was improved by Garcia-Malea et al. (2006) and they proposed another hyperbolic model:

$$\mu = \frac{\mu_{max} I_{av}^{(a+bI_0)}}{(c+d)^{(a+bI_0)} + I_{av}^{(a+bI_0)}} \quad (2-57)$$

where I_0 stands for incident light intensity at the surface of the vessel. Maximum specific growth rate characteristic for each strain, and a , b , c and d are constants that can be estimated by non-linear regression so that relates growth rate to average light intensity taking into account photoinhibition (Martinez et al., 2012).

Muller-Feuga (1999), proposed a model to estimate specific growth rate when it relates to saturation specific growth rate, μ_s , saturation light intensity, I_s , and average light intensity, I_{av} , Equation (2-58). At saturation irradiance, system reaches its saturation point; it means it can process all received energy. Then, by increasing light intensity over the saturation point, growth rate reduce because of excess photon flux and cell damage.

$$\mu = \frac{2\mu_s \left(1 - \frac{I_e}{I_s}\right) \left(\frac{I_{av}}{I_s} - \frac{I_e}{I_s}\right)}{\left(1 - \frac{I_e}{I_s}\right)^2 + \left(\frac{I_{av}}{I_s} - \frac{I_e}{I_s}\right)^2} \quad (2-58)$$

Martinez et al. (2012), found that simulation results predicted by Muller-Feuga model are closer to experimental data in compare with results from Garcia-Malea model when cyanobacterium *Synechocystis* sp. cultured at different light intensities. Muller-Feuga model can predict decrease in the specific growth rate after reaching maximum specific growth rate at saturation point which is realistic and was observed in experimental results as well.

Many other kinetic models proposed by researches can be seen in Table 2-6. However, Equations (2-59), (2-60) and (2-61) do not take into account photoinhibition and effect of excessive irradiance (Grima et al., 1999).

Table 2-6 Static kinetic models for light-dependent specific growth rate

Growth model		Reference
$\mu = \frac{\alpha\mu_{max}I}{\mu_{max} + \alpha I}$	(2-59)	(Tamiya et al., 1953)
$\mu = \mu_{max} \left[1 - \exp\left(-\frac{I}{I_{max}}\right)\right]$	(2-60)	(Oorschot, 1955)
$\mu = \frac{\mu_{max}I}{I_{max}} \exp\left(1 - \frac{I}{I_{max}}\right)$	(2-61)	(Steele, 1977)
$\mu = \frac{\mu_{max}I}{(K_t^m + I^m)^{1/m}}$	(2-62)	(Bannister, 1979)
$\mu = \frac{\mu_{max}I}{K_s + I + \frac{I^2}{K_t}}$	(2-63)	(Aiba, 1982)
$\mu = \frac{\mu_{max}I_{av}^{(b+(c/I_o))}}{I_k(1 + (I_o + K_i)^a)^{(b+(c/I_o))} + I_{av}^{(b+(c/I_o))}}$	(2-64)	(Grima et al., 1994)

2.12 Response Surface Methodology for Optimisation

Overall, process optimisation is traditionally accomplished by one-dimensional methods so that experiments are carried out at various values of one factor to find the optimum. Nevertheless, applying this method to find optimum value for few factors is time-consuming, in addition it can lead to inaccurate results since interaction between factors is missed. Statistical experimental designs minimise errors while consider relationships between factors. Optimisation can be done with minimum number of experiments, so enormously economise both material resources and time. Response Surface Methodology (RSM) is one of the most frequently applied tools (Jacob-Lopes et al., 2008a, Martinez et al., 2011). This is cost effective tools for design and optimisation for reducing time and material.

Response surface methodology is a mathematical and statistical technique for optimisation model building. By a particular design of experiments, response (dependent output variable) is optimised which is influenced by several independent input variables. The statistical method calculates the influence of changes in selected variables and their mutual interactions on the process via a specific experimental design. The three steps used in the statistical experimental design and optimisation including statistical design of experiments, estimation of coefficient of a mathematical model using experimental data and then an analysis of model applicability and mathematical optimisation which can be verified by experiment.

The response is increased to a maximum value by change in variables and after that the response starts decrease. Actually, when independent variables depart from their optimum values, dependent variable will fall. To describe this behaviour, model should be at least a second order polynomial. Most of the times, a second order model can explain the observed response, otherwise, a higher order model must be considered (Myers, 2002).

The most common way to design experiments is central composite design (CCD), so that 2^N factorial points (N is number of independent variables) are augmented by additional $2N$ axial points and one central point (Figure 2-12). Three replicates at central points are used to estimate the error.

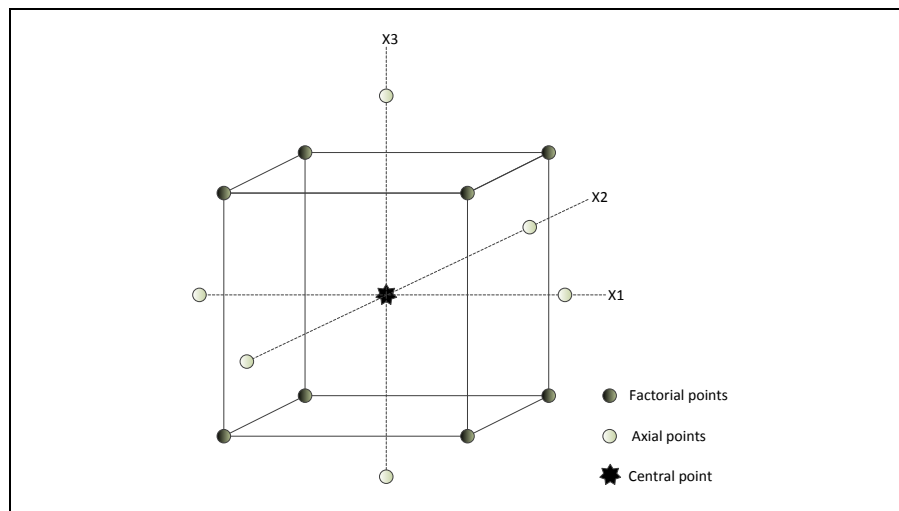


Figure 2-12 Central composite design for three variables

Many research works to find optimum cultivation conditions have been designed by CCD method. For instant, Bartley et al. (2015) used this method to investigate the influence of temperature, salinity and pH on marine microalga, *Nannochloropsis salina*; Karpagam et al. (2015) applied this design to evaluate effect of nutrients including nitrogen, phosphorous and iron on the growth; Muthuraj et al. (2015) also employed CCD tool to design some experiments to optimise seven component of medium. Optimisation of light intensity, agitation speed and temperature was carried out when experiments were designed via CCD (Imamoglu et al., 2015). These are some of the research works in this area that have been successfully done by applying CCD tool under RSM. Also some other researchers used another method of design which is called Box-Behnken Design

(BBD) (Kasiri et al., 2015) (Hallenbeck et al., 2015, Liu et al., 2015). While in CCD experimental points place on the face centres of the bounding box, BBD places experimental points on the edge centres. So BBD mostly is used when central point is not important or feasible (Kasiri et al., 2015, Myers, 2002)

Jacob-Lopes et al. (2008a), optimised three independent variables of CO₂ concentration, temperature and light intensity to achieve maximum CO₂ removal by applying RSM and conducting 17 experiments at designed conditions. They estimated optimum conditions of 15 % CO₂, 35 °C and 11 klux when cultured *Aphanothece microscopica Nägeli*.

This methodology was used to investigate the effects of initial pH, nitrogen and phosphate concentrations on the cultivation of few microalgae strains (Kim et al., 2012). The optimal growth conditions estimated are as follow: *Chlorella* sp., initial pH 7.2, ammonium 17 mM, phosphate 1.2 mM; *D. salina*, initial pH 8.0, nitrate 3.3 mM, phosphate 0.0375 mM and *Dunaliella* sp., initial pH 8.0, nitrate 3.7 mM, phosphate 0.17 mM.

Optimal conditions of light intensity, pH and temperature were estimated to be 686 $\mu\text{mol m}^{-2} \text{s}^{-1}$, 7.2 and 35.3 °C for maximum CO₂ biofixation by *Synechocystis* sp. (Martinez et al., 2011) by conducting 17 experiments when RSM applied. By conducting 12 experiments at different aeration rate and CO₂ concentration and applying RSM, optimum conditions were found to be 0.5 vvm and 6.5 %, respectively, to obtain maximum CO₂ biofixation with *Chlorella vulgaris*. Optimum conditions of initial pH, initial biomass concentration, light intensity and gas flow rate as well as concentration of KNO₃ and K₂HPO₄ in medium were evaluated to screen several microalgae species to find the most suitable one for CO₂ removal and lipid production. For this purpose two set of experiments were designed, each for three parameters at three levels were performed through RSM and it was found that the most suitable strain, *Chlorella* sp. can capture 89.3 % of carbon dioxide while mentioned parameters set at 8.7, 10^{7.5} cells, 4500 lux, 0.03 L min⁻¹, 0.80 g L⁻¹ and 0.06 g L⁻¹, respectively (Tongprawhan et al., 2014).

Some researchers used a multi-objective procedure to optimise two different target functions simultaneously. For instance, Kasiri et al. (2015) optimised CO₂ uptake rate and growth rate using same experimental results when they applied RSM. Many research studies have been done to optimise some chosen parameters at the same time to maximise biomass productivity or CO₂ removal, especially optimising

nutrients in the medium or operation conditions such as pH, agitation speed, gas flow rate, light intensity. But to the best of the authors' knowledge none of them considered the effect of light intensity, light period and carbon dioxide concentration together so far. These factors seem to be the most important parameters and necessary for high density biomass production and high carbon dioxide removal efficiency.

2.13 Summary

This chapter first, discussed necessity of CO₂ biofixation and different approaches for that while explained advantages and disadvantages of each approach. Then it continues with different methods and systems to achieve microalgal CO₂ biofixation as an advantageous sustainable approach which recently came to high attention of researchers. Thereafter, various factors affecting microalgae growth and CO₂ biofixation rate were discussed in details. Meanwhile, a review on researches on these subjects and their results summarised. This chapter was followed by explaining available light intensity and distribution modelling, and then available growth kinetic modelling equations and related studies. This chapter finished by explaining RSM method and its advantages as well as different experimental designs.

To conclude, among the all affecting parameters on microalgae growth and microalgal CO₂ biofixation, light can be a limiting factor in microalgae culturing and besides can be a prohibiting factor, so calculating optimised incident light intensity is remarkably beneficial which is attainable by an appropriate mathematical simulation on light gradient inside the photobioreactor. Except incident light intensity, light period also has a significant role to play to provide required energy for photosynthesis. Due to the dynamics nature of the system and absorption, scattering and shading, light intensity inside a microalgal photobioreactor is accordingly varied in different locations inside the culture and various biomass concentrations. Therefore, each cell inside the photobioreactor is exposed to different light intensity, however can assume that cells illuminated with an average light intensity. Discussed mathematical models have been investigated for continues culturing so that dealing with constant biomass concentration in steady state conditions. Although these equations are function of the biomass concentration, no change in microalgae concentration with time has been considered.

Different kinetic modes to predict biomass growth rate have been discussed. Limiting substrate in microalgae culturing is considered to be light, so an accurate estimate of available photon to the cells is of high importance. By estimating local light intensity and then averaging local light intensity through the whole vessel, average light intensity can be mathematically calculated and be used to estimate growth kinetic of microalgae.

Furthermore, experimental optimisation of the factors is essential task to maximise CO₂ biofixation rate. This target can be achieved by one factor optimisation and this can be repeated for different factors. However, in this way interaction between factors is ignored. By applying RSM interaction of factors come into consideration and it helps to achieve the object with less experiments and material.

3

Experimental Methods and Design

3.1 Introduction

This chapter explains the development of the laboratory equipment and procedures used for carrying out the experimental work of this study. The experimental results are presented in the following chapters. A bioreactor, which is a modified stirred tank reactor with a light enclosure, was used in the experiments. A CO₂ meter and a light meter were used for measuring CO₂ concentration and light intensity, respectively. The design, development, modification, and calibration of the major parts of the experimental equipment were carried out as part of this study.

In this study, a closed photobioreactor under aseptic conditions was used to investigate the productivity and CO₂ biofixation capability of *Chlorella vulgaris*. This strain was chosen because of its ability to produce biomass and CO₂ fixation, in addition to its capability for appropriate growth in Australian weather conditions. A diagram of lab work procedures is illustrated in Figure 3-1. In the following sections, the experimental equipment, their development, modifications, and calibration will be discussed.

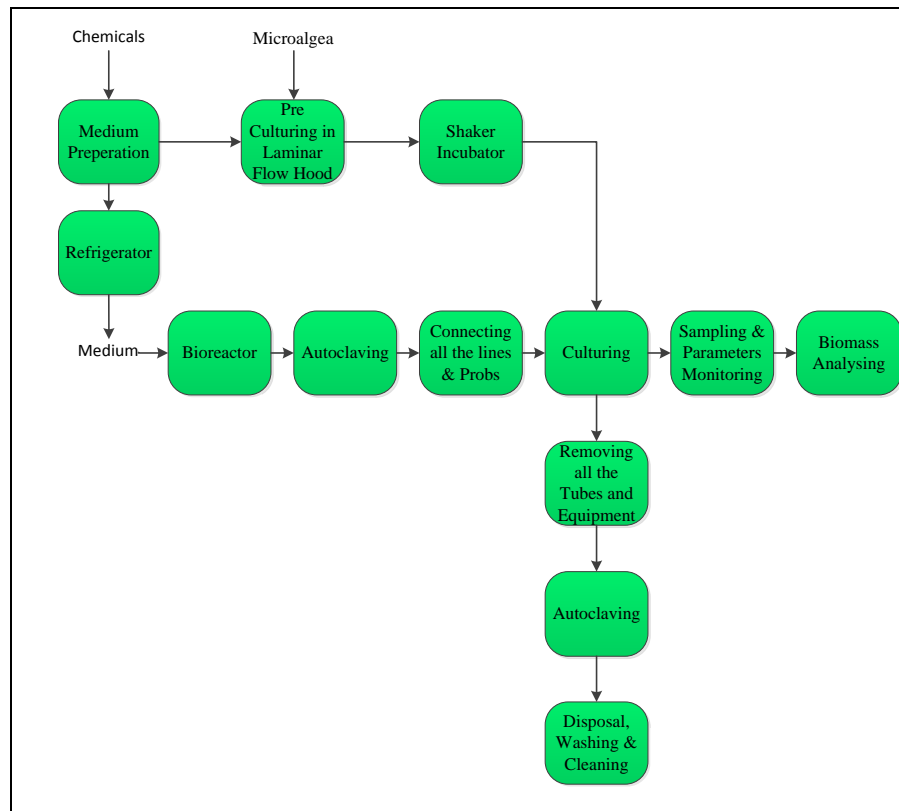


Figure 3-1 Lab work diagram

3.2 Microalgae and Medium

The freshwater microalgae strain *Chlorella vulgaris* was cultivated in this experiment. A culture of *C. vulgaris* (CCAP 211/11B, CS-42) was obtained from ANASS (Australian National Algae Supply Service), CSIRO (Commonwealth Scientific and Industrial Research Organisation), Tasmania, Australia. The culture was dispatched in a 250 ml tissue-culture flask and immediately subcultured to fresh media after arrival (Figure 3-2).

C. vulgaris was cultivated in fresh MLA media based on the CSIRO recipe, which was derived from the ASM-1 medium reported in Gorhan et al. (1964). To prepare media, we used five separate stock solutions, including $\text{MgSO}_4 \cdot 7\text{H}_2\text{O}$, NaNO_3 , K_2HPO_4 , H_3BO_3 and H_2SeO_3 . We also used a vitamin stock solution containing biotin, vitamin B12 and thiamine HCl, and micronutrient stock solutions including Na_2EDTA , $\text{FeCl}_3 \cdot 6\text{H}_2\text{O}$, NaHCO_3 , $\text{MnCl}_2 \cdot 4\text{H}_2\text{O}$, $\text{CuSO}_4 \cdot 5\text{H}_2\text{O}$, $\text{ZnSO}_4 \cdot 7\text{H}_2\text{O}$, $\text{CoCl}_2 \cdot 6\text{H}_2\text{O}$ and $\text{Na}_2\text{MoO}_4 \cdot 2\text{H}_2\text{O}$, and separate stock solutions of NaHCO_3 and $\text{CaCl}_2 \cdot 2\text{H}_2\text{O}$. All chemicals used in this study were of analytical grade and supplied by Sigma Aldrich or Perth Scientific. Media can be filter sterilised or

fully autoclaved. In this study they were fully sterilised. For this reason, the sodium bicarbonate concentration was adjusted to reduce precipitation. Before autoclaving, the pH of media must be adjusted from 7.5 to 8.0 with HCl; however, often no adjustment is necessary. For autoclave sterilisation, 15 mins at 121 °C followed by cooling down overnight is recommended. Finally, the media had the following composition (in mg L⁻¹): MgSO₄·7H₂O 49.4; NaNO₃ 170; K₂HPO₄ 34.8; H₃BO₃ 2.47; H₂SeO₃ 1.29×10⁻³; Biotin 50×10⁻⁶; Vitamin B12 50×10⁻⁶; Thiamine HCl 0.1; Na₂EDTA 4.36; FeCl₃·6H₂O 1.58; MnCl₂·4H₂O 0.36; CuSO₄·5H₂O 0.01; ZnSO₄·7H₂O 0.022; CoCl₂·6H₂O 0.01; Na₂MoO₄·2H₂O 6×10⁻³; NaHCO₃ 17.5; CaCl₂·2H₂O 29.4.

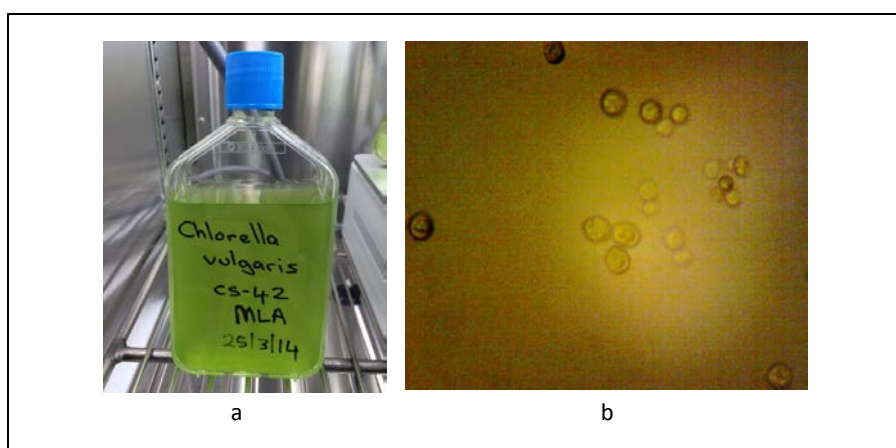


Figure 3-2 a) Tissue-culture flask from CSIRO, and b) microscopic photograph of *Chlorella vulgaris*

3.3 Subculturing

A culture of the selected strain was received from the CSIRO and subcultured immediately into appropriate growth media. A small amount of the original culture was kept in reserve. It can survive for two to four weeks under correct storage conditions.

A 300 litre capacity refrigerated cycling incubator (LABEC, ICC36) equipped with shelf lighting of two sets of 4 and 10 W fluorescent lamps provided a temperature- and light period-controlled environment for stock cultures. A rotational benchtop shaker (LABEC, J-USRC) was placed inside the incubator to shake Erlenmeyer flasks of stock culture (Figure 3-3).



Figure 3-3 a) Refrigerated incubator, and b) shaker

Stock cultures were propagated every two weeks by aseptically transferring 20 ml of old culture to 200 ml autoclaved fresh medium in a 250 ml Erlenmeyer flask. All stock cultures, including grandparent, parent and daughter, were kept inside the refrigerated incubator equipped with four 10 W daylight fluorescent tubes, so that a photon flux density of approximately $80 \mu\text{mol m}^{-2} \text{s}^{-1}$ was supplied to the flasks, with a light:dark period of 12:12 h. Temperature was controlled at 25 °C. To prevent sedimentation, Erlenmeyer flasks were continuously shaken in a rotational shaker at 200 rpm and occasionally shaken by hand to prevent microalgae from adhering to the inside surface of the glass. Unwanted old cultures were sterilised in an autoclave for 30 minutes at 121 °C. A schematic diagram is presented in Figure 3-4.

provided for pH, DO, agitation speed, broth temperature, the feeding or harvesting pump, liquid level, and foam. The bioreactor and all accessories were connected to a control cabinet for the monitoring and control of these factors (Figure 3-5).

Precise temperature control was achieved through a cool water jacket, heater and PI controller. The broth temperature was sensed by the RTD immersed in the thermowell. A refrigerated cooling bath was attached to the bioreactor to supply coolant to the water jacket, and the vessel sat on the jacket water heater. Through this cooling and heating system and the PI controller, the temperature could be controlled precisely. The culture temperature set point was selectable within the range of 20-70°C above the coolant temperature. The jacket water heater was equipped with a magnetic stirrer to achieve uniform temperature inside the jacket water.

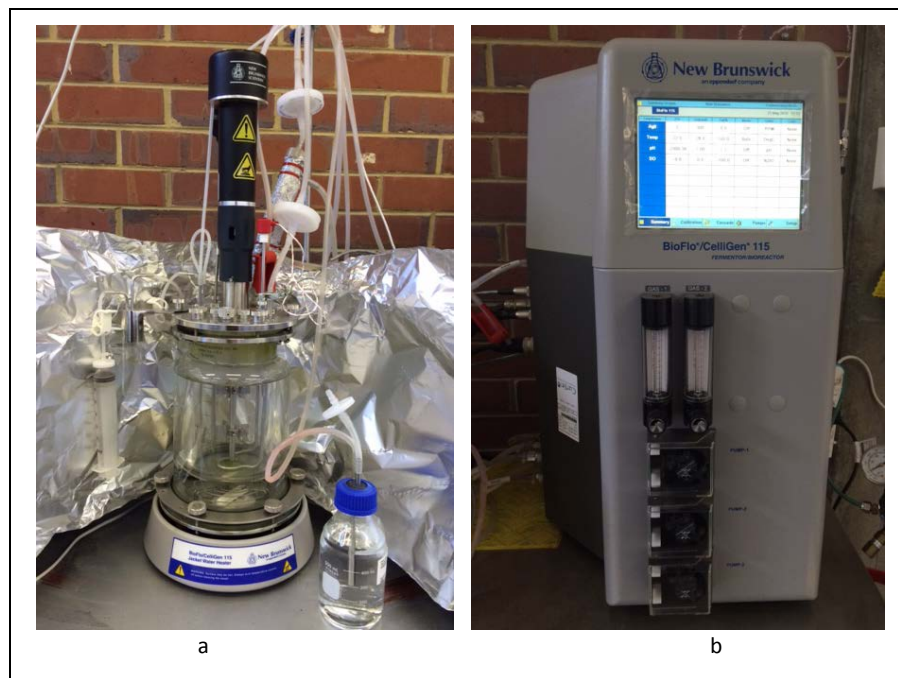


Figure 3-5 a) Bioreactor. b) Control cabinet

Dissolved oxygen and pH were monitored daily through the DO and pH meters installed at the top of the bioreactor. The DO and pH levels were sensed by a polarographic DO electrode and a gel-filled pH probe, respectively. Both were dedicated bioreactor accessories and were autoclavable (Figure 3-6). Additionally, two level probes were placed on the bioreactor head plate to monitor and control the liquid level. Make up water could be added to the vessel, and broth could be harvested automatically or manually using dosing pumps. Pumps were set to turn on

or off in response to the absence or presence of liquid. Three dosing pumps were fixed to the control cabinet.

Furthermore, the bioreactor was equipped with an agitation system comprising a motor and impeller. The agitation motor was located on top of the head plate and was removable. It could be easily disconnected before autoclaving the vessel and replaced afterwards. The agitation system had a speed range of 50 to 1200 rpm and was controlled with the PI controller. The impeller was made of stainless steel and was a Rushton-style standard.

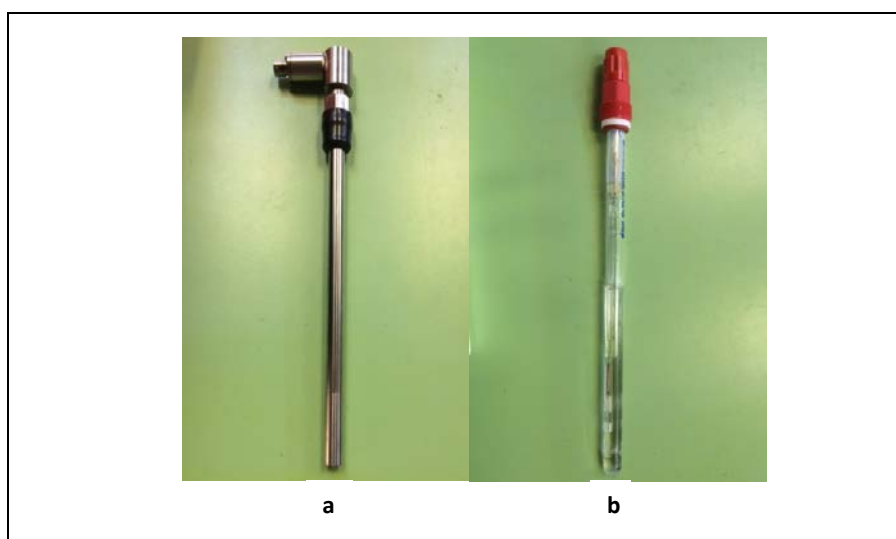


Figure 3-6 a) DO probe and b) pH probe

The control cabinet of the bioreactor was equipped with two push-in type gas tube connections on the rear panel. All gases were regulated using a two stage regulator, with the second stage regulating pressure from 3 to 10 psi. The gas was regulated at the minimum pressure to maintain the desired flow rate. Atmospheric air was supplied from an air compressor in the laboratory. A cylinder of pure CO₂ was ordered from BOC (British Oxygen Company, Ltd.). It was an anaerobic size E CO₂ cylinder with a purity of > 99.95 %. Moisture was reported as < 50 ppm, hydrocarbons (as methane) < 20 ppm, oxygen < 20 ppm, sulphur compounds < 0.5 ppm, and nitrogen oxides < 0.5 ppm. With separate gas sources of air and CO₂, two rotameters and a CO₂ meter (G110-10N, VIASENSOR), it was easy to regulate and supply the gas mixture with the desired concentration of CO₂. The CO₂ analyser was designed for accurate measurement of CO₂ percentage in a gas stream. It had a measurement range of 0—100 % CO₂ with an accuracy of ± 1 %, and allowed for quick verification of CO₂ levels and storage of large amounts of data (Figure 3-7).

The bioreactor included two gas inlet ports and two manual rotameters to adjust the flow rate. Gases were mixed, and then the inlet mixture was passed through a 0.2 μm PTFE membrane (Acro 50 PTFE vent filter, PALL) to remove living organisms, and then injected into the bottom of the bioreactor through a ring sparger that was placed centrally below the impeller. The exhaust gases passed through the exhaust condenser where moisture was condensed and returned to the vessel. The remaining gases then left the system through another 0.2 μm PTFE filter. After autoclaving, and also periodically, the exhaust condenser and filter were checked to ensure they were unobstructed. It was especially important to check that the particulate filter was not blocked due to autoclaving.

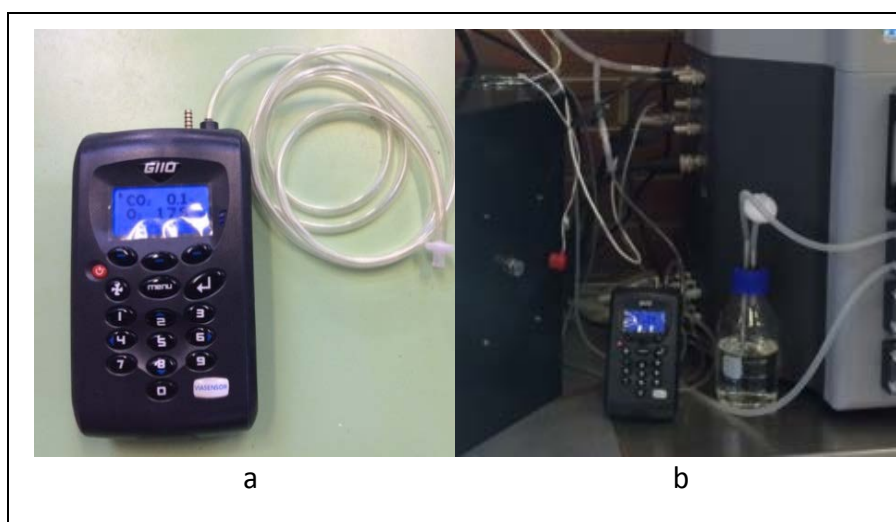


Figure 3-7 a) CO₂ analyser and b) CO₂ analyser connected to experimental setup.

The experiment was performed in batch mode so that gas continuously aerated a batch of broth inside the bioreactor. Culture samples were collected easily via a sampling port and syringe connected to the vessel. A schematic diagram and photo of the photobioreactor and cultivation system are shown in Figure 3-8.

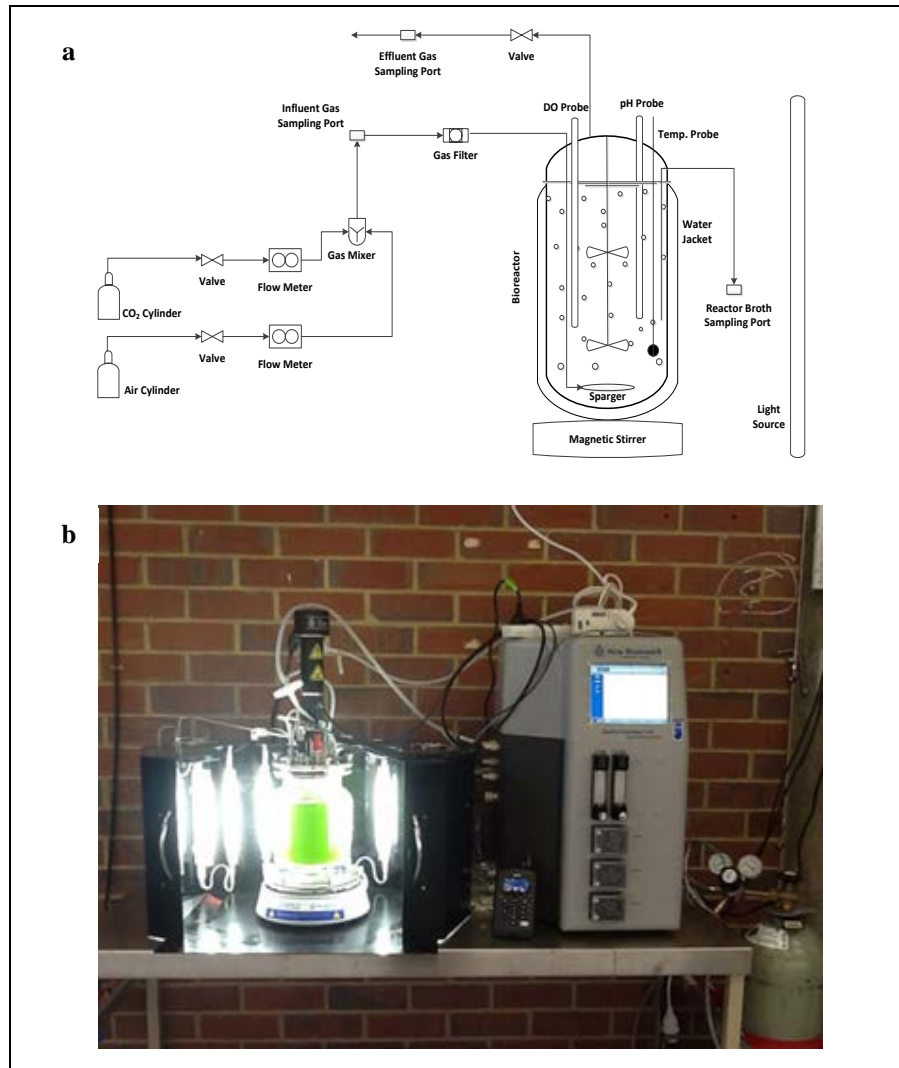


Figure 3-8 a) Experimental set up for the photobioreactor and b) Photobioreactor in the light enclosure.

3.4.2 Light Enclosure

A light enclosure was designed in the shape of an octagon, with sixteen 6 W cool white fluorescent tubes affixed inside (Figure 3-9). To prevent high temperatures inside the light enclosure, two fans were installed on top to generate airflow. Both the number of lamps, and the distance between the lamps and surface of the bioreactor were adjustable. This allowed adjustment of the light intensity emitted to the bioreactor surface. The bioreactor was surrounded by the light enclosure and was adjusted so that the desired light intensity was obtained. The light period was controlled by a timer switch.



Figure 3-9 Light enclosure

3.4.3 Cultivation procedure

To perform culturing in aseptic conditions, fresh media were added to the bioreactor and then sterilised for 15 minutes at 121 °C in a steam pressure autoclave (LABEC, AA20-HT; Figure 3-10). The autoclave had a stainless steel vessel of 100 L capacity, digital temperature and pressure settings, and a 0–300 h timer. Heating was done by electrical elements immersed in the base of the vessel. An electric switch turned off the power when the water level was below the minimum level required to protect the element. After autoclaving, the bioreactor was left inside the autoclave to cool down overnight. This was to minimise the amount of precipitate that occurred due to the presence of sodium bicarbonate in the media. As per CSIRO recommendations, the sodium bicarbonate for fully autoclaved media was reduced to one tenth (Sacasa Castellanos, 2013) and pH was maintained within 7.5–8.0 using 0.1 M HCl and 0.1 M NaOH (Chang et al., 2016); however, often no adjustment was necessary.

Afterwards, the bioreactor was connected to the control cabinet and the inlet gas tube, cooling water tubes, make-up tube, and pH and DO probes were connected. Also, the RTD sensor was inserted into the thermowell. The pH probe was calibrated before fixing to the bioreactor. It was calibrated using two external buffer solutions of known pH, usually 7.00 and 4.00. The pH probe calibration was checked after autoclaving, immediately prior to inoculation. To validate the pH calibration, the pH of a sample withdrawn from the bioreactor was measured using an external pH meter and compared with the pH value displayed on the control cabinet screen, and any

discrepancies were adjusted. The DO-electrode was polarised overnight after autoclaving and then calibrated.



Figure 3-10 Autoclave

Prior to every experimental run, a subculture of inoculum was prepared as explained in Section 3.3. Inoculation was performed by aseptically transferring stock culture with a two week lifetime to the bioreactor with a 1:10 inoculum ratio. Samples were taken for further analysis immediately after inoculation and daily at a regular time. Meanwhile, a sample of stock culture was taken and analysed to measure biomass concentration. Temperature, pH, aeration rate, and DO and CO₂ concentrations in the inlet and outlet tubes were monitored constantly. A schematic diagram of the procedure is illustrated in Figure 3-11.

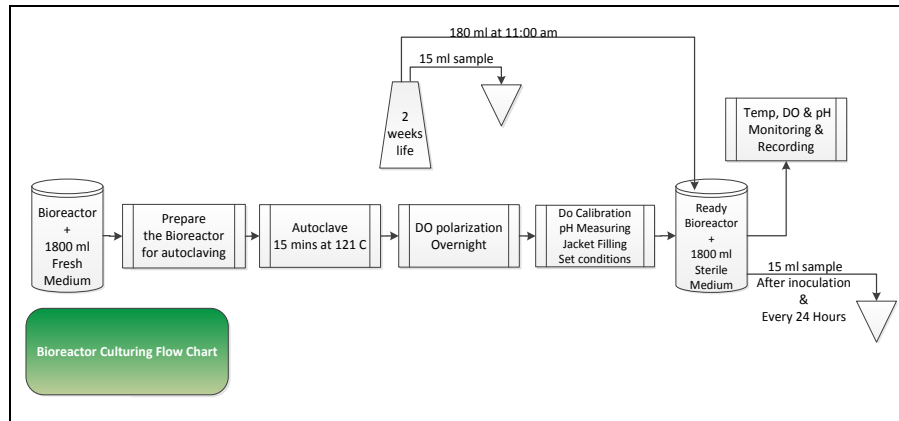


Figure 3-11 Diagram of cultivation procedure

3.4.4 Calibration and sterilisation

Enough medium was added to the bioreactor and then both were sterilised at 121 °C in a floor model steam autoclave (LABEC, AA20-HT; Figure 3-10). Before sterilising, the pH probe required calibration. This was done with two external buffer solutions, usually pH 7.00 and 4.00, while the pH probe was connected to the control cabinet. Then, the pH probe was installed in the bioreactor headplate. Additionally, pH calibration was checked after autoclaving and before inoculation. The DO probe was installed in the bioreactor headplate prior to sterilisation.

Prior to autoclaving, the motor was removed from top of the vessel and all gas and water lines were disconnected. The harvest tube, sample tube and all other tubes immersed in the media were clamped off. However, the gas outlet tube was not clamped off, to allow ventilation. The glass sample bottle was loosened and the water jacket was half full. All filters were wrapped with aluminium foil to protect them from steam, but the foil on the outlet filter was left loose to allow for ventilation. Immediately after autoclaving, the aluminium foil on the filters was closed off to maintain sterility. The bioreactor was left to cool down inside the autoclave overnight to minimise the formation of precipitants.

The day after autoclaving, the bioreactor was connected to the control panel and all probes and tubes were connected as appropriate. The DO probe was polarised overnight and the following day it was calibrated. This was done by zeroing it when disconnected, then setting the span to 100 after connecting it to the bioreactor that had been injected with air and mixed at 50 rpm for approximately 10 mins.

If a level probe was required, then after sterilisation it was calibrated by choosing the appropriate sensitivity in dry mode or wet mode. For dry mode, the

level probe was slowly immersed in the liquid until the raw value changed to wet. Conversely, for wet mode, it was immersed in the media and then slowly removed until the raw value changed to dry.

3.5 Analytical Procedures

3.5.1 Culture Sampling

Samples were taken daily at the same time as inoculation, by introducing a syringe through the sampling port of the photobioreactor. To make up for any evaporation losses, sterilised distilled water was added 15 minutes before sampling to allow enough time for mixing (da Silva Vaz et al., 2016, Sacasa Castellanos, 2013). The amount of evaporation loss from the system was estimated by two level probes fixed to the bioreactor.

Biomass concentration can be measured by 1) direct counting of cells using a microscope and haemocytometer, or 2) estimating biomass concentration by dry weight or optical density (Andersen, 2005). Among these methods, measurement of optical density is the fastest. It is also a simple method with a low possibility of human error. However, it is necessary to estimate the linear correlation between optical density and dry weight for specific algae species via a calibration equation.

To estimate biomass concentration, the optical density (OD) of the samples was measured by a UV-Vis spectrophotometer with a 1 cm light path. The OD was then converted to dry weight according to the calibration curve. The calibration curve was derived by measuring the dry weight of several samples of different concentrations that had known optical densities. The resulting calibration equation was used to calculate the biomass concentration of collected samples. These methods are explained in the following sections.

3.5.2 Optical Density Measurement

Optical density of the samples was measured using a UV-Vis spectrophotometer (Jasco, model V-670). It was equipped with a unique single monochromator optical system, and was able to measure the absorption spectrum of samples over a

wavelength range of 190—2700 nm, or it could be adjusted to measure optical density at one or a few particular wavelengths (Figure 3-12).

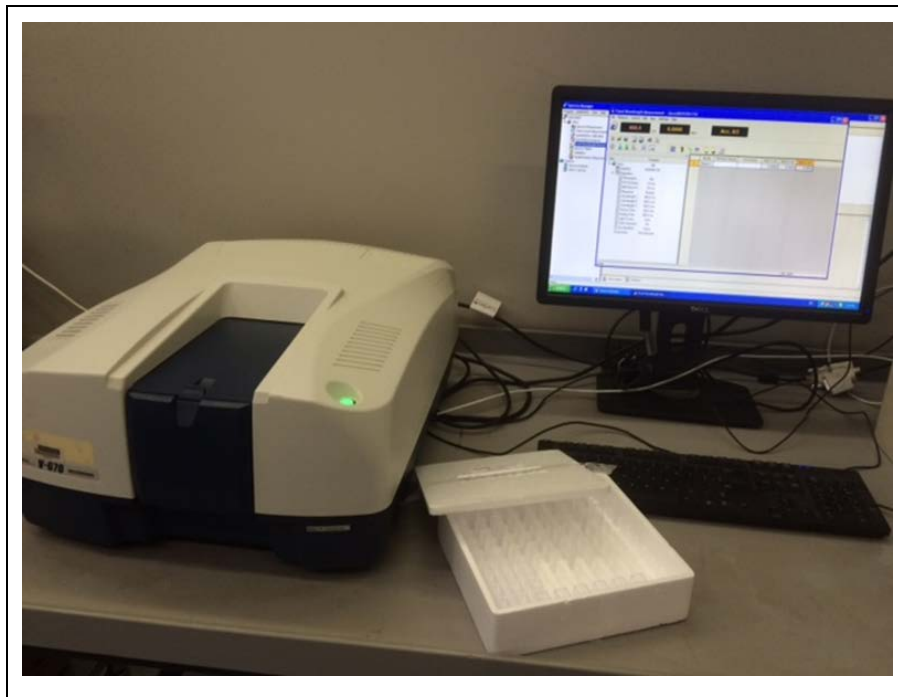


Figure 3-12 UV-Vis spectrophotometer

By measuring absorption over the 400—800 nm spectrum, which is the region of photosynthetically active radiation (PAR), the absorption peaks for *C. vulgaris* were determined (Figure 3-13). Maximum absorbance peaks were observed at 440 nm and 684 nm. Usually, absorption peaks for this strain are located in the blue (460—470 nm) and red (640—690 nm) regions (Fan et al., 2007). Red light wavelengths cause the greatest photosynthetic activity and, therefore, significantly higher growth is achieved in this wavelength range in comparison with 590—600 nm (yellow light) or 460—470 nm (blue light; Ge, Zhang, et al., 2013). Therefore, the OD of the samples was measured with 684 nm wavelength light. For comparison, the absorbance of the standard medium without *C. vulgaris* at 684 nm was 0.0074. Samples were diluted with deionised water to obtain an absorbance range of 0.1–1 before analysis.

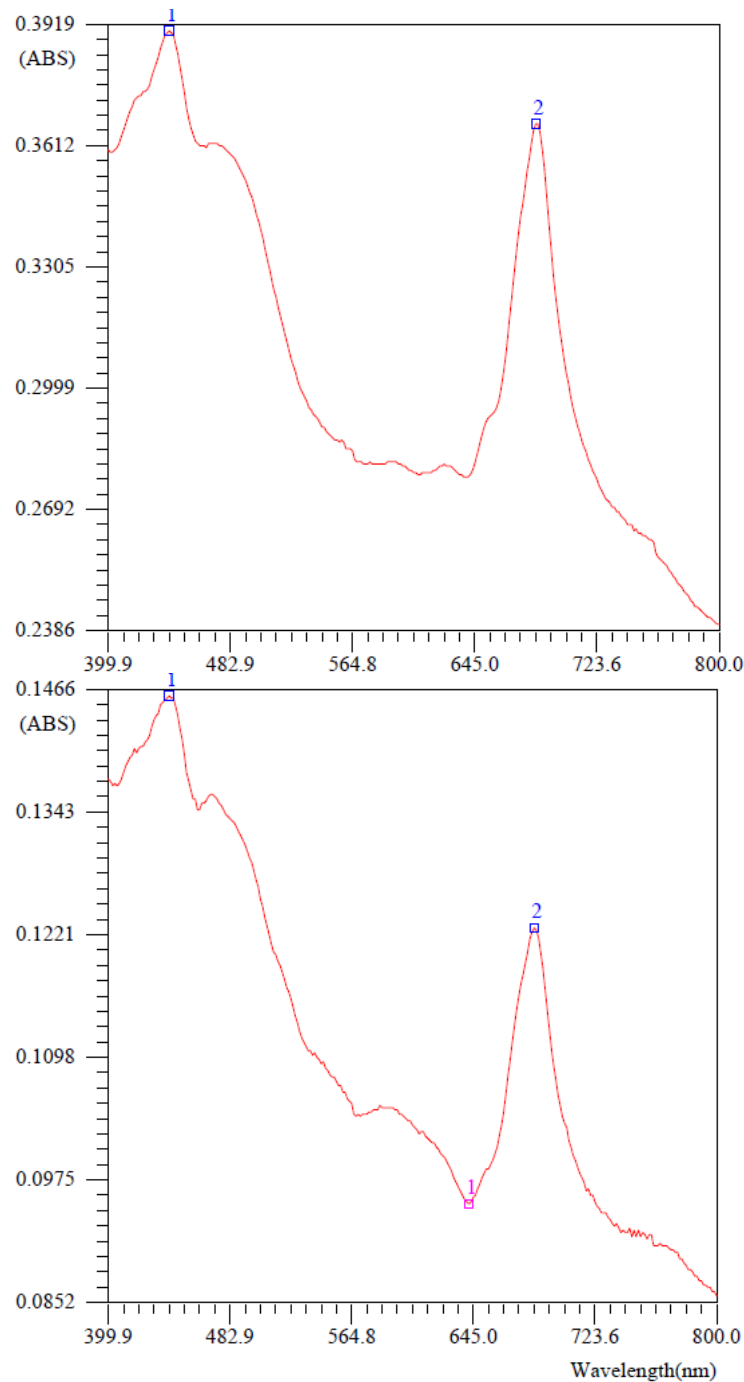


Figure 3-13 Absorbance spectra for two samples of *C. vulgaris* culture

3.5.3 Biomass Dry Weight Method

A known volume of the biomass samples (10 ml) were filtered through pre-weighed, pre-combusted Whatman glass fibre filters (GF/C, 1.2 μm), then rinsed with 10 ml distilled water and dried in an oven at 105 $^{\circ}\text{C}$ for 24 hours, then reweighed to determine the dry weight of the filtered microalgae.

Pre-combustion was carried out in a muffle furnace. First, filters were loosely wrapped in aluminium foil and combusted at a temperature of 450 °C for 3 hours and then left overnight for cooling to ambient temperature. Prior to setting this time for pre-combustion, some preliminary experiments were carried out to determine a suitable time for fixing the weight of the filters. Then, filters were removed and transferred to a desiccator and weighed with a 4 digit balance. For filtration, a Millipore unit connected to a vacuum pump was used (Figure 3-14).



Figure 3-14 Millipore unit and vacuum pump for biomass filtration

During filtration, the vacuum pressure differentials were maintained at 35 to 55 mm Hg to avoid cell damage (Zhu and Lee, 1997). The vacuum was applied before starting filtration to prevent liquid diffusing to the edge of the filter. Filtrates were rinsed to remove the salts precipitated on the surface of the cells. For freshwater algae species, washing with distilled water is recommended (Zhu and Lee, 1997). To avoid air exposure of the cells and to achieve perfect washing of all the cells, the vacuum pump was turned off during each rinse so that the water covered the filter, and was then turned on again to remove the rinsing solutions. Afterwards, filtrates were placed in a 105 °C oven for 24 hours, left in a desiccator to reach ambient temperature, and reweighed. Biomass concentration was calculated as the weight difference before and after filtration per unit volume of culture.

To minimise error in dry weight measurements, duplicate measurements were carried out for each sample and the results were averaged. Precision in measuring the volumes of replicates, and filtering and washing all samples in a consistent manner were of high importance in obtaining accurate results. A sufficient volume of culture was filtered so that a good amount of filtrate remained on the filter. This facilitated

accurate weight measurement. In my experience, the minimum dry weight on a filter should be more than 2 mg.

3.5.4 Calibration Equation for Biomass Concentration

Duplicate measurements were made of dry cell weight and OD (at 684 nm) for nine samples with various biomass concentrations and ODs between 0.1–0.9. The experimental biomass concentrations calculated from dry cell weight (DCW), were correlated to their optical density readings at 684 nm (OD_{684}). Figure 3-15 shows the correlation of dry cell weight (biomass concentration) with the culture's absorbance at 684 nm. Then, the following linear calibration equation with a correlation coefficient of 0.9968 was obtained:

$$C_b = 0.2036 OD_{684} - 0.0006 \quad (3-1)$$

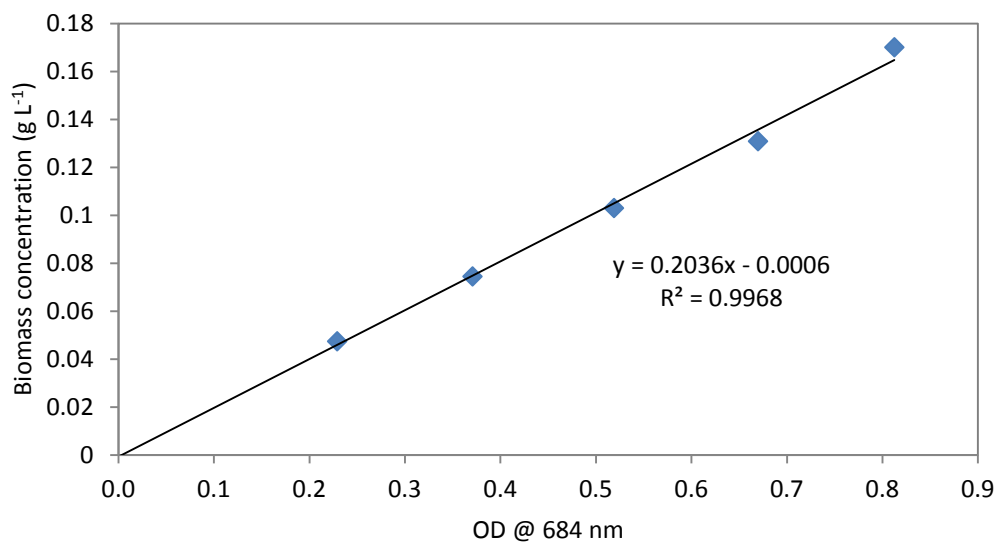


Figure 3-15 Optical density calibration line

It should be noted that the calibration equation varies for different species of algae. This equation is very close to the one obtained by Sacasa Castellanos (2013). Equation (3-2) calibrated the OD of the same strain at 686 nm.

$$C_b = 0.2936 OD_{686} + 0.0007 \quad (3-2)$$

3.5.5 Light Intensity Measurement

The light intensity on the surface of the bioreactor was measured using a quantum sensor (LI-192SA, LI-Core Inc.; Figure 3-16). This sensor has been designed to measure photosynthetically active radiation (PAR, 400-700 nm) in aquatic environments. Computer-tailored filter glass was used in the sensor to achieve the desired quantum response. Both underwater and atmospheric photosynthetic photon flux densities can be accurately measured by this sensor. However, this sensor is appropriate for measuring light intensity from one direction since it has a flat sensor. It is made of corrosion resistant metal with an acrylic diffuser (3.18 cm diameter \times 4.62 cm height) and has a flat, high-stability, silicon photovoltaic detector. It includes a 3 m underwater cable and BNC connector.



Figure 3-16 Quantum sensor (LI-192SA)

This quantum sensor is flat and can collect photons from one direction; therefore, it is appropriate for use to measure incident light intensity on the surface of the bioreactor. It is quite reasonable to use this sensor to measure light intensity in a vessel when that vessel is illuminated from one direction, and measuring of photon flux from only one direction is required. Nevertheless, to measure local light intensity inside the vessel, especially when it is illuminated from around the vessel, this sensor is not accurate. Indeed, in this case, a spherical sensor which can collect photons from all directions is needed. For this purpose, a spherical micro quantum sensor (US-SQS, WALZ; Figure 3-17) was used. This sensor has been designed to measure PAR. It has a 3.7 mm diameter sphere made from highly scattering plastic.

Since it is a quite small sensor, it can measure local light intensity very accurately. Also it includes a 3 m coaxial cable and a BNC connector. Sensors were cleaned with water and a mild detergent (dishwashing soap) after each use.



Figure 3-17 Spherical micro quantum sensor (US-SQS/L)

These sensors are connectable to any data logger with a microampere current measuring function. Here, a light meter (LI-250, LI-COR Inc.; Figure 3-18), was used which provided a direct digital readout. The digital LCD was updated every 0.5 seconds in instantaneous mode. Sensor output was collected and displayed as a 15-second average which represents approximately 60 readings. A typical accuracy of 0.4 % at 25 °C is specified for this device. Each sensor was supplied with a calibration multiplier factor which was provided by the factory and must be taken into account. Two calibration multipliers could be saved in the memory of this device, use with atmospheric and underwater measurements. When measuring light intensity, the correct choice of calibration multiplier is dependent on the sensor type and measuring environment. Measurements can be displayed in different units, including $\mu\text{mol m}^{-2} \text{s}^{-1}$, lux, klux or W m^{-2} . In this study, light intensity was measured in $\mu\text{mol m}^{-2} \text{s}^{-1}$.



Figure 3-18 Light meter (LI-250)

To measure incident light intensity, it is necessary to take the average of several measurements. This is because illumination on the surface of the bioreactor was not perfectly uniform. For this reason, average incident light intensity was calculated after measuring light intensity at 25 locations across the surface of the vessel. These locations were on a 5 x 5 point grid on half of the perimeter of the vessel, due to symmetry of the vessel and illumination. Then, the average light intensity was calculated as the weighted average of the measurements.

3.5.6 Elemental Analysis of Microalgae

To calculate CO₂ biofixation, we need to know the carbon content of the biomass. The elemental composition of *C. vulgaris* and the total carbon content of dried cells were determined using an element analyser (PerkinElmer, 2400 Series II CHNS/O; Figure 3-19). This instrument is fully automated and can be operated in either CHN or CHNS mode. Small quantities of the sample (typically about 2 mg) are accurately weighed into small tin capsules and are placed in the auto-sampler chamber. At elevated temperatures, in the presence of excess oxygen, organic materials combust to form CO₂, H₂O, various N_xO_y compounds, and SO₂ if sulfur is present. The resulting gas is sent to a thermal conductivity meter for analysis. In addition to carbon, total amounts of hydrogen, nitrogen and oxygen were measured. Indeed, CO₂, H₂O, N₂ and SO₂ are representatives of carbon content, hydrogen content, nitrogen content and sulfur content, respectively (only with the CHNS

configuration). Acetanilide was used as a standard with a composition of 71.09 % carbon, 6.71 % hydrogen, 10.36 % nitrogen and 11.84 % oxygen.



Figure 3-19 Elemental analyser

The molecular formula of the *C. vulgaris* used in this study ($\text{CH}_{1.83}\text{O}_{0.46}\text{N}_{0.05}$) was obtained by elemental analysis of several samples collected at different cultivation times (Table 3-1).

Table 3-1 Elemental analysis of *Chlorella vulgaris*

Run & sample description	Results			
	Carbon	Hydrogen	Nitrogen	Oxygen
1- Stock culture	43.31	6.64	5.06	44.99
2- Stock culture	43.60	6.66	5.34	44.40
3- Recently inoculated	54.29	9.12	3.24	33.35
4- Recently inoculated	54.97	8.96	3.25	32.82
5- Elderly inoculated	58.05	8.82	2.07	31.06
6- Elderly inoculated	60.45	9.26	2.13	28.16
7- Old culture	51.62	6.62	3.95	37.81
8- Old culture	50.03	7.65	4.13	38.19

3.5.7 Calculation of Microalgae Growth Rate, Biomass Productivity and CO_2 Biofixation

Microalgal growth was monitored by measuring OD, and then DCW was calculated using Equation (3-1). The specific growth rate was calculated according to the equation:

$$\mu_{max} = \frac{\ln(C_{b2}/C_{b1})}{(t_2 - t_1)} \quad (3-3)$$

where C_{b2} and C_{b1} are the biomass concentrations (g L^{-1}) at times t_2 and t_1 (d), respectively.

Biomass productivity ($\text{g DW L}^{-1} \text{d}^{-1}$) was calculated by the following equation:

$$\text{Biomass productivity} = \frac{C_{bt} - C_{b_0}}{t} \quad (3-4)$$

where C_{bt} is the final biomass concentration (g L^{-1}) at cultivation time t , and C_{b_0} is the initial biomass concentration (g L^{-1}).

The total carbon content of dried biomass (%C) was determined by the elemental analyser. Thus, the CO_2 biofixation rate ($\text{g CO}_2 \text{L}^{-1} \text{d}^{-1}$) was calculated according to Equation (3-5).

$$\text{CO}_2 \text{ biofixation rate} = \%C \times \text{Biomass productivity} \times \frac{44}{12} \quad (3-5)$$

Where %C is biomass carbon content, and 44 and 12 are the molecular weights of carbon dioxide and carbon, respectively.

CO_2 utilisation efficiency (%), the percentage of carbon dioxide fixed by microalgae from the total inlet carbon dioxide, was calculated by Equation (3-6) (Ketheesan and Nirmalakhandan, 2012, Ryu et al., 2009).

$$\text{CO}_2 \text{ utilisation efficiency} = \frac{\text{CO}_2 \text{ biofixation rate}}{V_{\text{CO}_2}} \times 100 \quad (3-6)$$

where V_{CO_2} is mass aeration rate of CO_2 supplied to the vessel ($\text{g CO}_2 \text{L}^{-1} \text{d}^{-1}$).

3.6 Light Distribution Measurement

To investigate light distribution inside the microalgae culture, two different vessels were used: a rectangular vessel measuring 20 x 34 x 30 cm (width x length x height; Figure 3-20); and a cylindrical vessel of 20 cm diameter (Figure 3-21).

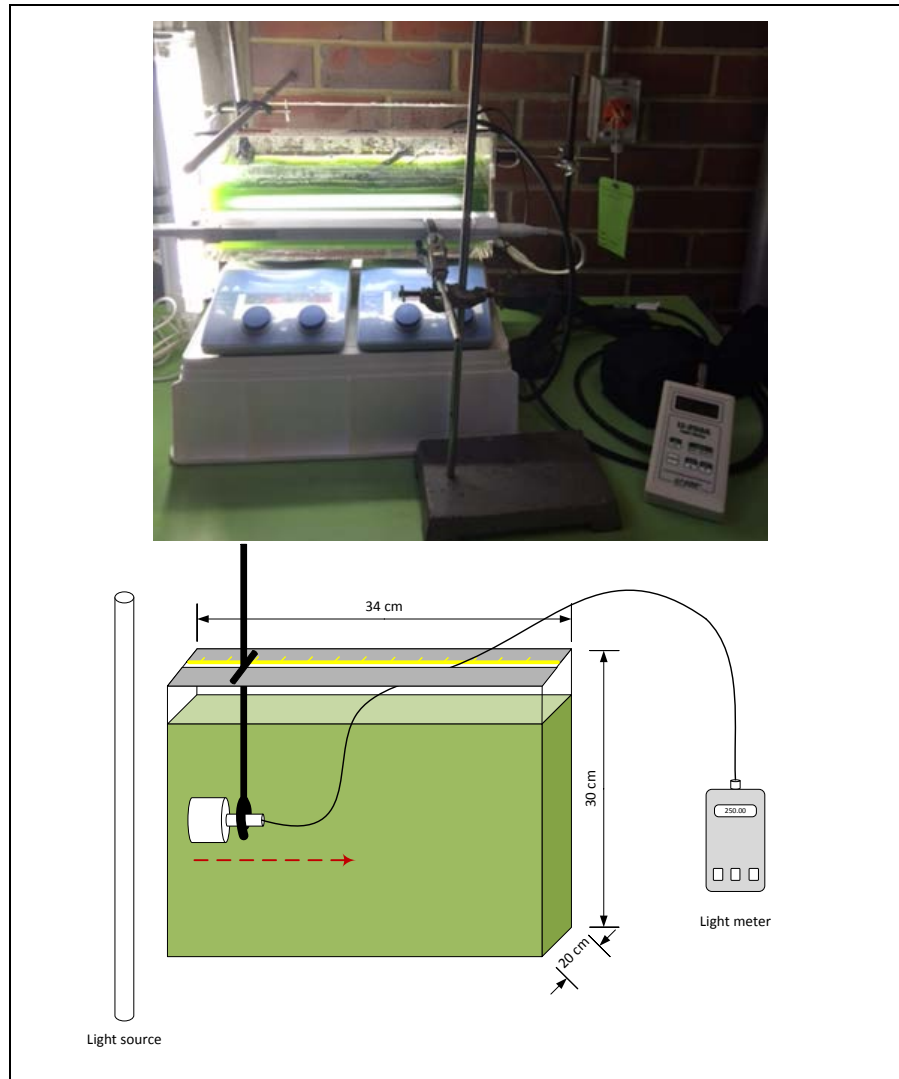


Figure 3-20 Light distribution experimental setup with rectangular vessel

The experiments were carried out in a rectangular vessel (Figure 3-20) illuminated from one side while the other sides were covered by black sheets, and then in a cylindrical vessel (Figure 3-21) with single-direction illumination, and illuminated evenly from all sides. Readings were repeated at various biomass concentrations and also at different incident light intensities while measuring local light intensity inside the culture at various distances from the surface of the vessels.

A quantum sensor (LI-192SA, LI-Core Inc.) was used to measure incident light intensity on the surface of the vessel (Figure 3-16). This quantum sensor measured light intensity from one direction. However, to measure local light intensity at different distances from the surface of the vessel, a spherical micro quantum sensor with a 3.7 mm diffusing sphere (US-SQS/L, WALZ; Figure 3-17) was used to accurately measure light intensity at a particular position. Both sensors were connected to a light meter (LI-250, LI-COR Inc.; Figure 3-18), and light intensity was measured in $\mu\text{mol m}^{-2} \text{s}^{-1}$.

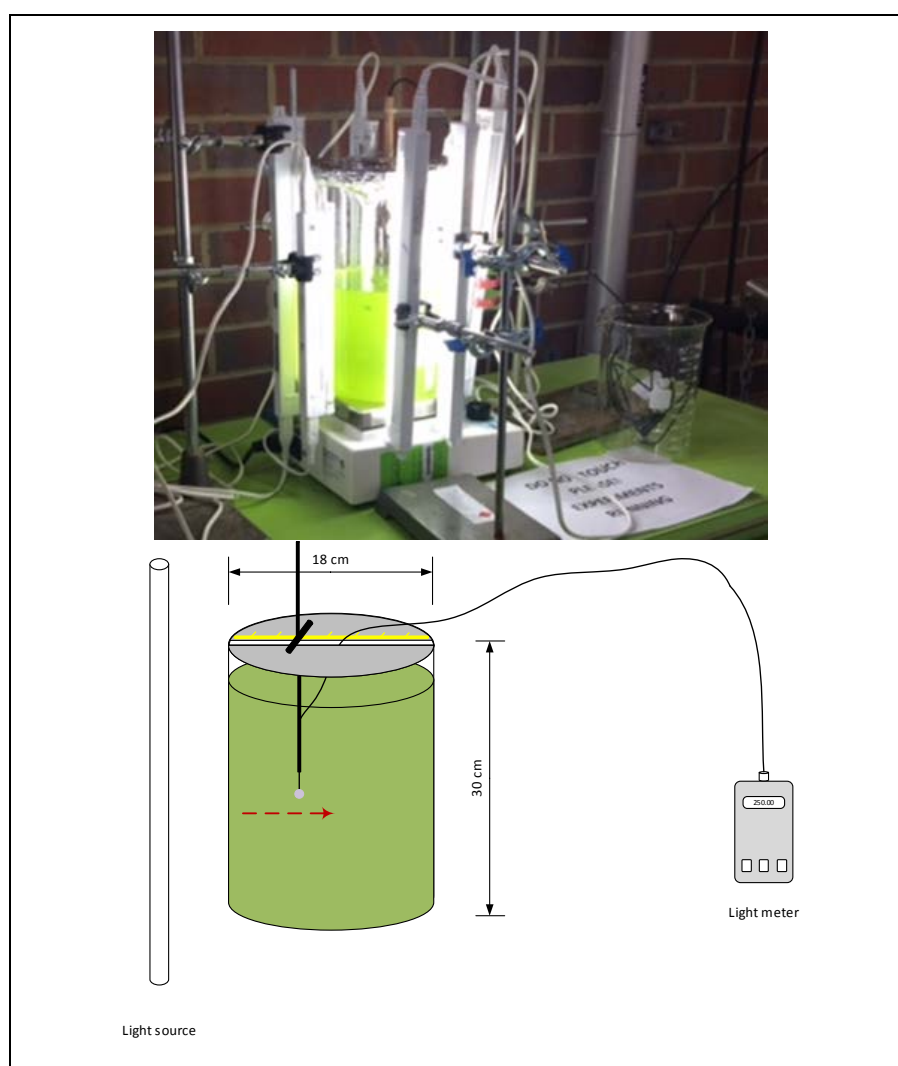


Figure 3-21 Light distribution experimental setup with cylindrical vessel

3.7 Experimental Design for Optimisation by RSM

A five level central composite design (CCD) with three replicates at central points was used to plan the experiment and evaluate the relationship between the factors.

To achieve this target, experiments designed by means of a 2^3 factorial central composite design, so that 17 experimental runs were conducted. For each experiment, the bioreactor was illuminated with various specific light intensities and light periods, and was also sparged with a particular percentage of CO₂-enriched air. CO₂-enriched air was aerated continuously at a constant rate of 0.5 vvm to the bottom of the bioreactor through a sparger. Temperature was kept constant at 28 °C and agitation was carried out via impeller at 300 rpm to create a uniform photon exposure to the cells, reduce temperature gradients and prevent biomass sedimentation. Each experiment was conducted for 10 days and every day, biomass growth was followed by measurement of optical density. Duplicate OD measurements were carried out at 684 nm for each sample. Then, cell density was calculated using the OD calibration equation (3-1). Regression, statistical analysis and ANOVA were carried out using MATLAB, Synthesis, and DOE++ (version 10.1) software. More details will be explained in the optimisation chapter.

4

Influence of Light Intensity on Growth and CO₂ Biofixation by *Chlorella vulgaris*

4.1 Introduction

Many factors such as temperature, pH, light intensity, aeration rate and agitation affect microalgae growth. However, light intensity is one of the most significant factors because when it is insufficient or exceedingly high, it can limit or inhibit microalgae growth. In other words, while microalgae cannot grow well in low light intensity (photolimitation), high light intensity causes cell damage and so leads to decrease in biomass growth (photoinhibition), (Grima et al., 1996, Martinez et al., 2012). Microalgae need a day/night light regimen with sufficient photon flux during the day for productive photosynthesis. Nevertheless, due to shading effects, including photon-absorption by cells and scattering by particles, there is a light gradient inside the culture, especially in dense cultures. It has been accepted by researchers that light illumination parameters such as light intensity and light period play a significant role toward optimising microalgae growth or CO₂ biofixation. In addition to the interaction of other factors such as light period on optimum light intensity, different strains also vary in their optimum conditions for maximum biomass production or CO₂ removal. *Chlorella vulgaris* is one of the promising microalgae species suitable for CO₂ sequestration due to fast growing, relatively high carbon content and also tolerance to high temperature and CO₂ concentration (Salih, 2011, Pires et al., 2012). Bhola et al. (2011) stated that *C. vulgaris* can tolerate light intensity between 150 to 350 $\mu\text{mol m}^{-2} \text{s}^{-1}$ and could achieved a 6.17 $\text{mg L}^{-1} \text{h}^{-1}$ CO₂ biofixation rate.

In this chapter, the biomass production rate and CO₂ biofixation rate by *C. vulgaris* in a batch photobioreactor at different light intensities are discussed. A light enclosure was designed for better and controlled illumination for the available bioreactor to explore the optimum light intensity for *C. vulgaris*. The performance of the modified bioreactor inside the light enclosure for carbon dioxide biofixation by *C. vulgaris* is investigated. The influence of different light intensities on CO₂ biofixation and biomass production rate is evaluated. Meanwhile, operational conditions of the photobioreactor such as pH, dissolved oxygen (DO) and inlet CO₂ concentration have been measured and discussed.

4.2 Materials and Methods

Chlorella vulgaris was cultivated in MLA medium in the described photobioreactor in section 3.4.1. Cultivation system and experimental procedure have been discussed in chapter three. The inoculation was performed by aseptically transferring stock culture to autoclaved fresh medium with an inoculation ratio of 10:100 to maintain an initial concentration of 0.01 g L⁻¹. Culturing was carried out at 20 °C by bubbling 2 % CO₂-enriched air at a flow rate of 1 L min⁻¹. The impeller was set at 200 rpm for better mixing and prevention of sedimentation. Samples were withdrawn daily at the same time at noon and used for further analysis.

To investigate the effect of light intensity, five experiments were conducted at light intensities of 30, 50, 100, 185 and 300 μmol m⁻² s⁻¹, and constant light period of 12:12 light:dark. Desired light intensity was adjusted with number of the lamps and their distance from the vessel's surface. For instance, a light intensity of 50 μmol m⁻² s⁻¹ was furnished by eight 6 W cool white fluorescent lamps located at approximately 10 cm from the bioreactor surface. Table 4-1 summarises the light enclosure set-up.

Table 4-1 Light enclosure set-up

Experiment	Light intensity μmol m ⁻² s ⁻¹	Light enclosure configuration
Run 1	30	4 lamps on, at 10-cm distance
Run 2	50	8 lamps on, at 10-cm distance
Run 3	100	16 lamps on, at 10-cm distance
Run 4	185	16 lamps on, at 5-cm distance
Run 5	300	16 lamps on, at 1-cm distance

Afterwards, two other experiments have been carried out in the same procedure explained but at incident light intensities of 120 and 280 $\mu\text{mol m}^{-2} \text{s}^{-1}$ when 4 % CO₂ enriched air at flow rate of 1 L min⁻¹ was sparged to the photobioreactor. Temperature and agitation speed set at 28 °C and 300 RPM, respectively, and with a 12:12 light:dark cycle and 0.1 g L⁻¹ initial concentration.

4.3 Results and Discussion

4.3.1 Carbon content and elemental analysing

As explained in chapter three, elemental analysing of dried biomass was used to measure carbon content of the cultivated biomass. Four different samples with different ages were selected to use for this purpose and duplicate measurements were carried out. Carbon content of the species used in this study, (*Chlorella vulgaris*), was 54 % as explained in section 3.5.6.

4.3.2 Effect of light intensity on *C. vulgaris* growth

Experiments were conducted at same initial concentration of microalgae and continued for same cultivation period but under different conditions of light intensities. It was observed that the appearance and colour of the culture inside the bioreactor was almost same and without sensible change in the first day after inoculation; however intensive change in density and colour of the biomass in second and third days of cultivation was apparently visible. Indeed, the colour of the broth was changed to relatively dark green. However, afterwards the colour of broth began to change to light green and yellowish green, especially in high incident light intensities. This is due to change in structure of the cells and chlorophyll which is adaptation behaviour of the cells to the environment (Cheirsilp and Torpee, 2012).

Figure 4-1 illustrates the growth curve of the fresh water *C. vulgaris* at five different light intensities including 30, 50, 100, 185 and 300 $\mu\text{mol m}^{-2} \text{s}^{-1}$, when cultivation was maintained for 17 days. The culture showed an exponential growth phase after two days lag phase for up to 6-7 days. The maximum biomass concentration of 1.25 g L⁻¹ in exponential growth was achieved at 100 $\mu\text{mol m}^{-2} \text{s}^{-1}$ light intensity in comparison with 0.33, 0.98, 0.60 and 0.69 g L⁻¹ at 30, 50, 185 and

300 $\mu\text{mol m}^{-2} \text{s}^{-1}$ light intensities, respectively. Then, although a slowdown in cell growth was observed, it did not stop growing completely. This fall in growth rate is a result of an increase in cell density and a decrease in available photon flux to the cells due to shading effects. As long as the photon flux exceeds a certain threshold, biomass will continue to increase. Moreover, light scattering causes less available photon flux for the deep part of the culture and therefore, a decreasing light gradient occurs in the cross-section of the vessel.

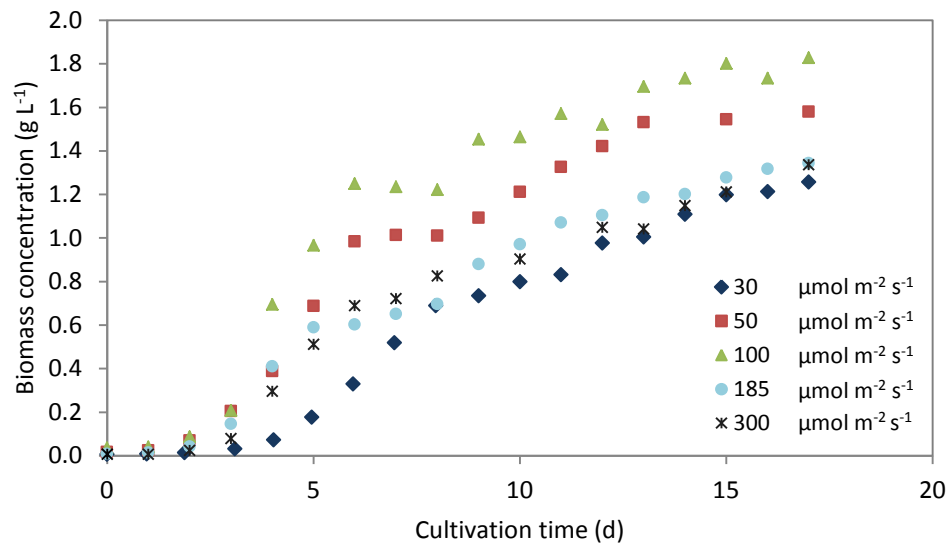


Figure 4-1 Growth curve of microalgae *C. vulgaris* at different light intensities in 17 days

A maximum biomass of 1.83 g L^{-1} was obtained on the last day with a light intensity of 100 $\mu\text{mol m}^{-2} \text{s}^{-1}$. Rise in light intensity from 100 to 185 and then to 300 $\mu\text{mol m}^{-2} \text{s}^{-1}$ led to drop in biomass concentration to 1.34 and 1.33 g L^{-1} , respectively. Even cultivation at 50 $\mu\text{mol m}^{-2} \text{s}^{-1}$ photon flux presented better growth and higher biomass concentration than 185 and 300 $\mu\text{mol m}^{-2} \text{s}^{-1}$ light intensities; in consequence, 1.58 g L^{-1} biomass was obtained when the bioreactor was illuminated under 50 $\mu\text{mol m}^{-2} \text{s}^{-1}$ while the maximum biomass concentration for light intensities of 185 and 300 $\mu\text{mol m}^{-2} \text{s}^{-1}$ was only 1.34 g L^{-1} . Considering this result and the idea that cell growth is almost the same at light intensities of 185 and 300 $\mu\text{mol m}^{-2} \text{s}^{-1}$, it can be concluded that the biomass growth is inhibited at 185 and 300 $\mu\text{mol m}^{-2} \text{s}^{-1}$. In the phenomena of photoinhibition that occurs at high light intensities, the photosynthetic receptor system of the cells is damaged and consequently biomass

growth decreases. Additionally, the colour of the cells changes and they appear lighter or even brown in the case of very high light intensities (Wahidin et al., 2013).

On the other hand, under the photolimitation condition, microalgae growth is limited because there is insufficient light and so not enough source of energy. It was observed that microalgae did not grow well when 30 $\mu\text{mol m}^{-2} \text{s}^{-1}$ of light intensity was exposed to the bioreactor, and the biomass reached to 0.33 g L⁻¹ in six days. With an increase in light intensity from 30 to 50 $\mu\text{mol m}^{-2} \text{s}^{-1}$, biomass concentration increased to 0.98 g L⁻¹, almost three times for the same cultivation time.

Because light provides the required energy for photosynthesis, it is one of the significant factors affecting microalgae growth along with other factors such as pH, temperature and aeration rate. However, both phenomena of photolimitation and photoinhibition, as well as the change in the light gradient inside the vessel with cultivation time and biomass concentration, make light regime analysis more complicated.

4.3.3 Effect of light intensity on specific growth rate

Figure 4-2 shows daily specific growth rate at various incident light intensities. Similar behaviour is observed for all cultivations so that growth rate reaches to maximum in the early days of culturing when biomass concentration is low and then sharply decreases to very small values.

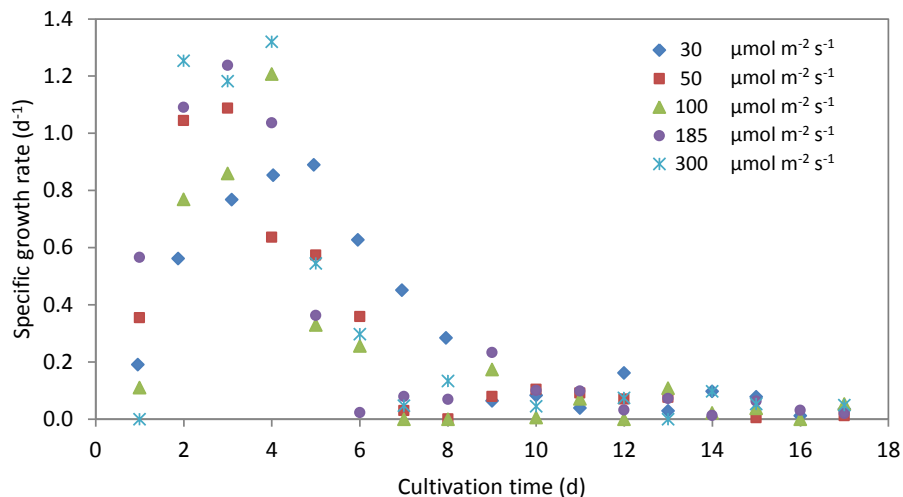


Figure 4-2 Daily specific growth rate at different incident light intensities of 30, 50, 100, 185 and 300 $\mu\text{mol m}^{-2} \text{s}^{-1}$

The maximum specific growth rate is occurred in day 3 or 4 and is almost same, around 1.2-1.3 d⁻¹, for light intensities of 100, 185 and 300 μmol m⁻² s⁻¹. Nevertheless, lower values, 1.0 and 0.9 d⁻¹, is observed for light intensities of 50 and 30 μmol m⁻² s⁻¹, respectively. The highest specific growth rate among the all experiments was 1.3 d⁻¹ and happened at incident irradiance of 300 μmol m⁻² s⁻¹ in day 4 of cultivation. It can concluded in the few first days up to 4 days higher light intensity is appreciated and very low light intensity results a very slow growth.

4.3.4 Effect of biomass growth on PH at different light intensities

The pH value of the MLA medium is approximately 7.8; however, after autoclaving it increases and again dramatically drops when sparging CO₂-enriched air. Indeed, pH of the autoclaved medium rose to nearly 8.1 due to high temperature and degassing in the autoclave. After gas injection it sharply dropped to approximately 5.4 as a result of increasing dissolved CO₂. After inoculation, the pH level started to slightly increase when biomass started to grow because inorganic carbon is consumed by the microalgae; however, a few days later, the pH value almost levelled off. Figure 4-3 shows pH evolution with cultivation time for different light intensities of 30, 50, 100, 185 and 300 μmol m⁻² s⁻¹. Generally, pH values ranged from 5.35 to 7.2 during cultivation in these experiments, which do not inhibit *C. vulgaris* growth (Concas et al., 2012); even at the highest level of pH up to 7.2, no negative effect on growth was observed.

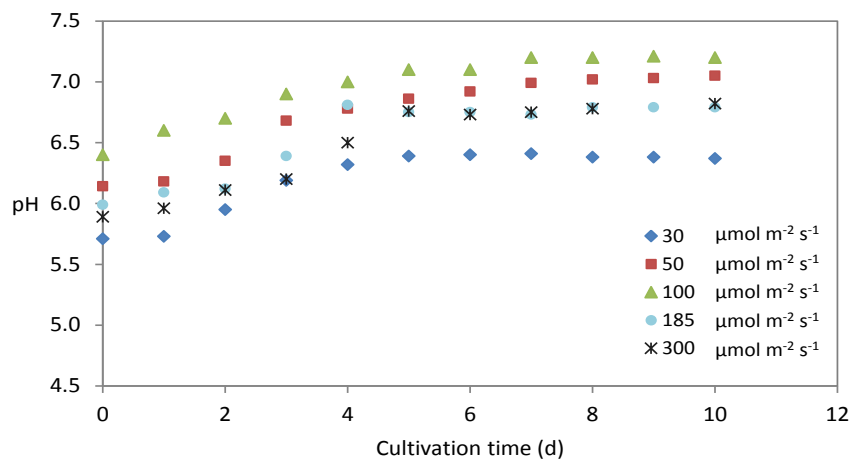


Figure 4-3 pH evolution for experiments in different light intensities of 30, 50, 100, 185 and 300 μmol m⁻² s⁻¹ over cultivation time

A sharper exponential growth rate in the first six days accompanied by a sharper increase in pH, and after a reduction in growth in the following days, less change in pH occurred. As it can be observed after six days of cultivation, the pH in each experiment became nearly constant and the final pH values in the different experiments ranged between 6.4 and 7.2.

The same pH evolution trend has been reported by Concas et al. (2013) when they cultured *C. vulgaris* in a batch photobioreactor, so that pH of the medium (7.5) decreased to 5.6 after gas inlet was added and then slowly increased to 6.2. In addition, a slight increase in pH from 6.3 to 7 followed by little fluctuation in pH has been reported by Li et al. (2013) when *C. vulgaris* was cultured in 0.035 L min⁻¹ aeration with 15 % CO₂ enriched air. However, steep variation in pH from 6.5 to 8.3 has been observed when the aeration was reduced to 0.025 L min⁻¹, which can cause a negative effect on alga growth. Although the optimal pH value for *C. vulgaris* ranges from 6-8, cell growth can take place even at pH 4 and 10 (Concas et al., 2012). Therefore, this strain can be a good choice for direct CO₂ sequestration from flue gas.

CO₂ as a source of carbon was consumed and converted to biomass via photosynthesis. On the other hand, aeration of CO₂ to the medium has a reduction effect on pH due to the reaction of CO₂ with water forming carbonic acid (Kumar et al., 2011). However, biomass grew and subsequently pH increased because of CO₂ consumption by photosynthesis reaction (Bhola et al., 2011). Meanwhile, there was a sharp increase in pH in the first few days (exponential growth phase) and then a slight increase of pH after reaching the stationary growth phase; which can be seen in Figure 4-4 for experiment with 185 μmol m⁻² s⁻¹ light intensity.

Overall, there is a close relationship between pH and biomass production. Consequently, photosynthetic growth and CO₂ utilisation rate will be limited in very high or very low pH values. Therefore, investigating pH evolution in microalga biomass culturing can be a key issue to properly optimise a microalgae photobioreactor. In particular, this aspect is significant when highly concentrated CO₂ flue gases from power plants as the source of CO₂ are used. In this case, the pH level can reach very low values and may inhibit microalgae growth (Pires et al., 2012).

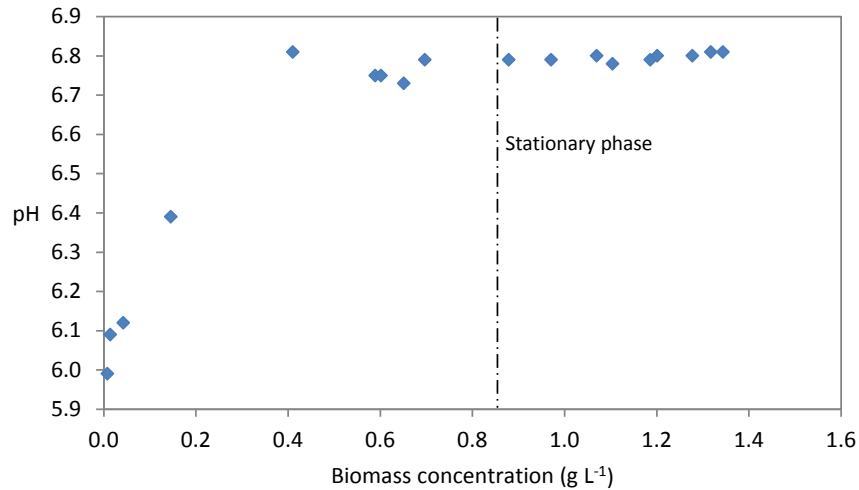


Figure 4-4 Effect of biomass growth on pH in experiment with $185 \mu\text{mol m}^{-2} \text{s}^{-1}$ light intensity

Figure 4-5 illustrates the variation in biomass concentration at days 6 and 17 as well as final pH value with light intensity. It was observed that the maximum pH value (7.35), which is accompanied by the highest biomass concentration, occurred at $100 \mu\text{mol m}^{-2} \text{s}^{-1}$ of light intensity. Meanwhile, the second maximum pH (7.25), which was obtained at $50 \mu\text{mol m}^{-2} \text{s}^{-1}$ photon fluxes, was associated with the second maximum biomass concentration. The lowest pH (6.3) occurred in the experiment with minimum biomass production and a light intensity of $30 \mu\text{mol m}^{-2} \text{s}^{-1}$.

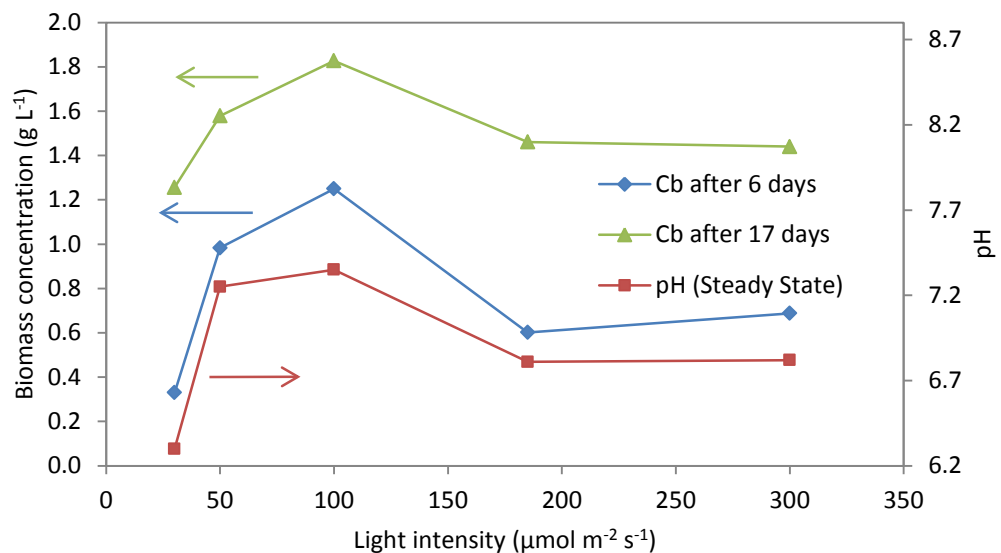


Figure 4-5 Biomass concentration at day 6 and day 17 and pH when culture was illuminated by various light intensities of $30, 50, 100, 185$ and $300 \mu\text{mol m}^{-2} \text{s}^{-1}$

Two factors can affect the final pH values: the volume of the carbon dioxide injected into the bioreactor and the amount of the biomass produced. High inlet CO₂ and less biomass production results in a lower pH value. In all experiments, CO₂ percentage in inlet gas was adjusted to be 2 %. The minimum pH of 6.4 was observed at a light intensity of 30 $\mu\text{mol m}^{-2} \text{s}^{-1}$ due to less biomass growth. In contrast, the maximum pH of 7.2 was achieved at a light intensity of 100 $\mu\text{mol m}^{-2} \text{s}^{-1}$ and associated with more biomass production (Figure 4-5).

4.3.5 Effect of light intensity and biomass growth on DO

Figure 4-6 shows the growth curve and dissolved oxygen over cultivation time for three experiments with 50, 100 and 185 $\mu\text{mol m}^{-2} \text{s}^{-1}$ light intensities.

Generally, there was a noticeable rise in the first few days and then a reduction in DO observed in all experiments. Indeed, exponential biomass growth caused an increase in DO levels and then a decrease in biomass growth rate accompanied by less oxygen and a decrease in DO. Overall it's very clear from the figure that there is an increase in DO% from day 0 until day 12 where the stationary phase is started. These results suggest that the steep change in DO during the exponential growth phase of microalgae is due to the photosynthesis, CO₂ consumption and O₂ generation. Consequently, DO monitoring can be used to predict the health of the microalgae. Chai et al. (2012) observed a gradual increase in the daily DO peak during the exponential growth phase and then after, reaching 135 %, it decreased during stationary phase, for a batch culture of *Chlorococcum* species.

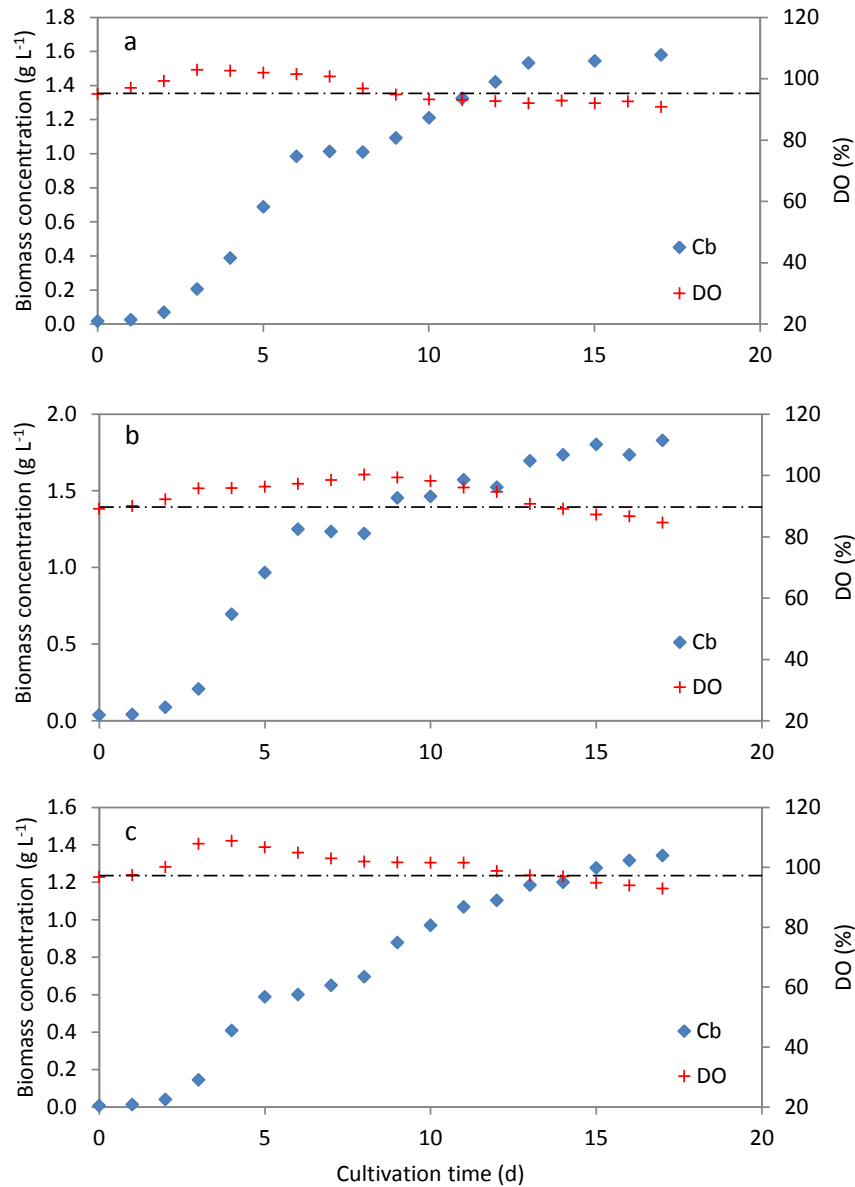


Figure 4-6 Biomass concentration and DO evolution over cultivation time, at light intensities of a) 50, b) 100 and c) 185 $\mu\text{mol m}^{-2} \text{s}^{-1}$

4.3.6 Interaction between light intensity and biomass growth

Effect of illuminating different light intensities to the surface of the bioreactor on maximum specific growth rate (μ_{max}), productivity and CO₂ biofixation rate have been shown in Figure 4-7. As expected, trend of change in productivity and CO₂ biofixation rate is similar to each other and also similar to biomass concentration.

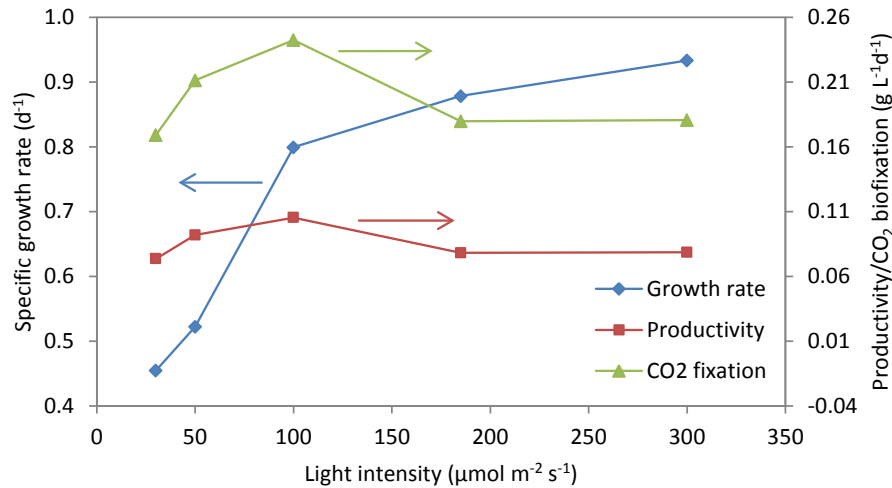


Figure 4-7 Maximum specific growth rate, productivity and CO₂ biofixation rate vs light intensity

Maximum and minimum values of productivity and CO₂ biofixation rate are happened at light intensities of 100 and 30 $\mu\text{mol m}^{-2} \text{s}^{-1}$, respectively. However, interestingly, specific growth rate increases with light intensity. Specific growth rate sharply increased from 0.45 to 0.52 and then to 0.8 d^{-1} when light intensity rose from 30 to 50 and then to 100 $\mu\text{mol m}^{-2} \text{s}^{-1}$, respectively. Although specific growth rate continued to increase while increasing light intensity to 185 and 300 $\mu\text{mol m}^{-2} \text{s}^{-1}$, it just slowly increased to 0.88 and 0.93 d^{-1} . Increasing specific growth rate with increasing light intensity shows positive effect, as more photon availability in the culture could leads to a great exponential growth of biomass. However after few days, due to cell damage at high light intensities of 185 and 300 $\mu\text{mol m}^{-2} \text{s}^{-1}$, biomass growth reduces and finally less biomass and productivity will be achieved. As it can be seen, even at 50 $\mu\text{mol m}^{-2} \text{s}^{-1}$ of light intensity, higher productivity and CO₂ biofixation rate was obtained in compare with 185 and 300 $\mu\text{mol m}^{-2} \text{s}^{-1}$.

4.3.7 Specific growth rate, productivity and CO₂ biofixation at various light intensities

The growth of biomass in the present study is being measured and the specific growth rate is being calculated by Equation (3-3). Biomass productivity and CO₂ biofixation rate are calculated using Equations (3-4) and (3-5). Figure 4-8 illustrates specific growth rate, biomass production rate and CO₂ biofixation rate at different light intensities. Specific growth rate increased with an increase in light intensity.

Increasing the light intensity from 50 to 100 $\mu\text{mol m}^{-2} \text{s}^{-1}$ resulted in enhancing the specific growth rate from 0.52 to 0.8 d^{-1} . Specific growth rate increased with increasing light intensity and no sharp change occurred. It finally reached a maximum of 0.93 d^{-1} at a light intensity of 300 $\mu\text{mol m}^{-2} \text{s}^{-1}$.

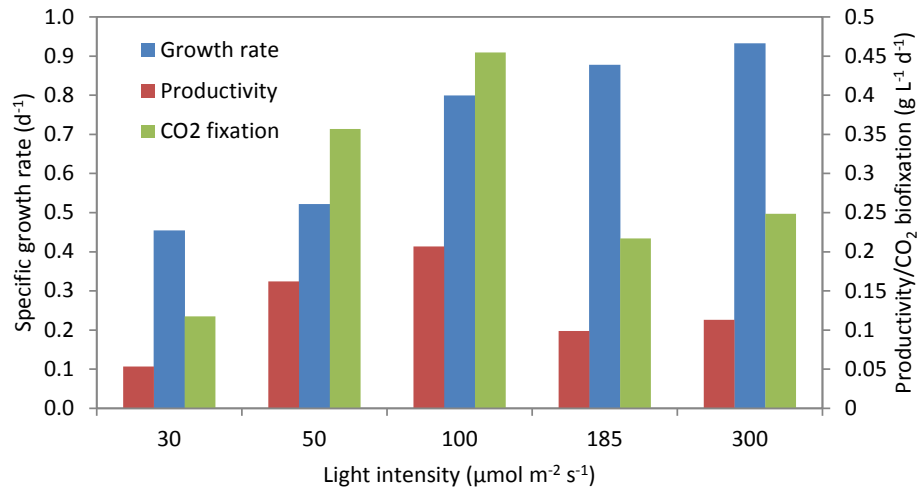


Figure 4-8 Effect of light intensity on specific growth rate, productivity and CO₂ biofixation rate

The specific growth rates in these experiments were calculated to be 0.455, 0.522, 0.799, 0.878 and 0.933 d^{-1} at 30, 50, 100, 185 and 300 light intensities, respectively. Maximum growth rates of 0.04 and 0.06 h^{-1} equated to 0.96 and 1.44 d^{-1} , and this has been reported for the same strain by Jacob et al. (2008a) and Concas et al. (2012) when 15 % and 100 % CO₂ were injected. Sacasa et al. (2013) cultivated the same strain in a similar bioreactor with 2 L min^{-1} of 3 % CO₂ inlet gas and achieved a maximum growth rate of 0.172 d^{-1} and a maximum biomass concentration of 0.470 g L^{-1} .

Despite the continuous increase of the specific growth rate with an increase of light intensity, the production rate did not show the same trend. Productivity increased when the light intensity changed from 30 to 50 and then 100 $\mu\text{mol m}^{-2} \text{s}^{-1}$; nevertheless, it was reduced at light intensities of 185 and 300 $\mu\text{mol m}^{-2} \text{s}^{-1}$. Productivity reached 0.21 $\text{g DCW L}^{-1} \text{d}^{-1}$ at a light intensity of 100 $\mu\text{mol m}^{-2} \text{s}^{-1}$ which was maximised in comparison with lower and higher light intensities. Similarly, CO₂ biofixation showed a similar trend because it is proportional to the production rate. Maximum CO₂ biofixation achieved at 100 $\mu\text{mol m}^{-2} \text{s}^{-1}$ was 0.45 $\text{g CO}_2 \text{ L}^{-1} \text{d}^{-1}$. This result was better than those obtained by Yun et al. (1997), who cultivated *C. vulgaris* at 27 °C, 15 % CO₂ and 110 $\mu\text{mol m}^{-2} \text{s}^{-1}$ and obtained a rate of 0.312 $\text{g L}^{-1} \text{d}^{-1}$, and

by Sydney et al. (2010), who achieved 0.252 g CO₂ L⁻¹ d⁻¹ for cultivation of the same strain at 30 °C, 5 % CO₂ and 3500 lux. Ho et al. (2012) saw the same trend for production rate and CO₂ biofixation rate when they cultured *Scenedesmus obliquus*. For this strain, productivity is maximised at light intensity of 420 μmol m⁻² s⁻¹ and then decreased with higher light intensity. A rate of 0.128 g CO₂ L⁻¹ h⁻¹ was removed by *C. vulgaris* when cultivated in a bubble column at 25 °C, 1.25 L min⁻¹ gas flow rate and 10800 lx light intensity (Fan et al., 2007b). Furthermore, daily CO₂ biofixation of 1.96 g d⁻¹ was obtained at 1600 μmol m⁻² s⁻¹ for *Synechocystis* sp. after six days cultivation, which was maximum in comparison with cultivation at lower or higher light intensities (Ho et al., 2012).

While lower biomass production and CO₂ removal at lower light intensities is due to light limitation, a drop in productivity and CO₂ fixation at higher light intensities occurred because of photoinhibition (Chiang et al., 2011, Wahidin et al., 2013). Furthermore, in dense cultures, both photolimitation and photoinhibition can take place simultaneously. Increasing light intensity to avoid light limitation in the deep parts of dense cultures may lead to inhibition of microalgae growth at the surface of the bioreactor (Ho et al., 2012).

Despite a higher specific growth rate in light intensities of 185 and 300 μmol m⁻² s⁻¹ compared with a light intensity of 100 μmol m⁻² s⁻¹, the production rate was less. This can be considered a result of inhibition. In reality, due to more photon flux available to microalga, it grew faster at first but afterwards, high light intensity damaged the cells and consequently, they did not continue to grow well. Many researchers concentrated on photoinhibition phenomena for variety of species. For instance, Wahidin et al. (2013) investigated the influence of light intensity on *Nannochloropsis* sp. and discussed that light intensity above saturation led to an inhibition effect. Microalgae growth can take place in light limitation, light saturation or light inhibition conditions (Ho et al., 2012). Saturation light intensity varies for different species and it ranges from 140 to 210 μmol m⁻² s⁻¹ (Kumar et al., 2011). For example, according to Hanagata (1992a), 200 μmol m⁻² s⁻¹ is the saturation light intensity for *Chlorella* sp. and *Scenedesmus*.

In this study, a maximum of 0.45 g CO₂ L⁻¹ d⁻¹ was fixed at a light intensity of 100 μmol m⁻² s⁻¹. In a study performed by Ryu et al. (2009), maximum productivity and maximum biofixation rate of 0.335 g DW L⁻¹ d⁻¹ and 0.35 g CO₂ d⁻¹

have been reported when *Chlorella* sp. was cultivated in 600 ml vertical photobioreactor aerated by 5 % CO₂ enriched air. However, they achieved 0.295 g DW L⁻¹ d⁻¹ productivity and 0.31 g CO₂ d⁻¹ biofixation when 2 % CO₂ was injected.

4.3.8 Experimental results at two different light intensities

Results of experiments at light intensities of 120 and 280 μmol m⁻² s⁻¹ while all other conditions kept same have been shown in Figure 4-9, (a,b,c), for biomass concentration, specific growth rate and productivity versus cultivation time.

First, biomass increased exponentially and then after 3 days continued to increase nearly linearly with low slope, for both experiments. However, at higher incident light intensity of 280 μmol m⁻² s⁻¹, biomass concentration increased faster at the early days after inoculation and reached to 0.79 g L⁻¹ in compare to 0.66 g L⁻¹ for 120 μmol m⁻² s⁻¹ light intensity. Afterwards, biomass growth dropped in both experiments but biomass growth in higher light intensity showed more decrease so that biomass concentration after ten days reached to 1.48 and 1.00 g L⁻¹ for light intensities of 120 and 280 μmol m⁻² s⁻¹.

It worth to mention that at previous set of experiments, for cultivation under 100 μmol m⁻² s⁻¹, a biomass concentration of 1.46 g L⁻¹ were achieved after 10 days, and similarly in recent experiments, a biomass concentration of 1.48 g L⁻¹ was achieved at 120 μmol m⁻² s⁻¹ light intensity. Besides, biomass concentration was 0.97 g L⁻¹ after 10 days at 300 μmol m⁻² s⁻¹ of light intensity in first set of the experiments, and then biomass concentration reached to 1.0 g L⁻¹ when light intensity was adjusted to 280 μmol m⁻² s⁻¹ in recent experiment. Although conditions were slightly different in first and second set of the experiments; 2 % CO₂, 20 °C and 200 rpm agitation speed in compare with 4 % CO₂, 28 °C and 300 rpm, and also light intensity was not exactly same but quite close, biomass growth was almost same. This could be a proof of significant importance of light intensity to compare with other factors.

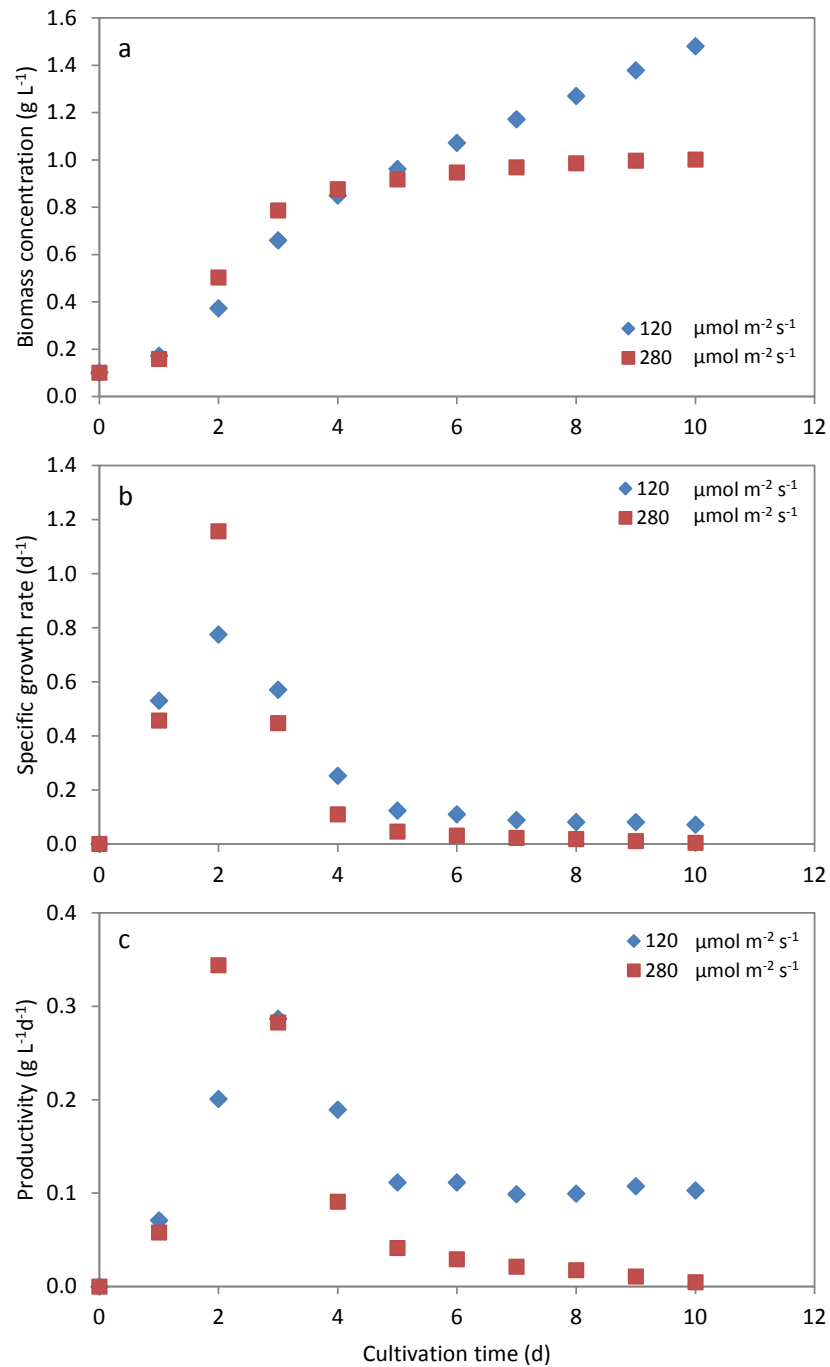


Figure 4-9 a) Biomass concentration , b) specific growth rate and c) productivity vs cultivation time for two light intensities of 120 and 280 $\mu\text{mol m}^{-2} \text{s}^{-1}$

Figure 4-9 b, illustrates specific growth rate over the time for these experiments. Specific growth rate increases sharply and reaches to maximum value in second day of culturing, which are 0.77 and 1.16 d^{-1} for 120 and 280 $\mu\text{mol m}^{-2} \text{s}^{-1}$ incident irradiance, respectively. Afterwards, it sharply falls to 0.12 and 0.05 d^{-1} and then slowly decreases and reaches to 0.07 and 0.005 d^{-1} , for light intensities of 120

and 280 $\mu\text{mol m}^{-2} \text{s}^{-1}$, respectively. Decrease of specific growth rate to very small values in fourth day leads to noticeable change at biomass concentration curve and drop in biomass growth.

The highest value of daily productivity was 0.78 $\text{g L}^{-1} \text{d}^{-1}$ in second day when 280 $\mu\text{mol m}^{-2} \text{s}^{-1}$ of light intensity was furnished to the bioreactor. For illumination with 120 $\mu\text{mol m}^{-2} \text{s}^{-1}$, productivity reached maximum to 0.64 $\text{g L}^{-1} \text{d}^{-1}$. Then, daily productivity declined to 0.23 and 0.01 $\text{g L}^{-1} \text{d}^{-1}$ for light intensity of 120 and 280 $\mu\text{mol m}^{-2} \text{s}^{-1}$, respectively. Productivity for whole duration of culturing which was ten days calculated to be 0.14 and 0.09 $\text{g L}^{-1} \text{d}^{-1}$, for the experiments with 120 and 280 $\mu\text{mol m}^{-2} \text{s}^{-1}$ of light intensity.

From what discussed above, two significant phenomena concluded. First, generally biomass growth shows a reduction after few days and that is due to increase in biomass concentration inside the bioreactor which leads to less availability of photons. Second, it can be deduced that first biomass grow faster in early days for higher light intensity but it experienced more decrease in following days which is due to cell damage as a result of high irradiance, and consequently, less biomass concentration is achieving.

CO₂ biofixation was estimated 0.32 $\text{g CO}_2 \text{L}^{-1} \text{d}^{-1}$ when light intensity of 120 $\mu\text{mol m}^{-2} \text{s}^{-1}$ is furnished on the surface of the bioreactor, while it is reduced to 0.21 $\text{g CO}_2 \text{L}^{-1} \text{d}^{-1}$ for 280 $\mu\text{mol m}^{-2} \text{s}^{-1}$. Actually, CO₂ biofixation rate is 34 % less for higher irradiance. CO₂ utilisation efficiency is a better parameter to analyse effectiveness of CO₂ removal. CO₂ utilisation efficiencies are calculated 0.56 % and 36 % for these experiments with 120 and 280 $\mu\text{mol m}^{-2} \text{s}^{-1}$ illuminations.

Because light provides the required energy for photosynthesis, it is one of the significant factors affecting microalgae growth along with other factors such as pH, temperature and aeration rate. However, both phenomena of photolimitation and photoinhibition, as well as the change in the light gradient inside the vessel with cultivation time and biomass concentration, make light regime analysis more complicated.

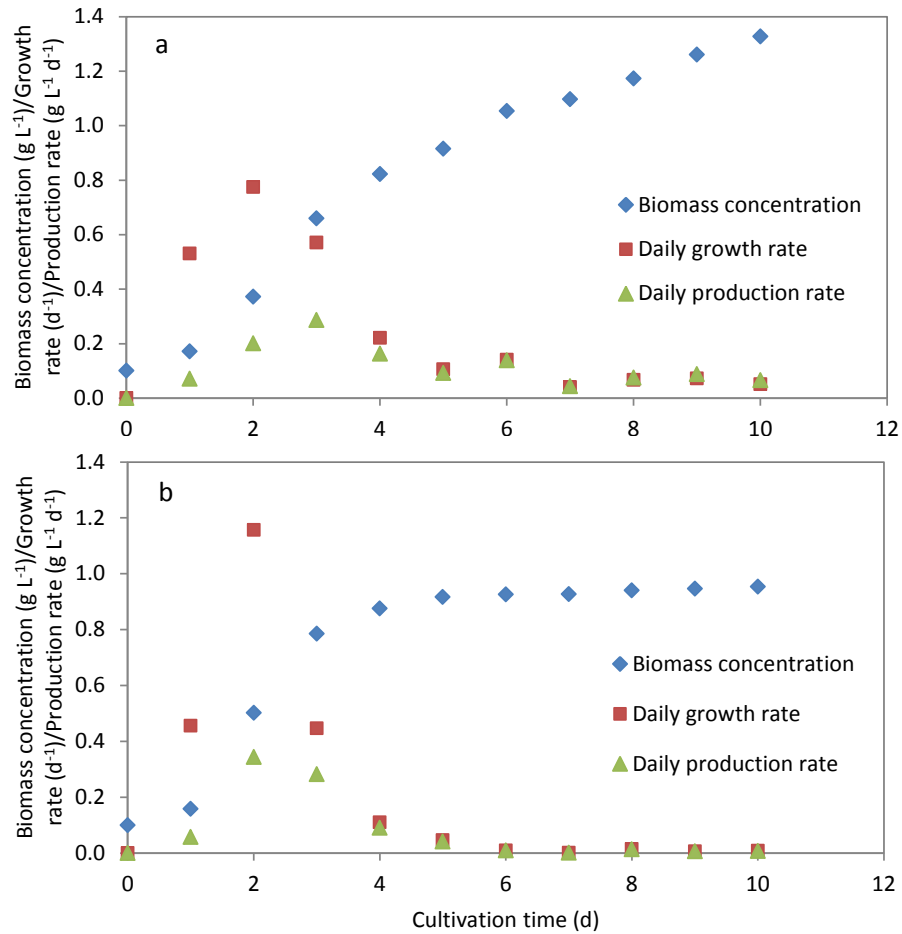


Figure 4-10 Biomass concentration, daily specific growth rate and daily production rate vs time at two different incident light intensities: a) 120 $\mu\text{mol m}^{-2} \text{s}^{-1}$ & b) 280 $\mu\text{mol m}^{-2} \text{s}^{-1}$

To discuss how growth rate and production rate changes during culturing time, these two factors along with biomass concentration have been plotted in same graph for two different values of incident light intensities (120 and 280 $\mu\text{mol m}^{-2} \text{s}^{-1}$) while all other parameters kept constant; 28 °C temperature, 300 rpm agitation speed, 0.5 vvm aeration rate, 4 % CO₂ and 12 h light period, Figure 4-10 (a, b). After one day lag phase, exponential growth phase continues for about two days and then after 3-4 days of culturing, biomass growth decreases. Daily growth rate sharply increases for first two days in both cases and then severely drops to very small value. Although trend of changes in daily growth rate are same for both incident light intensities, it reaches to higher value at peak point when incident light intensity is 280 $\mu\text{mol m}^{-2} \text{s}^{-1}$. Maximum daily growth rates approximately are 0.8 and 1.2 d^{-1} for incident light intensities of 120 and 280 $\mu\text{mol m}^{-2} \text{s}^{-1}$, respectively. As expected, daily production

rate shows same behaviour of daily growth rate and reaches to a maximum in second or third day of cultivation time and then fall down to small value.

To evaluate how light intensity inside the culture changes as biomass grows at these two experiments which were conducted at two different incident light intensities of 120 and 280 $\mu\text{mol m}^{-2} \text{s}^{-1}$, every day after sampling and measuring OD of the sample, local light intensity was measured with spherical micro quantum sensor at the centre of the bioreactor. Results have been illustrated in Figure 4-11 (a, b). As it can be seen as soon as biomass grows, light intensity drops to smaller values even for a little increase in biomass concentration in first day after inoculation. Indeed, in day 5 in the first experiment and in day 6 in the second experiment, when biomass concentration reaches to around 0.8 g L⁻¹, light intensity at centre of the bioreactor is almost zero. At the same time a drop in biomass growth occurs. Even increasing incident light intensity from 120 to 280 $\mu\text{mol m}^{-2} \text{s}^{-1}$, does not positively change this phenomena. Indeed, reduction at biomass growth is observed when local light intensity drops to less than 10 $\mu\text{mol m}^{-2} \text{s}^{-1}$ at the centre of the bioreactor. In this situation the calculated average light intensity using Equation (2-11) is 65-85 $\mu\text{mol m}^{-2} \text{s}^{-1}$. Hence, this is the minimum boundary of light intensity for the algae used in this study and limiting effect occurs. Overall, saturation light intensity is in the range of 45-120 $\mu\text{mol m}^{-2} \text{s}^{-1}$, while higher light intensities of 120 $\mu\text{mol m}^{-2} \text{s}^{-1}$ causes inhibitory influence of light intensity (Latala, 1991). Although, microalgae species can adopt themselves to higher light intensity, their growth is not pronounced as at saturation light intensity. As it was observed in this study optimum light intensity for *C. vulgaris* is around 100 $\mu\text{mol m}^{-2} \text{s}^{-1}$, however it can grow even at 350 $\mu\text{mol m}^{-2} \text{s}^{-1}$ but inhibitory effects is observe and leads to less productivity. Light distribution and average light intensity will discuss in following chapters in detail.

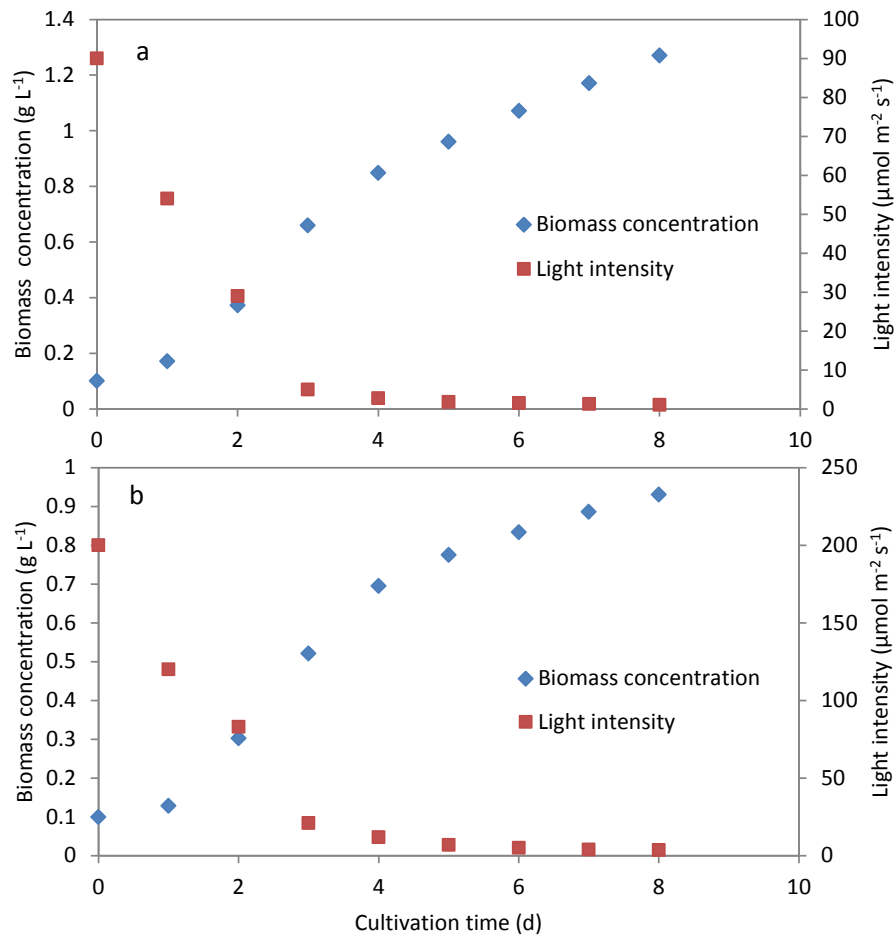


Figure 4-11 Biomass concentration and light intensity at centre of the bioreactor vs cultivation time at two different incident light intensities: a) 120 $\mu\text{mol m}^{-2} \text{s}^{-1}$ b) 280 $\mu\text{mol m}^{-2} \text{s}^{-1}$

4.4 Summary

The performance of a modified bioreactor inside a light enclosure for carbon dioxide (CO₂) bio-fixation by *Chlorella vulgaris* was investigated. The influence of different light intensities on CO₂ biofixation and biomass production rates was evaluated. The results showed that the photon flux available to microalgal cultures can be a key issue in properly optimising microalgae photobioreactor performance, particularly at high cell concentrations. Although the optimal pH values for *C. vulgaris* range from 6-8, cell growth can take place even at pH 4 and 10. Batch microalgal cultivation in a photobioreactor was used to investigate the effect of different light configurations and intensities, including 30, 50, 100, 185 and 300 $\mu\text{mol m}^{-2} \text{s}^{-1}$. The maximum

biomass concentration of 1.83 g L⁻¹ was obtained at a light intensity of 100 μmol m⁻² s⁻¹ and 1 L min⁻¹ of 2 % CO₂ enriched air aeration. Meanwhile, suitable range of light intensity and also range of light intensity that can lead to photolimitation or photoinhibition was discussed. Overall, this species can grow properly and tolerate in light intensity in range of 50-150 μmol m⁻² s⁻¹.

Furthermore, experimentally it was deduced that among these five light intensities (30, 50, 100, 185 and 300 μmol m⁻² s⁻¹), *C. vulgaris* can grow better at light intensity of 100 μmol m⁻² s⁻¹. However, to find an accurate optimum value for light intensity which leads to maximum CO₂ biofixation, a mathematical and statistical optimisation must be carried out.

Additionally, biomass concentration, specific growth rate and productivity versus cultivation time for two light intensities of 120 and 280 μmol m⁻² s⁻¹ were discussed. The results from these experiments were in agreement with the previous set of the experiments. Then light intensity variation at centre of the bioreactor versus cultivation time at these two different incident light intensities and its relation to biomass concentration were discussed.

5

Enhancement of CO₂ Biofixation Rate and CO₂ Utilisation Efficiency in an Algal PBR

5.1 Introduction

Today, the biofixation of carbon dioxide (CO₂) as an alternative, sustainable CO₂ mitigation approach has received much attention due to increasing atmospheric CO₂ levels which seem to be the major cause of global warming. Photon availability to the biofixing cells is of high importance and is presently the main obstacle to the successful scaling-up of microalgae cultivation systems and their commercialisation. Regardless of photobioreactor (PBR) geometry or cultivation conditions, photon availability to the cells inside the PBR depends mainly on the light intensity and light period (Barsanti and Gualtieri, 2014, Dasgupta et al., 2010). Microalgae need alternating light:dark periods with sufficient photon flux during the light period for effective photosynthesis. However, due to shading effects, including photon-absorption by cells and scattering by particles, there are light gradients inside cultures, particularly in dense ones (Wahidin et al., 2013). On the other hand, it has been stated that only a small fraction of the CO₂ injected to a bioreactor can be utilised for biomass production (Jacob-Lopes et al., 2008b). Therefore, optimum illumination and CO₂ aeration are crucial factors for achieving a satisfactory level of CO₂ fixation in sustainable microalgae cultures.

Traditionally, process optimisation is accomplished by one-dimensional methods. Experiments are carried out while varying specific factors so that the optimum values can be determined. Nevertheless, applying this method to find optimum values for several factors is time-consuming. In addition, it can lead to

inaccurate results when interactions between factors are missed. Statistical experimental designs not only minimise the number of experiments, but also minimise errors while accounting for interactions between factors. Response surface methodology (RSM) is one of the most frequently applied tools in engineering optimisation (Jacob-Lopes et al., 2008a, Martinez et al., 2011).

The RSM is a mathematical and statistical technique for optimising models. Within a particular experimental design, the response (the output dependent variable) is optimised according to the influences of the input independent variables. The three steps employed in the statistical experimental design and optimisation include (i) statistical design of experiments and estimation of a mathematical model coefficient using experimental data, (ii) an analysis of the model applicability, and (iii) mathematical optimisation which can be verified experimentally. Usually, a second-order model can explain the observed response, otherwise, a higher order model should be considered (Myers, 2002).

Jacob-Lopes et al. (2008a), optimised the three independent variables most relevant to PBRs, being CO₂ concentration, temperature and light intensity. Maximum CO₂ removal was achieved by applying RSM and conducting the 17 experiments designed. They estimated the optimum conditions for the culturing of *Aphanothece microscopica Nägeli* to be 15 % CO₂, 35 °C and 11 klux. This methodology was also used to investigate the effects of initial pH, light and temperature on the cultivation of the freshwater cyanobacterium *Synechocystis* sp. (Martinez et al., 2011). The optimal growth conditions estimated from the mathematical relations were as follows: average light intensity of 686 $\mu\text{mol m}^{-2} \text{s}^{-1}$, temperature of 35.3 °C and pH of 7.2. Many researchers have investigated the effects of illumination on CO₂ biofixation but none of them considered both light intensity and light period simultaneously (Table 5-1). Wahidin et al. (2013) investigated the influence of light intensity and light period on CO₂ biofixation by *Nannochloropsis* sp.; however, the optimum biofixation rate was obtained experimentally with each factor being considered individually and their interactions being ignored. Recent studies (Table 5-1) have clearly demonstrated that only small fractions of the CO₂ injected into the photobioreactor can be bio-fixed and utilised for biomass production.

Table 5-1 CO₂ biofixation rate for various microalgae species under various conditions

Microalgae species	Temperature (°C)	CO ₂ (%)	Light intensity (μmol m ⁻² s ⁻¹)	Photoperiod (Light:dark)	Specific growth rate (d ⁻¹)	Biomass Productivity (g L ⁻¹ d ⁻¹)	Reactor type	Reference
<i>Chlorella</i> sp.	40	20	500	24:0	5.76	0.7	Tubular	(Sakai et al., 1995)
<i>Synechocystis aquatulis</i>	N.A.	N.A.	N.A.	24:0	5.5	0.59	N.A.	(Murakami and Ikenouchi, 1997)
<i>Scenedesmus obliquus</i>	30	12	3200 lx	12:12	0.22	0.14 ^a	Tubular	(De Morais and Costa, 2007a)
<i>Spirulina</i> sp.	30	6	3200 lx	12:12	0.44	0.2 ^a	Tubular	(De Morais and Costa, 2007a)
<i>Chlorella vulgaris</i>	25	0.093	3600 lx	24:0	N.A	0.15	Membrane tubular	(Fan et al., 2008)
<i>Chlorella</i> sp.	26	2	300	24:0	0.49	0.17	Bubble column	(Chiu et al., 2008)
<i>Chlorella</i> sp.	Ambient	5	100	N.A	N.A	0.34	Tubular	(Ryu et al., 2009)
<i>Aphanothece microscopica</i> Nägeli	35	15	150	24:0	N.A	0.77	Bubble column	(Jacob-Lopes et al., 2009a)
<i>Scenedesmus obliquus</i>	28	10	60	24:0	1.19	0.29	N.A.	(Ho et al., 2010)
<i>Anabaena</i> sp.	30	300 ppm	1625	N.A.	N.A.	0.5	Bubble column	(Sánchez et al., 2012)
<i>Synechocystis</i> sp.	25	5	1600	16:8	0.095	1.56	Bubble column	(Martinez et al., 2012)
<i>Chlorella</i> sp.	27	1	100	12:12	0.58	0.028	Tubular	(Kim et al., 2012)
<i>Dunaliella salina</i>	27	3	80	12:12	0.78	0.054	Tubular	(Kim et al., 2012)
<i>Dunaliella</i> sp.	25	1	100	12:12	0.56	0.03	Tubular	(Kim et al., 2012)
<i>Nannochloropsis</i> sp.	23	300 ppm	100	18:6	0.34	N.A.	N.A.	(Wahidin et al., 2013)
<i>Spirulina platensis</i>	25	300 ppm	90-125	24:0	N.A.	0.087	Bubble column	(Arata et al., 2013)
<i>Tetraselmis suecica</i>	Ambient	N.A.	Sunlight	-	N.A.	0.52	Tubular	(Michels et al., 2014)
<i>Scenedesmus obliquus</i>	25	350 ppm	150	16:8	0.18	0.077	Airlift	(Massart et al., 2014)
<i>Chlorella vulgaris</i>	30	2	250	N.A.	N.A.	0.72	Airlift	(Fernandes et al., 2014)
<i>Chlorella sorokiniana</i>	35	5	1500	24:0	N.A.	8.6	Flat plate	(Tuantet et al., 2014)
<i>Scenedesmus obliquus</i>	23	5	350	N.A	0.49	0.35	Flat plate	(Gris et al., 2014)

Therefore, this study was devoted to understanding the synergistic effects of the key important factors including light intensity, light period and CO₂ concentration, on biomass growth, CO₂ biofixation rate and CO₂ utilisation, using *C. vulgaris* in a batch PBR system. Response surface methodology optimisation based on CCD will be applied for optimising the algal PBR performance.

5.2 Materials and Methods

The freshwater microalgae strain *C. vulgaris* was cultivated in a fresh MLA medium in a three litre stirred-tank bioreactor in which accurate adjustment of light intensity, light period and CO₂ concentration were possible. Batch cultivations of microalgae were conducted at in experiments designed to optimise the three independent variables of light intensity, light period and CO₂ concentration. Culture samples were collected daily to estimate biomass concentration by measuring the OD. Medium preparation, microalgae cultivation, the PBR system and biomass analyses were detailed in Chapter 3.

Relationships between three independent variables of light intensity, light period and CO₂ concentration, and their influences on the CO₂ biofixation rate were determined by a second-order mathematical model according to the RSM statistical method. In this study, central composite design (CCD) was utilised to design the experiments for estimating optimum response. Design was carried out in a fractional factorial of five levels for each variable, with alpha equal to 1.68. Simultaneously, optimum CO₂ utilisation efficiency was estimated using the same experimental data. Table 5-2 shows the levels of experimental conditions.

Table 5-2 Independent variable values for different levels of experimental design

Independent variable	Symbol	Level				
		-1.68	-1	0	1	1.68
Light intensity ($\mu\text{mol m}^{-2} \text{s}^{-1}$)	x_1	65.6	120	200	280	334.4
Light period (hours)	x_2	9.3	12	16	20	22.7
CO ₂ concentration (%)	x_3	1.3	4	8	12	14.7

To achieve the target, 17 experimental runs were conducted, as stated in Table 5-3. The actual and coded values of the variables in each experiment can also be found in this table. Each experiment was carried out under constant conditions of

28 °C temperature, 0.5 vvm aeration rate, 300 rpm agitation speed, 0.1 g L⁻¹ initial biomass concentration, and 10 day duration. Biomass productivity, CO₂ biofixation rate and CO₂ utilisation efficiency were estimated by Equations (3-4), (3-5) & (3-6), respectively. Then, a second-order polynomial equation that included interaction terms (Equation (5-1)) was fitted to the experimental data using non-linear regression and least squares methods by means of minimising the sum of the squares of the errors.

$$\begin{aligned}
 \text{CO}_2 \text{ biofixation rate} & \quad (5-1) \\
 & = \beta_0 + \beta_1 X_1 + \beta_2 X_2 + \beta_3 X_3 + \beta_{11} X_1^2 + \beta_{22} X_2^2 \\
 & \quad + \beta_{33} X_3^2 + \beta_{12} X_1 X_2 + \beta_{13} X_1 X_3 + \beta_{23} X_2 X_3
 \end{aligned}$$

where X_1 , X_2 , and X_3 represent the coded independent variables of light intensity, light period and CO₂ concentration, respectively; β_0 is a constant coefficient; β_i is the first-order coefficient; β_{ii} is the second-order coefficient; and β_{ij} is the interaction coefficient. Also, maximum productivity and maximum CO₂ utilisation were estimated. To calculate maximum productivity, Equation (5-1) at maximum CO₂ biofixation rate can be used, since productivity is proportional to CO₂ biofixation; therefore, both of them will be maximised at the same conditions of light intensity, light period and CO₂ concentration. However, optimum CO₂ utilisation efficiency can vary according to the CO₂ utilisation efficiency achieved under the conditions of maximum CO₂ biofixation. This means that the conditions that maximise CO₂ utilisation efficiency might be different from the conditions that maximise CO₂ biofixation rate. This is due to definition of CO₂ utilisation efficiency so that inlet CO₂ concentration effects on both numerator and denominator values, Equation (3-6). So, maximum CO₂ utilisation will be calculated by Equations (3-6) and (5-1) and will be compared with CO₂ utilisation efficiency obtained under the conditions of maximum CO₂ biofixation. Regressions, statistical analyses and ANOVAs were carried out using MATLAB, and also The Synthesis, and DOE++ software (version 10.1).

Table 5-3 Experimental runs, actual and coded levels of variables

Run		Actual level of variables			Coded level of variables		
		Light intensity ($\mu\text{mol m}^{-2} \text{s}^{-1}$)	Light period	CO ₂ concentration (%)	X ₁	X ₂	X ₃
1	Factorial portion	120	12:12	4	-1	-1	-1
2	“	120	12:12	12	-1	-1	+1
3	“	120	20:4	4	-1	+1	-1
4	“	120	20:4	12	-1	+1	+1
5	“	280	12:12	4	+1	-1	-1
6	“	280	12:12	12	+1	-1	+1
7	“	280	20:4	4	+1	+1	-1
8	“	280	20:4	12	+1	+1	+1
9	Axial portion	65.6	16:8	8	-1.68	0	0
10	“	334.4	16:8	8	+1.68	0	0
11	“	200	9.3:14.7	8	0	-1.68	0
12	“	200	22.7:1.3	8	0	+1.68	0
13	“	200	16:8	1.3	0	0	-1.68
14	“	200	16:8	14.7	0	0	+1.68
15	Central portion	200	16:8	8	0	0	0
16	“	200	16:8	8	0	0	0
17	“	200	16:8	8	0	0	0

5.3 Results and Discussion

Since microalgal CO₂ biofixation is indicative of cell growth, the CO₂ biofixation ability of microalgal species is positively correlated with their cell growth rate and biomass productivity (Ho et al., 2011). Therefore, enhancing the factors affecting biomass growth is essential to maximise CO₂ biofixation (Tebbani et al., 2014). The RSM method is a reliable and relatively fast way to estimate the influence of various factors on objective function. In this research, RSM was used to derive a model to investigate how CO₂ biofixation rate changes with light intensity, light period and CO₂ concentration. In the following sections, the experimental results and the individual and synergistic effects of various factors will be discussed. This will lead to optimisation results for both CO₂ biofixation and CO₂ utilisation efficiency.

5.3.1 Experimental results

As explained previously, light intensity, light period and CO₂ concentration are three of the most significant factors affecting biomass growth in algae. In this section, experimental results are conferred to see the effect of these three parameters on biomass growth.

Maximum specific growth rates of between 0.6131—1.3379 d⁻¹ were observed under different cultivation conditions. This indicates that there was a dependence of biomass growth rate and PBR performance on light intensity, light period and the percentage of CO₂ in the enriched air. It should be noted that this microalgae species was able to grow in all applied conditions (light intensity ranged from 65.6—334.4 μmol m⁻² s⁻¹, light period ranged from 9.3—22.7 h, and CO₂ concentration ranged from 1.3—14.7 %); however, different amount of biomass grew in each experiment. Biomass concentrations ranged from 0.4855 to 1.5517 g L⁻¹, and the maximum was obtained under cultivation conditions of 200 μmol m⁻² s⁻¹ incident light intensity, 16 h light period, and 8 % CO₂ concentration. The maximum productivity rate (0.1443 g L⁻¹ d⁻¹) and maximum CO₂ biofixation rate (0.3318 g CO₂ L⁻¹ d⁻¹) were achieved under the same conditions. The CO₂ biofixation rate in these experiments was between 0.08—0.33 g CO₂ L⁻¹ d⁻¹. The CO₂ biofixation results reported by Lopez et al. (2009) for same species varied from 0.08—1.1 g CO₂ L⁻¹ d⁻¹.

However, maximum CO₂ utilisation may not have occurred under these conditions. Actually, since CO₂ utilisation efficiency is defined as the percentage of input CO₂ that has been processed, it depends on both CO₂ concentration and CO₂ biofixation rate. In this study, among the experiments, the maximum CO₂ utilisation efficiency of 0.50 % was achieved when *C. vulgaris* was cultivated under incident light intensity, light period and CO₂ concentration of 120 $\mu\text{mol m}^{-2} \text{s}^{-1}$, 20 h and 4 %, respectively.

5.3.1.1 Influence of light intensity

Figure 5-1 shows the results of three experiments conducted under incident light intensities of 65.6, 200 and 334.4 $\mu\text{mol m}^{-2} \text{s}^{-1}$, while light period and CO₂ concentration were held constant at 16 h and 8 %, respectively. Among these, the experiment with 200 $\mu\text{mol m}^{-2} \text{s}^{-1}$ light intensity produced the maximum biomass concentration (1.55 g L⁻¹). Optimum light intensity for *C. vulgaris* is reported to be between 150—350 $\mu\text{mol m}^{-2} \text{s}^{-1}$, while a light intensity of 369 $\mu\text{mol m}^{-2} \text{s}^{-1}$ leads to lower biomass growth (Bhola et al., 2011).

Figure 5-2 shows the influence of light intensity (65.6, 200 and 334.4 $\mu\text{mol m}^{-2} \text{s}^{-1}$) on the maximum specific growth rate, CO₂ biofixation rate and CO₂ utilisation efficiency under a constant light period and inlet CO₂ concentration of 16:8 h and 8 %, respectively. All factors were maximal at the 200 $\mu\text{mol m}^{-2} \text{s}^{-1}$ light intensity. The minimum growth rate was observed at the lowest tested light intensity (65.6 $\mu\text{mol m}^{-2} \text{s}^{-1}$). The CO₂ biofixation rate and CO₂ utilisation efficiency were lowest at the highest light intensity (334.4 $\mu\text{mol m}^{-2} \text{s}^{-1}$). Indeed, although specific growth rate was higher with 334.4 $\mu\text{mol m}^{-2} \text{s}^{-1}$ of light than with 65.6 $\mu\text{mol m}^{-2} \text{s}^{-1}$, less biomass concentration and consequently, less CO₂ biofixation, occurred under the higher light intensity. Among these experiments, the maximum specific growth rate was 1.1 d⁻¹ and occurred at 200 $\mu\text{mol m}^{-2} \text{s}^{-1}$ light intensity, 16 h light period and 8 % CO₂. A higher maximum specific growth rate of 1.37 d⁻¹ has been reported for *C. vulgaris* cultivated under 15 % CO₂, a light period of 16:8 h, and a light intensity of 45-50 $\mu\text{mol m}^{-2} \text{s}^{-1}$ (Ji et al., 2013).

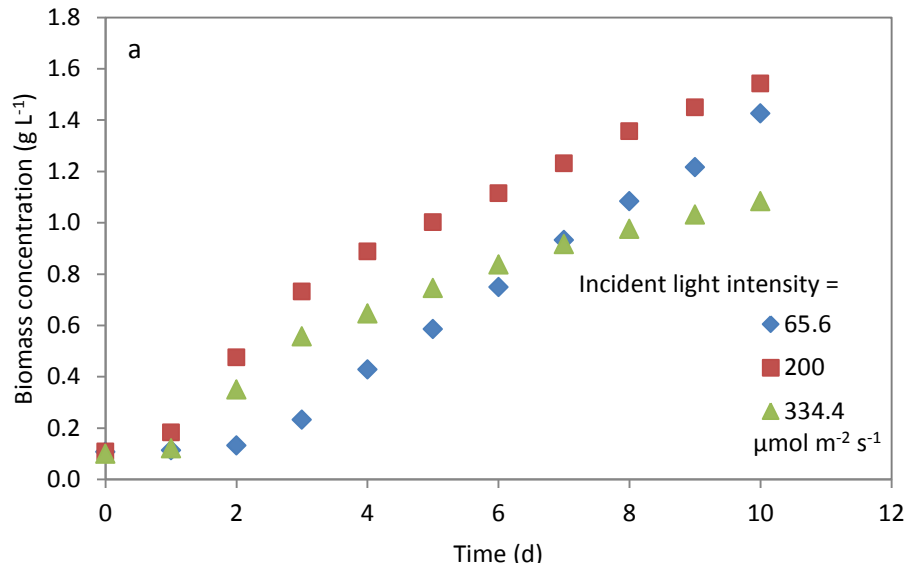


Figure 5-1 Biomass concentration vs cultivation time for incident light intensities of 65.6, 200 & 334.4 $\mu\text{mol m}^{-2} \text{s}^{-1}$ with light period of 16 h and CO₂ concentration of 8 %

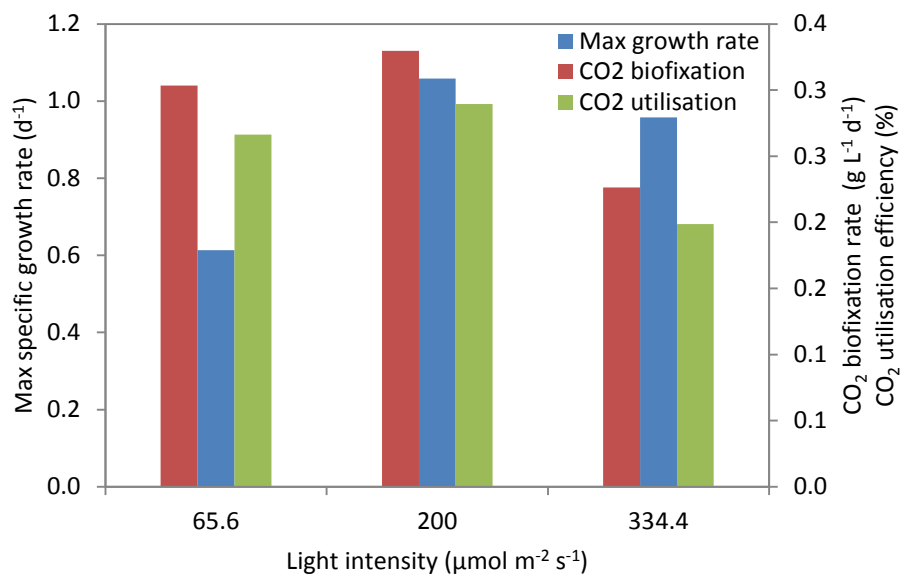


Figure 5-2 Maximum specific growth rate, CO₂ biofixation rate and CO₂ utilisation efficiency under different light intensities

5.3.1.2 Influence of light period

Results for experiments conducted with different light periods (9.3, 16 and 22.7 h) with constant light intensity (200 $\mu\text{mol m}^{-2} \text{s}^{-1}$) and CO₂ concentration (8 %) are illustrated in Figure 5-3. Maximum biomass (1.55 g L^{-1}) was observed when light period was 16 h. Minimum biomass (1.1 g L^{-1}) was achieved at 9.3 h light period. There are no published reports of the optimum light period for CO₂ biofixation by *C.*

vulgaris. However, maximum biomass concentration for *C. vulgaris* was achieved with a 16 h light period among the three periods (8, 12, 16 h) tested by Amini Khoeyi et al. (2012) which is in agreement with the present study. Wahidin et al. (2013) examined three light periods (24:0, 18:06 and 12:12 h) for *Nannochloropsis* sp. and found 18 h to be optimum. Optimum light period for the cyanobacterium *Aphanothece microscopica Nægeli* was investigated under 12 light periods (0:24 up to 24:0) in a bubble column photobioreactor with light intensity and CO₂ concentration of 150 $\mu\text{mol m}^{-2} \text{s}^{-1}$ and 15 %, respectively (Jacob-Lopes et al., 2009a). A linear increase in biomass production (from 0.002 up to 0.77 $\text{g L}^{-1} \text{d}^{-1}$) and CO₂ biofixation (from 0.004 up to 1.44 $\text{g CO}_2 \text{L}^{-1} \text{d}^{-1}$) was evident with increasing light period (from 0 up to 24 h), with the exception being under a 12:12 h regime. CO₂ biofixation intensively dropped ($< 0.065 \text{g CO}_2 \text{L}^{-1} \text{d}^{-1}$) with light periods of less than 8 h. Biomass production of *Chlorococcum* sp. was higher with a 16 h light period than with 12 or 24 h light periods (Chai et al., 2012).

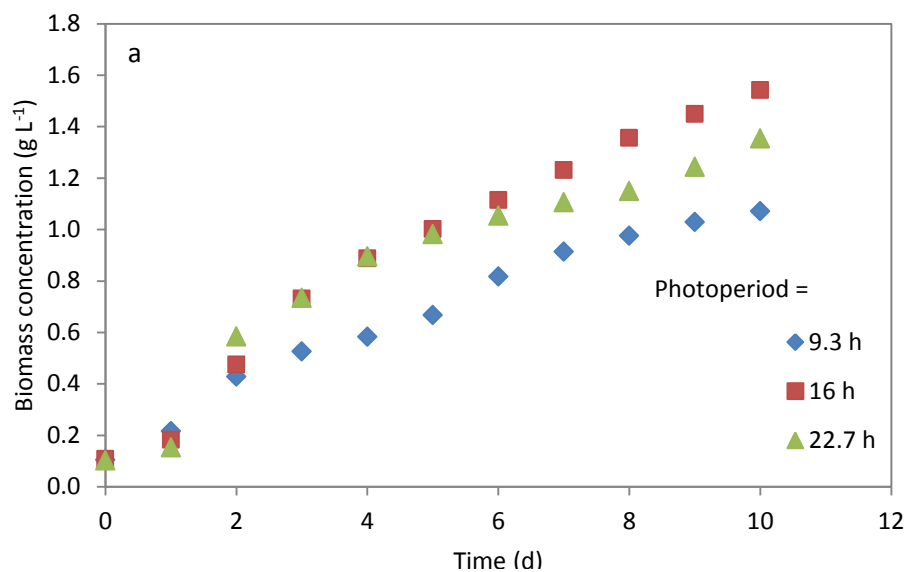


Figure 5-3 Biomass concentration vs cultivation time for light periods of 9.3, 16 and 22.7 h, with light intensity of 200 $\mu\text{mol m}^{-2} \text{s}^{-1}$ and CO₂ concentration of 8 %

The influence of different light periods (9.3, 16, 22.7 h) on the maximum specific growth rate, CO₂ biofixation rate and CO₂ utilisation efficiency at a constant light intensity of 200 $\mu\text{mol m}^{-2} \text{s}^{-1}$ and constant CO₂ concentration of 8 % are depicted in Figure 5-4. Maximum specific growth rate increased as light period increased. The highest specific growth rate of the three experiments was 1.34 d^{-1} , which is very close to that achieved by Ji et al. (2013) (1.37 d^{-1}) with the same species

under PBR conditions of 45—50 $\mu\text{mol m}^{-2} \text{s}^{-1}$, 16:8 light period and 15 % CO₂. The CO₂ biofixation rate and CO₂ utilisation efficiency showed significant increases when increasing light period from 9.3 to 16 h; however, they decreased slightly with a 22.7 h light period. Greater photon availability may lead to fast initial growth, but with time it may cause cell damage which lowers the biomass concentration.

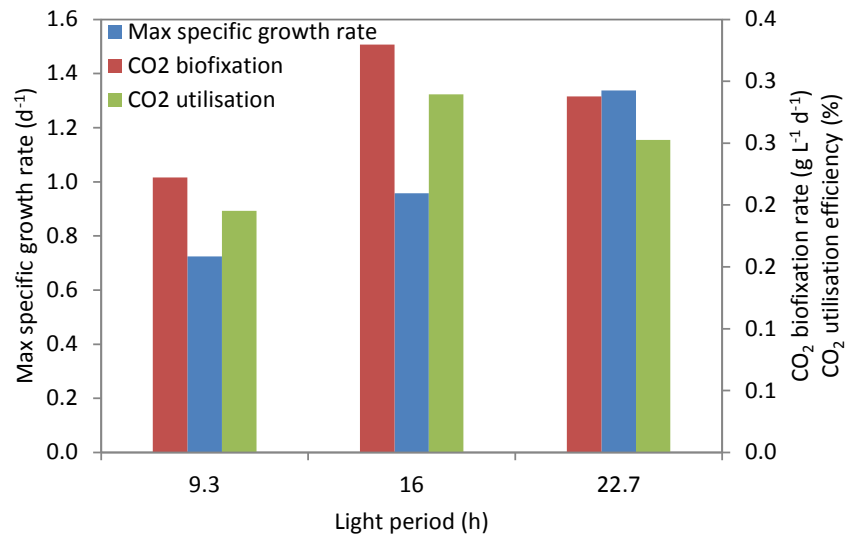


Figure 5-4 Maximum specific growth rate, CO₂ biofixation rate and CO₂ utilisation efficiency at different light periods

5.3.1.3 Influence of CO₂ concentration

The algal biomass concentrations that resulted after injecting gas at various CO₂ concentrations (1.3, 8, and 14.7 %) under constant conditions of incident light intensity (200 $\mu\text{mol m}^{-2} \text{s}^{-1}$) and light period (16 h) are shown in Figure 5-5. Interestingly, a very low biomass concentration (0.49 g L⁻¹) was achieved by aerating with 1.3 % CO₂-enriched air, and a similarly low biomass concentration (0.96 g L⁻¹) was observed with a much greater CO₂ concentration (14.7 %). However, biomass concentration was higher (1.55 g L⁻¹) when the CO₂ concentration was moderate (8 %). In previous studies, a promising CO₂ biofixation ability for *C. vulgaris* has been reported (Li et al., 2013). A range of CO₂ biofixation rates, of 0.73—1.79 g CO₂ L⁻¹ d⁻¹, was reported by Ho et al. (2011) for this species. Anjose et al. (2013) examined CO₂ biofixation by *C. vulgaris* with different CO₂ concentrations (2, 6 and 10 %) and achieved biofixation rates of 1.15—2.29 g CO₂ L⁻¹ d⁻¹, with maximum biofixation occurring at 6 % CO₂ concentration.

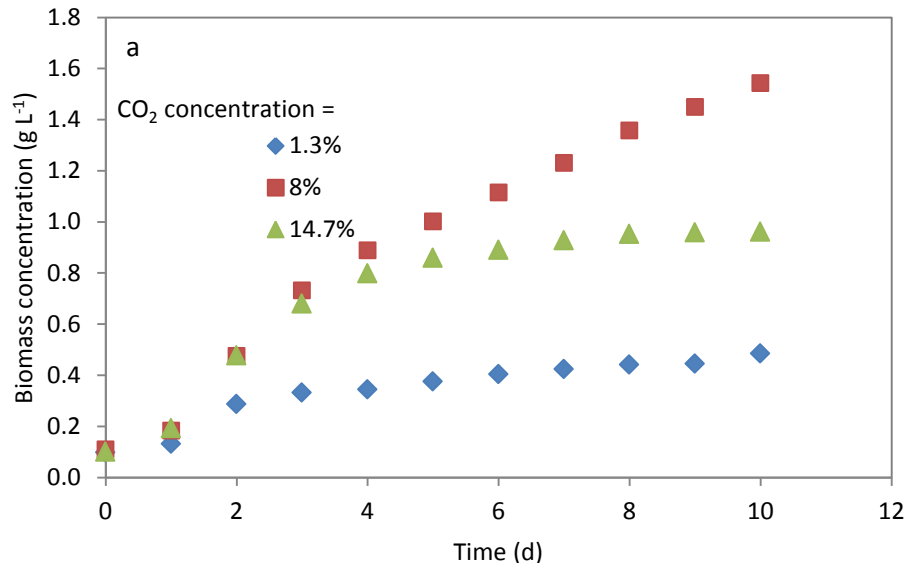


Figure 5-5 Biomass concentration vs cultivation time for CO₂ concentrations of 1.3, 8.0 and 14.7 % with light intensity of 200 $\mu\text{mol m}^{-2} \text{s}^{-1}$ and light period of 16 h

Concentration of CO₂ has a significant impact on the CO₂ biofixation rate and CO₂ utilisation efficiency. Therefore, different CO₂ concentrations (1.3, 8 and 14.7 %) were used in the PBR with a constant light intensity of 200 $\mu\text{mol m}^{-2} \text{s}^{-1}$ and light period of 16 h (Figure 5-6). The highest specific growth rate (0.96 d⁻¹) was obtained at 8 % CO₂ concentration. A slightly reduced rate of 0.91 d⁻¹ resulted with 14.7 % CO₂. A maximum specific growth rate of 1.55 d⁻¹ was reported for *C. vulgaris* after cultivation with 100 % CO₂ and a light intensity of 84 $\mu\text{mol m}^{-2} \text{s}^{-1}$ and 12 h light period (Concas et al., 2012). *C. vulgaris* even can grow well under a 20 % CO₂ concentration (Salih, 2011). The ability of *C. vulgaris* to grow in atmospheres with high CO₂ concentrations is a significant advantage of this species and makes it suitable for CO₂ biofixation of power plant flue gases. In the present study, the maximum CO₂ biofixation rate (0.33 g CO₂ L⁻¹ d⁻¹) was achieved at 8 % CO₂ concentration. Furthermore, CO₂ biofixation was very low (0.09 g CO₂ L⁻¹ d⁻¹) when the CO₂ concentration was 1.3 %. The maximum CO₂ biofixation rate attained in these three experiments (0.33 g CO₂ L⁻¹ d⁻¹, with 200 $\mu\text{mol m}^{-2} \text{s}^{-1}$ light intensity, 16 h light period and 8% CO₂ concentration) was much higher than that obtained by Bhola et al. (2011), who obtained 0.15 g CO₂ L⁻¹ d⁻¹ when cultivating *C. vulgaris* with 80 $\mu\text{mol m}^{-2} \text{s}^{-1}$ of light intensity for a light period of 16:8 h and 4 % CO₂.

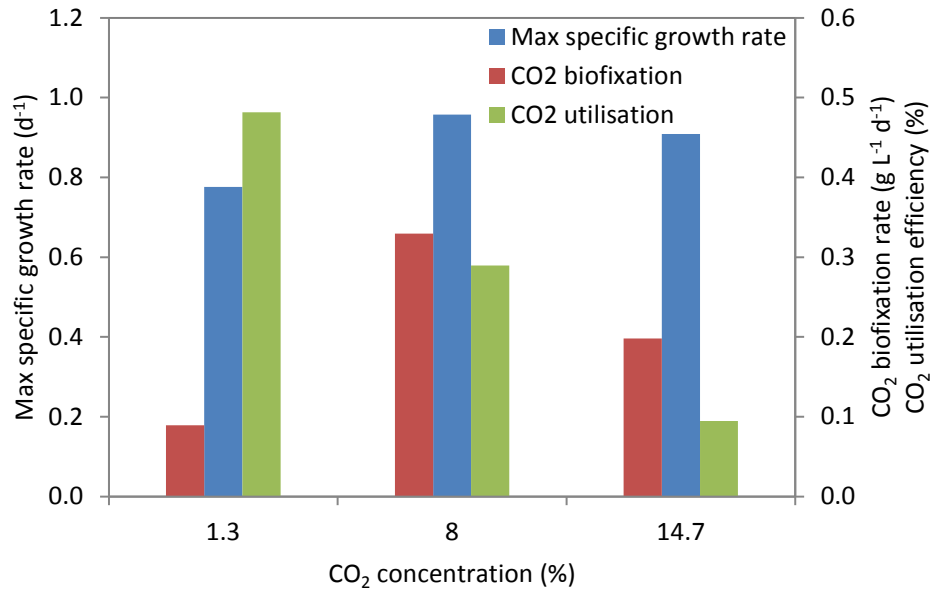


Figure 5-6 Maximum specific growth rate, CO₂ biofixation rate and CO₂ utilisation efficiency at different CO₂ concentrations

5.3.2 RSM results

Response surface methodology was used to fit a second-order polynomial equation to the experimental data to model the effects of incident light intensity, light period and CO₂ concentration on CO₂ biofixation rate. The experimental data were used to determine linear and quadratic coefficients of CO₂ biofixation (Equation (5-1)). These coefficients for coded and actual independent variables are listed in Table 5-4.

Table 5-4 Model coefficients for both coded and actual values of parameters

Equation (coded values)		Equation (actual values)	
CO ₂ biofixation rate =		CO ₂ biofixation rate =	
0.329195		-0.299774	
-0.033048	X_1 : Light intensity	+0.000494	x_1 : Light intensity
+0.012806	X_2 : Light period	+0.038877	x_2 : Light period
+0.015763	X_3 : CO ₂ concentration	+0.067082	x_3 : CO ₂ concentration
-0.015118	$X_1 \cdot X_1$	-0.000002	$x_1 \cdot x_1$
-0.018601	$X_2 \cdot X_2$	-0.001158	$x_2 \cdot x_2$
-0.058028	$X_3 \cdot X_3$	-0.003642	$x_3 \cdot x_3$
+0.003338	$X_1 \cdot X_2$	+0.000010	$x_1 \cdot x_2$
-0.005538	$X_1 \cdot X_3$	-0.000017	$x_1 \cdot x_3$
-0.001413	$X_2 \cdot X_3$	-0.000088	$x_2 \cdot x_3$

Table 5-5 represents the experimental and predicted results of each experimental run under the various conditions.

Table 5-5 Experimental conditions and observed and predicted results

Run	Actual level of variables			CO ₂ biofixation (g L ⁻¹ d ⁻¹)		CO ₂ utilisation (%)	
	Light intensity ($\mu\text{mol m}^{-2} \text{s}^{-1}$)	Light period (light:dark h)	CO ₂ concentration (%)	Observed	Predicted	Observed	Predicted
1	120	12:12	4	0.2819	0.2383	0.4951	0.4185
2	120	12:12	12	0.2944	0.2837	0.1724	0.1661
3	120	20:4	4	0.2848	0.2601	0.5002	0.4568
4	120	20:4	12	0.3106	0.2999	0.1818	0.1756
5	280	12:12	4	0.1964	0.1766	0.3449	0.3102
6	280	12:12	12	0.2057	0.1999	0.1204	0.1170
7	280	20:4	4	0.2316	0.2117	0.4068	0.3718
8	280	20:4	12	0.2163	0.2294	0.1266	0.1343
9	65.6	16:8	8	0.3034	0.3420	0.2664	0.3003
10	334.4	16:8	8	0.2263	0.2309	0.1987	0.2028
11	200	9.3:14.7	8	0.2223	0.2551	0.1952	0.2240
12	200	22.7:1.3	8	0.2877	0.2981	0.2526	0.2618
13	200	16:8	1.3	0.0891	0.1386	0.4815	0.5790
14	200	16:8	14.7	0.1979	0.1916	0.0946	0.0916
15	200	16:8	8	0.3296	0.3292	0.2894	0.2891
16	200	16:8	8	0.3318	0.3292	0.2914	0.2891
17	200	16:8	8	0.3311	0.3292	0.2908	0.2891

5.3.3 Statistical analysis

The response results from the CCD were assimilated into a regression model and coefficients were estimated. Afterwards, the individual coefficients were statistically analysed for null hypothesis tests and fitness to identify the significant parameters affecting the CO₂ biofixation rate. Analysis of variance (ANOVA) was performed by Synthesis, DOE++ software (version 10.1) to verify the model and determine its statistical significance (Table 5-6). The regression coefficient of determination (R^2) was 92.91 %, indicating that the quadratic equations adequately described the relationship between the variables. A relatively high F -ratio indicates that the model can reasonably explain the variance in the response. The p -value represents the probability of estimating a factor by model as much as closer to what actually observed; thus, a smaller p -value indicates that the resultant coefficient is significant. The small p -value (< 0.05) obtained from the ANOVA demonstrates that the experimental and predicted values are in good agreement.

Table 5-6 ANOVA results

Source of variation	Degrees of freedom	Sum of squares [partial]	Mean squares [partial]	F-ratio	p-value
Model	10	0.07684	0.007684	11.80242	0.000502
Main effects	3	0.020551	0.00685	10.521925	0.00267
2-way interactions	3	0.00035	0.000117	0.179394	0.907702
Quadratic effects	3	0.051831	0.017277	26.536881	0.000084
Residual	6	0.005859	0.000651		
Lack of fit	5	0.005843	0.001169	291.305515	0.000033
Pure error	1	0.000016	0.000004		
Total	16	0.082699			

$R^2 = 92.91\%$

$R^2(\text{adj}) = 85.04\%$

From the statistical hypothesis tests and the p -values calculated for each linear, quadratic and interaction term, it was deduced that the effect of all linear and quadratic terms (for light intensity, light period and CO₂ concentration) were statistically significant and the null hypotheses were rejected. The statistical significance of the interaction terms was not low enough to justify rejecting the null hypotheses. Meanwhile, p -values for linear terms of light intensity and CO₂ concentration were < 0.01 , so there is strong evidence that the null hypothesis is false for these two factors (99 % confidence). However, since the p -value for light period was > 0.05 but < 0.1 , the null hypothesis was rejected (at a 95 % confident level) but with less confidence than the other two factors. Moreover, fairly high R^2 values indicate that the model is good enough to predict the response.

5.3.4 Validation of the model

The quadratic model generated by RSM was used to predict *C. vulgaris* CO₂ biofixation rates, and these were compared with observed results (Figure 5-7). The values predicted by Equation (5-1) were in reasonable agreement with those determined experimentally.

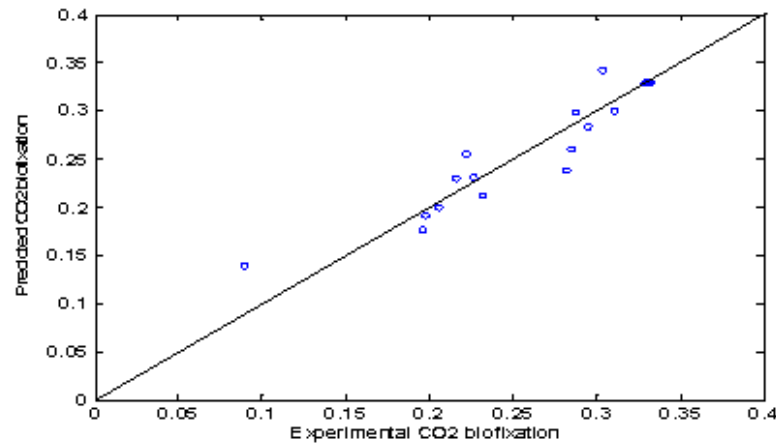


Figure 5-7 Correlation of modelled and observed CO₂ biofixation rates

5.3.5 Individual influence of parameters on CO₂ biofixation

Next, the model was used to plot three dimensional graphs of CO₂ biofixation in relation to two of the three parameters while the third parameter was kept constant (either 8 % CO₂ concentration, 18 h light period, or 200 $\mu\text{mol m}^{-2} \text{s}^{-1}$ light intensity). The results are shown in Figure 5-8. Variation in biofixation rate as a function of these three parameters also can be presented as contour curves (Figure 5-9). They indicate that photoperiod and CO₂ concentration must be fixed around a central point, while for maximum CO₂ biofixation, a lower amount of central light intensity is desirable.

In the experiments, the effect of varying light intensity while all other conditions were kept constant was investigated (at 65.6, 200 and 334.4 $\mu\text{mol m}^{-2} \text{s}^{-1}$). Increasing light intensity from 65.6 to 200 $\mu\text{mol m}^{-2} \text{s}^{-1}$ increased CO₂ biofixation, but with a further increase (to 334.4 $\mu\text{mol m}^{-2} \text{s}^{-1}$), CO₂ biofixation dropped to the lowest value. Therefore, the optimum light intensity might be between 65.6—200 $\mu\text{mol m}^{-2} \text{s}^{-1}$.

Figure 5-8a shows the impacts of light intensity and light period (at constant 8 % CO₂) on the CO₂ biofixation rate. Figure 5-8b shows the influences of light intensity and CO₂ concentration with a constant light period of 16 h. It can be clearly seen in Figure 5-8a that variation in light intensity does not greatly change CO₂ biofixation within a certain light period. In the range of 50—300 $\mu\text{mol m}^{-2} \text{s}^{-1}$ light intensity, within each light period, the maximum variation in the CO₂ biofixation rate was approximately 0.08—0.1 g CO₂ L⁻¹d⁻¹. Meanwhile, the maximum and minimum CO₂ biofixation rates within each light period apparently occurred at specific

intensities of light—approximately 125 and 300 $\mu\text{mol m}^{-2} \text{s}^{-1}$, respectively (Figure 5-8b). Similarly, for a constant CO₂ concentration with light period set at a central value, the CO₂ biofixation rate gradually varied with light intensity variations between 50—300 $\mu\text{mol m}^{-2} \text{s}^{-1}$ (Figure 5-8b). The range of variation in CO₂ biofixation was even lower, at approximately 0.05—0.08 g CO₂ L⁻¹d⁻¹. Correspondingly, slight changes in CO₂ biofixation rate at various light intensities can be seen in the counter plots (Figure 5-9).

To investigate influence of light period, experiments were conducted at light periods of 9.3, 16 and 22.7 h, with other conditions kept constant at a central level (in the middle of the range of tested values). The 16 h light period produced the maximum CO₂ biofixation rate, followed by the 22.7 h period. Therefore, the optimum light period is between 16—22.7 h.

Light period influences on the CO₂ biofixation rate can be discussed with respect to Figure 5-8 a and c. For each particular light intensity, the CO₂ biofixation rate changed noticeably when the light period was increased from 2 h to 17 h. Beginning at almost zero, it reached the maximum at 17 h and then dropped at 24 h (by 0.2 g CO₂ L⁻¹d⁻¹). Indeed, for a specified light intensity level and optimum CO₂ concentration, the CO₂ biofixation rate varied from 0.29—0.34 g CO₂ L⁻¹d⁻¹ as light periods varied from 2—24 h. Likewise, changes in light period significantly influenced CO₂ biofixation when light intensity was set at a central value and CO₂ concentration was kept constant (even at different concentrations). In this case, the CO₂ biofixation rate varied between approximately 0.3—0.32 g CO₂ L⁻¹ d⁻¹.

Individual effects of CO₂ concentration were determined by the three experiments that varied CO₂ concentration (1.3, 8 and 14.7 %) while keeping light intensity and period constant (at 200 $\mu\text{mol m}^{-2} \text{s}^{-1}$ and 16 h, respectively). The CO₂ biofixation rate at 1.3 % CO₂ was somewhat low, and maximum CO₂ biofixation occurred at 8 % CO₂. This shows the importance of CO₂ concentration to the CO₂ biofixation yield. Meanwhile, relatively good biomass growth at high percentages of CO₂ demonstrates the high tolerance of *C. vulgaris* to high CO₂ concentrations.

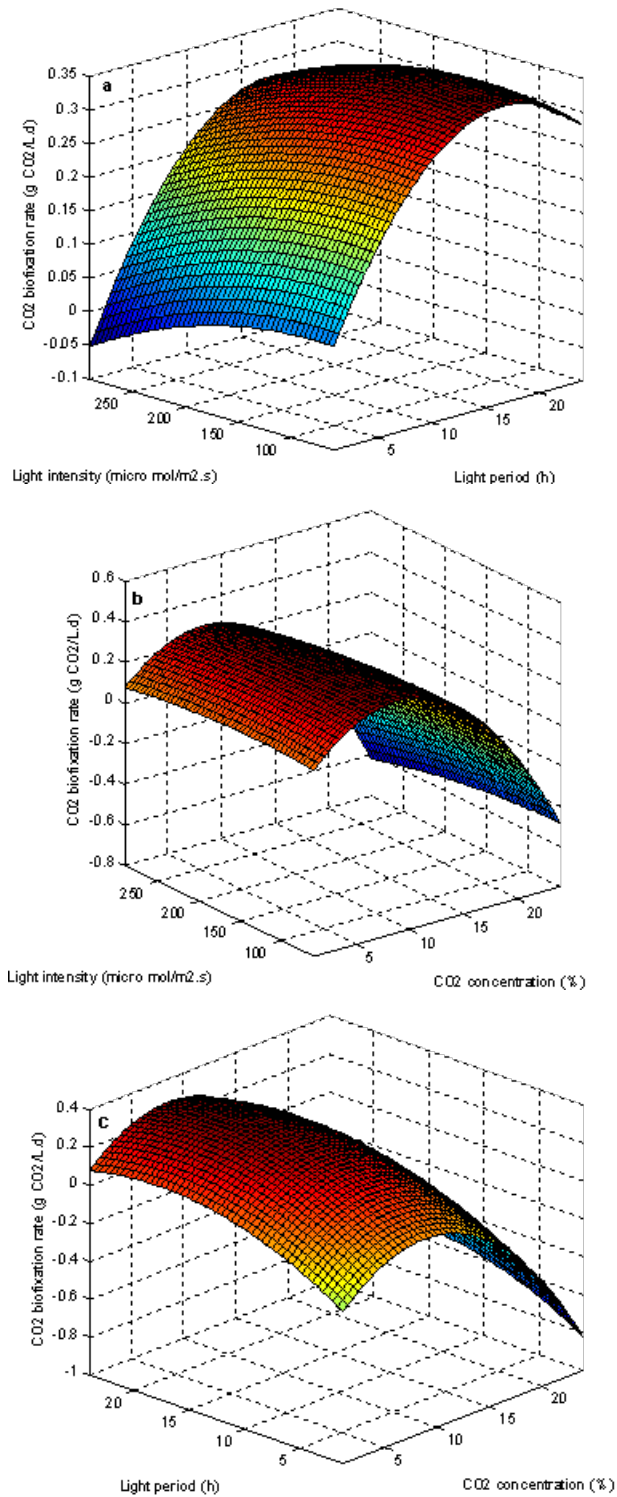


Figure 5-8 Three dimensional plots for CO₂ biofixation rate vs a) light intensity and light period, b) CO₂ concentration and light intensity, and c) light period and CO₂ concentration. In each plot the third parameter was kept constant at central point.

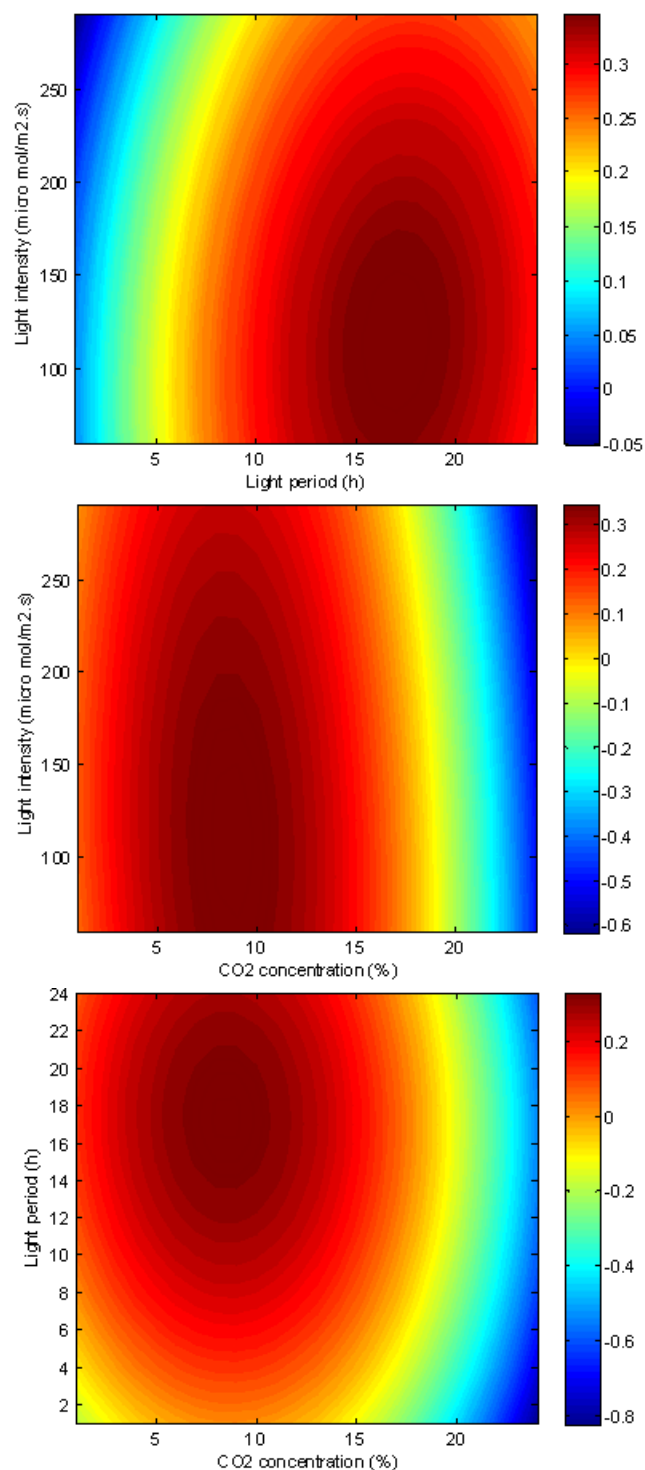


Figure 5-9 Contour plots of CO₂ biofixation rate for two of the three influencing factors. The third factor was kept constant at central value.

From both 3D plots in Figure 5-8 b and c, it can be seen that the CO₂ concentration strongly influences the CO₂ biofixation rate. The optimum CO₂ concentration was about 8–9 %, and reducing or increasing it lowered CO₂ biofixation rates. Meanwhile, from the contour plots (Figure 5-9), it is clear that a wide range of CO₂ biofixation rates (from 0.1–0.35 g CO₂ L⁻¹ d⁻¹) can be achieved

at CO₂ concentrations of 1—15 %. This is consistent with the *C. vulgaris* CO₂ biofixation rate of 0.15 g CO₂ L⁻¹ d⁻¹ reported by (Bhola et al., 2011) under a 4 % CO₂ atmosphere.

5.3.6 Synergistic effect of parameters on CO₂ biofixation

With CO₂ concentration fixed at central level, the optimum light intensity increased with longer light periods (Figure 5-8 a). For instance, when light period was about 2 h, optimum light intensity was 78.4 μmol m⁻² s⁻¹. It increased to 92.2, 110.6 and 124.4 μmol m⁻² s⁻¹ for light periods of 6.7, 15.4 and 22.1 h, respectively. In the same way, light intensity was varied and CO₂ concentration fixed at 8 %, the optimum light period did not change greatly. It only increased from 16.8 to 17.77 h when light intensity was increased from 69 to 290 μmol m⁻² s⁻¹.

The synergistic effect of light intensity and CO₂ concentration is evident in Figure 5-8 b. With light period held constant, the optimum light intensity ranged between 87.6—138.2 μmol m⁻² s⁻¹ as the CO₂ concentration decreased from 15 to 1 %. In fact, with higher CO₂ concentrations, the optimum light intensity decreases. For example, with a constant light period of 16 h and CO₂ concentration varied at 1, 3.4, 9 and 13 %, the light intensities required to optimise CO₂ biofixation were 138.2, 129, 110.6 and 92.2 μmol m⁻² s⁻¹, respectively. As CO₂ concentrations in the PBR are increased, light intensity must be reduced to obtain maximum CO₂ biofixation. Interestingly, the optimum CO₂ percentage for biofixation is similar and about 8.7 % for a wide range of light intensities (~100—220 μmol m⁻² s⁻¹).

The influences of light period and CO₂ percentage on CO₂ biofixation (with constant light intensity) can be seen in Figure 5-8 c. It was observed that for a wide range of CO₂ concentrations (4—15 %), the optimum light period remained constant at 17 h. Only at very low percentages of CO₂ (less than 4 %) did the optimum light period increase to 18 h. So, the effects of CO₂ concentration and light period on biofixation rates have very little interaction. Likewise, by applying different light periods, the optimum CO₂ concentration remained constant at 8.7 %, except at very long periods (> 21.7 h) where it reduced slightly to 8.2 %.

5.3.7 Maximising CO₂ biofixation

The calculated maximum CO₂ biofixation rate was 0.3504 g CO₂ L⁻¹ d⁻¹ when incident light intensity, light period and CO₂ concentration were 112 μmol m⁻² s⁻¹, 17 h, and 8.7 %, respectively (Figure 5-10). Additionally, maximum productivity should occur under the same conditions, since it is proportional to CO₂ biofixation, and was calculated as 0.1570 g DCW L⁻¹ d⁻¹.

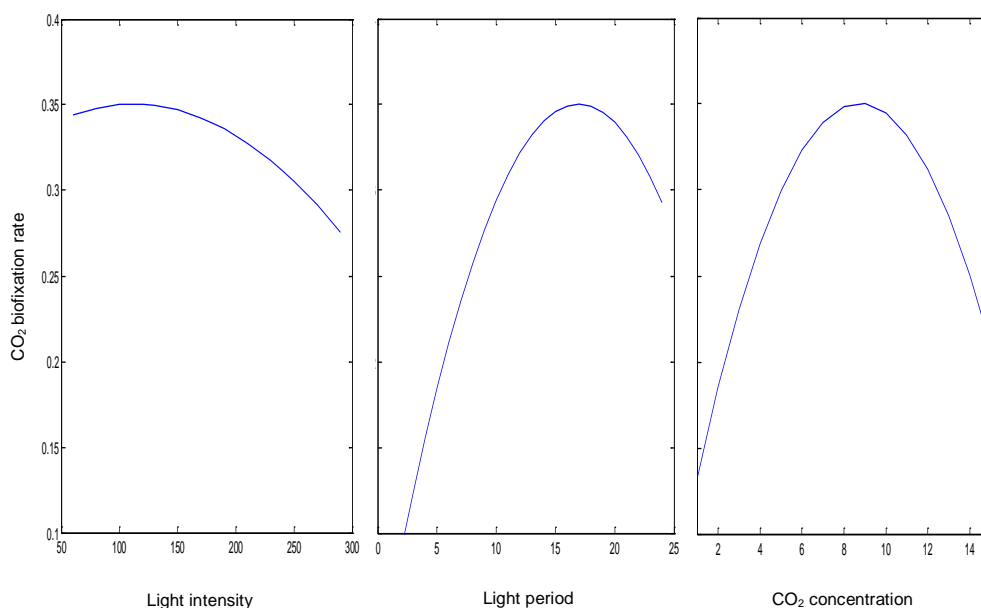


Figure 5-10 CO₂ biofixation rate optimisation results

The calculated optimum light intensity is in agreement with results reported for *C. vulgaris*, although the study only considered the effects of light intensity on CO₂ biofixation (Naderi et al., 2015). In that study, among the five light intensities tested (30, 50, 100, 185, 300 μmol m⁻² s⁻¹), maximum CO₂ biofixation was achieved at 100 μmol m⁻² s⁻¹. Another study reported the maximum cell growth of *Nannochloropsis* sp. to occur at a light intensity of 100 μmol m⁻² s⁻¹ (using an 18 h light period; (Wahidin et al., 2013). However, the interaction of factors has been generally ignored as each one has been studied separately, and only one factor at a time has been varied in the experiments.

Response surface analysis in this study gave an optimum CO₂ concentration of 8.7 %, indicating that *C. vulgaris* has a good tolerance to gas enriched with high levels of CO₂. This makes it a good choice for removing carbon from power plant outlet gases. Also, further increases in CO₂ concentration did not stop microalgae

growth. As discussed before, microalgae can grow at even higher carbon dioxide percentages of up to 14.7 %. Meanwhile, it is worthy to mention that these experiments were conducted at a relatively high temperature (28 °C), which demonstrates the high temperature tolerance advantage of this strain.

The RSM was successfully applied to maximise the CO₂ biofixation rate of *Aphanothece microscopica Nägeli* in a bubble column PBR for optimising temperature, light intensity and CO₂ concentration (Jacob-Lopes et al., 2008a). While maximum CO₂ biofixation was obtained at 35 °C, 9 klux and 15 % CO₂, by applying RSM optimisation, conditions of 11 klux, 35 °C and 15% CO₂ was estimated to be optimum. This is comparable to the results of the present study.

5.3.8 Maximising CO₂ utilisation efficiency

While the CO₂ biofixation rate is indicative of the average amount of CO₂ consumed daily, CO₂ utilisation efficiency is the percentage of CO₂ input to the system that was consumed. Therefore, although the CO₂ biofixation rate indicates the capacity of the system for CO₂ fixation and biomass production, the efficiency of the system for CO₂ fixation is evaluated by CO₂ utilisation efficiency.

Utilisation of CO₂ is defined by Equation (3-6) as the mass fraction of consumed CO₂ to total input CO₂. Total input CO₂ can be calculated easily when the aeration rate and CO₂ percentage of the inlet gas is known. Then, a second-order polynomial can be used to estimate the amount of CO₂ converted to biomass. Finally, the CO₂ utilisation efficiency can be estimated.

Three dimensional and contour plots for CO₂ utilisation efficiency optimisation are illustrated in Figure 5-11 and Figure 5-12.

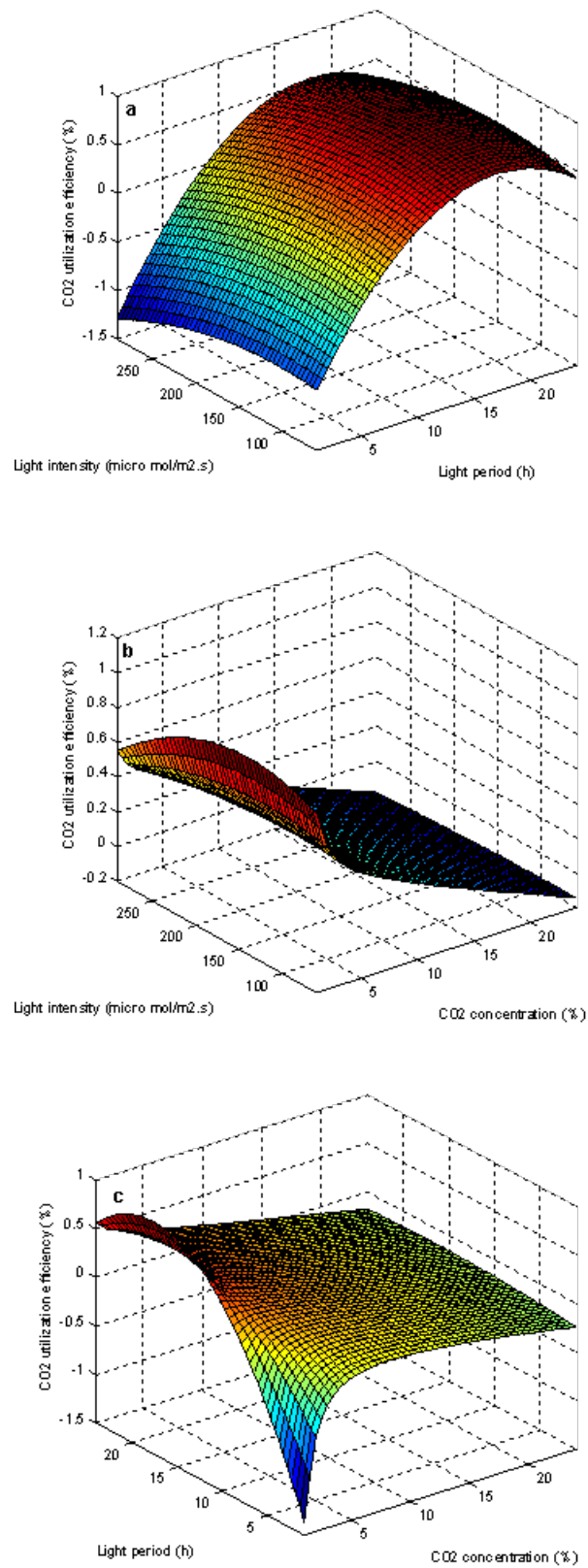


Figure 5-11 Three dimensional plots of CO₂ utilisation efficiency vs two of the three influencing factors (light intensity, light period, CO₂ concentration)

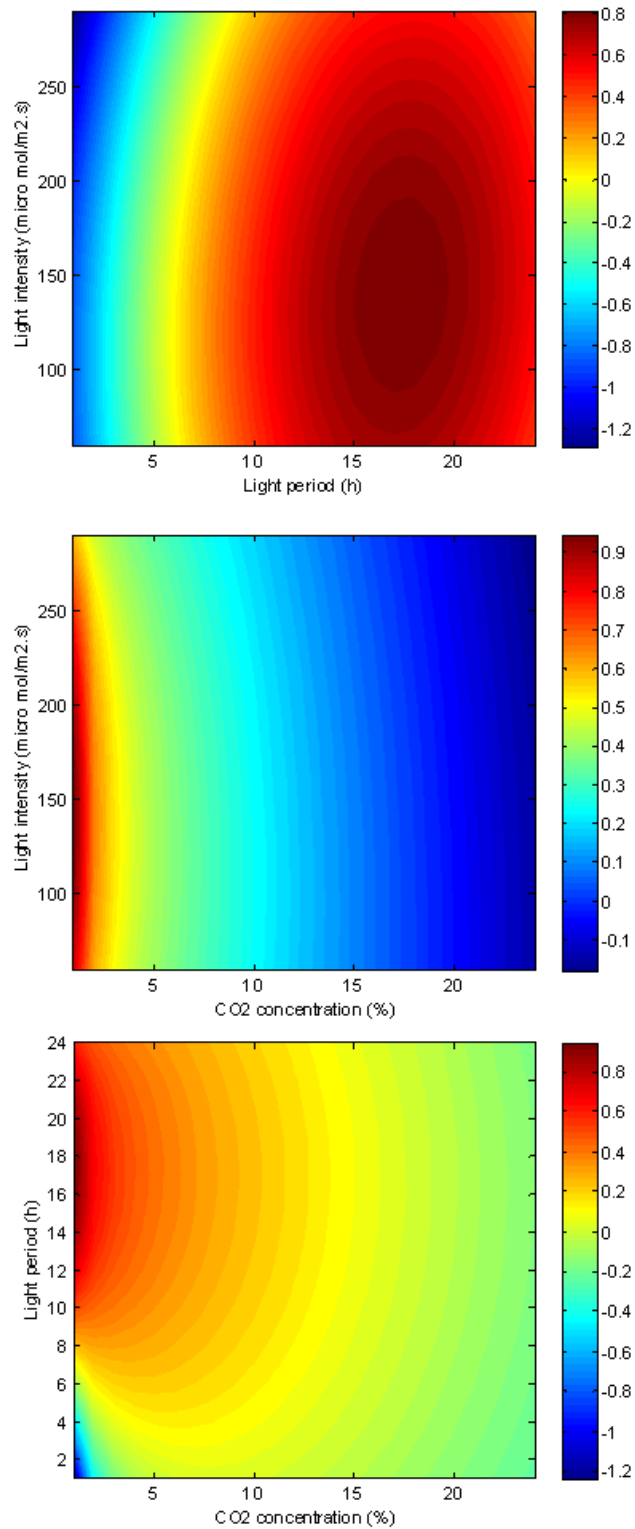


Figure 5-12 Contour plots of CO₂ utilisation according to a) light intensity vs light period, b) light intensity vs CO₂ concentration, and c) light period vs CO₂ concentration

A CO₂ utilisation efficiency of 0.2829 % was achieved with the light intensity, light period and CO₂ concentration that is optimal for CO₂ biofixation. Whereas CO₂ utilisation efficiency optimisation predicts that a maximum CO₂

utilisation efficiency of 0.8146 % will be achieved with 140 $\mu\text{mol m}^{-2} \text{s}^{-1}$ of light over a 17.4 h period with 1.3 % CO₂. Obviously, the CO₂ concentration that gives maximum CO₂ utilisation efficiency is much less than that required for optimum CO₂ biofixation. Meanwhile, the light intensity that maximises CO₂ utilisation efficiency (140 $\mu\text{mol m}^{-2} \text{s}^{-1}$) is higher than that needed to achieve maximum CO₂ biofixation (112 $\mu\text{mol m}^{-2} \text{s}^{-1}$). However, the optimum light period is almost the same for both cases. Although increasing the CO₂ concentration from 1.3 % to 8.7 % leads to increased biomass growth and, accordingly, CO₂ biofixation, it is not enough of an increase to increase the CO₂ utilisation efficiency. That is why maximum CO₂ utilisation occurs at a lower CO₂ concentration.

5.3.9 Verification of optimisation results

A quadratic model resulting from RSM was used to estimate the light intensity, light period and CO₂ concentration required for optimal CO₂ biofixation. It predicted that a maximum of 0.3504 g CO₂ L⁻¹ d⁻¹ can be fixed by *C. vulgaris* when cultivated under 112 $\mu\text{mol m}^{-2} \text{s}^{-1}$ of light intensity with a 17 h light period and an atmosphere of 8.7 % CO₂-enriched air. To validate this prediction, an experiment was conducted under the modelled optimum conditions. Some 0.3564 g CO₂ L⁻¹ d⁻¹ of CO₂ biofixation was observed, which is slightly more than the estimate, and the highest among all the experiments conducted in this study. Under these conditions, CO₂ utilisation of 0.2878 % was obtained.

The model predicted that to achieve maximum CO₂ utilisation efficiency (0.8146 %), the light intensity, light period and CO₂ concentration should be 140 $\mu\text{mol m}^{-2} \text{s}^{-1}$, 17.4 h and 1.3 %, respectively. Accordingly, another experiment was conducted under these conditions, and a CO₂ utilisation efficiency of 0.8003 was observed, which is close to the prediction. The CO₂ biofixation rate was 0.1481 g CO₂ L⁻¹ d⁻¹.

5.3.10 Regression Analysis and Statistically Significant Terms

Regression analysis results are presented in Table 5-7. Regression coefficients of the quadratic equation with coded independent variables are listed in this table with standard errors for each term. Regression coefficients represent the contribution of each term to the variation in the response. Standard errors, which are the deviations

of the regression coefficients, show how precisely the model estimates the coefficient. They were quite small and acceptable for all terms. Lower and upper confidence bounds for regression coefficients are also listed. The T value is normalised regression coefficient and is equal to the coefficient divided by the standard error. The *p*-value shows the probability that the amount of variation in the response is due to chance. When the *p*-value is lower than the risk level, then that source of variation is considered to have a significant effect on the response. In this case, all linear terms and quadratic terms were statistically significant while interaction terms were not.

Table 5-7 Regression table

Term	Coefficient	Standard error	Lower confidence limit	Upper confidence limit	T-Value	<i>p</i> -Value
Intercept	0.329195	0.010519	0.307694	0.346258	31.085222	1.8088E-10
X_1 : Light intensity	-0.033048	0.006908	-0.045732	-0.020407	-4.78746	0.000991
X_2 : Light period	0.012806	0.006908	0.000146	0.025471	1.854304	0.096686
X_3 : CO ₂ concentration	0.015763	0.006908	0.003101	0.028425	2.282008	0.048403
$X_1 \cdot X_1$	-0.015118	0.006735	-0.02745	-0.00276	-2.242871	0.051601
$X_2 \cdot X_2$	-0.018601	0.006735	-0.03094	-0.006249	-2.761089	0.022073
$X_3 \cdot X_3$	-0.058028	0.006735	-0.070445	-0.045755	-8.627207	0.000012
$X_1 \cdot X_2$	0.003338	0.009021	-0.013199	0.019874	0.369964	0.719966
$X_1 \cdot X_3$	-0.005538	0.009021	-0.022074	0.010999	-0.613835	0.554521
$X_2 \cdot X_3$	-0.001413	0.009021	-0.017949	0.015124	-0.156576	0.879035

Table 5-8 Significant terms

Term	<i>p</i> -Value
X_1 : Light intensity	0.000991
X_2 : Light period	0.096686
X_3 : CO ₂ concentration	0.048403
$X_1 \cdot X_1$	0.051601
$X_2 \cdot X_2$	0.022073
$X_3 \cdot X_3$	0.000012

The Pareto charts for ANOVA and regression are illustrated in Figure 5-13. The first one demonstrates the inverse *p*-value of each selected term. The second one shows the standardised effects of the all factors or combinations of factors. If a bar is beyond the blue line (threshold value), this indicates that the effect of that term is significant. Based on these plots, all three parameters (light intensity, light period and CO₂ percentage) were statistically significant factors for CO₂ biofixation.

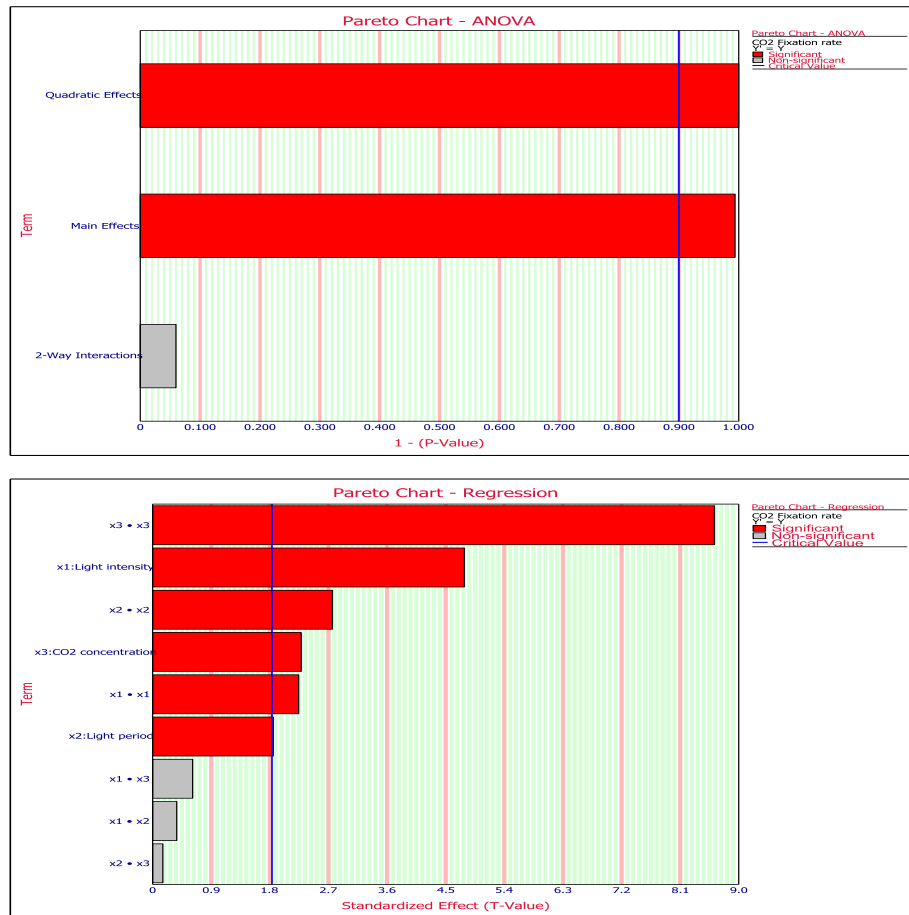


Figure 5-13 Pareto charts of ANOVA and regression

5.3.11 Scatter plots

Scatter plots (Figure 5-14) show the dispersion of CO₂ biofixation rate vs each of the influencing factors (light intensity, light period and CO₂ concentration) at experimental points. It can clearly be seen that all 4 points of factorial portions at 120 $\mu\text{mol m}^{-2} \text{s}^{-1}$ and also at 280 $\mu\text{mol m}^{-2} \text{s}^{-1}$ are quite close to each other. Meanwhile, the central points are widely scattered within CO₂ biofixation rates of near zero to 0.33 g CO₂ L⁻¹ d⁻¹. Factorial points for light period are almost close but again, the central points are broadly distributed between maximum and minimum CO₂ biofixation. In the CO₂ concentration scatter plot, it can be seen that the central points and each set of factorial points are nearly close.



Figure 5-14 Scatter plots for CO₂ biofixation vs a) light intensity, b) light period and c) CO₂ percentage

5.3.12 Residual and interaction plots

From the residual plot vs run order plot (Figure 5-15), we see that there are no outliers and the majority of our data set perfectly fits the model. It is evident that the test sequence of the experiment had no effect since the points are randomly distributed. If there was a pattern, it might be due to a time-related variable affecting

the experiment. There were no points outside the critical value lines. Thus, if desired, the model can be used to predict CO₂ biofixation rate under different combinations of light intensity, light period and CO₂ concentration.

In this study, more than one factor affected the response, and so interactions between them must be considered. Actually, the effect of one independent variable may depend on the value of the other independent variable. An interaction matrix (Figure 5-16) shows the mean effect of each of the three selected factors versus another selected factor at two levels. In this study, there was no significant interaction between the two factors since the mean effect lines at level 1 and level 2 are nearly parallel in all cases. The strongest interaction between factors is the interaction between CO₂ concentration and light intensity; nevertheless, it is quite negligible.

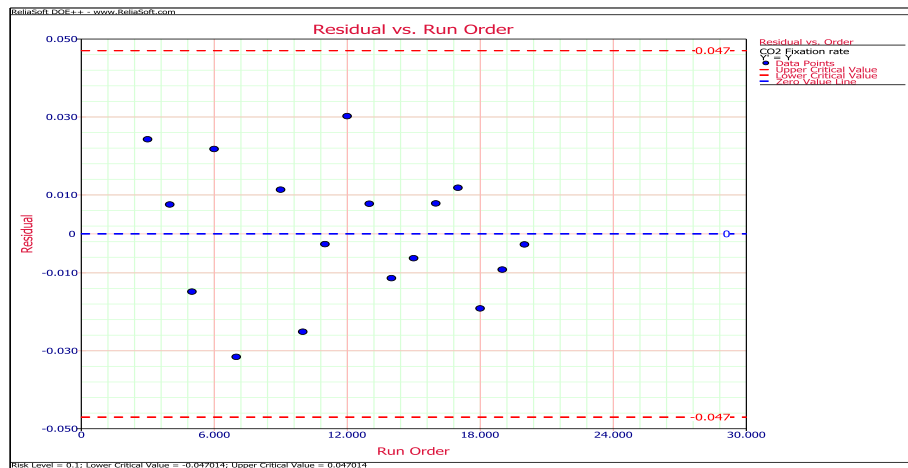


Figure 5-15 Residual plot vs run order

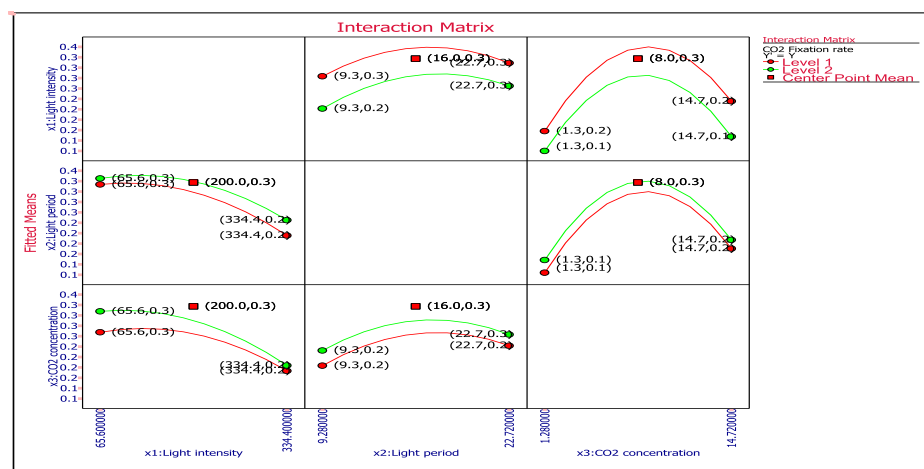


Figure 5-16 Interaction plot

5.4 Summary

Recent studies have clearly demonstrated that only a small fraction of the CO₂ injected into PBRs can be biofixed and utilised for biomass production. Therefore, this chapter was devoted to understanding the synergistic effects of the key factors that influence biomass growth in *C. vulgaris*, i.e., injected CO₂ concentration, light intensity, and the photoperiod. For that purpose, a response surface methodology (RSM) was employed and the set of experiments was designed based on a rotatable central composite design (CCD) of five levels. Light intensity ranged from 65.6—334.4 $\mu\text{mol m}^{-2} \text{s}^{-1}$, light periods were between 9.3—22.7 h, and CO₂ concentration ranged from 1.3—14.7 %. The experiments were conducted in a 3 L photobioreactor at 28 °C with an aeration rate of 0.5 vvm, impeller speed of 300 rpm and initial biomass concentration of 0.1 g L⁻¹. Results of the 17 experiments were analysed and optimised by RSM. It was deduced that the conditions needed to achieve the maximum CO₂ biofixation rate (0.3504 g CO₂ L⁻¹ d⁻¹) were 112 $\mu\text{mol m}^{-2} \text{s}^{-1}$ of light for 17 h per day under a 8.7 % CO₂ atmosphere. Alternatively, to maximise CO₂ utilisation (0.8146 %), the optimum conditions are 140 $\mu\text{mol m}^{-2} \text{s}^{-1}$ light for duration of 17.4 h d⁻¹ under 1.3 % CO₂. In addition to environmental stress optimisation, the individual and synergistic effects of these parameters on biomass growth and CO₂ fixation were discussed. Overall, the results obtained in the present study suggest that this type of process has the potential to be applied for obtaining carbon credits.

6

Investigating and Modelling of Light Intensity Distribution inside the Photobioreactor

6.1 Introduction

Microalgal biofixation of carbon dioxide in photobioreactors has recently received significant research attention as an alternative, sustainable CO₂ removal approach. However, it has not yet been commercialised due to several problems, of which photon availability inside the cultures is foremost.

Light distribution inside microalgal cultures in photobioreactors is of high importance since due to shading effects, light intensity sharply diminishes inside the culture. Light availability determines the algal growth rate and is the main limiting factor in photobioreactor performance (Chiang et al., 2011). On the other hand, due to strong light attenuation inside the culture, light availability cannot simply be determined by measuring incident light on the surface of the bioreactor. It has been accepted and is quite reasonable to assume that cells are exposed to a volumetric average light intensity which is calculated mathematically in consideration of the shape of the vessel and the local light intensity inside the bioreactor. Average light intensity can be considered a limiting factor in photobioreactors with which to investigate biomass growth rates.

Therefore, an accurate model of light distribution inside cultures has a significant role to play in investigating the efficiencies of illumination and photosynthesis. The most common light distribution model is based on the Beer-

Lambert law (Yun and Park, 2001). However, it is not accurate enough, especially in dense cultures (see discussion in Chapter 2, Section 2.7.1), as it overestimates local light intensity, particularly at high biomass concentrations (Sevilla and Grima, 1997). Many researchers have used equations based on the Beer-Lambert law to estimate average light intensity inside photobioreactors (Martínez et al., 2011, Concas et al., 2013, Walter et al., 2003). Suh and Lee (2003) investigated and developed a light distribution model for an internally-illuminated photobioreactor, then the model was successfully applied for different types of internal illumination. Perner and Posten (2007) used computational fluid dynamics and particle tracking to investigate light flashes in a tubular photobioreactor. The simulation results showed the usefulness of static mixers for improving light availability to the cells. Quantitative evaluation of light distribution in cuboidal and cylindrical photobioreactors was investigated and modelled by Ogbonna et al. (1995); however, local light intensity inside the photobioreactor was not discussed. Some other researchers used RTE to model light distribution in photobioreactors which is very difficult, time consuming, and needs complex mathematical methods.

In this study, a new quantitative model has been developed by adapting the Beer-Lambert model to describe light distribution inside algal cultures and predict local light intensity inside the culture. To investigate interior light distribution in microalgae culture, local light intensity inside the culture at different incident light intensities and various biomass concentrations was measured in different geometries. Then, the data was used to develop a mathematical model of light distribution by non-linear regression of the experimental variables and determination of statistical parameters. Afterwards, average light intensity was calculated and different kinetic models were used to model growth rate and biomass concentration. Light distribution and kinetic modelling are explained and discussed in this chapter.

In this chapter, the characteristics of light distribution inside cultures of different geometries and configurations, as well as the influences on light profiles, are discussed. Then, the model was used to calculate average volumetric light intensity inside the vessel and modelling of kinetics.

6.2 Materials and Methods

To investigate light distribution, a transparent rectangular vessel (34 cm L × 20 cm W × 30 cm H) was used to cultivate microalgae. Autoclaved media were added to the sterile vessel and inoculation was aseptically performed using stock culture. Also, a sterile light meter was fixed inside the vessel to measure light intensity. Two heated magnetic stirrers were used to keep the culture temperature at 28 °C and provide mixing. Light was applied to the vessel from all sides during culturing to allow biomass growth; however, during light distribution measurements, light was illuminated from one side while the other sides were covered by black paper. Cool white 10 W fluorescent tubes were used as light sources, and different incident light intensities were maintained by varying the number and distances of the lamps.

First, two preliminary experiments were conducted at fixed incident light intensities of 120 $\mu\text{mol m}^{-2} \text{s}^{-1}$ and then 190 $\mu\text{mol m}^{-2} \text{s}^{-1}$ for initial investigations of light distribution. For this set of experiments, a highly concentrated broth obtained from a photobioreactor was added to the vessel and light distribution at different distances was measured after consecutive dilution of the culture with a sterile medium. Therefore, for a specific intensity of incident light, light distributions at different biomass concentrations were measured.

To model the light intensity distribution inside the culture at different distances from the surface, a set of experiments were conducted at various incident light intensities (350, 310, 275, 235, 160, 100 and 70 $\mu\text{mol m}^{-2} \text{s}^{-1}$) and biomass concentrations (0.09, 0.18, 0.26, 0.47, 0.67, 0.89 and 1.33 g L⁻¹). Light intensity inside the culture, along with biomass growth, was measured at different incident light intensities. Light intensity at the surface of the vessel, as well as at different points inside the culture (1 cm intervals up to 10 cm distance), were measured for each level of incident light intensity. Biomass concentration was measured as explained in Chapter 3. This data was used to model light distribution as a function of incident light intensity, biomass concentration and distance.

Afterwards, a cylindrical vessel was used in the same way to simulate bioreactor light distribution. This cylindrical vessel was made of glass and had an 18 cm diameter. A spherical flat quantum sensor was used to measure incident light intensity on the surface of the vessel while a quantum sensor was used to measure local light intensity inside the culture (Section 3.5.5). This vessel was used to

investigate light distribution in a cylindrical geometry when it was illuminated from one side, and also when it was evenly illuminated from all sides. Light distribution measurements were collected at different distances from the surface of the vessel as far as the centre of the vessel. This was repeated every few days as long as there was biomass growth, so data were collected at different biomass concentrations. Each time, light distributions inside the culture were measured for different particular incident light intensities. These were set at 130, 110 and 80 $\mu\text{mol m}^{-2} \text{s}^{-1}$ for the single-sided illumination experiments and at 310, 220 and 130 $\mu\text{mol m}^{-2} \text{s}^{-1}$ for the even illumination experiments.

Model parameters were estimated using non-linear regression and MATLAB fitting tools. Average light intensity was mathematically calculated for the cylindrical bioreactor which was used to perform microalgae culturing under various conditions. Then, different kinetic models were applied to simulate biomass growth with respect to average light intensity.

6.3 Results and Discussion

6.3.1 Light distribution at constant incident irradiance in a rectangular vessel

It is well known that there are light gradients inside cultures, and light diminishes while traveling inside the material. Light absorption and scattering by the cells lead to decreasing light intensity as it penetrates the culture. Therefore, homogenous light distribution along the vessel is not possible. To evaluate light attenuation inside the culture, light intensity inside the bioreactor was measured at different distances from surface of the vessel, at different concentrations of biomass, while incident light intensity at the vessel's surface was fixed at the optimum value of 120 $\mu\text{mol m}^{-2} \text{s}^{-1}$.

Figure 6-1 shows the light intensity distribution inside the culture, from the surface of the vessel up to 10 cm distance from the surface, at different biomass concentrations and a constant incident light intensity of 120 $\mu\text{mol m}^{-2} \text{s}^{-1}$. Light intensity sharply diminishes even at very shallow depths, particularly at higher biomass concentrations. For example, at biomass concentrations higher than 0.2 g L⁻¹, light intensity decreases to less than half after just 2 cm. Interestingly, light intensity attenuated by 47 % at 2 cm distance when the biomass concentration was

about 0.13 g L^{-1} ; however, when the biomass concentration increased by 10 times (to 1.4 g L^{-1}), the light intensity decreased by 83 %. Cultures with high biomass concentrations of 1.7 g L^{-1} , show significant reductions in light intensity ($< 10 \mu\text{mol m}^{-2} \text{ s}^{-1}$) even at 2 cm distance, reaching almost zero after 4 cm.

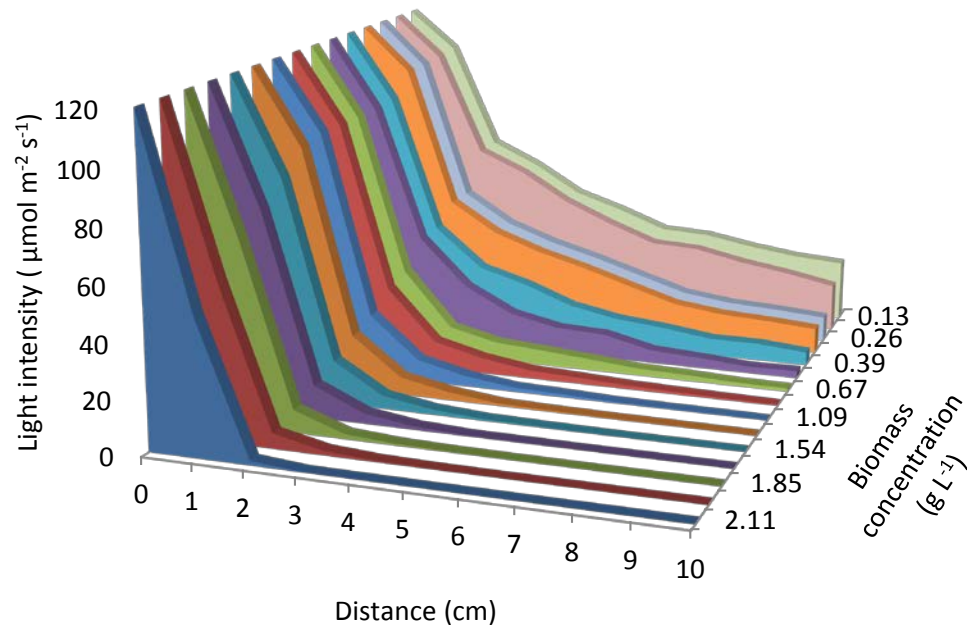


Figure 6-1 Local light intensity vs distance from the vessel surface and biomass concentration at an incident light intensity of $120 \mu\text{mol m}^{-2} \text{ s}^{-1}$ when was measured in 1 cm intervals

Another set of experiments with the same procedure was performed except that incident light intensity at surface of the vessel was changed to $190 \mu\text{mol m}^{-2} \text{ s}^{-1}$. The results are shown in Figure 6-2. At a biomass concentration less than 0.1 g L^{-1} , light intensity level is relatively good ($> 40 \mu\text{mol m}^{-2} \text{ s}^{-1}$), even at 10 cm distance. However, even by increasing incident light intensity from 120 to $190 \mu\text{mol m}^{-2} \text{ s}^{-1}$, light intensity diminished to less than $10 \mu\text{mol m}^{-2} \text{ s}^{-1}$ at > 2 cm depth for biomass concentrations $> 1 \text{ g L}^{-1}$. It can be deduced that simply increasing incident light intensity does not supply enough photon flux for microalgae cells, particularly at high biomass concentrations. On the other hand, increasing incident light intensity at low biomass concentrations may damage the cells. It seems that decreasing the light path and providing good mixing to create homogeneous availability of photons to cells is the best approach.

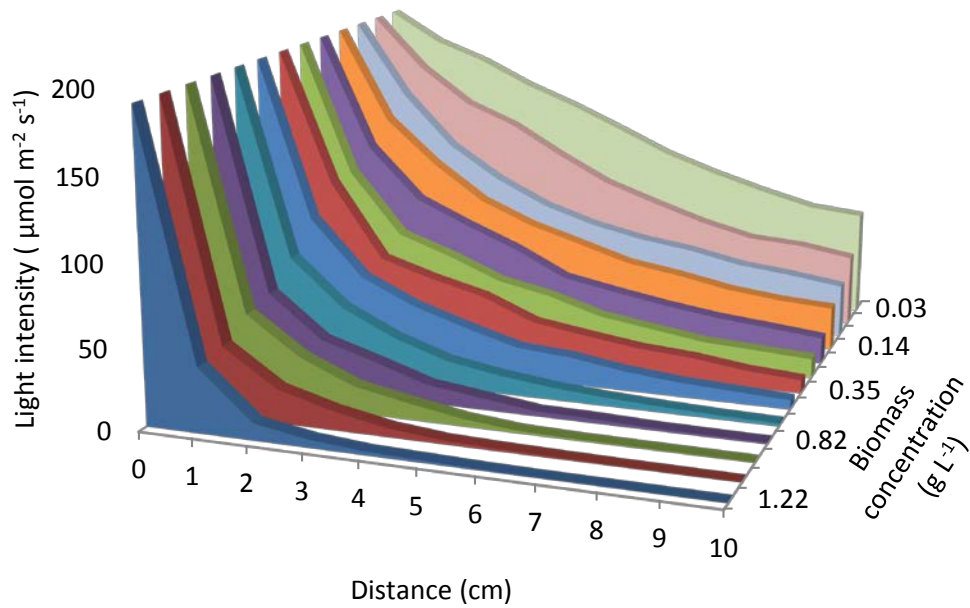


Figure 6-2 Local light intensity vs distance from the vessel surface and biomass concentration at an incident light intensity of $190 \mu\text{mol m}^{-2} \text{s}^{-1}$ when was measured in 1 cm intervals

As discussed in Chapter 4, high light intensity leads to photoinhibition, so applying high light intensity to a low concentration culture can damage the cells. On the other hand, since light availability inside the culture falls with biomass growth, increasing the incident light intensity as biomass concentration increases could be a solution. However, the results of experiments conducted with a high incident light intensity ($190 \mu\text{mol m}^{-2} \text{s}^{-1}$) prove that even increasing incident light intensity in dense cultures is not effective. Besides, it could damage cells close to the surface of the bioreactor.

6.3.2 Light distribution at different incident irradiance in rectangular vessel

A set of experiments was conducted at different biomass concentrations and various incident light intensities and light distribution data were collected. These data are discussed in this chapter and then used to model light distributions inside cultures in Chapter 7. To compare the effect of incident light intensity on light distribution, the results were plotted in Figure 6-3 to show light intensity vs light path at various incident light intensities. Each curve shows light distribution along the vessel at seven different incident light intensities ($70, 100, 160, 235, 275, 310$ and $350 \mu\text{mol m}^{-2} \text{s}^{-1}$), at a specified biomass concentration. Meanwhile, to analyse the influence of

biomass concentration on the light distribution inside the culture, the experimental results were replotted in Figure 6-4. This figure shows light intensity vs light path at different biomass concentrations. Each graph represents a different incident light intensity. These results and the remarkable aspects of these figures are discussed in following section.

6.3.2.1 Effect of incident light intensity

The effect of incident light intensity on light attenuation at different biomass concentrations is presented in Figure 6-3. At a particular biomass concentration, reductions in light intensity over a specific distance are almost the same for any incident light intensity. In addition, it can be seen that a high biomass concentration tends to attenuate the light at 2—3 cm distance from the illuminated surface, so that the level of incident light intensity does not extensively change the rate of attenuation. In addition, it is clear that for long distances from the surface of the bioreactor (> 4 cm), and high biomass concentrations (> 0.5 g L⁻¹) the influence of incident light intensity is insignificant.

Furthermore, as it can be seen in the figures that the slope of the curves decreases for lower incident light intensities, especially at 70 $\mu\text{mol m}^{-2} \text{s}^{-1}$. Therefore, when biomass grows, less reduction in light will occur for lower incident intensities. For instance, at a biomass concentration of 0.09 g L⁻¹ and incident light intensity of 350 $\mu\text{mol m}^{-2} \text{s}^{-1}$, the light intensity decreases by 17 % (290 $\mu\text{mol m}^{-2} \text{s}^{-1}$) after 1 cm. However, a lower incident light intensity of 70 $\mu\text{mol m}^{-2} \text{s}^{-1}$ is only attenuated by 10 % (63 $\mu\text{mol m}^{-2} \text{s}^{-1}$) over the same distance. Correspondingly, at a higher biomass concentration of 1.34 g L⁻¹, light intensity drops from 350 to 82 $\mu\text{mol m}^{-2} \text{s}^{-1}$ and from 70 to 23 $\mu\text{mol m}^{-2} \text{s}^{-1}$ over a 1 cm distance from the illuminated surface. Furthermore, at greater distances from the illuminated surface, local light intensities are very similar, even with different incident light intensities, particularly at higher biomass concentrations. These observations suggest that increasing incident light intensity is not an efficient solution for facilitating photosynthesis in dense cultures.

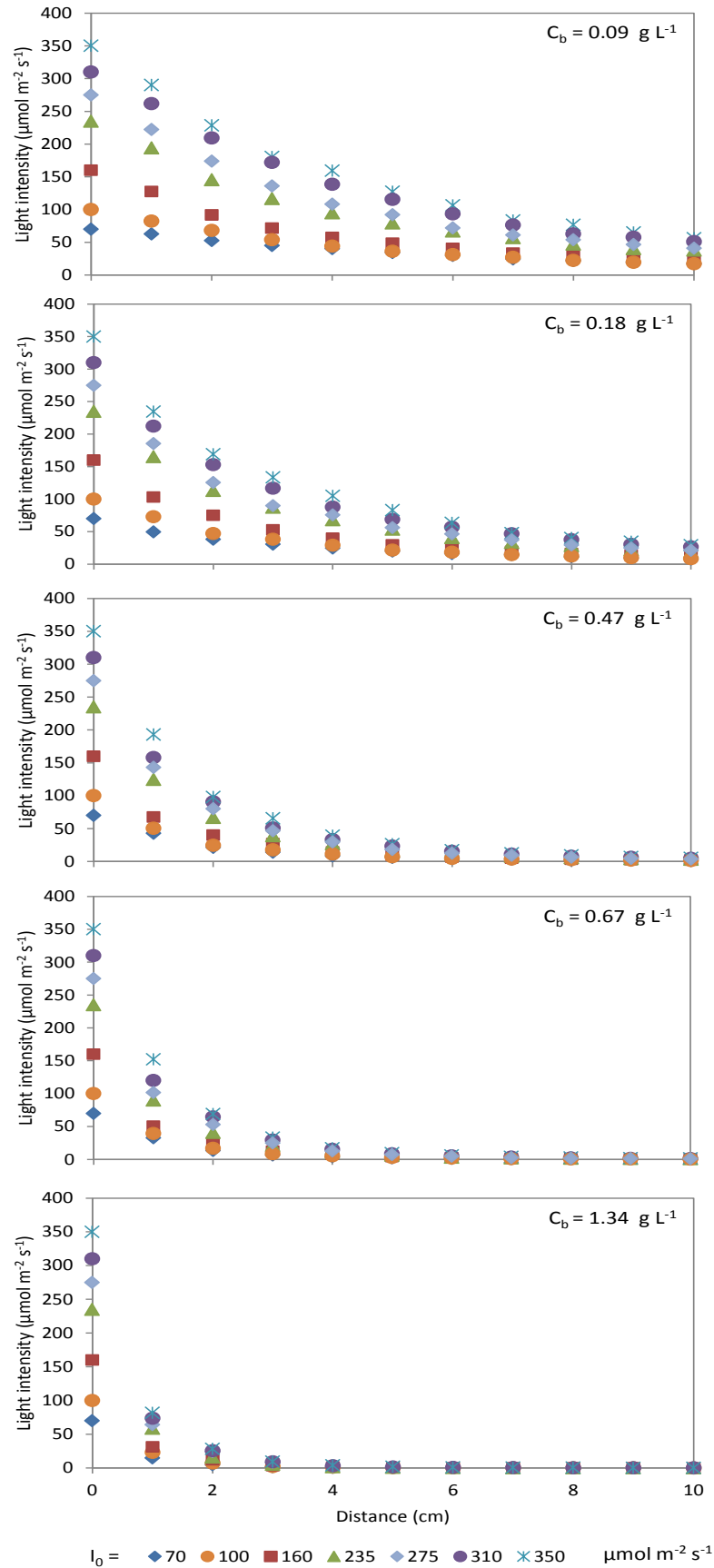


Figure 6-3 Local light intensity vs distance from the vessel surface for various incident light intensities (I_0) at five different biomass concentrations (C_b)

6.3.2.2 Effect of biomass concentration

Figure 6-4 shows light distribution at different biomass concentrations and a constant incident light intensity. Local light intensity of less than $10 \mu\text{mol m}^{-2} \text{s}^{-1}$ limits algal growth, so these areas are considered as dark zones. Dark zones noticeably increase with increases in biomass concentration. For instance, there is no dark zone when the biomass concentration is $\leq 0.16 \text{ g L}^{-1}$, but when biomass concentration increases to 0.67 g L^{-1} , the dark zone occurs $\geq 4 \text{ cm}$ from the surface.

Light intensity inside the culture reduces rapidly over the first 2 cm from the surface. This effect intensifies with increasing biomass concentration. For example, with a biomass concentration of 1.34 g L^{-1} and incident light intensity of $70 \mu\text{mol m}^{-2} \text{s}^{-1}$, light intensity decreases by 79 % over the first 1 cm. However, when biomass concentration is 0.09 g L^{-1} , light intensity only falls by 10 %. In other words, the influence of biomass concentration on light attenuation is strong, especially close to the illuminated surface.

For a biomass concentration of 0.09 g L^{-1} , light intensity decreased by 35 % over the first 2 cm. For biomass concentrations of 0.47 and 1.34 g L^{-1} , light intensity decreased by 71 and 92 %, respectively. Likewise, at the same biomass concentrations ($0.09, 0.47$ and 1.34 g L^{-1}) but at 5 cm from the surface, light intensity was reduced by 67, 93 and 99.6 %, respectively.

Variation in Transmittance (I/I_0) vs biomass concentration is independent of incident light intensity and it has been illustrated in Figure 6-5 for three different locations inside the culture (2, 5 and 10 cm from the illuminated surface). The results show that at low biomass concentrations (< 0.7), light transmittance reduces significantly with increasing biomass concentration. However, for biomass concentrations $> 0.7 \text{ g L}^{-1}$, I/I_0 levelled off at 0.1 for the region near the illuminated surface (2 cm distance) and was almost zero at 5 and 10 cm.

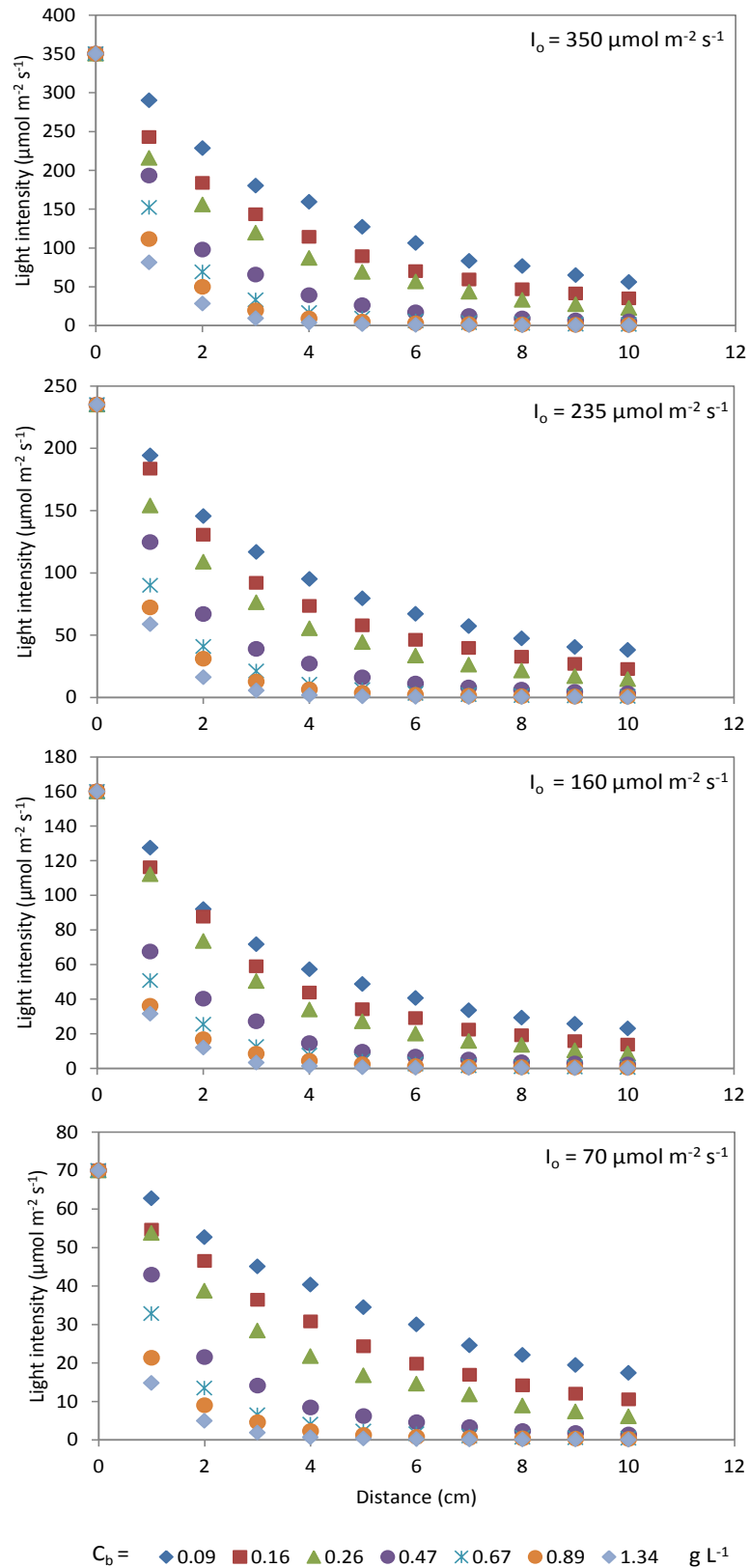


Figure 6-4 Local light intensity vs distance from the vessel surface for various biomass concentrations (C_b) at different incident light intensities (I_0)

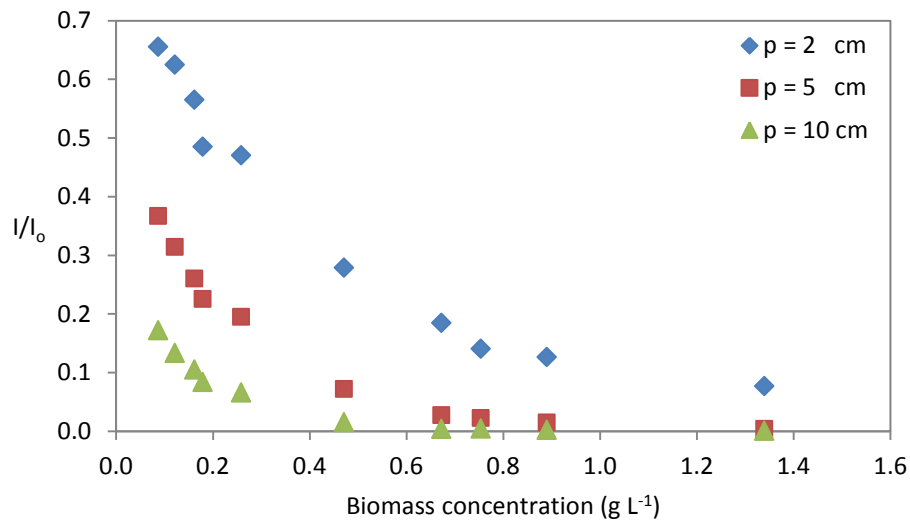


Figure 6-5 Transmittance (I/I_0) vs biomass concentration at different distances (p) from the illuminated surface

6.3.2.3 Effect of distance

Overall, light intensity decreases with distance from the illuminated surface. This relationship is non-linear—the effect is stronger for regions closer to the illuminated surface. For areas far from the vessel's surface, decreases in light intensity continue at a smaller rate. For instance, for a biomass concentration of 0.47 g L^{-1} with incident light intensity of $350 \mu\text{mol m}^{-2} \text{ s}^{-1}$, light inside the culture fell by approximately 55 % over the first 2 cm, then fell another 28 % over the next 8 cm. From Figure 6-3, it can be seen that at a particular biomass concentration, less attenuation of light with distance is observed for lower incident light intensities. On the other hand, at a particular incident light intensity, rapid attenuation occurs over small distances from the surface, especially for higher biomass concentrations (Figure 6-4). Moreover, at high biomass concentrations ($> 1.0 \text{ g L}^{-1}$) and distances of $> 2\text{--}3 \text{ cm}$, the culture is almost dark for all incident light intensities.

Transmittance (I/I_0) vs distance at various biomass concentrations is illustrated in Figure 6-6. Again, it is obvious that the effect of distance on transmittance is stronger in areas close to the surface ($< 4 \text{ cm}$).

The results of these experiments are consistent with those of Suh and Lee (2003). They used an internally-radiating cylindrical illuminated vessel to develop a light distribution model for estimating local light intensity inside photobioreactors culturing *Synechococcus* sp. microalgae. The effect of biomass concentration and

light path were investigated by measuring local light intensity at different distances from an internal light source. This was done at various biomass concentrations but with incident light intensity kept constant. The influence of light path and biomass concentration on light attenuation were determined. At high biomass concentrations, light intensity attenuated rapidly over very small distances from the light source.

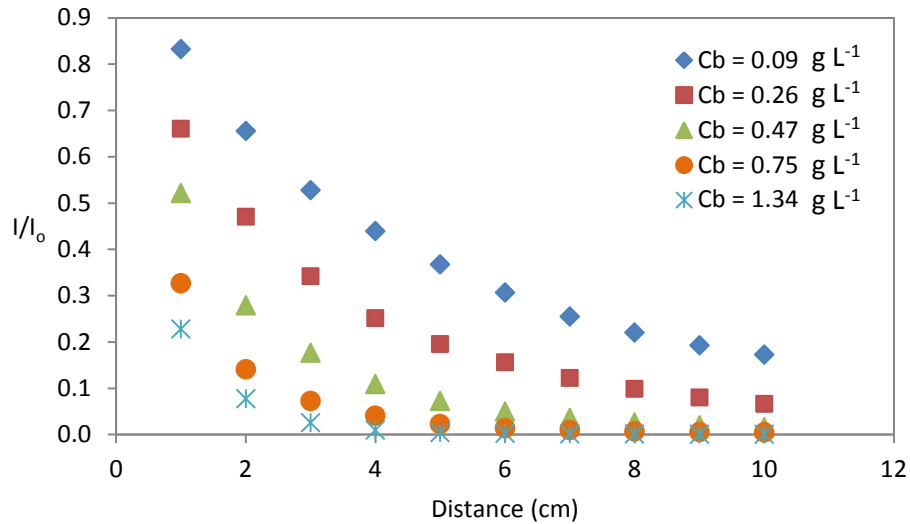


Figure 6-6 Transmittance (I/I_0) vs distance at different biomass concentrations (C_b)

6.3.3 Light distribution in cylindrical vessels

6.3.3.1 Single direction illumination

Local light intensity at different distances from the surface of the cylindrical vessel was measured with the vessel illuminated from one direction. Light distribution for different incident light intensities at various biomass concentrations can be seen in Figure 6-7. A light intensity profile similar to that of a rectangular vessel was observed; however, the dark zone occurred at higher biomass concentrations. For example, no local light intensity of less than $10 \mu\text{mol m}^{-2} \text{ s}^{-1}$ was observed at a biomass concentration of 0.28 g L^{-1} . In addition, at a high biomass concentration of 1.22 g L^{-1} , a dark zone was observed after 6 cm from the surface. In Figure 6-8, a comparison of light distributions in rectangular and cylindrical geometries is made for two biomass concentrations at similar incident light intensities.

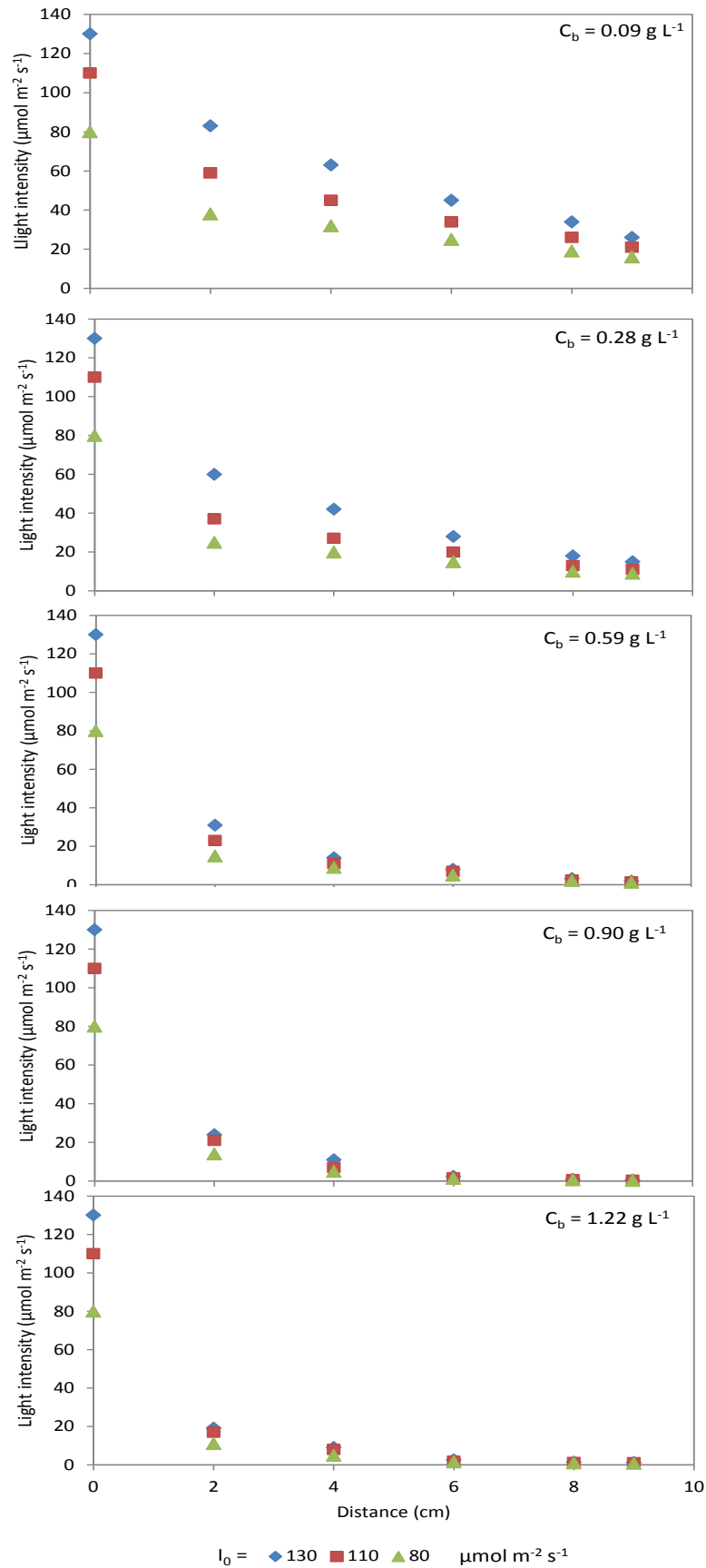


Figure 6-7 Light distribution in a single-direction illuminated cylindrical vessel at various incident intensities (I_0) and biomass concentrations (C_b)

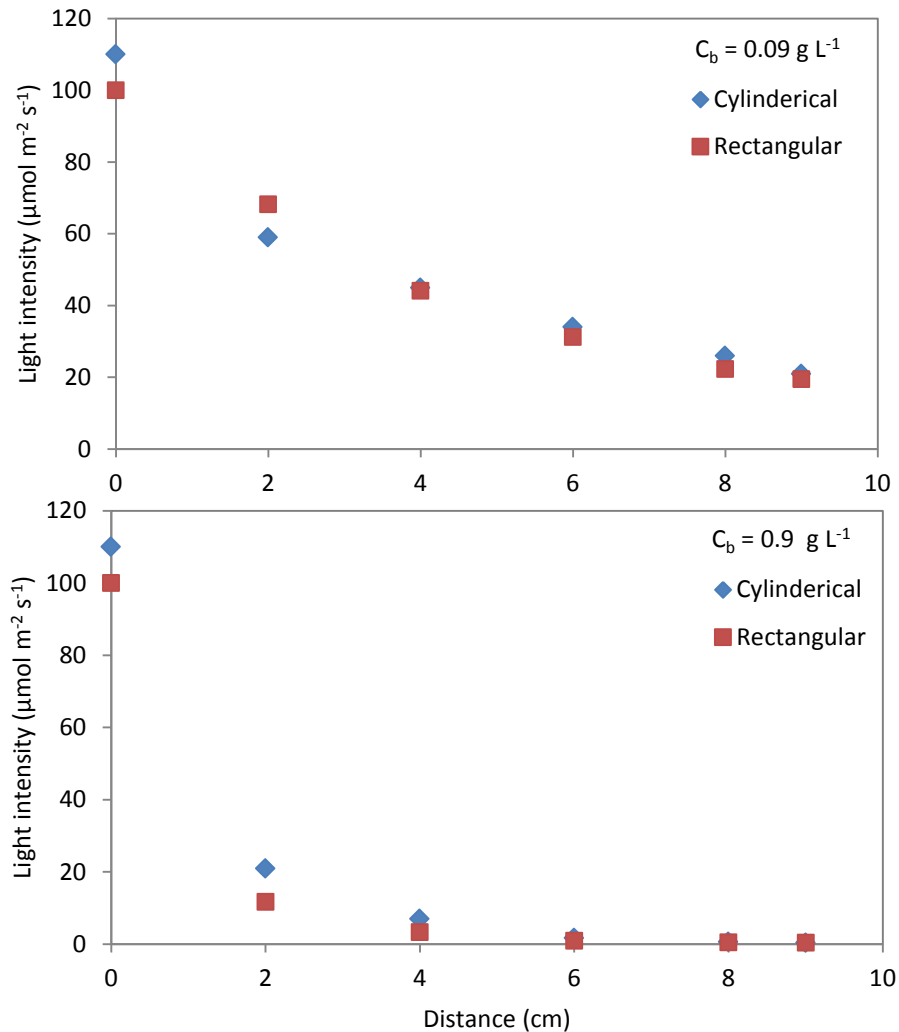


Figure 6-8 Light distribution two different geometries (rectangular and cylindrical) at biomass concentrations of 0.09 and 0.9 g L⁻¹

6.3.3.2 Even illumination

Figure 6-9 illustrates light distribution inside a cylindrical vessel illuminated evenly from all sides. Local light intensity was measured within different biomass concentrations while various intensities of incident light were applied to the surface of the vessel. Light intensity diminished more slowly in this case, especially when the culture was not very dense. However, at high biomass concentrations, light intensity decreased sharply. To compare light distributions in a cylindrical vessel that was either illuminated from one side or from all sides, experimental data were plotted for two biomass concentrations (Figure 6-10). When biomass concentration was low (0.09 g L⁻¹), light distributions were quite different and no great

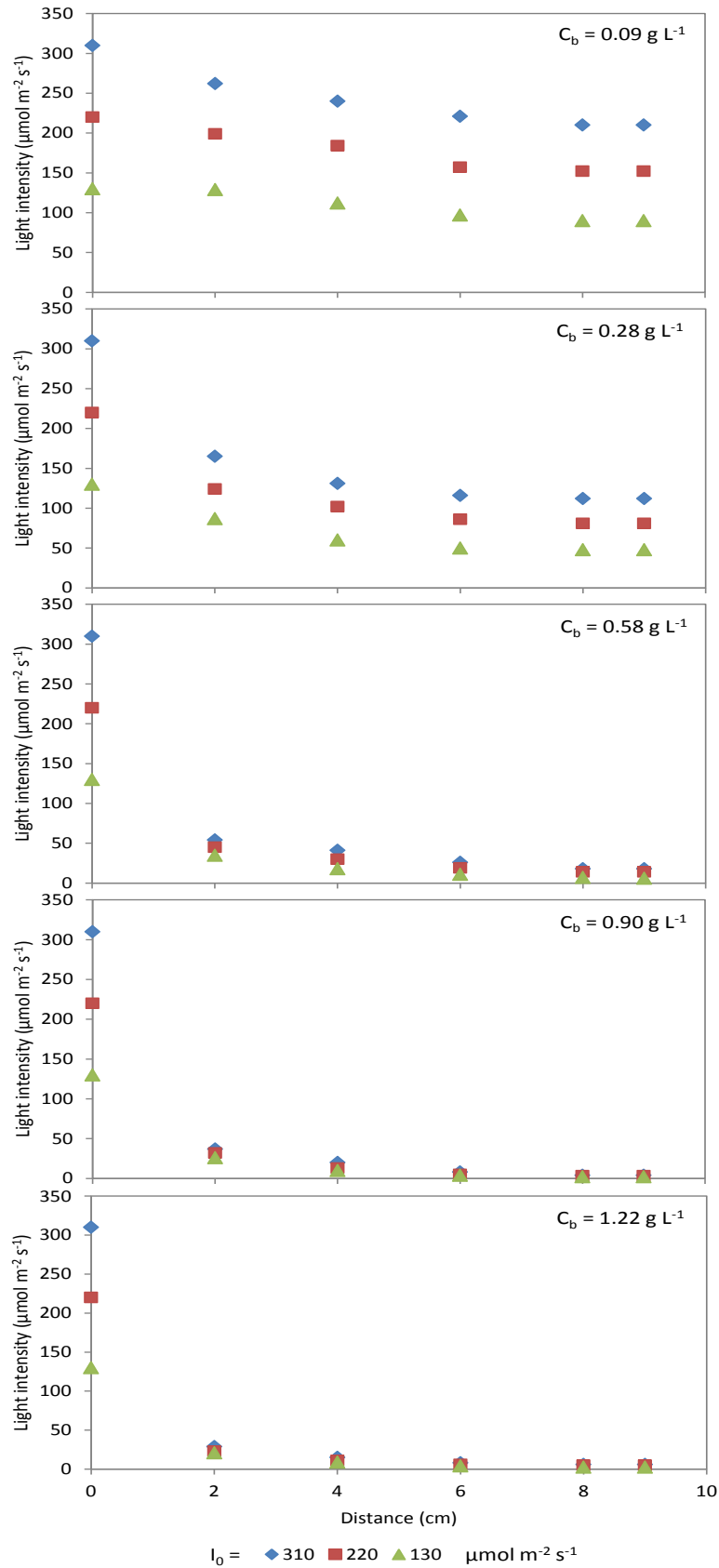


Figure 6-9 Light distribution in evenly illuminated cylindrical vessel at different biomass concentrations

decrease in light intensity was observed when the vessel was evenly illuminated. However, at a higher biomass concentration (0.9 g L^{-1}), light distributions were quite similar.

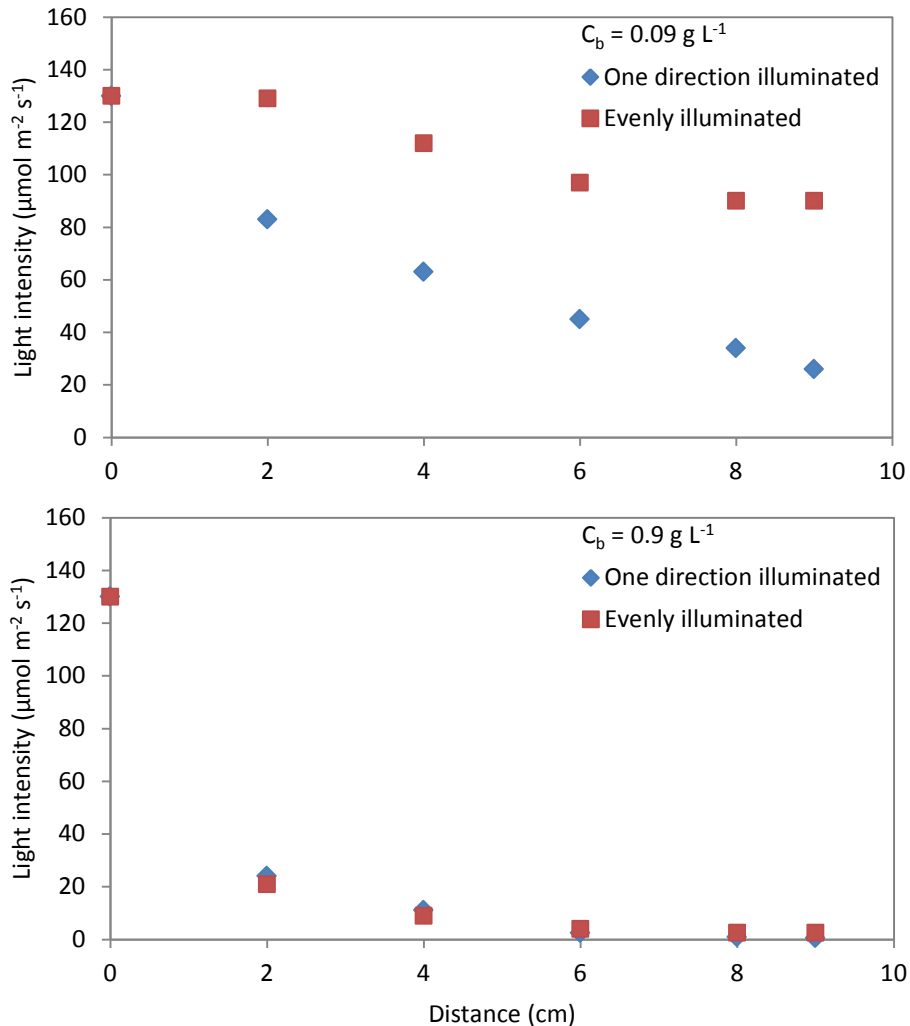


Figure 6-10 Light distribution in a cylindrical vessel illuminated evenly or from a single direction, at two biomass concentrations (C_b)

6.3.4 Light distribution modelling

Usually, in dense cultures, photon flux attenuates sharply due to absorption and scattering. The most common model for predicting light attenuation is the Beer-Lambert model. However, the estimates of this model are not always accurate, especially when the culture is dense (see explanation in Chapter 2), and it tends to overestimate local light intensity.

Overall, the exponential decay of light intensity with biomass concentration and distance is accepted. A simple one-dimensional exponential model (Beer-

Lambert) has been proposed; however, it is not accurate enough, especially at high biomass concentrations. A more accurate modelling approach is possible using radiative transfer equations, but this involves complex mathematical equations which are very time-consuming to solve.

In present study, an effort was made to model light distribution inside cultures by modifying the simple Beer-Lambert model; however, it only gives estimates of average light intensity and not local light intensity. The exponential decay of light with biomass concentration and distance is accepted. However, with greater distances from the illuminated surface, the effect of distance diminishes, especially in dense cultures. In other words, at a given point far from the illuminated surface, the gradient of local light intensity is remarkably less than that near the surface. This case cannot be captured accurately by Beer-Lambert model.

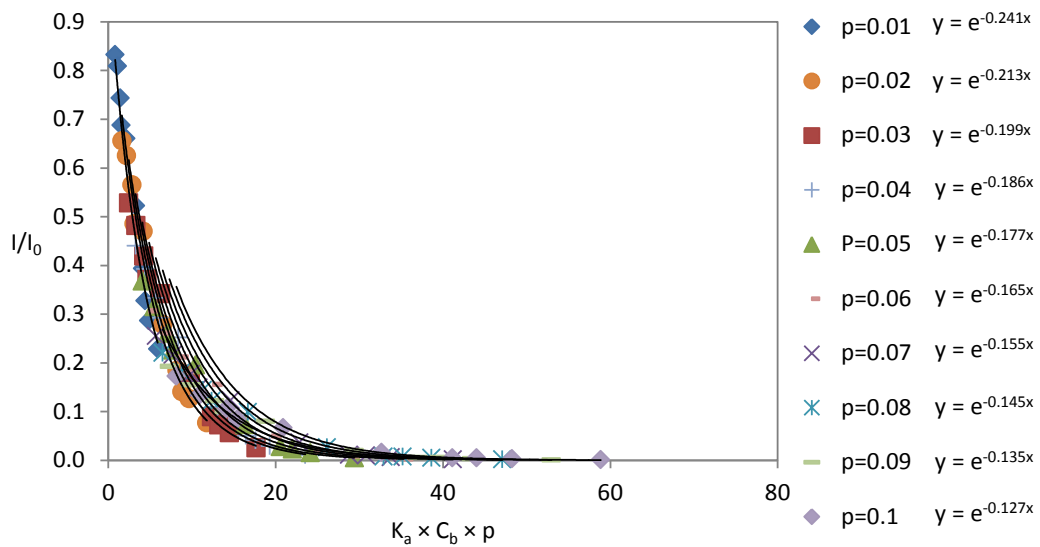


Figure 6-11 Transmittance (I/I_0) versus $K_a.C_b.p$ at different distances from the illuminated surface

It was found that including a hyperbolic light path term in the exponential expression of the Beer-Lambert model, has significantly improved the light attenuation prediction. Accordingly, a hyperbolic term for light path was included in an attempt to experimentally develop a model of one-dimensional light distribution that simulates local light intensity. The parameters of the model, were estimated through non-linear fitting of experimental data of biomass concentration, light path and incident light intensity. It was assumed that the effects at the top and bottom of the culture could be neglected, and that the attenuation coefficient (including in-

scattering and absorption) could be calculated as explained in Section 2.10.1. Furthermore, it was assumed that the light source emitted a unidirectional light beam at a constant rate, and that light travels in a straight direction. Light distribution was experimentally modelled. Equation (6-1) represents the proposed light distribution model.

$$I(p, C_b) = I_o \cdot \exp\left(-p \cdot K_a \cdot C_b \cdot \frac{p^q}{p_k + p^q}\right) \quad (6-1)$$

where I_o , p , K_a and C_b are incident light intensity ($\mu\text{mol m}^{-2} \text{s}^{-1}$), light path, absorption coefficient and biomass concentration, respectively, and q and p_k are model parameters. K_a was calculated below Equation (Sevilla and Grima, 1997):

$$K_a = \frac{K_{a,max} \cdot C_b}{b + C_b} \quad (6-2)$$

Where $K_{a,max}$ and b are maximum attenuation coefficient (m^{-1}) and model parameter (kg m^{-3}), respectively. For *C. vulgaris* these parameters are respectively 1041 m^{-1} and 1.03 kg m^{-3} as calculated by Yun and Park (Yun and Park, 2001).

Experimental data of local light intensity at various biomass concentrations and incident light intensities was used to fit the model and estimate its parameters. Coding in MATLAB software (R2014a) was performed using a nonlinear least squares method. The best fitting surfaces are shown in Figure 6-12. The model fit to the experimental data had a non-linear regression coefficient of 0.9920, and the parameters were estimated as follows:

$$q = -0.3128 \quad \& \quad p_k = 12.66 \quad (6-3)$$

6.3.4.1 Model validation

The validity of the model was examined by using it to predict local light intensity in other conditions and comparing the predictions with experimental observations of local light intensity. Some of the results (at different biomass concentrations ranging from $0.09\text{--}1.33 \text{ g L}^{-1}$) are shown in Figure 6-13. The model

predictions fit the experimental data appropriately; however, at high biomass concentrations, local light intensities are slightly overestimated by the model.

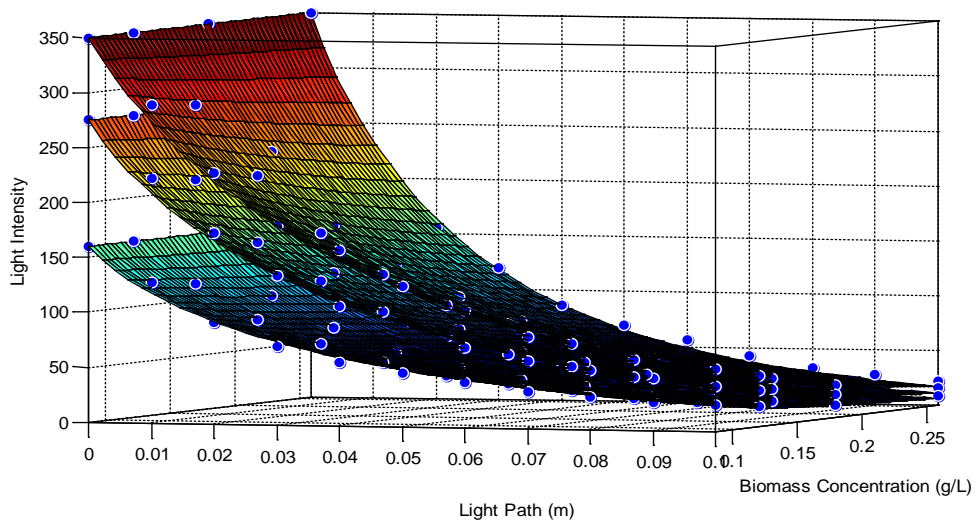


Figure 6-12 Surface fitting of the light distribution model (Equation 6-1) to experimental data of light intensity, light path and biomass concentration (blue dots)

6.3.4.2 Average light intensity

Light, apart from being the main energy source for photosynthesis, is a substrate, and can limit or enhance growth according to its intensity. Therefore, the amount of microalgal growth is dependent on the light intensity received by cells. The light intensity received by cells can be estimated by average light intensity. This is simpler than using local light intensity, as it accounts for incident light, light path and cell density (Martinez et al., 2012). Hence, average light intensity represents the photons available to each cell moving randomly in the culture, where there is a heterogeneous light distribution and different local light intensities due to shading effects (Sevilla et al., 1998). Therefore, the use of average light intensity is generally accepted in algal culture research. It is assumed that cells are influenced by the volumetric average light intensity in the total working volume of cultures. Hence, kinetic and growth rate are dependent on average light intensity rather than local photon flux and local kinetics. These issues were discussed in detail in Chapter Two.

For any geometry, average volumetric light intensity can be calculated by Equation (2-10):

$$I_{av} = \frac{\sum_{i=1}^n V_i \cdot I_{pi}}{\sum_{i=1}^n V_i} = \frac{\sum_{i=1}^n V_i \cdot I_{pi}}{V_T} \quad (2-10)$$

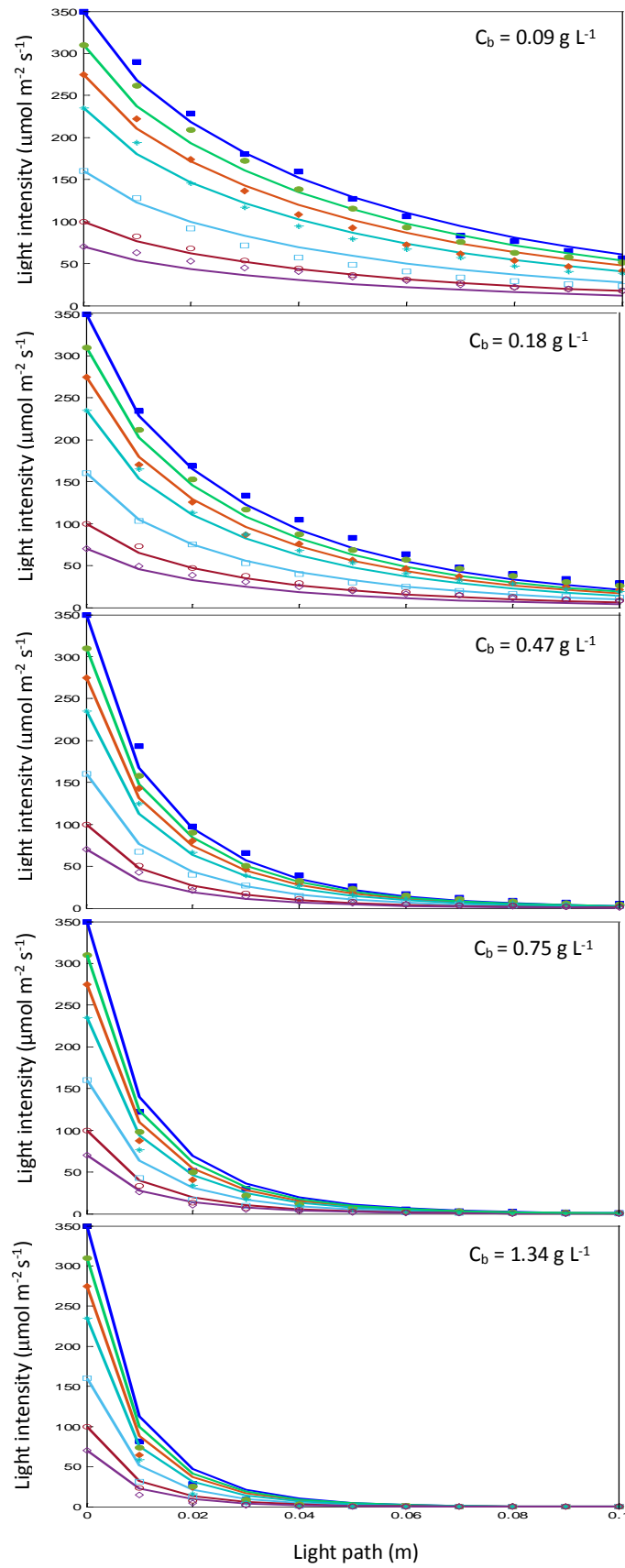


Figure 6-13 Experimental and modelled results for light intensity vs light path at biomass concentrations (C_b) of 0.09, 0.18, 0.47, 0.75 and 1.34 g L^{-1}

Then, local light intensity can be estimated using Equation (2-10), remembering that light path must be calculated based on the appropriate geometry, as explained in Chapter Two. In the case of rectangular vessels with illumination from one side, the light path is simply the distance from the illuminated surface. However, for an evenly illuminated cylindrical vessel, the light path can be estimated by Equation) 6-4).

$$p = a + b = (R - s) \cos \theta + [R^2 - (R - s)^2 \sin^2 \theta]^{0.5} \quad (6-3)$$

The average light intensity for any geometry can be estimated via Equation (2-10). Therefore, adapting Equation (6-1) to estimate local light distribution in an evenly illuminated cylindrical vessel results in Equation (6-4).

$$I_{av} = \frac{I_o}{\pi R} \int_0^R \int_0^\pi \exp(-p(s) \cdot K_a \cdot C_b \cdot \frac{p(s)^q}{p(s)_k^q + p(s)^q}) ds d\theta \quad (6-4)$$

where $p(s)$ is calculated by Equation (6-3).

In Figure 6-14, the results for changes in average light intensity with increasing biomass are presented for an incident light intensity of $120 \mu\text{mol m}^{-2}\text{s}^{-1}$. Average light intensity decreases sharply with increasing cell density. For biomass concentrations $> 0.5 \text{ g L}^{-1}$, it is almost the same and at a very low level.

The unit of average light intensity is useful, as it makes it possible to study photosynthetic response based on the actual light intensity that cells in a culture receive, instead of irradiance on the photobioreactor surface. Therefore, optimal light intensity can be determined. Then, in order to optimise microalgal biomass productivity and CO_2 biofixation, the influence of average light intensity on growth rate must be investigated.

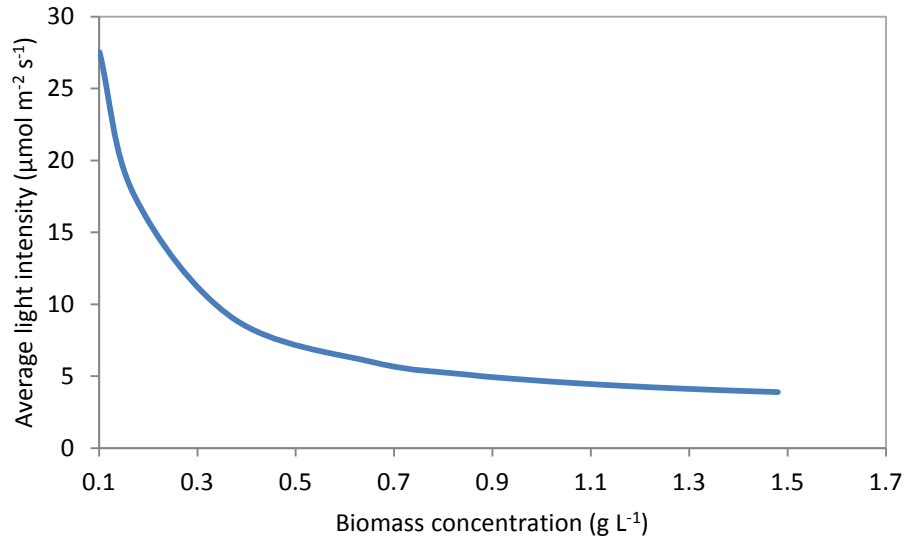


Figure 6-14 Average light intensity vs biomass concentration at an incident light intensity of $I_0 = 120 \mu\text{mol m}^{-2} \text{s}^{-1}$

Figure 6-15 shows how the average light intensity in a cylindrical bioreactor changes with time due to cell growth. The cell growth results for these experiments were discussed in Section 4.3.2 and Figure 4-1.

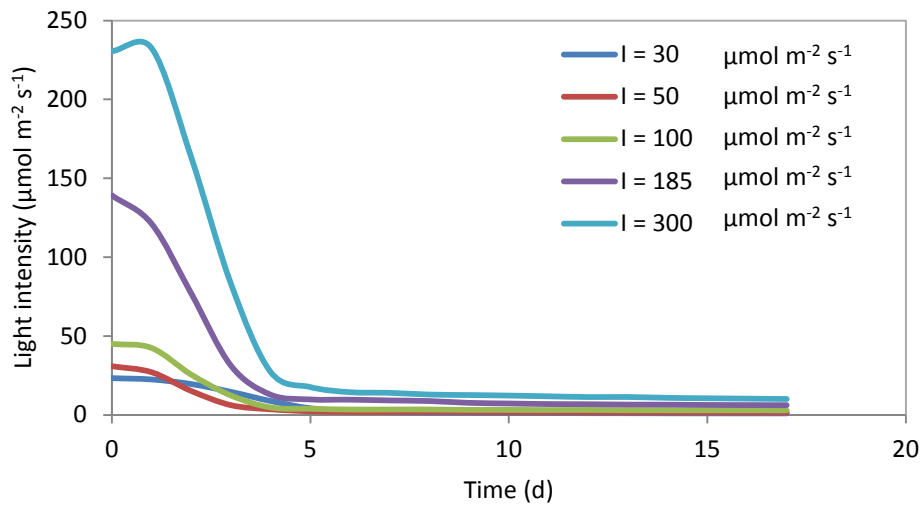


Figure 6-15 Average light intensity vs time for various incident light intensities

Figure 6-16 plots cell growth rate (calculated from experimental data, Chapter 3) vs average light intensity. Average light intensity can be considered as a substrate, and growth rate can be related to it. The experimental growth rate, μ , vs average light intensity, I_{av} , was fitted to a kinetic model by non-linear regression. In this study, two different kinetic models were used to model growth rate, as explained in the following section.

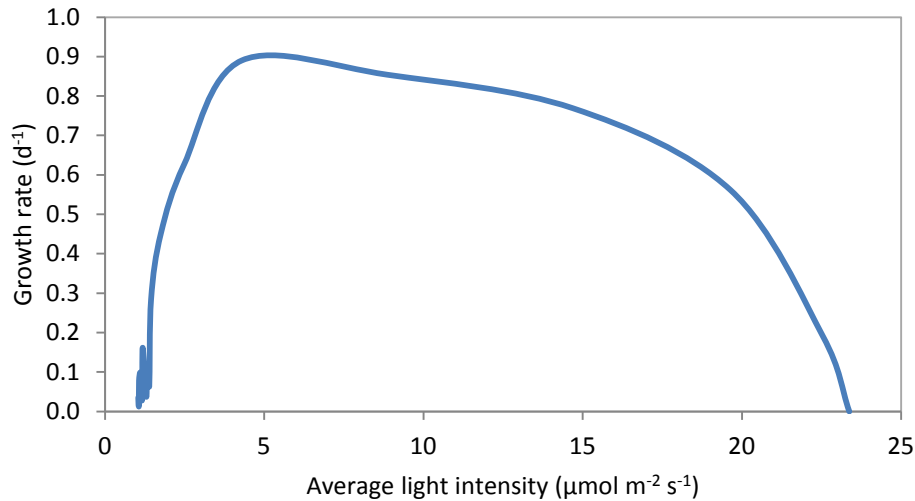


Figure 6-16 Growth rate vs average light intensity

6.3.4.3 Comparison of improved model with Beer-Lambert model

Experimental observations of light distribution inside a culture in a vessel with a rectangular cross-section were used to develop a new, modified Beer-Lambert model. To see the improvements made by this model, simulation results from these two models were plotted against experimental data for various biomass concentrations and incident light intensities. First, two figures were plotted for a biomass density of 0.16 g L^{-1} with incident light intensities of 100 and $275 \mu\text{mol m}^{-2} \text{ s}^{-1}$ (Figure 6-17 a & b). The two other figures are for the same incident light intensities but at a higher biomass concentration of 1.34 g L^{-1} (Figure 6-17 c & d). All figures were plotted versus light path distance from the surface of the vessel.

It can be clearly seen in all plots that the Beer-Lambert model overestimates light intensity at every distance, especially in dense biomass cultures. The new model is more accurate in all conditions. It almost completely corresponds with data at low biomass concentrations, and even at high concentrations it is very accurate. As can be seen and has been discussed before, in dense cultures, due to absorption and scattering, sharp decreases in light intensity are observed near the surface, which are not predicted by the Beer-Lambert model at all. The new model shows this phenomenon relatively well. The results are significantly improved in comparison with the Beer-Lambert model, and are acceptable and reliable.

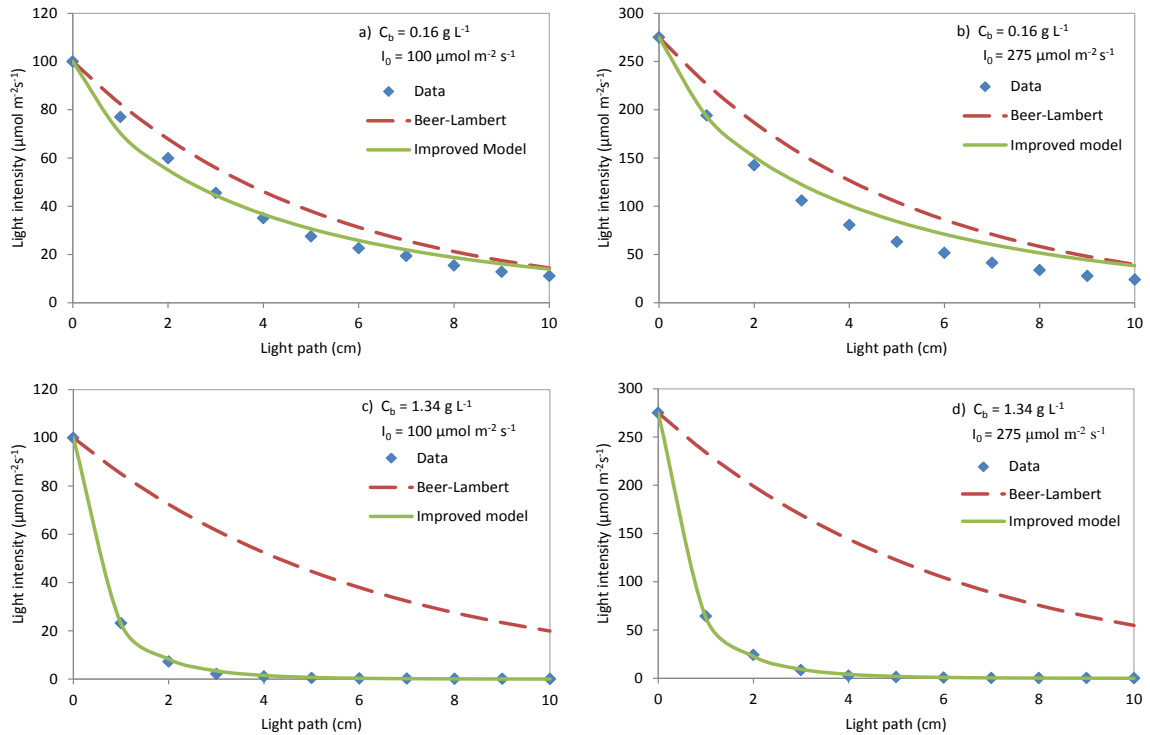


Figure 6-17 Light distribution in a rectangular vessel with single-sided illumination at different incident light intensities and biomass concentrations, dots represent experimental data, while dash and solid lines are show the predicted results using the Beer-Lambert model and the new model, respectively.

6.3.5 Kinetic modelling

Modelling growth rate as a function of culture conditions would be a useful tool for determining biomass concentration and productivity. The growth rate of a microorganism can be estimated by a kinetic model of the consumed substrate. In the case of phototrophic microalgae cultivation, photon flux can be considered as a substrate when nutrients are in excess of that required for algal growth. As reviewed in Chapter 2, many equations have been proposed to model specific cell growth rate as a function of average light intensity. Three models are considered in this study for predicting biomass growth where irradiance changes over time.

6.3.5.1 Molina-Grima model

The Molina-Grima model is one of the simplest models. It uses a hyperbolic relationship between specific growth rate, μ , and average light intensity, I_{av} :

$$\mu = \frac{\mu_{max} I_{av}^n}{I_k^n + I_{av}^n} \tag{6-4}$$

Maximum specific growth rate, μ_{max} , and the other two model parameters, n and I_k , can be estimated by fitting the model to a set of experimental data. Models are specific for each algae strain. The model parameters were determined by non-linear regression with experimental data in MATLAB. The model fit was determined by the non-linear regression coefficient, R^2 .

In this model, growth rate increases with average light intensity up to a maximum point, after which there are no further increases. The results for *Chlorella vulgaris*, the microalgal species used in this study, are shown in Figure 6-18. The model fits the experimental data acceptably ($R^2 = 0.9314$). The estimated model parameters are:

$$\mu_{max} = 0.9243; \quad I_k = 16.66; \quad n = 9.095$$

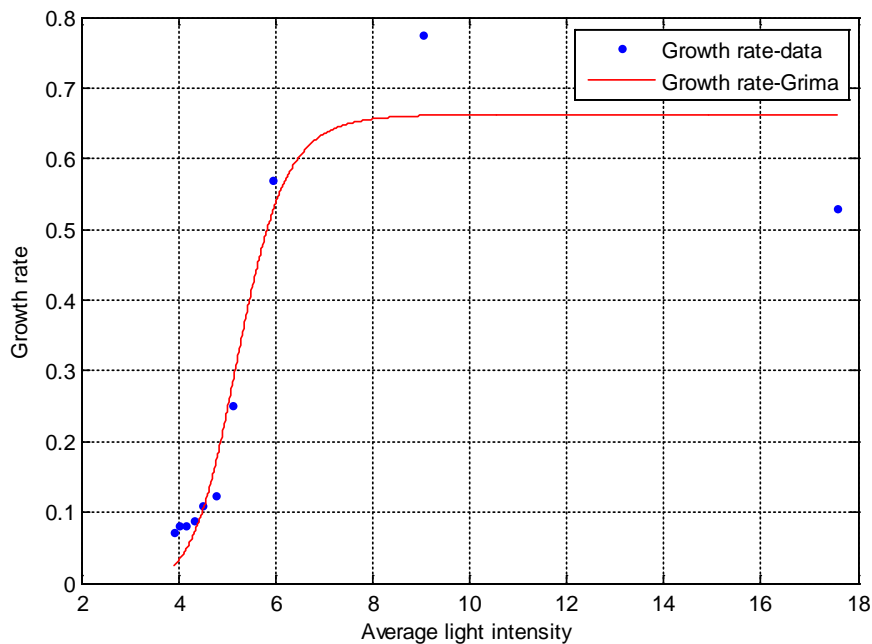


Figure 6-18 Molina-Grima hyperbolic model of specific growth rate (d^{-1}) vs average light intensity ($\mu\text{mol m}^{-2} \text{s}^{-1}$), compared with experimental observations

It should be noted that the strain used in this study was not previously adapted to irradiance. The microalgae cells have the ability to adapt their photosynthetic rate to the local light level. Cells that have been exposed to low light levels show relatively high photosynthetic efficiency when illuminated by favourable levels of light (Martinez et al., 2012).

6.3.5.2 Muller-Feuga model

In this model, proposed by Muller-Feuga (1999), a maximum growth rate, μ_s , is achieved when the average light intensity, I_{av} , reaches the saturation light intensity, I_s . In this situation, the maximum amount of photons that can be processed by the cells is being received. Any further increases in light intensity lead to cell damage, photoinhibition and reduced productivity. Meanwhile, I_e represents compensation energy, which is the minimum amount of energy needed for sustaining the microalgae, below which any lower levels of light cause weight μ loss.

$$\mu = \frac{2\mu_s(1 - \frac{I_e}{I_s})(\frac{I_{av}}{I_s} - \frac{I_e}{I_s})}{(1 - \frac{I_e}{I_s})^2 + (\frac{I_{av}}{I_s} - \frac{I_e}{I_s})^2} \tag{6-5}$$

Model parameters, estimated by non-linear regression with experimental data, are listed below ($R^2 = 0.9431$):

$$\mu_s = 1.1556; I_e = 3.1053; I_s = 12.4871$$

Figure 6-19 displays the Muller-Feuga kinetic model fitted to the experimental data. As can be seen, the model can predict decreased growth rates at high values of irradiance.

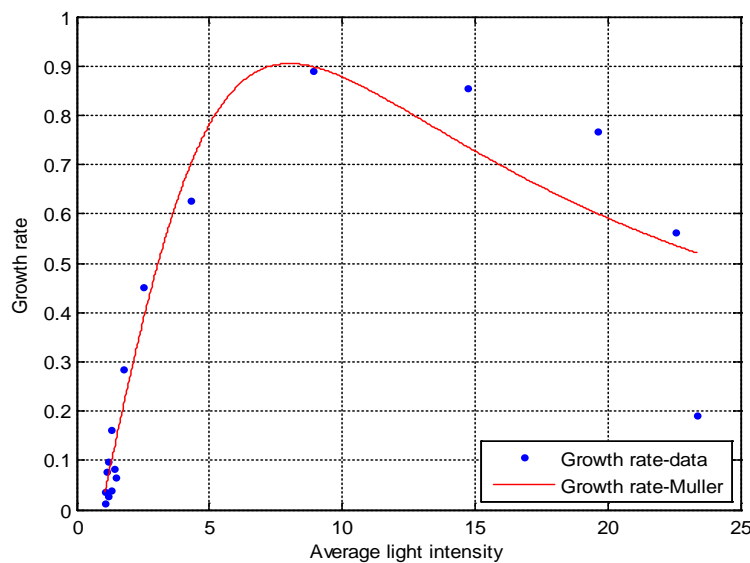


Figure 6-19 Muller-Feuga model of specific growth rate (d^{-1}) vs average light intensity ($\mu\text{mol m}^{-2} \text{s}^{-1}$), compared with experimental data

6.3.5.3 Comparing results from different kinetic models

As can be seen in Figure 6-18, the Molina-Grima model cannot explain the decreases in growth rate at high light intensities that correspond with photoinhibition. In practice, after the growth rate reaches its maximum it decreases with further irradiance. However, this model predicts that growth rate stays constant after reaching its maximum. In contrast, the Muller-Feuga model is able to estimate this reduction in growth rate. Although both models fit the experimental data with an acceptable level of statistical significance, the Molina-Grima model cannot describe all features of microalgal growth.

Biomass concentration vs time was estimated with the two models and compared with experimental data (Figure 6-20). Clearly, the Muller-Feuga model is better. A similar figure, but showing growth rate vs time, is presented in Figure 6-21.

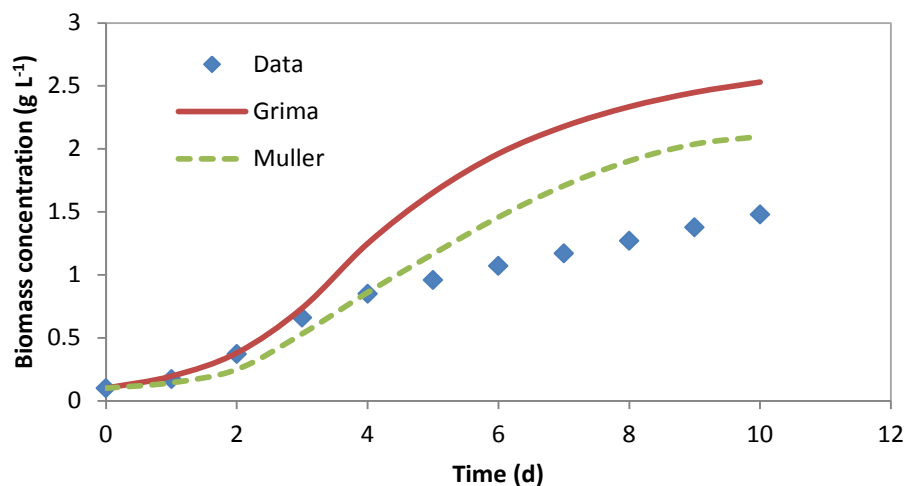


Figure 6-20 Biomass concentration vs time predicted by Grima and Muller models and compared with experimental data.

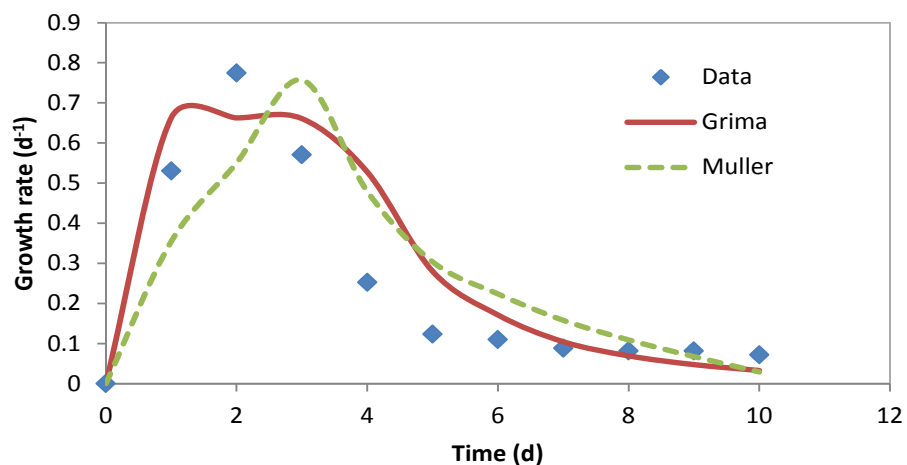


Figure 6-21 Growth rate vs time predicted by Grima and Muller models and compared with experimental data.

6.3.6 Summary

Investigating the quality of light availability and distribution inside cultures could enhance microalgal productivity and improve photobioreactor performance. Light intensity distributions across microalgal cultures inside rectangular and cylindrical bioreactors were analysed and discussed in this chapter. In addition to the influence of incident light intensity, the effects of distance from the illuminated surface and biomass concentration were addressed. Increasing incident light intensity to an optimum value, or evenly illuminating vessels, can lead to better light availability. However, this becomes inefficient at high biomass concentrations or at large distances from the culture surface. A light distribution model that accurately estimates local light intensity is of importance as it can be used to estimate photon availability inside cultures (or in other words, average light intensity).

In this study, a large dataset of experimentally-measured local light intensities was used to develop a light distribution model based on the Beer-Lambert law. This model was used to estimate local light intensity under different conditions. The results were compared with experimental data and the predictions of a conventional Beer-Lambert model. The new model gave greatly improved estimates, especially in dense cultures. Use of the new model, and consideration of vessel geometry, allows average light intensity to be calculated mathematically. Two different kinetic models of growth rate in light-limited photobioreactors were fitted to data obtained from biomass cultivation experiments. They were used to estimate specific growth rate, and results from different models were discussed.

7

Conclusions and Recommendations

7.1 Introduction

This chapter details the conclusions drawn from the present study and also the suggested recommendations for further research. Microalgae that can grow rapidly and convert solar energy to chemical energy via CO₂ biofixation are now being considered as a promising renewable source of energy and an atmospheric CO₂ mitigation.

7.1.1 Conclusions

This study focused on light availability and CO₂ biofixation, therefore, the influence of light intensity, the light period and CO₂ concentration on biomass growth, CO₂ biofixation and CO₂ utilisation were investigated. Furthermore, light distribution inside the culture was studied and discussed for different algal PBRs under different conditions. Thereafter, it was experimentally modelled. The newly developed model was used for the simulation of average light intensity and light-limited growth kinetic. The following conclusions can be drawn:

- The influence of the light intensity on the biomass growth of *Chlorella vulgaris* and the performance of the photobioreactor was investigated. Different levels of light intensity, namely 30, 50, 100, 185 and 300 $\mu\text{mol m}^{-2} \text{s}^{-1}$, were examined. The influence of light intensity on growth and other parameters (e.g. pH and DO) were discussed. While maximum biomass growth was different at various conditions, biomass growth presented a similar trend in all conditions and after rapidly increasing and reaching a maximum, it dropped steeply to small values and levelled off. Since biomass productivity and the CO₂ biofixation rate directly depend on biomass growth,

following the reduction in growth rate, they also reduced. Through these experiments, optimum light intensity was among the five light intensities identified at $100 \mu\text{mol m}^{-2} \text{s}^{-1}$. While the biomass grew relatively well at a light intensity of $50 \mu\text{mol m}^{-2} \text{s}^{-1}$, biomass growth was limited at $30 \mu\text{mol m}^{-2} \text{s}^{-1}$. Growth was inhibited at light intensities of 185 and $300 \mu\text{mol m}^{-2} \text{s}^{-1}$.

- For the first time the simultaneous influence of light intensity, light period and CO_2 concentration on biomass growth was investigated. These parameters are among the most effective factors that influence the CO_2 biofixation rate, which to the best knowledge of the author, have not been optimised together when interaction between them is considered. It was revealed that CO_2 concentration is the most effective parameter has a strong influence on the process of carbon removal and widely changes the CO_2 biofixation rate. Then, the CO_2 biofixation demonstrates more change with the changing light period than the changing of light intensity. The influence of these parameters on biomass growth as well as the CO_2 biofixation rate and utilisation efficiency was discussed considering the individual and synergistic effect of the parameters.
- Statistical design and analysis was used to systematically explore the influence of light intensity, light period and CO_2 concentration on inlet gas for achieving optimum growth and maximum CO_2 uptake rate. The CCD method was used to design experiments and a five-level fractional factorial design was carried out. Then RSM was used to analyse results from 17 experiments conducted at designed levels while the interaction effect of the parameters was also considered. Among these experiments, the highest rate of CO_2 biofixation was achieved at $200 \mu\text{mol m}^{-2} \text{s}^{-1}$ light intensity, 16 h light period and 8 % CO_2 . Statistical optimisation of these parameters gave $112 \mu\text{mol m}^{-2} \text{s}^{-1}$ of light intensity, a 17 h light period and 8.7 % CO_2 as the optimum conditions that produced the maximum CO_2 biofixation rate of $0.3504 \text{ g CO}_2 \text{ L}^{-1} \text{ d}^{-1}$ which was validated experimentally. Meanwhile, CO_2 utilisation was optimised and $140 \mu\text{mol m}^{-2} \text{s}^{-1}$ of light intensity, 17.4 h light period and 1.3 % CO_2 was found as the optimum conditions to achieve maximum CO_2 utilisation efficiency (0.8146 %). Another experiment was carried out to validate the optimisation results for CO_2 utilisation efficiency.

While the CO₂ biofixation rate only demonstrates the total amount of carbon dioxide that has been fixed, CO₂ utilisation efficiency determines the percentage of carbon dioxide removal from the total amount of introduced CO₂ to the system. Different aspects of the statistical analysis, including ANOVA and regression analysis, were discussed.

- Light distribution inside the culture in different photobioreactor geometries and configurations was studied and discussed. The influence of incident light intensity, biomass concentration and the distance from the illuminated surface was investigated. It was deduced that by increasing the biomass density of the culture, light availability significantly drops and even increasing the incident light intensity did not prove useful. Despite the noticeable reduction in the local light intensity at the first few centimetres of the light beam travelling inside the culture, for distances far from the illuminated surface, the local light intensity levelled off and no significant change was observed. It was revealed that the Beer-Lambert model cannot predict local light intensity accurately and the necessity of adding another term to the Beer-Lambert model was discussed.
- A newly modified light distribution model was proposed and used to estimate local light intensity. The predicted results from this model were evaluated by experimental results and compared with the Beer-Lambert model, verifying great improvement, particularly in dense cultures. Afterwards, the average light intensity was mathematically calculated and used to simulate light-limited biomass growth kinetic and investigate the performance of the photobioreactor. The estimated average light intensity and its influence on biomass growth was investigated and explained. Two previously proposed kinetic models were used for kinetic modelling while the new proposed light model was used to estimate the average light intensity. Among the two kinetic models (Grima and Muller) that were applied, Muller described the growth rate better since it considers photoinhibition.

7.1.2 Recommendations for future research

This study has opened a range of future research subjects that may be of interest to researchers:

-
- It was observed that RSM is good enough and reliable for optimising biomass growth parameters and parameter optimisation is a beneficial method to enhance biomass productivity and CO₂ biofixation. Despite reducing the number of experiments when experiments are designed by this method, considering more than three parameters for optimisation led to a steep increase in the number of experiments, which makes the optimisation process very difficult and time consuming, particularly for microalgae research since it must be cultivated for at least one week to reach a reasonable level of growth. However, it is good practice to choose some other factors that influence microalgae growth and apply the optimisation method. This study clarified that parameters of light intensity, light period and CO₂ concentration have significant influence on CO₂ biofixation. Light source and light wavelength are two other significant factors that could have high potential to be investigated and optimised. In all experiments in this study, cool white fluorescent lamps were used to illuminate light to the bioreactor. Different light sources can be used, particularly LED lamps that have recently come to the researchers' attention. Fluorescent lamps have been used and investigated as a light source to grow microalgae for quite a long time; however, LED lamps have recently been used for this purpose and need to be studied further. LED lamps have good potential as a light source for microalgae growing since they are very energy efficient and can reduce production costs. Nevertheless, because of the characteristics of LED lamps, microalgae species may need to adapt to this light source. Light wavelength is another parameter of light; its influence on microalgae growth has been investigated by some researchers. However, little research has been done in this regard and it seems optimising light wavelength along with other parameters of light, for instance, light source and light intensity can potentially yield useful results whereas the current study briefly discussed variation in the amount of light absorbed by microalgae cells in different light wavelengths.
 - In this study, a new light distribution model was proposed and an improvement in estimating local light intensity using this model was explained. However, some parts of previously proposed kinetic model were used to simulate biomass growth. Although many kinetic models have been

developed for biomass growth and some of them demonstrate great improvements, it seems there is still potential for carrying out more research in this area. Accurate kinetic simulation of microalgae growth could be a beneficial tool for optimising biomass growth and the enhancement of photobioreactor efficiency. It can even be applied to develop novel photobioreactors.

- Current research has proposed a light intensity model that has been used to mathematically calculate the average light intensity in an evenly illuminated photobioreactor and then used for a light-limited growth kinetic model. It will be useful to see how accurately light distribution and average light intensity can be estimated by this model for different photobioreactor configurations, and particularly for the flat plate bioreactor as it is one of the most popular photobioreactors for growing microalgae.
- How the optimum conditions of the studied parameters (light intensity, light period and CO₂ concentration) can be different for different optimisation objectives was demonstrated. In other words, for optimising the CO₂ biofixation rate the optimum conditions are different from the optimum conditions that lead to optimising CO₂ utilisation. Although, reducing the level of carbon dioxide in the atmosphere is the objective and so the CO₂ biofixation rate must be considered as the optimisation function, thus including the cost of aeration to the bioreactor indicates the necessity of optimising the CO₂ utilisation efficiency. Aerating the high rate of carbon dioxide (actually) has a low percentage of carbon removal, leading to increases in the cost. Not much research has been performed on this subject and it still needs to be studied further. Furthermore, multi-objective optimisation methods that involve minimising or maximising two or more conflicting objectives could be beneficial and is recommended to optimise both objectives of the CO₂ biofixation rate and CO₂ utilisation efficiency.
- Owing to the fact light scattering is proportional to $1/\lambda^4$ (Rayleigh scattering), scattering effect by algal cells is more prominent at shorter wavelengths. Since the absorption spectra (Figure 3-26) contain prominent scattering effect, the use of opal-glass method (Shibata, 1959) is recommended to

reduce this effect. Otherwise, scattering can be corrected according to the method described (Hirani et al., 2001).

- In the future work it is a good practice to investigate the hydrodynamics of the large scale algal photobioreactors.

8

References

- ACIÉN FERNÁNDEZ, F., FERNÁNDEZ SEVILLA, J. & MOLINA GRIMA, E. 2013. Photobioreactors for the production of microalgae. *Reviews in Environmental Science and Bio/Technology*, 12, 131-151.
- AIBA, S. 1982. Growth kinetics of photosynthetic microorganisms. *Microbial Reactions*, 85-156.
- AMINI KHOEYI, Z., SEYFABADI, J. & RAMEZANPOUR, Z. 2012. Effect of light intensity and photoperiod on biomass and fatty acid composition of the microalgae, *Chlorella vulgaris*. *Aquaculture International*, 20, 41-49.
- ANDERSEN, R. A. 2005. *Algal culturing techniques*, Academic press.
- ANJOS, M., FERNANDES, B. D., VICENTE, A. A., TEIXEIRA, J. A. & DRAGONE, G. 2013. Optimization of CO₂ bio-mitigation by *Chlorella vulgaris*. *Bioresource Technology*, 139, 149-154.
- ARATA, S., STRAZZA, C., LODI, A. & DEL BORGHI, A. 2013. Spirulina platensis Culture with Flue Gas Feeding as a Cyanobacteria-Based Carbon Sequestration Option. *Chemical Engineering & Technology*, 36, 91-97.
- BALIGA, R. & POWERS, S. E. 2010. Sustainable algae biodiesel production in cold climates. *International Journal of Chemical Engineering*, 2010.
- BANNISTER, T. 1979. Quantitative description of steady state, nutrient-saturated algal growth, including adaptation. *Limnology and Oceanography*, 24, 76-96.
- BARBOSA, M. J., HOOGAKKER, J. & WIJFFELS, R. H. 2003. Optimisation of cultivation parameters in photobioreactors for microalgae cultivation using the A-stat technique. *Biomolecular Engineering*, 20, 115-123.
- BARSANTI, L. & GUALTIERI, P. 2014. *Algae: anatomy, biochemistry, and biotechnology*, CRC press.
- BARTLEY, M. L., BOEING, W. J., DANIEL, D., DUNGAN, B. N. & SCHAUB, T. 2015. Optimization of environmental parameters for *Nannochloropsis salina* growth and lipid content using the response surface method and invading organisms. *Journal of Applied Phycology*, 1-10.
- BASU, S., ROY, A. S., MOHANTY, K. & GHOSHAL, A. K. 2013. Enhanced CO₂ sequestration by a novel microalga: *Scenedesmus obliquus* SA1 isolated from bio-diversity hotspot region of Assam, India. *Bioresource Technology*, 143, 369-377.
- BENSON, B. C., GUTIERREZ-WING, M. T. & RUSCH, K. A. 2007. The development of a mechanistic model to investigate the impacts of the light dynamics on algal productivity in a hydraulically integrated serial turbidostat algal reactor (HISTAR). *Aquacultural engineering*, 36, 198-211.

- BENSON, B. C. & RUSCH, K. A. 2006. Investigation of the light dynamics and their impact on algal growth rate in a hydraulically integrated serial turbidostat algal reactor (HISTAR). *Aquacultural Engineering*, 35, 122-134.
- BERBEROGLU, H., GOMEZ, P. S. & PILON, L. 2009. Radiation characteristics of *Botryococcus braunii*, *Chlorococcum littorale*, and *Chlorella* sp. used for CO₂ fixation and biofuel production. *Journal of Quantitative Spectroscopy and Radiative Transfer*, 110, 1879-1893.
- BHOLA, V., DESIKAN, R., SANTOSH, S. K., SUBBURAMU, K., SANNIYASI, E. & BUX, F. 2011. Effects of parameters affecting biomass yield and thermal behaviour of *Chlorella vulgaris*. *Journal of bioscience and bioengineering*, 111, 377-382.
- BILANOVIC, D., ANDARGATCHEW, A., KROEGER, T. & SHELEF, G. 2009. Freshwater and marine microalgae sequestering of CO₂ at different C and N concentrations—response surface methodology analysis. *Energy Conversion and Management*, 50, 262-267.
- BLANKEN, W., CUARESMA, M., WIJFFELS, R. H. & JANSSEN, M. 2013. Cultivation of microalgae on artificial light comes at a cost. *Algal Research*, 2, 333-340.
- BOROWITZKA, M. A. & MOHEIMANI, N. R. 2013. *Algae for biofuels and energy*, Springer.
- BOSMA, R., VAN ZESSEN, E., REITH, J. H., TRAMPER, J. & WIJFFELS, R. H. 2007. Prediction of volumetric productivity of an outdoor photobioreactor. *Biotechnology and bioengineering*, 97, 1108-1120.
- BRINDLEY, C., FERNANDEZ, F. G. A. & FERNANDEZ-SEVILLA, J. M. 2011. Analysis of light regime in continuous light distributions in photobioreactors. *Bioresource Technology*, 102, 3138-3148.
- CAMACHO, F. G. A., GOMEZ, A. C., SOBCZUK, T. M. & GRIMA, E. M. 2000. Effects of mechanical and hydrodynamic stress in agitated, sparged cultures of *Porphyridium cruentum*. *Process Biochemistry*, 35, 1045-1050.
- CARVALHO, A. P., MEIRELES, L. A. & MALCATA, F. X. 2006. Microalgal reactors: a review of enclosed system designs and performances. *Biotechnology Progress*, 22, 1490-1506.
- CHAI, X., ZHAO, X. & BAOYING, W. 2012. Biofixation of carbon dioxide by *Chlorococcum* sp. in a photobioreactor with polytetrafluoroethylene membrane sparger. *African Journal of Biotechnology*, 11, 7445-7453.
- CHANDRASEKHAR, S. 1960. *Radiative transfer*, Courier Dover Publications.
- CHANG, H.-X., HUANG, Y., FU, Q., LIAO, Q. & ZHU, X. 2016. Kinetic characteristics and modeling of microalgae *Chlorella vulgaris* growth and CO₂ biofixation considering the coupled effects of light intensity and dissolved inorganic carbon. *Bioresource technology*, 206, 231-238.
- CHEIRSILP, B. & TORPEE, S. 2012. Enhanced growth and lipid production of microalgae under mixotrophic culture condition: Effect of light intensity, glucose concentration and fed-batch cultivation. *Bioresource Technology*, 110, 510-516.
- CHEN, C.-Y., YEH, K.-L., AISYAH, R., LEE, D.-J. & CHANG, J.-S. 2011. Cultivation, photobioreactor design and harvesting of microalgae for biodiesel production: a critical review. *Bioresource Technology*, 102, 71-81.
- CHENG, L., ZHANG, L., CHEN, H. & GAO, C. 2006. Carbon dioxide removal from air by microalgae cultured in a membrane-photobioreactor. *Separation and purification technology*, 50, 324-329.

- CHIANG, C. L., LEE, C. M. & CHEN, P. C. 2011. Utilization of the cyanobacteria *Anabaena* sp CH1 in biological carbon dioxide mitigation processes. *Bioresource Technology*, 102, 5400-5405.
- CHISTI, Y. 2007. Biodiesel from microalgae. *Biotechnology advances*, 25, 294-306.
- CHIU, S.-Y., KAO, C.-Y., CHEN, C.-H., KUAN, T.-C., ONG, S.-C. & LIN, C.-S. 2008. Reduction of CO₂ by a high-density culture of *Chlorella* sp. in a semicontinuous photobioreactor. *Bioresource technology*, 99, 3389-3396.
- CHIU, S. Y., TSAI, M. T., KAO, C. Y., ONG, S. C. & LIN, C. S. 2009. The air-lift photobioreactors with flow patterning for high-density cultures of microalgae and carbon dioxide removal. *Engineering in life sciences*, 9, 254-260.
- CHOJNACKA, K. & NOWORYTA, A. 2004. Evaluation of *Spirulina* sp. growth in photoautotrophic, heterotrophic and mixotrophic cultures. *Enzyme and Microbial Technology*, 34, 461-465.
- CONCAS, A., LUTZU, G. A., PISU, M. & CAO, G. 2012. Experimental analysis and novel modeling of semi-batch photobioreactors operated with *Chlorella vulgaris* and fed with 100%(v/v) CO₂. *Chemical Engineering Journal*.
- CONCAS, A., PISU, M. & CAO, G. 2013. Mathematical Modelling of *Chlorella Vulgaris* Growth in Semi-Batch Photobioreactors Fed with Pure CO₂. *CHEMICAL ENGINEERING*, 32.
- CORNET, J.-F., DUSSAP, C. & GROS, J.-B. 1998. Kinetics and energetics of photosynthetic micro-organisms in photobioreactors. *Bioprocess and Algae Reactor Technology, Apoptosis*. Springer.
- CORNET, J.-F., DUSSAP, C., GROS, J.-B., BINOIS, C. & LASSEUR, C. 1995. A simplified monodimensional approach for modeling coupling between radiant light transfer and growth kinetics in photobioreactors. *Chemical Engineering Science*, 50, 1489-1500.
- CORNET, J., DUSSAP, C., CLUZEL, P. & DUBERTRET, G. 1992a. A structured model for simulation of cultures of the cyanobacterium *Spirulina platensis* in photobioreactors: II. Identification of kinetic parameters under light and mineral limitations. *Biotechnology and bioengineering*, 40, 826-834.
- CORNET, J., DUSSAP, C. & DUBERTRET, G. 1992b. A structured model for simulation of cultures of the cyanobacterium *Spirulina platensis* in photobioreactors: I. Coupling between light transfer and growth kinetics. *Biotechnology and Bioengineering*, 40, 817-825.
- CORNET, J., DUSSAP, C. & GROS, J. 1994. Conversion of radiant light energy in photobioreactors. *AIChE Journal*, 40, 1055-1066.
- DA SILVA VAZ, B., COSTA, J. A. V. & DE MORAIS, M. G. 2016. CO₂ Biofixation by the cyanobacterium *Spirulina* sp. LEB 18 and the green alga *Chlorella fusca* LEB 111 grown using gas effluents and solid residues of thermoelectric origin. *Applied biochemistry and biotechnology*, 178, 418-429.
- DANIEL, K., LAURENDEAU, N. & INCROPERA, F. 1979. Prediction of radiation absorption and scattering in turbid water bodies. *Journal of Heat Transfer*, 101, 63-67.
- DASGUPTA, C. N., GILBERT, J. J., LINDBLAD, P., HEIDORN, T., BORGVANG, S. A., SKJANES, K. & DAS, D. 2010. Recent trends on the development of photobiological processes and photobioreactors for the improvement of hydrogen production. *International Journal of Hydrogen Energy*, 35, 10218-10238.

- DE MORAIS, M. G. & COSTA, J. A. V. 2007a. Biofixation of carbon dioxide by *Spirulina* sp. and *Scenedesmus obliquus* cultivated in a three-stage serial tubular photobioreactor. *Journal of Biotechnology*, 129, 439-445.
- DE MORAIS, M. G. & COSTA, J. A. V. 2007b. Carbon dioxide fixation by *Chlorella kessleri*, *C. vulgaris*, *Scenedesmus obliquus* and *Spirulina* sp. cultivated in flasks and vertical tubular photobioreactors. *Biotechnology Letters*, 29, 1349-1352.
- DE MORAIS, M. G. & COSTA, J. A. V. 2007c. Isolation and selection of microalgae from coal fired thermoelectric power plant for biofixation of carbon dioxide. *Energy Conversion and Management*, 48, 2169-2173.
- DEMIRBAS, A. & DEMIRBAS, M. F. 2010. *Algae energy: algae as a new source of biodiesel*, Springer Science & Business Media.
- DOUSKOVA, I., DOUCHA, J., LIVANSKY, K., MACHAT, J., NOVAK, P., UMYSOVA, D., ZACHLEDER, V. & VITOVA, M. 2009. Simultaneous flue gas bioremediation and reduction of microalgal biomass production costs. *Applied Microbiology and Biotechnology*, 82, 179-185.
- ELYASI, S. & TAGHIPOUR, F. 2010. Simulation of UV photoreactor for degradation of chemical contaminants: model development and evaluation. *Environmental science & technology*, 44, 2056-2063.
- EVERS, E. G. 1991. A Model for Light-Limited Continuous Cultures - Growth, Shading, and Maintenance. *Biotechnology and Bioengineering*, 38, 254-259.
- FAN, L.-H., ZHANG, Y.-T., ZHANG, L. & CHEN, H.-L. 2008. Evaluation of a membrane-sparged helical tubular photobioreactor for carbon dioxide biofixation by *Chlorella vulgaris*. *Journal of Membrane Science*, 325, 336-345.
- FAN, L. H., ZHANG, Y. T., CHENG, L. H., ZHANG, L., TANG, D. S. & CHEN, H. L. 2007a. Optimization of Carbon Dioxide Fixation by *Chlorella vulgaris* Cultivated in a Membrane-Photobioreactor. *Chemical Engineering & Technology*, 30, 1094-1099.
- FAN, L. H., ZHANG, Y. T., CHENG, L. H., ZHANG, L., TANG, D. S. & CHEN, H. L. 2007b. Optimization of Carbon Dioxide Fixation by *Chlorella vulgaris* Cultivated in a Membrane-Photobioreactor. *Chemical engineering & technology*, 30, 1094-1099.
- FERNANDES, B. D., MOTA, A., FERREIRA, A., DRAGONE, G., TEIXEIRA, J. A. & VICENTE, A. A. 2014. Characterization of split cylinder airlift photobioreactors for efficient microalgae cultivation. *Chemical Engineering Science*, 117, 445-454.
- FUNAHASHI, H., NISHIYAMA, Y., ASANO, M. & NAKAO, K. 1999. Effects of pH shift and agitation speed on chlorophyll biosynthesis in heterotrophic culture of *Chlorella*. *KAGAKU KOGAKU RONBUNSHU*, 25, 214-219.
- GADHAMSSETTY, V., SUKUMARAN, A. & NIRMALAKHANDAN, N. 2010. Photoparameters in photofermentative biohydrogen production. *Critical Reviews in Environmental Science and Technology*, 41, 1-51.
- GARCÍA-MALEA, M., BRINDLEY, C., RÍO, E. D., ACIÉN, F., FERNÁNDEZ, J. & MOLINA, E. 2005. Modelling of growth and accumulation of carotenoids in *Haematococcus pluvialis* as a function of irradiance and nutrients supply. *Biochemical Engineering Journal*, 26, 107-114.
- GARCIA-MALEA, M. C., ACIEN, F. G., FERNANDEZ, J. M., CERON, M. C. & MOLINA, E. 2006. Continuous production of green cells of *Haematococcus*

- pluvialis*: Modeling of the irradiance effect. *Enzyme and Microbial Technology*, 38, 981-989.
- GRIMA, E. M., CAMACHO, F. G., PEREZ, J. A. S., FERNANDEZ, F. G. A. & SEVILLA, J. M. F. 1997. Evaluation of photosynthetic efficiency in microalgal cultures using averaged irradiance. *Enzyme and Microbial Technology*, 21, 375-381.
- GRIMA, E. M., CAMACHO, F. G., PEREZ, J. A. S., SEVILLA, J. M. F., FERNANDEZ, F. G. A. & GOMEZ, A. C. 1994. A Mathematical-Model of Microalgal Growth in Light-Limited Chemostat Culture. *Journal of Chemical Technology and Biotechnology*, 61, 167-173.
- GRIMA, E. M., FERNANDEZ, F. G. A., CAMACHO, F. G. & CHISTI, Y. 1999. Photobioreactors: light regime, mass transfer, and scaleup. *Journal of Biotechnology*, 70, 231-247.
- GRIMA, E. M., PEREZ, J. A. S., CAMACHO, F. G., SANCHEZ, J. L. G. & ALONSO, D. L. 1993. N-3 Pufa Productivity in Chemostat Cultures of Microalgae. *Applied Microbiology and Biotechnology*, 38, 599-605.
- GRIMA, E. M., SEVILLA, J. M. F., PEREZ, J. A. S. & CAMACHO, F. G. 1996. A study on simultaneous photolimitation and photoinhibition in dense microalgal cultures taking into account incident and averaged irradiances. *Journal of Biotechnology*, 45, 59-69.
- GRIS, B., MOROSINOTTO, T., GIACOMETTI, G., BERTUCCO, A. & SFORZA, E. 2014. Cultivation of *Scenedesmus obliquus* in Photobioreactors: Effects of Light Intensities and Light-Dark Cycles on Growth, Productivity, and Biochemical Composition. *Applied Biochemistry and Biotechnology*, 172, 2377-2389.
- GUTIERREZ-SANCHEZ, R. & NAFIDI, A. 2008. Trend analysis using nonhomogeneous stochastic diffusion processes. Emission of CO₂; Kyoto protocol in Spain. *Stochastic Environmental Research and Risk Assessment*, 22, 57-66.
- HALLENBECK, P. C., GROGGER, M., MRAZ, M. & VEVERKA, D. 2015. The use of Design of Experiments and Response Surface Methodology to optimise biomass and lipid production by the oleaginous marine green alga, *Nannochloropsis gaditana* in response to light intensity, inoculum size and CO₂. *Bioresource technology*, 184, 161-168.
- HANAGATA, N., TAKEUCHI, T., FUKUJU, Y., BARNES, D. J. & KARUBE, I. 1992a. Tolerance of Microalgae to High CO₂ and High-Temperature. *Phytochemistry*, 31, 3345-3348.
- HANAGATA, N., TAKEUCHI, T., FUKUJU, Y., BARNES, D. J. & KARUBE, I. 1992b. Tolerance of microalgae to high CO₂ and high temperature. *Phytochemistry*, 31, 3345-3348.
- HARRINGTON, L. & FOSTER, R. 1999. Australian residential building sector greenhouse gas emissions 1990–2010. *Australian Greenhouse Office*.
- HIRANI, T. A., SUZUKI, I., MURATA, N., HAYASHI, H. & EATON-RYE, J. J. 2001. Characterization of a two-component signal transduction system involved in the induction of alkaline phosphatase under phosphate-limiting conditions in *Synechocystis* sp. PCC 6803. *Plant molecular biology*, 45, 133-144.
- HO, S.-H., CHEN, C.-Y. & CHANG, J.-S. 2012. Effect of light intensity and nitrogen starvation on CO₂ fixation and lipid/carbohydrate production of an

- indigenous microalga *Scenedesmus obliquus* CNW-N. *Bioresource technology*, 113, 244-252.
- HO, S.-H., CHEN, W.-M. & CHANG, J.-S. 2010. *Scenedesmus obliquus* CNW-N as a potential candidate for CO₂ mitigation and biodiesel production. *Bioresource Technology*, 101, 8725-8730.
- HO, S. H., CHEN, C. Y., LEE, D. J. & CHANG, J. S. 2011. Perspectives on microalgal CO₂-emission mitigation systems--a review. *Biotechnol Adv*, 29, 189-98.
- IMAMOGLU, E., DEMIREL, Z. & CONK DALAY, M. 2015. Process optimisation and modeling for the cultivation of *Nannochloropsis* sp. and *Tetraselmis striata* via response surface methodology. *Journal of Phycology*, 51, 442-453.
- IMBERDORF, G. & MOHSENI, M. 2011. Modeling and experimental evaluation of vacuum-UV photoreactors for water treatment. *Chemical Engineering Science*, 66, 1159-1167.
- INCROPERA, F. & THOMAS, J. 1978. A model for solar radiation conversion to algae in a shallow pond. *Solar Energy*, 20, 157-165.
- JACOB-LOPES, E., LACERDA, L. M. C. F. & FRANCO, T. T. 2008a. Biomass production and carbon dioxide fixation by *Aphanothece microscopica Nageli* in a bubble column photobioreactor. *Biochemical Engineering Journal*, 40, 27-34.
- JACOB-LOPES, E., SCOPARO, C. H. G. & FRANCO, T. T. 2008b. Rates of CO₂ removal by *Aphanothece microscopica Nægeli* in tubular photobioreactors. *Chemical Engineering and Processing: Process Intensification*, 47, 1365-1373.
- JACOB-LOPES, E., SCOPARO, C. H. G., LACERDA, L. M. C. F. & FRANCO, T. T. 2009a. Effect of light cycles (night/day) on CO₂ fixation and biomass production by microalgae in photobioreactors. *chemical engineering and Processing: Process Intensification*, 48, 306-310.
- JACOB-LOPES, E., SCOPARO, C. H. G., LACERDA, L. M. C. F. & FRANCO, T. T. 2009b. Effect of light cycles (night/day) on CO₂ fixation and biomass production by microalgae in photobioreactors. *chemical engineering and Processing: Process Intensification*, 48, 306-310.
- JANSSEN, M., JANSSEN, M., DE WINTER, M., TRAMPER, J., MUR, L. R., SNEL, J. & WIJFFELS, R. H. 2000. Efficiency of light utilisation of *Chlamydomonas reinhardtii* under medium-duration light/dark cycles. *Journal of biotechnology*, 78, 123-137.
- JI, M.-K., ABOU-SHANAB, R. A. I., KIM, S.-H., SALAMA, E.-S., LEE, S.-H., KABRA, A. N., LEE, Y.-S., HONG, S. & JEON, B.-H. 2013. Cultivation of microalgae species in tertiary municipal wastewater supplemented with CO₂ for nutrient removal and biomass production. *Ecological Engineering*, 58, 142-148.
- KARPAGAM, R., RAJ, K. J., ASHOKKUMAR, B. & VARALAKSHMI, P. 2015. Characterisation and fatty acid profiling in two fresh water microalgae for biodiesel production: lipid enhancement methods and media optimisation using response surface methodology. *Bioresource technology*, 188, 177-184.
- KASIRI, S., ABDUSALAM, S., ULRICH, A. & PRASAD, V. 2015. Optimisation of CO₂ fixation by *Chlorella kessleri* using response surface methodology. *Chem. Eng. Sci.*, 127, 31-39.
- KATSUDA, T., FUJII, N., TAKATA, N., OOSHIMA, H. & KATOH, S. 2002. Light Attenuation in Suspension of the Purple Bacterium *Rhodobacter capsulatus*

- and the Green Alga *Chlamydomonas reinhardtii*. *Journal of chemical engineering of Japan*, 35, 428-435.
- KETHEESAN, B. & NIRMALAKHANDAN, N. 2012. Feasibility of microalgal cultivation in a pilot-scale airlift-driven raceway reactor. *Bioresource Technology*, 108, 196-202.
- KIM, W., PARK, J. M., GIM, G. H., JEONG, S. H., KANG, C. M., KIM, D. J. & KIM, S. W. 2012. Optimisation of culture conditions and comparison of biomass productivity of three green algae. *Bioprocess and Biosystems Engineering*, 35, 19-27.
- KUMAR, K., DASGUPTA, C. N., NAYAK, B., LINDBLAD, P. & DAS, D. 2011. Development of suitable photobioreactors for CO₂ sequestration addressing global warming using green algae and cyanobacteria. *Bioresource Technology*, 102, 4945-4953.
- LAN, C. *Microalgae for biofuel production and CO₂ sequestration* / Christopher Q. Lan and Bei Wang.
- LATALA, A. 1991. Effects of salinity, temperature and light on the growth and morphology of green planktonic algae. *Oceanologia*.
- LEE, H. Y. & ERICKSON, L. E. 1987. Theoretical and Experimental Yields for Photoautotrophic, Mixotrophic, and Photoheterotrophic Growth. *Biotechnology and Bioengineering*, 29, 476-481.
- LEE, H. Y., ERICKSON, L. E. & YANG, S. S. 1984. The Estimation of Growth-Yield and Maintenance Parameters for Photoautotrophic Growth. *Biotechnology and Bioengineering*, 26, 926-935.
- LEE, J.-Y., YOO, C., JUN, S.-Y., AHN, C.-Y. & OH, H.-M. 2010. Comparison of several methods for effective lipid extraction from microalgae. *Bioresource technology*, 101, S75-S77.
- LEE, Y. K. U. N. & PIRT, S. J. 1981. Energetics of photosynthetic algal growth: influence of intermittent illumination in short (40 s) cycles. *Journal of General Microbiology*, 124, 43-52.
- LEHANA, M. 1990. Kinetic analysis of the growth of *Chlorella vulgaris*. *Biotechnology and Bioengineering*, 36, 198-206.
- LI, D., XIONG, K., LI, W., YANG, Z., LIU, C., FENG, X. & LU, X. 2010. Comparative study in liquid-phase heterogeneous photocatalysis: model for photoreactor scale-up. *Industrial & Engineering Chemistry Research*, 49, 8397-8405.
- LI, S., LUO, S. & GUO, R. 2013. Efficiency of CO₂ Fixation by Microalgae in a Closed Raceway Pond. *Bioresource Technology*.
- LIU, J., SONG, Y., LIU, Y. & RUAN, R. 2015. Optimisation of growth conditions toward two-stage cultivation for lipid production of *chlorella vulgaris*. *Environmental Progress & Sustainable Energy*, 34, 1801-1807.
- LOPEZ, C., FERNANDEZ, F., SEVILLA, J., FERNANDEZ, J., GARCIA, M. C. C. & GRIMA, E. 2009. Utilisation of the cyanobacteria *Anabaena* sp ATCC 33047 in CO₂ removal processes. *Bioresour. Technol.*, 100, 5904-5910.
- MARTINEZ, L., MORAN, A. & GARCIA, A. I. 2012. Effect of light on *Synechocystis* sp and modelling of its growth rate as a response to average irradiance. *Journal of Applied Phycology*, 24, 125-134.
- MARTÍNEZ, L., MORÁN, A. & GARCÍA, A. I. 2012. Effect of light on *Synechocystis* sp. and modelling of its growth rate as a response to average irradiance. *Journal of Applied Phycology*, 24, 125-134.

- MARTINEZ, L., REDONDAS, V., GARCIA, A. I. & MORAN, A. 2011. Optimisation of growth operational conditions for CO₂ biofixation by native *Synechocystis* sp. *Journal of Chemical Technology and Biotechnology*, 86, 681-690.
- MARTÍNEZ, L., REDONDAS, V., GARCÍA, A. I. & MORÁN, A. 2011. Optimisation of growth operational conditions for CO₂ biofixation by native *Synechocystis* sp. *Journal of Chemical Technology and Biotechnology*, 86, 681-690.
- MASSART, A., MIRISOLA, A., LUPANT, D., THOMAS, D. & HANTSON, A.-L. 2014. Experimental characterization and numerical simulation of the hydrodynamics in an airlift photobioreactor for microalgae cultures. *Algal Research*, 6, Part B, 210-217.
- MEIRELES, L. A., GUEDES, A. C., BARBOSA, C. R., AZEVEDO, J. L., CUNHA, J. P. & MALCATA, F. X. 2008. On-line control of light intensity in a microalgal bioreactor using a novel automatic system. *Enzyme and Microbial Technology*, 42, 554-559.
- MICHELS, M. H. A., VASKOSKA, M., VERMUË, M. H. & WIJFFELS, R. H. 2014. Growth of *Tetraselmis suecica* in a tubular photobioreactor on wastewater from a fish farm. *Water Research*, 65, 290-296.
- MIRÓN, A. S., GARCÍA, M. C. C., GÓMEZ, A. C., CAMACHO, F. G., GRIMA, E. M. & CHISTI, Y. 2003. Shear stress tolerance and biochemical characterisation of *Phaeodactylum tricornutum* in quasi steady-state continuous culture in outdoor photobioreactors. *Biochemical Engineering Journal*, 16, 287-297.
- MIYAIRI, S. 1995. CO₂ assimilation in a thermophilic cyanobacterium. *Energy conversion and management*, 36, 763-766.
- MIYAMOTO, K. 1997. *Renewable biological systems for alternative sustainable energy production*, Food & Agriculture Organization of the UN (FAO).
- MODEST, M. F. 2013. *Radiative heat transfer*, Academic Press.
- MOLINA, E., FERNÁNDEZ, J., ACIÉN, F. & CHISTI, Y. 2001. Tubular photobioreactor design for algal cultures. *Journal of biotechnology*, 92, 113-131.
- MULLER-FEUGA, A. 1999. Growth as a function of rationing: a model applicable to fish and microalgae. *Journal of Experimental Marine Biology and Ecology*, 236, 1-13.
- MURAKAMI, M. & IKENOUCI, M. 1997. The biological CO₂ fixation and utilisation project by rite (2)—Screening and breeding of microalgae with high capability in fixing CO₂—. *Energy Conversion and Management*, 38, S493-S497.
- MUTHURAJ, M., CHANDRA, N., PALABHANVI, B., KUMAR, V. & DAS, D. 2015. Process Engineering for High-Cell-Density Cultivation of Lipid Rich Microalgal Biomass of *Chlorella* sp. FC2 IITG. *BioEnergy Research*, 8, 726-739.
- MYERS, R. H. 2002. *Response surface methodology : process and product optimization using designed experiments / Raymond H. Myers, Douglas C. Montgomery*, New York, New York : J. Wiley.
- NADERI, G., TADE, M. O. & ZNAD, H. 2015. Modified Photobioreactor for Biofixation of Carbon Dioxide by *Chlorella vulgaris* at Different Light Intensities. *Chemical Engineering & Technology*, 38, 1371-1379.

- NEWELL, R. G., PIZER, W. A. & RAIMI, D. 2013. Carbon markets 15 years after kyoto: Lessons learned, new challenges. *The Journal of Economic Perspectives*, 123-146.
- OGBONNA, J. C., YADA, H. & TANAKA, H. 1995. Light supply coefficient: a new engineering parameter for photobioreactor design. *Journal of Fermentation and Bioengineering*, 80, 369-376.
- ONO, E. & CUELLO, J. 2007. Carbon dioxide mitigation using thermophilic cyanobacteria. *Biosystems engineering*, 96, 129-134.
- ONO, E. & CUELLO, J. L. Selection of optimal microalgae species for CO₂ sequestration. Proceedings 2nd Annual Conference on Carbon Sequestration, 2003. 1-7.
- OORSCHOT, J. L. P. V. 1955. Conversion of light energy in algal culture.
- OTA, M., KATO, Y., WATANABE, H., WATANABE, M., SATO, Y., SMITH, R. L. & INOMATA, H. 2009. Effect of inorganic carbon on photoautotrophic growth of microalga *Chlorococcum littorale*. *Biotechnology progress*, 25, 492-498.
- PAREEK, V., CHONG, S., TADÉ, M. & ADESINA, A. A. 2008. Light intensity distribution in heterogenous photocatalytic reactors. *Asia-Pacific Journal of Chemical Engineering*, 3, 171-201.
- PAYNE, W. J. 1970. Energy yields and growth of heterotrophs. *Annual review of microbiology*, 24, 17-52.
- PEGALLAPATI, A. K. & NIRMALAKHANDAN, N. 2012. Modeling algal growth in bubble columns under sparging with CO₂-enriched air. *Bioresource Technology*, 124, 137-45.
- PERNER-NOCHTA, I. & POSTEN, C. 2007. Simulations of light intensity variation in photobioreactors. *Journal of Biotechnology*, 131, 276-285.
- PHILLIPS JR, J. N. & MYERS, J. 1954. Growth Rate of *Chlorella* in Flashing Light. *Plant Physiology*, 29, 152.
- PILON, L., BERBEROĞLU, H. & KANDILIAN, R. 2011. Radiation transfer in photobiological carbon dioxide fixation and fuel production by microalgae. *Journal of Quantitative Spectroscopy and Radiative Transfer*, 112, 2639-2660.
- PIRES, J. C. M., ALVIM-FERRAZ, M. C. M., MARTINS, F. G. & SIMOES, M. 2012. Carbon dioxide capture from flue gases using microalgae: Engineering aspects and biorefinery concept. *Renewable & Sustainable Energy Reviews*, 16, 3043-3053.
- PULZ, O. 2001. Photobioreactors: production systems for phototrophic microorganisms. *Applied Microbiology and Biotechnology*, 57, 287-293.
- RENAUD, S. M., THINH, L. V., LAMBRINIDIS, G. & PARRY, D. L. 2002. Effect of temperature on growth, chemical composition and fatty acid composition of tropical Australian microalgae grown in batch cultures. *Aquaculture*, 211, 195-214.
- RÍO, E. D., ACIÉN, F. G., GARCÍA-MALEA, M. C., RIVAS, J., MOLINA-GRIMA, E. & GUERRERO, M. G. 2005. Efficient one-step production of astaxanthin by the microalga *Haematococcus pluvialis* in continuous culture. *Biotechnology and Bioengineering*, 91, 808-815.
- RÍOS, A. F., FRAGA, F., PÉREZ, F. F. & FIGUEIRAS, F. G. 1998. Chemical composition of phytoplankton and particulate organic matter in the Ría de Vigo (NW Spain). *Scientia Marina*, 62, 257-271.

- ROSELLO SASTRE, R., CSÖGÖR, Z., PERNER-NOCHTA, I., FLECK-SCHNEIDER, P. & POSTEN, C. 2007. Scale-down of microalgae cultivations in tubular photo-bioreactors—a conceptual approach. *Journal of biotechnology*, 132, 127-133.
- RYU, B., KANG, K.-H., NGO, D.-H., QIAN, Z.-J. & KIM, S.-K. 2012. Statistical optimisation of microalgae *Pavlova lutheri* cultivation conditions and its fermentation conditions by yeast, *Candida rugopelliculosa*. *Bioresource Technology*, 107, 307-313.
- RYU, H. J., OH, K. K. & KIM, Y. S. 2009. Optimisation of the influential factors for the improvement of CO₂ utilisation efficiency and CO₂ mass transfer rate. *Journal of Industrial and engineering chemistry*, 15, 471-475.
- SACASA CASTELLANOS, C. 2013. Batch and Continuous Studies of *Chlorella Vulgaris* in Photo-Bioreactors.
- SAKAI, N., SAKAMOTO, Y., KISHIMOTO, N., CHIHARA, M. & KARUBE, I. 1995. *Chlorella* strains from hot springs tolerant to high temperature and high CO₂. *Energy Conversion and Management*, 36, 693-696.
- SALIH, F. M. 2011. Microalgae Tolerance to High Concentrations of Carbon Dioxide: A Review. *Journal of environmental protection*, 2, 648-654.
- SÁNCHEZ, F. J., GONZÁLEZ-LÓPEZ, C., ACIÉN, F. F., FERNÁNDEZ, S. J. & MOLINA, G. E. 2012. Utilisation of *Anabaena* sp. in CO₂ removal processes: modelling of biomass, exopolysaccharides productivities and CO₂ fixation rate. *Applied Microbiology and Biotechnology*, 94, 613.
- SAYRE, R. 2010. Microalgae: The potential for carbon capture. *Bioscience*, 60, 722-727.
- SECKBACH, J. & IKAN, R. 1972a. Sterols and chloroplast structure of *Cyanidium caldarium*. *Sterols and chloroplast structure of Cyanidium caldarium*, Mar, 457-459.
- SECKBACH, J. & IKAN, R. 1972b. Sterols and chloroplast structure of *Cyanidium caldarium*. *Plant physiology*, 49, 457.
- SEVILLA, J. F. & GRIMA, E. M. 1997. A model for light distribution and average solar irradiance inside outdoor tubular photobioreactors for the microalgal mass culture. *Biotechnology and Bioengineering*, 55.
- SEVILLA, J. M. F., GRIMA, E. M., CAMACHO, F. G., FERNANDEZ, F. G. A. & PEREZ, J. A. S. 1998. Photolimitation and photoinhibition as factors determining optimal dilution rate to produce eicosapentaenoic acid from cultures of the microalga *Isochrysis galbana*. *Applied Microbiology and Biotechnology*, 50, 199-205.
- SHEN, Y., YUAN, W., PEI, Z. J., WU, Q. & MAO, E. 2009. Microalgae Mass Production Methods. *Microalgae Mass Production Methods*, 52, 1275-1287.
- SHIBATA, K. 1959. Spectrophotometry of translucent biological materials—opal glass transmission method. *Methods of Biochemical Analysis, Volume 7*, 77-109.
- SIERRA, E., ACIEN, F., FERNANDEZ, J., GARCIA, J., GONZALEZ, C. & MOLINA, E. 2008. Characterisation of a flat plate photobioreactor for the production of microalgae. *Chemical Engineering Journal*, 138, 136-147.
- SILVA, H. J., CORTIFAS, T. & ERTOLA, R. J. 1987. Effect of hydrodynamic stress on *Dunaliella* growth. *Journal of chemical technology and biotechnology*, 40, 41-49.

- SOBCZUK, T. M., CAMACHO, F. G., GRIMA, E. M. & CHISTI, Y. 2006. Effects of agitation on the microalgae *Phaeodactylum tricornutum* and *Porphyridium cruentum*. *Bioprocess and Biosystems Engineering*, 28, 243-250.
- SPADONI, G., BANDINI, E. & SANTARELLI, F. 1978. Scattering effects in photosensitised reactions. *Chemical Engineering Science*, 33, 517-524.
- STEELE, J. H. 1977. *Chemical reactor theory: a review : dedicated to the memory of Richard H. Wilhelm*, Englewood Cliffs, N.J.: Prentice-Hall.
- STEWART, C. & HESSAMI, M.-A. 2005a. A study of methods of carbon dioxide capture and sequestration—the sustainability of a photosynthetic bioreactor approach. *Energy Conversion and Management*, 46, 403-420.
- STEWART, C. & HESSAMI, M. A. 2005b. A study of methods of carbon dioxide capture and sequestration—the sustainability of a photosynthetic bioreactor approach. *Energy Conversion and Management*, 46, 403-420.
- SUH, I. S. & LEE, S. B. 2003. A light distribution model for an internally radiating photobioreactor. *Biotechnology and bioengineering*, 82, 180-189.
- SUKENIK, A., LEVY, R., LEVY, Y., FALKOWSKI, P. & DUBINSKY, Z. 1991. Optimising algal biomass production in an outdoor pond: a simulation model. *Journal of Applied Phycology*, 3, 191-201.
- SYDNEY, E. B., STURM, W., DE CARVALHO, J. C., THOMAZ-SOCCOL, V., LARROCHE, C., PANDEY, A. & SOCCOL, C. R. 2010. Potential carbon dioxide fixation by industrially important microalgae. *Bioresource Technology*, 101, 5892-5896.
- TAMIYA, H., HASE, E., SHIBATA, K., MITUYA, A., IWAMURA, T., NIHEI, T. & SASA, T. 1953. Kinetics of growth of *Chlorella*, with special reference to its dependence on quantity of available light and on temperature. *Algal culture from laboratory to pilot plant*, 204-32.
- TEBBANI, S., LOPES, F., FILALI, R., DUMUR, D. & PAREAU, D. 2014. Nonlinear predictive control for maximisation of CO₂ bio-fixation by microalgae in a photobioreactor. *Bioprocess and Biosystems Engineering*, 37, 83-97.
- TERRY, K. L. 1986. Photosynthesis in Modulated Light - Quantitative Dependence of Photosynthetic Enhancement on Flashing Rate. *Biotechnology and Bioengineering*, 28, 988-995.
- TONGPRAWHAN, W., SRINUANPAN, S. & CHEIRSILP, B. 2014. Biocapture of CO₂ from biogas by *oleaginous* microalgae for improving methane content and simultaneously producing lipid. *Bioresour. Technol.*, 170, 90-99.
- TUANTET, K., TEMMINK, H., ZEEMAN, G., JANSSEN, M., WIJFFELS, R. H. & BUISMAN, C. J. N. 2014. Nutrient removal and microalgal biomass production on urine in a short light-path photobioreactor. *Water Research*, 55, 162-174.
- VAN BERGEIJK, S. A., SALAS-LEITON, E. & CANAVATE, J. P. 2010. Low and variable productivity and low efficiency of mass cultures of the haptophyte *Isochrysis aff. galbana* (T-iso) in outdoor tubular photobioreactors. *Aquacultural Engineering*, 43, 14-23.
- WAHIDIN, S., IDRIS, A. & SHALEH, S. R. M. 2013. The influence of light intensity and photoperiod on the growth and lipid content of microalgae *Nannochloropsis* sp. *Bioresource Technology*, 129, 7-11.
- WALTER, C., STEINAU, T., GERBSCH, N. & BUCHHOLZ, R. 2003. Monoseptic cultivation of phototrophic microorganisms - development and scale-up of a

- photobioreactor system with thermal sterilisation. *Biomolecular Engineering*, 20, 261-271.
- WANG, B. 2010. *Microalgae for biofuel production and CO₂ sequestration*, Hauppauge, N.Y., Nova Science Publishers.
- WANG, B., LI, Y., WU, N. & LAN, C. Q. 2008. CO₂ bio-mitigation using microalgae. *Applied Microbiology and Biotechnology*, 79, 707-718.
- WESTERHOFF, P., HU, Q., ESPARZA-SOTO, M. & VERMAAS, W. 2010. Growth parameters of microalgae tolerant to high levels of carbon dioxide in batch and continuous-flow photobioreactors. *Environmental technology*, 31, 523-532.
- WIDJAJA, A., CHIEN, C.-C. & JU, Y.-H. 2009. Study of increasing lipid production from fresh water microalgae *Chlorella vulgaris*. *Journal of the Taiwan Institute of Chemical Engineers*, 40, 13-20.
- YOO, J. J., CHOI, S. P., KIM, B. W. & SIM, S. J. 2012. Optimal design of scalable photo-bioreactor for phototropic culturing of *Haematococcus pluvialis*. *Bioprocess and Biosystems Engineering*, 35, 309-315.
- YUN, Y. S., LEE, S. B., PARK, J. M., LEE, C. I. & YANG, J. W. 1997. Carbon dioxide fixation by algal cultivation using wastewater nutrients. *Journal of Chemical Technology and Biotechnology*, 69, 451-455.
- YUN, Y. S. & PARK, J. M. 2001. Attenuation of monochromatic and polychromatic lights in *Chlorella vulgaris* suspensions. *Applied Microbiology and Biotechnology*, 55, 765-770.
- ZHANG, K., MIYACHI, S. & KURANO, N. 2001. Evaluation of a vertical flat-plate photobioreactor for outdoor biomass production and carbon dioxide bio-fixation: Effects of reactor dimensions, irradiation and cell concentration on the biomass productivity and irradiation utilisation efficiency. *Applied Microbiology and Biotechnology*, 55, 428-433.
- ZHONGMING, Z., LINONG, L. & WEI, L. 2012. Simulation of the light evolution in an annular photobioreactor for the cultivation of *Porphyridium cruentum*.
- ZHU, C. & LEE, Y. 1997. Determination of biomass dry weight of marine microalgae. *Journal of Applied Phycology*, 9, 189-194.
- ZOLNER, W. J. & WILLIAMS, J. A. 1971. Three-dimensional light intensity distribution model for an elliptical photoreactor. *AIChE Journal*, 17, 502-503.

Every reasonable effort has been made to acknowledge the owners of copyright material. I would be pleased to hear from any copyright owner who has been omitted or incorrectly acknowledged.